Aus dem Institut für Physiologische Chemie
Geschäftsführender Direktor: Prof. Dr. Gerhard Schratt
des Fachbereichs Medizin der Philipps-Universität Marburg

Regulation of microRNA function in neuronal development by the transcription co-activator Ncoa3

Kumulative Dissertation

zur

Erlangung des Doktorgrades
der gesamten Naturwissenschaften
(Dr. rer. nat.)

Dem Fachbereich Medizin
der Philipps-Universität Marburg
Vorgelegt von

Peter Harry Störchel
aus München

Marburg, 2015

Angenommen vom Fachbereich Medizin der Philipps-Universität Marburg am: 09.11.2015

Gedruckt mit Genehmigung des Fachbereichs.

Dekan: Prof. Dr. Helmut Schäfer
Referent: Prof. Dr. Gerhard Schratt
1. Korreferent: Prof. Dr. Bernd Schmeck

Table of contents

Summary

Tightly orchestrated gene expression programs enable proper neuronal development as well as the synaptic adaptations that are responsible for learning and memory processes. MicroRNAs (miRNAs) are a class of short regulatory RNA molecules which negatively affect the translation of target mRNAs, thereby contributing to the regulation of gene expression during brain development and cognitive functions.

In the present cumulative thesis, I summarize my contributions to three research articles which describe the impact of specific miRNAs and an upstream regulator, the nuclear receptor co-activator 3 (Ncoa3), on neuronal growth and synaptic function.

In the first publication, we identified miR-181a to be enriched at synaptic sites of the nucleus accumbens, a brain region of the dopaminergic mesolimbic system which is involved in the development of addiction. Using primary neurons, we demonstrated that miR-181a directly regulates the expression of the AMPA-receptor (AMPA-R) subunit GluA2. Neuromorphological analysis and electrophysiological measurements showed that miR-181a affects transmission at excitatory synapses. Dopamine signaling stimulated the expression of miR-181a which further influenced the dopamine-dependent control of GluA2 expression. Treatment of mice with several drugs of abuse specifically upregulated miR-181a levels in different brain regions. Taken together, this publication established miR-181a as novel regulator of synaptic efficacy and in the context of the present literature as a potential modulator of addiction behavior.

Based on previous findings that showed the synaptic localization of miR-137 and that identified mutations in the MIR137 gene associated with schizophrenia and cognitive disabilities, we investigated the postsynaptic functions of miR-137 in the second publication. Manipulations of miR-137 expression provided evidence that the AMPA-R subunit GluA1 mRNA is a direct target of miR-137. Intriguingly, morphological and electrophysiological measurements revealed that miR-137 regulates the number but not the strength of excitatory synapses. MiR-137 further promoted the formation of silent synapses, since miR-137 manipulations affected AMPA-R-, but not NMDA-receptor (NMDA-R)-dependent currents. Furthermore, induction of miR-137 expression was required for mGluR-dependent long term depression (LTD). Therefore, this research article provides experimental support for a postsynaptic function of miR-137

in the regulation of synapse formation and plasticity, with possible implications for schizophrenia and cognitive disabilities.

In the third publication, which includes the main part of my PhD project, 10 novel regulators of miRNA-dependent gene silencing in neurons were identified by performing an RNAi-based screen. One of the newly ascertained proteins was Ncoa3, a transcription co-activator whose function in hippocampal neurons was not studied. Reporter gene assays showed that Ncoa3 was required for miRNA-mediated repression of a specific set of miRNA target genes, including Limk1. In addition, Ncoa3-knockdown increased endogenous Limk1 protein levels and interfered with miR-134-induced spine shrinkage. At the same time, Ncoa3 deficiency by itself reduced the size of dendritic spines and the amplitude of miniature excitatory postsynaptic currents (mEPSCs) while it stimulated dendrite growth. The latter phenotype was dependent on proper miRNA-expression. Ago2 is a central effector of miRNA repression and we established it further as a direct transcriptional target gene of Ncoa3. Epistasis experiments confirmed that both impaired dendritogenesis and miRNA function upon Ncoa3 knockdown were a result of reduced Ago2 expression. Thus, this publication uncovered a novel transcriptional mechanism for the control of miRNA-dependent repression during neuronal development.

In summary, these findings decipher neuronal gene expression programs which control synaptic adaptations and thus are potentially involved in learning and memory processes.

Zusammenfassung

Präzise koordinierte Genexpressionsprogramme ermöglichen korrekte neuronale Entwicklung und synaptische Anpassungen, die für Lern- und Gedächtnisprozesse verantwortlich sind. MicroRNAs (miRNAs) sind eine Klasse kurzer regulatorischer RNA-Moleküle, welche die Translation von spezifischen Ziel-mRNAs unterdrücken und dadurch zur Regulation der Genexpression während der Entwicklung des Gehirns und kognitiver Fähigkeiten beitragen.

In der vorliegenden kumulativen Dissertation fasse ich meinen Beitrag zu drei Forschungsartikeln zusammen. Sie beschreiben den Einfluss von bestimmten miRNAs, sowie eines vorgeschalteten Regulators (Nuclear receptor co-activator 3 (Ncoa3)) auf neuronales Wachstum und synaptische Funktion.

In der ersten Veröffentlichung entdecken wir eine Anreicherung von miR-181a an Synapsen des Nucleus Accumbens, einer Hirnregion des dopaminergen mesolimbischen Systems, die an der Entwicklung von Suchterkrankungen beteiligt ist. Mittels primärer Neuronen wiesen wir nach, dass miR-181a die Expression der AMPA-Rezeptor(AMPA-R)-Untereinheit GluA2 direkt reguliert. Neuromorphologische Analysen und elektrophysiologische Messungen zeigten zudem, dass miR-181a die Reizübertragung an exzitatorischen Synapsen beeinflusst. Aktivierung des Dopamin-Signalwegs stimulierte die Expression von miR-181a, was sich wiederum auf die Dopamin-abhängige Kontrolle der GluA2 Expression auswirkte. Die Gabe von unterschiedlichen psychoaktiven Substanzen führte bei Mäusen ebenfalls zu einer spezifischen Erhöhung der miR-181a Expression in verschiedenen Hirnregionen. Zusammengefasst etabliert diese Veröffentlichung miR-181a als neuen Regulator von synaptischer Übertragung und im Kontext aktueller Literatur als potentiellen Modulator von Suchtverhalten.

Basierend auf früheren Befunden, welche die synaptische Lokalisierung von miR-137 zeigten, und eine Assoziation von Mutationen im MIR137 Gen mit Schizophrenie und geistiger Behinderung identifizierten, untersuchten wir in der zweiten Veröffentlichung die postsynaptische Funktion von miR-137. Einflussnahme auf die miR-137 Expressionslevels belegte, dass die AMPA-R-Untereinheit GluA1 mRNA ein direktes Ziel von miR-137 ist. Interessanterweise zeigten morphologische und elektrophysiologische Messungen, dass miR-137 nur die Anzahl, nicht jedoch die

Stärke von exzitatorischen Synapsen reguliert. Ferner begünstigte miR-137 die Bildung von stummen Synapsen, da veränderte miR-137 Expression zwar AMPA-R-abhängige, nicht jedoch NMDA-Rezeptor(NMDA-R)-abhängige Ströme beeinflusste. Außerdem war der Anstieg von miR-137 notwendig für mGluR-abhängige Langzeit-Depression (LTD). Diese Publikation untermauert somit eine postsynaptische Funktion von miR-137 in der Regulation von Synapsenbildung und –plastizität, sowie eine damit verbundene mögliche Bedeutung für Schizophrenie und geistige Behinderung.

In der dritten Veröffentlichung, die den Hauptteil meiner Doktorarbeit beinhaltet, wurden mittels einem RNAi-basierten Screen zehn neue Regulatoren der miRNA-abhängiger Geneexpressionshemmung in Neuronen identifiziert. Eines der neu ermittelten Proteine war Ncoa3, ein Transkriptionscoaktivator dessen Funktion in Hippocampus-Neuronen bislang noch nicht untersucht war. Reportergen-Assays zeigten, dass Ncoa3 für miRNA-vermittelte Repression bei einer spezifischen Gruppe von miRNA-Zielgenen, inklusive Limk1, erforderlich ist. Zusätzlich hatte Ncoa3-knockdown zur Folge, dass endogene Limk1 Proteinmengen erhöht waren, und dass das miR-134-induzierte Schrumpfen von dendritischen Dornfortsätzen gestört war. Alleinige Ncoa3-Defizienz war zudem ausreichend die Größe von dendritischen Dornfortsätzen und die Amplitude von Miniatur exzitatorischen postsynaptischen Strömen (mEPSCs) zu reduzieren, während sie das Dendritenwachstum stimulierte. Dieser letztere Phänotyp war abhängig von ordnungsgemäßer miRNA-Expression. Ago2 ist ein zentraler Effektor von miRNA-Repression und wir etablierten es ferner als direktes transkriptionelles Zielgen von Ncoa3. Epistase-Experimente bestätigten, dass sowohl das durch Ncoa3-knockdown beeinträchtigte Dendritenwachstum, als auch die gestörte miRNA-Funktion, ein Ergebnis der reduzierten Ago2 Expression ist. Folglich enthüllt diese Veröffentlichung einen neuen transkriptionellen Mechanismus für die Kontrolle von miRNA-abhängiger Repression in neuronaler Entwicklung.

Zusammenfassend entziffern diese Befunde neuronale Genexpressionsprogramme, die synaptische Anpassungen kontrollieren und so möglicherweise in Lern- und Gedächtnisprozessen involviert sind.

Introduction

1.1 Dendritic protein synthesis and synaptic plasticity

The intriguing cognitive capabilities of our brain are enabled by ~100 billion (10^{11}) nerve cells (neurons) which are interconnected by ~100 trillion (10^{14}) specialized junctions (synapses) within complex neural circuits. In order to receive and integrate this extraordinary high number of synaptic inputs, neurons increase their surface through the formation of multiple, branched processes known as dendrites. Dendrites carry small protrusions called dendritic spines which are the major contact sites of excitatory synapses. Based on the results from many studies, spine size represents a good correlate of synaptic strength (Matsuzaki et al., 2004; Lippman and Dunaevsky, 2005). During postnatal development and in the adult organism, dendrites and synapses can adapt to changes in the environment in an activity-dependent manner. These adaptations are commonly referred to as neuronal plasticity and are thought to underlie both the correct development of neural circuits and memory formation in the adult (Flavell and Greenberg, 2008). The establishment of long-lasting morphological and functional changes of dendrites and synapses requires elaborate gene expression programs that include the regulation of transcription and translation. The activity-dependent translation of dendritically localized mRNAs appears to be particularly important for excitatory synaptic plasticity during memory-related processes (Richter and Klann, 2009). Dendritic protein synthesis requires the active transport of thousands of mRNAs to synaptic sites within dendrites, where they are available for the rapid supply of new synaptic proteins in response to stimulation. Dendritically localized mRNAs encode for proteins involved in signaling (e.g. protein kinases), translational control (e.g. RNA-binding proteins), membrane trafficking (e.g. adapter molecules), and neurotransmission (e.g. neurotransmitter receptors) (Cajigas et al., 2012). The most widely expressed neurotransmitter receptors in the mammalian brain are α-amino-3-hydroxy-5-methyl-4-isoxazolepropionic acid receptors (AMPA-Rs). AMPA-Rs are ligand-gated cation channels composed of four subunits (GluA1-4) which are activated by the neurotransmitter glutamate. They are located at the postsynaptic side of glutamatergic synapses and their dynamic membrane trafficking is involved in the bidirectional modification of synaptic strength (Huganir and Nicoll, 2013). Since AMPA-

Rs reside in the plasma membrane, the modification of their surface expression is mediated by orchestrated translational and membrane trafficking events. GluA1 and 2 mRNAs are dendritically localized (Cajigas et al., 2012) and their local translation is tightly controlled, e.g. by the translational repressor protein eIF4E-BP2 (Ran et al., 2013). As shown by several groups, microRNAs (miRNAs, see below) are also important regulators of GluA1 and 2 expression in the context of synaptic activity (Ho et al., 2014; Letellier et al., 2014; Hu et al., 2015).

1.2 MicroRNAs

MiRNAs are a family of non-coding RNAs with a length of ~21 nucleotides which negatively regulate the translation of specific mRNAs. In most cases, miRNAs bind via partial complementarity to the 3' untranslated region (3' UTR) of target mRNAs, thereby leading to translational repression and/or mRNA decay (Krol et al., 2010; Huntzinger and Izaurralde, 2011).

Since miRNA binding requires only a relatively short complementary region within target 3'UTRs (the so-called seed pairing region), a single miRNA regulates up to hundreds of target mRNAs. This pleiotropic effect offers the possibility to coordinately control genes working in the same pathway.

1.3 MiRNAs in the nervous system

Especially in the nervous system, orchestrated translational control by miRNAs is an attractive concept in the context of activity-dependent protein synthesis. Indeed, many miRNAs are expressed in particular cell-types of the nervous system (Jovicic et al., 2013). Several neuronal miRNAs were identified in the synaptodendritic compartment by microarray analysis of synaptosomes which are biochemical brain preparations enriched in pre- and postsynaptic components (Siegel et al., 2009). MiR-137, which is present at high levels in synaptosomes, was shown to regulate dendrite development (Smrt et al., 2010) and synaptic plasticity by acting presynaptically (Siegert et al., 2015). Intriguingly, genetic variants of MIR137 are associated with schizophrenia (Cummings et al., 2013; Ripke et al., 2014) and intellectual disability (Willemsen et al., 2011).

Another well-characterized dendritic miRNA is miR-134. MiR-134-dependent regulation of Pumilio2 (Pum2) is required for activity-dependent dendrite growth and homeostatic synaptic plasticity (Fiore et al., 2009; Fiore et al., 2014). In addition, miR-134 negatively

affects dendritic spine size by inhibiting local translation of LIM-domain kinase 1 (Limk1) mRNA. MiR-134-dependent inhibition of Limk1 can be reversed by brain-derived neurotrophic factor (BDNF) (Schratt et al., 2006). Furthermore, overexpression of miR-134 in mice interferes with memory formation by repression of the cyclic AMP-responsive element-binding protein 1 (CREB1) and its downstream target BDNF (Gao et al., 2010). Under pathophysiological conditions, miR-134 is induced by epileptiform activity, and miR134 reduces epilepsy-associated cell death and seizure activity (Jimenez-Mateos et al., 2012). MiR-138 is another crucial miRNA in the brain which regulates the development of dendritic spines through the local translational control of the acyl-protein thioesterase 1 (APT1) (Siegel et al., 2009). A different important miRNA is miR-181a. It was described as a regulator of immune system function by controlling the expression of the cytokine TNF-alpha (Dan et al., 2015). In addition, miR-181a has been shown to function as a tumor suppressor in multiple studies (Shi et al., 2008; Shin et al., 2011; Huang et al., 2015). Within neurons, miR-181a is present in neuronal processes (Kye et al., 2007) and negatively regulates dendrite outgrowth (Liu et al., 2013).

1.4 MiRNA biogenesis and function

MiRNA genes occur either as single genes, gene clusters or within introns of protein-coding genes. The majority of miRNAs are transcribed by RNA polymerase II. The resulting primary miRNA transcript (pri-miRNA) contains a typical hairpin structure which serves as a substrate for the RNase III family enzymes Drosha and Dicer for two consecutive nucleolytic processing steps. In the nucleus, the microprocessor complex consisting of Drosha and DiGeorge syndrome critical region 8 (DGCR8) generates a ~70 nucleotide precursor miRNA (pre-miRNA) by liberating the hairpin from the remaining pri-miRNA. After export to the cytoplasm, Dicer is assisted by Trans-activation-responsive RNA-binding protein (TRBP) to cleave off the loop region of the pre-miRNA hairpin yielding a miRNA/miRNA* duplex. One of the two strands of the duplex is incorporated into the miRNA-induced silencing complex (miRISC) which mediates the repressive activity. The miRISC consists of two core factors, Argonaute (Ago) and GW182 proteins. Mammals express four Ago proteins (Ago1-4) which catalyze the binding of the miRNA to the target mRNA and further recruit GW182

proteins (Tnrc6a-c in mammals). The multi-domain GW182 proteins act as scaffolds to recruit further protein complexes involved in translational repression, mRNA decapping and mRNA degradation. In addition, a number of miRISC accessory proteins that are able to modulate the repressive activity have been identified (van Kouwenhove et al., 2011).

1.5 Regulation of miRNA activity

The expression of miRNAs can be regulated at all stages of biogenesis (transcription, export and processing), which often involves the function of specific pre-miRNA-binding proteins (Krol et al., 2010). In addition, the gene regulatory activity of miRNAs can be regulated by altering miRISC function. Mechanistically, miRISC regulation can be achieved by posttranslational modification of the core miRISC components Ago or GW182 (Qi et al., 2008; Zeng et al., 2008; Rybak et al., 2009; Li et al., 2014). Furthermore the activity of the miRISC can be influenced by proteins that modulate miRISC recruitment to target mRNAs. These factors are often RNA-binding proteins (RBPs) that bind to sequence motifs that either overlap or are adjacent to miRNA binding sites within target 3'UTRs. Such RBPs have been shown to either promote or impede miRISC recruitment (Höck et al., 2007; Kedde et al., 2007; Nolde et al., 2007; Edbauer et al., 2010; Engels et al., 2012). The activity of RBPs which modulate miRISC can be modified by extracellular signals. For example, in response to cellular stress, HuR translocates from the nucleus to the cytoplasm where it relieves miR-122 dependent repression of the cationic amino acid transporter 1 (CAT-1) mRNA (Bhattacharyya et al., 2006). Such signal-dependent switches in miRNA-dependent repression could be highly relevant for the regulation of dendritic protein synthesis and plasticity in neurons, however few examples have been described so far. They include the signal-dependent modification of the Ago-interacting proteins FMRP and Mov10/Armitage (Banerjee et al., 2009; Muddashetty et al., 2011).

In principle, specific usage of the different Ago proteins by certain miRNAs could be a further means to control miRNA repressive function. However, conclusive evidence for a specific sorting of different miRNAs into the four mammalian Ago proteins is still missing (Azuma-Mukai et al., 2008; Hafner et al., 2010). Ago2 is the only family member with endonuclease activity, which enables target degradation in the case of perfect

complementarity between target mRNA and miRNA (Krol et al., 2010). Moreover, Ago2 has essential roles which are independent of its nuclease activity but cannot be compensated by the other Ago proteins, e.g. during hematopoiesis (O'Carroll et al., 2007). Together, these findings underscore apparently unique functions of Ago2 which cannot be compensated by the other Ago proteins.

1.6 Ncoa3

Ncoa3 (SRC-3, AIB-1) is a transcription factor belonging to the family of nuclear receptor co-activators (Ncoa 1-3) (Leo and Chen, 2000; Dasgupta et al., 2014). Ncoa3 does not contact DNA directly, but interacts with nuclear receptors (e.g. estrogen and retinoic acid receptors) in a ligand-dependent manner. Nuclear receptor binding recruits Ncoa3 to specific elements in the promoters of target genes, where it interacts with general co-activators that modify chromatin structure. By controlling hormone-dependent gene expression, Ncoa3 functions as an oncogene in various tumor types (Xu et al., 2009). Furthermore, Ncoa3 has cytoplasmic functions in signaling and translational control (Yu et al., 2007; Long et al., 2010). The transition of Ncoa3 between cytoplasm and nucleus was shown to depend on phosphorylation (Amazit et al., 2007). In the brain, the function of Ncoa3 remains largely unknown. In a study performed in cortical neurons, Ncoa3 was shown to be phosphorylated upon treatment with all-trans retinoic acid, a lipid hormone that regulates local protein synthesis in the context of homeostatic synaptic plasticity (Aoto et al., 2008; Chai et al., 2009). However, Ncoa3 has not been implicated in the control of miRNA activity so far.

1.7 Aims of this thesis

Although previous studies have identified a number of miRNAs involved in the regulation of neuronal development and plasticity, the target genes regulated by these miRNAs were still poorly characterized. In particular, a direct modulation of synaptic glutamate receptor function by miRNAs had not been established. Moreover, the mechanisms that modulate miRNA function in neurons were similarly unexplored, especially with respect to an involvement of RNA-binding proteins.

Therefore, in the context of two collaborative projects, I explored a potential regulation of AMPA-type glutamate receptor expression by the synaptic miRNAs miR-181a and

miR-137, with the aim to unravel the mechanism that underlies the regulation of synapse morphology and physiology by these miRNAs.

As a main project, I investigated the function of a specific protein (Ncoa3) that was identified in a large-scale screen for miRNA modulatory factors in neurons. The objective here was to clarify the mechanism whereby the transcription factor Ncoa3 controls miRNA activity and neuronal development.

2. Summary and personal contribution to cumulated publications

2.1 Publication 1: "Dopamine-regulated microRNA miR-181a controls GluA2 surface expression in hippocampal neurons." (Saba et al., 2012)

In the present publication, miR-181a was identified as a novel regulator of GluA2 expression, with potential implications for synaptic plasticity mechanisms involved in the control of addiction. The nucleus accumbens processes reward and motivation as part of the mesolimbic system and is therefore involved in the establishment of addiction. Since miRNAs are important regulators of gene expression and synaptic plasticity, the study investigated synaptically localized miRNAs in the nucleus accumbens using microarray analysis. Using synaptosome fractionation, nine miRNAs were identified that were enriched more than 2-fold in synaptosomes compared to nucleus accumbens tissue (Table 1). For further analysis, we focused on miR-181a, since *in silico* miRNA target prediction algorithms detected this miRNA to target GluA2 which is an important modulator of synaptic transmission (Fig. 2C). Furthermore, all follow-up experiments were performed in hippocampal neurons, since these cells are more amenable to experimental manipulation compared to neurons from nucleus accumbens. A functional interaction between miR-181a and GluA2 mRNA could be confirmed using overexpression and inhibition of miR-181a in reporter gene assays (Fig. 2D and 3C). MiR-181a expression was found to increase during *in vitro* development of neurons with highest levels at 14-20 days in vitro (DIV, Fig. 3A), a time period of intense synapse formation and remodeling. Overexpression of miR-181a reduced total GluA2 protein levels as well as GluA2 expression on the neuronal plasma membrane (Fig. 2F, 4B and C). Neuromorphological measurements by confocal microscopy in cells overexpressing miR-181a further showed a reduction in dendritic spine size and density (Fig. 4E and F). In agreement with the morphological data, electrophysiological recordings of neurons overexpressing miR-181a revealed a reduction in the frequency but not in the amplitude of mEPSCs (Fig. 5). Finally, treatment of neurons with the dopamine agonist SKF-38393 resulted in increased miR-181a expression (Fig. 6A and B) and reduced expression of the miR-181a target GluA2 in reporter gene assays (Fig. 6D). This effect was dependent on miR-181a, since mutation of the miR-181a site in the GluA2 reporter abolished dopamine

responsiveness. Furthermore, acute administration of cocaine and amphetamine affected the expression of miR-181a in various regions of the mouse brain (Fig. 6E). In conclusion, this publication describes miR-181a as a critical regulator of AMPA-type glutamate receptors with implications for drug-induced adaptations.

My contribution to this publication was to analyze the effects of miR-181a overexpression on GluA2 expression. The results of these experiments are presented in Figs. 2F, 4B, 4F. The methods used here are GluA2 protein quantification after miR-181a overexpression in primary neurons by Western Blot (Fig. 2F) and immunocytochemistry (Fig. 4B). Furthermore, I analyzed the density of dendritic spines of hippocampal neurons after miR-181a overexpression (Fig. 4F). The results from my experiments helped to establish endogenous GluA2 as a target of miR-181a and provided support for a functional role of miR-181a in the regulation of dendritic spine density.

2.2 Publication 2: "MicroRNA-137 controls AMPA-receptor-mediated transmission and mGluR-dependent LTD." (Olde Loohuis et al., 2015)

Disease-associated mutations in the MIR-137 gene have been linked to intellectual disability and schizophrenia. In this publication, the molecular mechanisms underlying a potential synaptic function of miR-137 were investigated. The functionality of a bioinformatically predicted miR-137 binding site in the AMPA-type glutamate receptor subunit GluA1 was validated by reporter gene assays and endogenous protein analysis using miR-137 overexpression and inhibition (Fig. 1). Inhibition of miR-137 resulted in an increased density of dendritic spines, whereas neither overexpression nor inhibition of miR-137 altered the size of dendritic spines (Fig. 3B). In parallel, miR-137 manipulation affected AMPA-R-dependent, but not NMDA-R-dependent mEPSC frequency as measured by patch-clamp recordings (Fig. 2). In agreement with the spine data, no alterations in either AMPA-R- or NMDA-R-dependent mEPSC amplitude were observed (Fig. 2E). Similarly, the number of silent synapses, i.e. synapses which contain NMDA- but not AMPA-Rs, were reduced after miR-137 inhibition and increased after miR-137 overexpression (Fig. 3I). This finding supports a mechanism whereby miR-137 controls the surface expression of functional AMPA-Rs. Since AMPA-R dynamics is important for activity-dependent synapse remodeling, a paradigm of synaptic plasticity (LTD) was used to further study the influence of miR-137. Pharmacological induction of LTD with the mGluR group I agonist Dihydroxyphenylglycine (DHPG) significantly increased mature miR-137 levels (Fig. 4) in an mGluR5-dependent manner. Furthermore, DHPG-mediated induction of miR-137 was essential for the establishment of LTD (Fig. 4E). In summary, this publication provided evidence for an important role of miR-137 in synapse function and plasticity. Therefore, these findings might help to explain neurological symptoms associated with polymorphisms in the MIR-137 gene observed in mental retardation and schizophrenia. My contribution to the present publication was to demonstrate that miR-137 directly controls GluA1 translation. This was carried out with reporter gene assays using the GluA1 3'UTR. The expression of the reporter was increased after miR-137 inhibition in primary neurons which was not the case when the miR-137 binding site in the GluA1 3'UTR was mutated (Fig. 1A, B). Together these data show that miR-137 actively represses the translation of GluA1 in neurons.

2.3 Publication 3: "A large-scale functional screen identifies Nova1 and Ncoa3 as regulators of neuronal miRNA function." (Störchel et al., 2015)

As illustrated in the previous two publications, synaptic miRNAs are crucially involved in the control of neuronal growth, synapse formation and plasticity by regulating the translation of specific mRNAs. In order to identify neuronal proteins which regulate the repressive activity of miRNAs, a luciferase-based RNAi screen was performed. The screening of 286 RBPs in primary neurons identified 12 RBPs that were required for miRNA repressive activity. Among them were 10 RBPs that were previously unknown to be involved in miRNA regulation (Fig. 1A and B). Based on results from further validation experiments, we decided to focus on two of these candidates, Ncoa3 and Nova1 (Fig. 1C). Both proteins were shown to be expressed in the cytoplasm and nucleus of primary neurons in a developmental-dependent manner (Fig. 2). Further luciferase-based experiments showed that both proteins are required for the repressive activity of miR-134, let-7 and miR-138 on reporters carrying the 3'UTR of Limk1, Lin-41 and APT1, respectively (Fig. 3). However, only Nova1 was essential for the regulation of an isolated miR-138 binding site (Fig. 3F). The endogenous protein levels of Limk1, a known miR-134 target, were elevated upon shRNA-mediated knockdown of Nova1 and Ncoa3 (Fig. 4A and B). Also, the knockdown of both proteins blocked miR-134-induced shrinkage of dendritic spines (Fig. 4C and D). Mechanistically, we demonstrated that Nova1 directly interacts with Ago proteins and target mRNAs using immunoprecipitation experiments (Fig. 5A and B). Direct recruitment of Nova1 to a reporter mRNA in tethering assays was sufficient to inhibit reporter gene expression (Fig. 5D). Together, our results suggest that Nova1 represses mRNA translation in neurons as a miRISC-interacting protein. Concerning the analysis of Ncoa3, we found that is essential for proper dendritic spine development and synaptic transmission (Fig. 7). An shRNA-mediated knockdown of Ncoa3 reduced the amplitude of mEPSC, but not their frequency in dissociated hippocampal neurons (Fig. 7C-F). Furthermore, Ncoa3 knockdown significantly increased dendrite outgrowth in wild-type neurons, but not in neurons that lack miRNAs due to knockdown of Drosha (Fig. 6). Therefore we conclude that the dendrite growth regulatory function of Ncoa3 is dependent on miRNAs. Comparative gene expression analysis of wild-type and Ncoa3-deficient neurons by microarrays identified Ago2 as an Ncoa3-regulated gene (Fig. 8B). These

results were further confirmed by qPCR and Western Blotting (Fig. 8C and D). By using chromatin immunoprecipitation (ChIP) and luciferase reporter gene assays, we found that Ncoa3 was associated with the Ago2 promoter (Fig. 8E and F) which suggests that Ncoa3 transcriptionally regulates Ago2 expression. Finally, restoring Ago2 expression rescued the effects of Ncoa3 knockdown on dendrite outgrowth and expression of miRNA reporter genes (Fig. 9), which supports the concept that the cellular defects caused by Ncoa3 knockdown are a result of reduced Ago2 expression. In summary, this publication describes the identification and validation of two novel miRNA regulatory factors in neurons, with implications for nervous system development and brain physiology.

In this publication, where I share first authorship, I generated most of the data related to Ncoa3. This includes the generation of expression vectors, reporter gene assays (Fig. 3B, 3D, 8F, 9B), dendrite growth analysis (Fig. 6 all, 9C-E), dendritic spine size analysis (Fig. 4C, 4D, 7A, 7B), gene expression analysis by microarray (Fig. 8B), qPCR (Fig. 8A, 8C), Western Blot (Fig. 2B, 2G, 4B, 8D), Immunocytochemistry (Fig. 2E, 2F, 9A) and ChIP experiments (Fig. 8E).

3. Discussion

3.1 miR-181a and miR-137 as synaptic regulators of AMPA-receptor subunits

The first two publications to which I contributed describe in detail the molecular mechanisms whereby two synaptic miRNAs, miR-181a and miR-137, control synapse development and physiology. Intriguingly, both miRNAs were found to regulate subunits of the AMPA-type glutamate receptor, which plays a pivotal role in excitatory synapse function and plasticity. As such, these publications depict a potential mechanism whereby miRNA dysregulation could contribute to disorders such as addiction and schizophrenia.

Our results obtained from synaptosome preparations of the rat nucleus accumbens (Pub. 1: Fig. 1) are consistent with an earlier study where qPCR analysis of total RNA isolated from laser-dissected dendrites of cultured rat hippocampal neurons identified the dendritic localization of miR-181a (Kye et al., 2007). This suggests that synapto-dendritic localization of miR-181a might be commonly observed in different neuron types. In addition, miR-181a might not be exclusively transported to postsynaptic sites, since a passenger strand of miR-181a (miR-181a-1*) was detected in the axons of mouse cortical neurons (Sasaki et al., 2014). Earlier findings that miR-181a expression increases during mouse brain development, reaching highest levels in the adult (Miska et al., 2004), already indicated that miR-181a could be involved in synaptic plasticity and brain physiology. Consistently, the pattern of miR-181a expression during the maturation of cultured rat hippocampal neurons follows a similar trend (Pub. 1: Fig. 3A). An important finding was that application of a dopamine-agonist in mature neurons induced miR-181a expression (Pub. 1: Fig. 6A), directly implicating dopamine signaling in miR-181a biology. A connection between miR-181a and dopamine signaling is supported by previous publications which showed that miR-181a associates with Ago2 in dopamine-receptor 2 (Drd2)-positive neurons of the mouse striatum, and that miR-181a expression was induced in this region by administration of cocaine, a drug that stimulates dopamine signaling (Schaefer et al., 2010). Induction of miR-181a in the nucleus accumbens was also necessary for the establishment of cocaine-induced plasticity (Chandrasekar and Dreyer, 2009, 2011). Intriguingly, synaptic rearrangements induced by cocaine involve a specific removal of the GluA2 subunit

from AMPA-R heterodimers (Bellone and Lüscher, 2006). Indeed, we could provide a link between miR-181a induction and GluA2 removal by showing that miR-181a overexpression reduced both total GluA2 protein levels and GluA2 cluster size (Pub. 1: Fig. 2, 3, 4). Interestingly, when the cocaine-evoked dopaminergic innervations were mimicked in cell culture by application of a dopamine agonist, expression of a GluA2 3'UTR reporter gene was reduced in a miR-181a-dependent manner (Pub. 1: Fig. 6D). Furthermore, the morphological changes caused by miR-181a expression (Pub. 1: Fig. 4E and F) could be a direct consequence of reduced GluA2 levels, since GluA2 is both necessary and sufficient for dendritic spine formation and stability (Passafaro et al., 2003).

Taken together, publication 1 establishes miR-181a as a critical regulator of synapse development through the translational control of the AMPA-type glutamate receptor subunit GluA2. This mechanism could be involved in cocaine-induced neuroadaptations and addictive behavior that were previously shown to be miR-181a-dependent (Chandrasekar and Dreyer, 2011).

Deregulated dopaminergic signaling is also observed in schizophrenia and commonly used drugs to treat the symptoms of schizophrenia antagonize the dopamine receptor Drd2 (van Os and Kapur, 2009). Intriguingly, another miR-181 family member (miR-181b) exhibits elevated levels in schizophrenia (Beveridge et al., 2008). Furthermore, GluA2 was identified as a target of miR-181b in a glioblastoma cell culture model used in the same study. Therefore, the regulation of GluA2 by miR-181 family members might also be relevant in deregulated dopaminergic transmission in schizophrenia.

The synaptic enrichment of miR-137 was previously demonstrated by microarray profiling of rat forebrain synaptosomes from juvenile (postnatal day 15) rats (Siegel et al., 2009). Further validation experiments by independent methods (e.g. qPCR, Northern Blot or *in-situ* hybridization) are required to confirm synaptic enrichment of miR-137, especially since other studies failed to demonstrate dendritic or synaptic localization of miR-137 (Kye et al., 2007; Lugli et al., 2008). Interestingly, in publication 2 we found an increase in mature miR-137 with a concomitant decrease in pre-miR-137 after DHPG-induced LTD (Pub. 2: Fig. 4A and B). These findings are most easily explained by stimulus-dependent processing of pre-miR-137. Since pre-miR-137 is absent from dendrites, processing is likely happening within the neuronal cell soma

(Bicker et al., 2013). According to this model, accumulation of miR-137 at synapses during LTD would have to involve a rapid transport of the mature miRNA from the soma to the dendrite after pre-miRNA processing. Future mechanistic studies are required to resolve the molecular mechanisms underlying the dendritic transport of mature miR-137 and other synaptic miRNAs in response to synaptic activity.

Importantly, inhibition of endogenous miR-137 interfered with the establishment of mGluR-dependent LTD (Pub. 2: Fig. 4E, F and G). This might be clinically relevant since mGluRs are considered as potential drug targets for the treatment of schizophrenia (Chaki and Hikichi, 2011). mGluR-LTD requires dendritic protein synthesis and the miR-137 target GluA1 mRNA is dendritically localized. This together raises the possibility that the miR-137-dependent regulation of GluA1 happens postsynaptically in dendrites. In agreement with a dendritic function of miR-137, other established miR-137 target mRNAs, such as CACNA1C, CSMD1 and TCF4, were also identified in dendrites (Cajigas et al., 2012; Kwon et al., 2013). In addition to this putative postsynaptic function, miR-137 was recently found to affect synaptic vesicle release probability and their distribution as well as the expression of presynaptic proteins (Siegert et al., 2015). Although this study clearly delineates a functional involvement of miR-137 in presynaptic processes, it does not provide data with regard to the subcellular localization of miR-137. In conclusion, miR-137 appears to orchestrate both post- and presynaptic processes important for neurotransmission.

3.2 Ncoa3 positively regulates miRNA activity by activating Ago2 expression

Luciferase-based RNAi screens to identify miRNA regulators have been carried out before (Horman et al., 2013; Li et al., 2014), but we were the first to perform such a screen in primary neurons. Moreover, we focused on RBPs expressed in the mammalian brain based on a previous *in-situ* hybridization study (McKee et al., 2005). Together, these unique aspects of our screen allowed us to identify 10 novel miRNA regulatory proteins that had not been reporter before. Since I mainly focused on one of the newly identified regulators (Ncoa3) during my PhD thesis, I will limit the following discussion to this protein.

As a family member of the nuclear receptor co-activators (Ncoa1-3 or also known as SRC1-3), Ncoa3 has been extensively studied in the context of nuclear receptor-

dependent transcription, e.g. in estrogen receptor signaling related to breast cancer (Gojis et al., 2010). However, two studies assign additional cytoplasmic functions to Ncoa3, either as a signaling molecule in focal adhesions or as a translational co-repressor in the immune response (Yu et al., 2007; Long et al., 2010). Consistent with this dual function of Ncoa3, I found that Ncoa3 is expressed in both the nuclear and cytoplasmic compartment of primary neurons (Pub. 3: Fig. 2). Having shown that Ncoa3 stimulates miRNA function in neurons, I collected several lines of evidence that support a nuclear role of Ncoa3 in this process: I) By using UV-crosslinking experiments, I was unable to demonstrate a specific interaction of Ncoa3 with RNA (data not shown); II) the recruitment of Ncoa3 to the 3'UTR of a reporter gene mRNA in tethering assays had no effect on reporter gene expression (Pub. 3: Fig. 5) ; and III) using compartment-specific expression of Ncoa3, I found that only nuclear expression of Ncoa3 was sufficient to restore miRNA-dependent repression of reporter genes in the context of Ncoa3 knockdown (data not shown). In support of a mechanism whereby Ncoa3 promotes miRNA repression by inducing the expression of miRNA regulatory proteins, I was able to establish Ago2 as a direct transcriptional target of Ncoa3 using multiple independent approaches (Pub. 3: Fig. 8). Although the observed reduction of Ago2 transcript levels after Ncoa3 knockdown is relatively small (30-40%), my results from rescue experiments (Pub. 3: Fig. 9) indicate that Ago2 regulation plays an important role in the control of miRNA activity and neuronal morphology by Ncoa3. In addition, Ncoa3 likely regulates neuronal morphogenesis by controlling other pathways. In fact, a set of genes which are implicated in microtubule dynamics, e.g. MAP9, Spastin and UHMK1 (Venoux et al., 2008; Cambray et al., 2009; Roll-Mecak and McNally, 2010), were downregulated by Ncoa3 knockdown. Future experiments are needed to determine the relevance of Ncoa3-regulated microtubule dynamics for neuronal development and plasticity.

Given the redundancy of Ago proteins in mammalian RNAi, the strong phenotypic and gene regulatory consequences observed upon a 30-40% reduction specifically of Ago2 are surprising at first. However, Ago2 was found to be rate-limiting in the RNAi pathway. Accordingly, excessive amounts of siRNAs are able to reduce available endogenous Ago2 complexes, with large consequences on cellular and organismal homeostasis (Grimm and Kay, 2006; Börner et al., 2013). I therefore speculate that Ago2 levels are

similarly rate-limiting in Ncoa3-regulated processes, e.g. dendrite development. Since global loss of miRNAs (e.g. induced by Drosha knockdown) does not affect dendrite outgrowth, the Ncoa3-Ago2 pathway likely affects only a specific subset of miRNA-target interactions, in particular those involved in the negative control of dendrite growth. In the past, several miRNAs have been identified that negatively affect dendrite growth, e.g. miR-34a, miR-375, miR-137 and miR-181a (Abdelmohsen et al., 2010; Smrt et al., 2010; Agostini et al., 2011; Liu et al., 2013). Interestingly, the latter two were studied in the context of publications 1 and 2, where they were shown to regulate the translation of the AMPA-R subunits GluA1 and GluA2 respectively. However, both the GluA1 and GluA2 3'UTRs were unresponsive to Ncoa3 knockdown (data not shown). Two possibilities could help to explain this controversy. First, miR-137 and miR-181a could be loaded into Ago proteins other than Ago2, which would make them unresponsive to Ncoa3 manipulation. Although it was not assessed in primary neurons, Ago proteins exhibit only weak or no sorting preferences for particular miRNA sequences (Azuma-Mukai et al., 2008; Hafner et al., 2010). Furthermore, both miR-181a and miR-137 have been previously shown to associate with Ago2 in the mouse brain *in vivo* (Schaefer et al., 2010). Therefore, the absence of miR-137 and miR-181a from Ago2-containing miRISC unlikely explains the failure of Ncoa3 to regulate GluA1/2. Alternatively, a specific mechanism which guides particular miRNA-Ago complexes to target mRNAs dependent on their 3'UTR context could be involved. In agreement with this model, we observed that two different target mRNAs (HMGA2 and Lin-41) of the same miRNA (let-7) displayed a differential responsiveness to Ncoa3 knockdown. Moreover, reporters containing isolated miRNA-binding sites without 3'UTR context were not affected by Ncoa3 knockdown (Pub. 3: Fig. 3d, E3d and data not shown). To identify Ncoa3-Ago2-dependent miRNA-complexes that inhibit dendrite growth, a candidate approach could be chosen in which miRNA-target pairs with known functions in dendrite growth are analyzed for their dependency on Ncoa3, e.g. the miR-137/Mib1 interaction (Smrt et al., 2010). In addition, genome-wide Ago2 cross-linking immunoprecipitation (CLIP) experiments in wild-type and Ncoa3 knockdown neurons would represent a comprehensive and unbiased approach to identify Ncoa3-regulated Ago2 target mRNAs.

It should also be considered that Ago2 is not solely involved in miRISC function, but also plays an important role in controlling miRNA abundance by regulating the processing and stability of specific subsets of miRNAs (Diederichs and Haber, 2007; Cheloufi et al., 2010; Cifuentes et al., 2010). Profiling of miRNA expression by small RNA sequencing upon Ncoa3 knockdown could be used to systematically analyze a potential regulation of miRNA abundance by Ncoa3.

It is noteworthy that Ncoa3 knockdown results in additional phenotypes in mature neurons, such as a reduction in dendritic spine size and synaptic strength (Pub. 3: Fig. 7). These findings support a role of Ncoa3 in synapse physiology. At present, it is unclear if these phenotypes are similarly due to impaired miRNA function. If so, it will be important to identify the specific miRNA-target interactions regulated by Ncoa3 in the context of spine morphogenesis and synapse physiology.

Finally, our findings in neurons establish a link between Ncoa3 and the miRNA pathway that could have important implications in other biological systems. For instance Ncoa3 is widely studied in cancer where it positively influences hormone signaling and cell proliferation. Similarly, several miRNAs and miRNA pathway genes have been demonstrated to have oncogenic potential (Iorio and Croce, 2012). This raises the possibility that de-regulated miRNA activity might contribute to Ncoa3-dependent carcinogenesis. Therefore, a better understanding of how the Ncoa3-Ago2 pathway is regulated by nuclear hormones could provide important new insight into both neuronal plasticity (e.g. retinoic-acid induced homeostatic plasticity) (Aoto et al., 2008) and carcinogenesis (e.g. estrogen signaling in breast cancer) (Gojis et al., 2010).

4. Reprints of original publications

MCB Journals.ASM.org

Dopamine-Regulated MicroRNA MiR-181a Controls GluA2 Surface Expression in Hippocampal Neurons

Reuben Saba,[a*] Peter H. Störchel,[a,b] Ayla Aksoy-Aksel,[b] Frauke Kepura,[c] Giordano Lippi,[d*] Tim D. Plant,[c] and Gerhard M. Schratt[a,b]

Interdisziplinäres Zentrum für Neurowissenschaften, SFB488 Junior Group, Universität Heidelberg, and Institut für Neuroanatomie, Universitätsklinikum, Heidelberg, Heidelberg, Germany[a]; Biochemisch-Pharmakologisches Centrum Marburg, Institut für Physiologische Chemie, Philipps-Universität-Marburg, Marburg, Germany[b]; Biochemisch-Pharmakologisches Centrum Marburg, Pharmakologisches Institut, Philipps-Universität-Marburg, Marburg, Germany[c]; and MRC Toxicology Unit, University of Leicester, Leicester, United Kingdom[d]

The dynamic expression of AMPA-type glutamate receptors (AMPA-R) at synapses is a key determinant of synaptic plasticity, including neuroadaptations to drugs of abuse. Recently, microRNAs (miRNAs) have emerged as important posttranscriptional regulators of synaptic plasticity, but whether they target glutamate receptors to mediate this effect is not known. Here we used microarray screening to identify miRNAs that regulate synaptic plasticity within the nucleus accumbens, a brain region critical to forming drug-seeking habits. One of the miRNAs that showed a robust enrichment at medium spiny neuron synapses was miR-181a. Using bioinformatics tools, we detected a highly conserved miR-181a binding site within the mRNA encoding the GluA2 subunit of AMPA-Rs. Overexpression and knockdown of miR-181a in primary neurons demonstrated that this miRNA is a negative posttranscriptional regulator of GluA2 expression. Additionally, miR-181a overexpression reduced GluA2 surface expression, spine formation, and miniature excitatory postsynaptic current (mEPSC) frequency in hippocampal neurons, suggesting that miR-181a could regulate synaptic function. Moreover, miR-181a expression was induced by dopamine signaling in primary neurons, as well as by cocaine and amphetamines, in a mouse model of chronic drug treatment. Taken together, our results identify miR-181a as a key regulator of mammalian AMPA-type glutamate receptors, with potential implications for the regulation of drug-induced synaptic plasticity.

Addiction to drugs of abuse is considered a chronic neurological disease characterized by compulsive drug abuse regardless of the consequences to the individual's well-being. Most drugs of abuse share common modes of action on the brain's pathways related to motivation and reward (mesolimbic dopamine system) through the release of the neurotransmitter dopamine (13, 32). Altered dopamine signaling can lead to neuroadaptations at these sites that can manifest in an individual's decreased sensitivity and/or increased propensity for the abused drug. At the cellular level, neuroadaptations consist of functional changes in synaptic connectivity or strength, such as changes in the number and size of dendritic spines, analogous to the long-lasting modulations of synaptic plasticity during learning and memory (42, 62). A hallmark of synaptic plasticity is the differential trafficking and cell surface expression of alpha-amino-3-hydroxy-5-methyl-4-isoxazolepropionic acid receptor (AMPA-R) subunits (25, 37). Moreover, several studies have now identified alterations in synaptic AMPA-R levels as a possible mechanism by which drugs of abuse may elicit long-lasting neuroadaptations (65, 66). AMPA-R subunits (GluA1/2, formerly referred to as GluR1/2 or GluRA/B) are locally translated near synaptic sites in response to stimulation (23, 25, 26, 57). MicroRNAs (miRNAs), an abundant class of posttranscriptional gene regulatory molecules, are present in the vicinity of synapses, where they regulate the local expression of synaptic proteins (48). However, it is not known whether miRNAs are involved in regulating local protein synthesis of mammalian AMPA-R subunits in brain areas associated with addiction.

Recently, evidence for a role of miRNAs in the brain's reward circuitry has emerged. miRNAs have been implicated in mediating the effects of cocaine (8, 9, 18, 22), nicotine (19, 20), alcohol (41, 44), and several other classes of drugs of abuse (17, 33, 67). In the case of cocaine addiction in rats, the upregulation of miR-181a and the downregulation of two other miRNAs, let-7d and miR-124a, has been revealed in addiction-relevant regions of the brain (8). Extended access to the drug has been shown to increase the expression of striatal miR-212 (and the closely related miR-132), leading to downstream consequences on signaling pathways that ultimately decrease cocaine's motivational properties and provide protection against drug overconsumption (18, 22). Manipulating the alterations of miRNAs in the nucleus accumbens appears to be sufficient to either attenuate or enhance drug-seeking behavior (9, 18, 22). In general, it is possible that by targeting even a single miRNA, drugs of abuse may alter the expression levels of a number of downstream target genes that modulate addiction-related neuronal mechanisms.

In the present study, we pursued the following three main objectives: (i) to define the population of miRNAs enriched in the synaptodendritic compartment of a region critical to the mesolimbic dopamine pathway (nucleus accumbens), (ii) to identify physiological miRNA target mRNAs that are relevant to synaptic

Received 4 July 2011 **Returned for modification** 8 August 2011
Accepted 23 November 2011

Published ahead of print 5 December 2011

Address correspondence to Gerhard M. Schratt, gerhard.schratt@staff.uni-marburg.de.

* Present address: R. Saba, Molecular PathoBiology Program, Public Health Agency of Canada, Winnipeg, Manitoba, Canada; G. Lippi, Neurobiology Section, Division of Biological Sciences, University of California, San Diego, La Jolla, California, USA.

Supplemental material for this article may be found at http://mcb.asm.org/.

doi:10.1128/MCB.05896-11

plasticity, and (iii) to characterize the functional interaction between a synaptic miRNA and its target mRNA within the context of addiction to drugs of abuse. Our results indicate that the modulation of miR-181a, an miRNA strongly enriched in the synaptodendritic compartment of the nucleus accumbens, can regulate the glutamate receptor 2 subunit (GluA2) of AMPA-Rs at the posttranscriptional level. Since AMPA-R dynamics are vitally involved in synaptic plasticity, this regulation has the potential to impinge on the brain reward circuitry and therefore may play a putative role in addiction-related neuroplastic changes.

MATERIALS AND METHODS

Primary neuronal cell culture. Cultures of dissociated primary cortical and hippocampal neurons from embryonic day 18 (E18) Sprague-Dawley rats (Charles River Laboratories, Sulzfeld, Germany) were prepared and cultured as described previously by Schratt et al. (50).

Preparation of synaptoneurosomes. Synaptoneurosomes were prepared from the microdissected nucleus accumbens regions of strain P15 Sprague-Dawley rat pups as described previously by Rao and Steward (45), from three independent litters. Specifically, from a single rat litter consisting of 15 pups, 10 were used for the preparation of synaptoneurosomes whereas the remaining nucleus accumbens regions from the other pups of the litter were saved as whole tissue. Briefly, nucleus accumbens regions were microdissected in 50 ml of homogenization buffer (0.32 M sucrose, 0.1 mM EDTA, 0.25 mM dithiothreitol [DTT], 2 mM HEPES, pH 7.4) and disrupted with a Teflon-coated Dounce-Potter homogenizer (Wheaton) by eight up-and-down strokes. Nuclei and cell debris were pelleted by a 2-min centrifugation at 2,000 × *g*. The supernatant was centrifuged for an additional 10 min at 14,000 × *g* to pellet a crude synaptoneurosome-containing fraction. The fraction was subsequently layered over a 5 to 13% discontinuous Ficoll gradient that had been equilibrated at 4°C for 1 h. Synaptoneurosomes were collected from the gradient interface after centrifugation at 45,000 × *g* for 45 min at 4°C. Samples were obtained from every step of the procedure for Western blot analysis to ensure the quality and purity of the preparations.

Total RNA extraction and qRT-PCR. Total RNA (including small RNA fraction) was purified using either Qiazol (Qiagen) or the miRVana kit (Ambion) and treated with TURBO DNase (Ambion) to remove DNA contamination. Quantitative real-time PCR (qRT-PCR) was performed with a 7300 real time PCR system (Applied Biosystems) using TaqMan MicroRNA assays (Applied Biosystems) and iTaq SybrGreen Supermix with ROX (Bio-Rad) for the detection of miRNAs and mRNAs, respectively. Primers used for the detection of miRNA and mRNA targets are listed in Table S1 in the supplemental material. RT-PCR data were processed and analyzed using the comparative ΔC_T method (34). The ΔC_T values were then expressed relative to the control sample (defined for each experiment and set to 1) and the mean ± standard deviation (SD) calculated from the separate experiments performed ($n \geq 3$).

Microarray analysis. Total RNA (including small RNA fraction) was extracted from both the nucleus accumbens whole tissue and from synaptoneurosomes prepared from these tissues from P15 rat pups. The extracted RNA was either Cy3 (RNA from synaptoneurosomes) or Cy5 (RNA from whole tissue) labeled and hybridized to miRNA microarrays. Assays were performed using the service provider LC Sciences, LLC (Houston, TX). The microarrays (μParaflo microfluidic chip technology) contained multiple redundant probes for each *Rattus norvegicus* miRNA listed in Sanger miRBase release 13.0 (http://www.sanger.ac.uk/Software/Rfam/mirna/). Each detection probe consisted of a chemically modified nucleotide coding segment complementary to target miRNA or another RNA control sequence. The detection probes were made by *in situ* synthesis using photo-generated reagent chemistry. The hybridization melting temperatures were balanced, and hybridization images were collected using a laser scanner and subsequently digitized. Data were analyzed by first subtracting the background and then normalizing signals using a lowess filter (locally weighted regression) (5). Because we conducted two-color experiments, the ratio of the two sets of detected signals (log2 transformed) and *P* values of the *t* test were calculated for all three microarrays; differentially detected signals were those with $P < 0.01$. Samples with dye bias as indicated by the manufacturer were omitted from the analysis. To identify miRNAs that were the most significantly different in expression between the synaptoneurosomes and the whole tissue, a one-class significance analysis of microarrays (SAM analysis) with a false discovery rate (FDR) of <10% was used (64). To further increase the confidence level of our results, only those miRNAs that were consistently identified in all three arrays were used for SAM analysis.

Northern blot analysis. Northern blots to detect neuronal mature miRNAs and U6 snRNA were performed as described previously (49) with radiolabeled DNA oligonucleotides serving as detection probes. The same RNA that was extracted by Qiazol (Qiagen) for miRNA microarray analysis was used again for Northern blot analysis. The probe sequences are provided in Table S1 in the supplemental material. For molecular markers, the Decade Marker system (Ambion) was utilized.

Western blot analysis. Proteins were separated by SDS-PAGE and blotted onto a polyvinylidene difluoride (PVDF) membrane. Nonspecific bindings were blocked with Tris-buffered saline plus 5% milk powder and 0.2% Tween 20. The following primary antibodies were used: mouse anti-PSD95 (1:1,000; MA1-046; Dianova), mouse anti-EEA1 (1:10,000; 610456; Becton Dickinson), mouse anti-β-actin (A5441; Sigma), and rabbit anti-GluA2 (AB1768; Millipore). Primary antibodies were recognized by either a horseradish peroxidase (HRP)-conjugated goat anti-rabbit antibody (1:20,000; 401315; Calbiochem) or an HRP-conjugated rabbit anti-mouse antibody (1:20,000; 402335; Calbiochem). Secondary antibodies were detected by enhanced chemiluminescence with the ECL Plus Western blotting detection system (GE Healthcare). Sizes of resolved protein bands were determined using the precision protein dual color standard (Bio-Rad).

Transfections. Neuronal transfections were performed with Lipofectamine 2000 (Invitrogen). For each well of a 24-well plate, a total of 1 μg of DNA/RNA was mixed with a 1:50 dilution of Lipofectamine 2000 in neurobasal medium, incubated at room temperature (15 to 25°C) for 20 min, and then further diluted 1:5 in neurobasal medium. Neurons were incubated with the transfection mix for 2 h (4 h for small RNA transfections). Nucleofections were performed with the Rat Neuron Nucleofector kit (Lonza) and program O-003. Primary cortical neurons of rat embryos (E18) were nucleofected with 2 to 3 μg of total DNA per condition and plated on six-well dishes in DMEM-Glutamax containing 10% fetal bovine serum (FBS) (Invitrogen). After 4 h, medium was replaced with standard neuronal culture medium. For dual-luciferase assays, transfections were performed on cells at 5 days *in vitro* (5DIV cells) (for cortical cells) and on 13DIV cells (for hippocampal cells). Cell lysates were harvested at day 2 posttransfection for cortical cells and day 5 posttransfection for hippocampal cells. In total, 20 μl of cell lysates was then used for the dual-luciferase assay following the manufacturer's protocol for the dual-luciferase reporter assay system (Promega).

Immunostaining. For GluA2-surface staining, 18DIV neurons were incubated with 0.5 μg of mouse anti-GluA2 antibody (clone 6C4; Millipore) in 240 μl of growth medium for 1 h at 37°C (live staining). After this time, the coverslips were washed four times with ice-cold phosphate-buffered saline (PBS) and fixed with 4% paraformaldehyde-4% sucrose in PBS for 10 min at room temperature. Coverslips were subsequently washed five times with PBS for 5 min each time and washed once in 1 × GDB (30 mM phosphate buffer at pH 7.4, 0.5 M NaCl, 0.5% Triton X-100, 0.2% gelatin). Incubation with the secondary antibody was performed at room temperature using goat anti-mouse Alexa Red 546 diluted in 1 × GDB (1:1,000; 400 μl/well). Coverslips were then mounted after three rapid and three slow washes in PBS. For staining of permeabilized neurons, the cells were fixed for 15 min, incubated for 30 min with 1 × GDB, and subjected to immunostaining for GluA2 using primary and secondary antibodies as described above.

DNA constructs. The GluA2 3′ untranslated region (UTR) (full length) was amplified from a mouse brain cDNA library (C57BL/6) and subsequently cloned into the XbaI site of pGL3promoter vector (luciferase vector) (Promega). A version with a mutated miR-181a-binding site within the GluA2 3′ UTR (mutant GluA2-3′ UTR) was generated with the QuikChange site-directed mutagenesis kit (Stratagene) using overlapping PCR. Approximately 25 ng of this and *Renilla* luciferase plasmid was used per experiment. See Table S1 in the supplemental material for primer sequences.

Image analysis. For image analysis, hippocampal neurons were transfected at 13DIV with the indicated miRNAs and miRNA inhibitors in combination with an enhanced green fluorescent protein (eGFP) plasmid and processed for confocal microscopy at 18DIV. For spine analysis, high-resolution *z*-stack images of GFP-positive neurons were taken with a confocal laser scanning microscope (Zeiss). Random neurons displaying pyramidal morphology were chosen from data sets that had been blinded to the experimental conditions. Spine volumes were subsequently analyzed with the ImageJ software (50). At least nine individual neurons per experimental condition were measured in three or more independent experiments. For each of the experimental conditions, 100 to 150 spines per neuron were analyzed. The size of GluA2 surface clusters was determined with the Analyze Particle function of ImageJ, using threshold images taken of at least 12 neurons per condition. Particles smaller than 0.1 μm^2 were excluded from the analysis.

Chronic drug treatment in adult mice. Chronic drug treatments were performed as described by Ziviani et al. (68). In brief, male C57BL6 adult mice (Charles River) were treated with either saline, cocaine hydrochloride (10 mg/kg), or D-amphetamine-d_3 sulfate salt (5 mg/kg) via a single intraperitoneal injection once a day for 5 days. Animals were then sacrificed via rapid decapitation and brain regions dissected on ice for immediate RNA extraction.

miRNA target prediction. To determine the gene targets of the differentially expressed miRNAs, we used three of the leading miRNA target prediction algorithms: miRanda (http://microrna.sanger.ac.uk/sequences/) (24), PicTar (http://pictar.mdc-berlin.de/) (29), and TargetScan (http://www.targetscan.org/) (16). To determine genes that were similarly identified by two or more of these algorithms, the online program Matchminer (http://discover.nci.nih.gov/matchminer/index.jsp) was used (7).

Functional analysis of miRNA target genes. Functional analysis of miRNA target genes was performed using Ingenuity Pathways Analysis (IPA-Ingenuity Systems). This software analysis lists genes in the context of known biological response and regulatory networks as well as other higher-order response pathways. miRNA targets that were associated with biological functions in the Ingenuity Pathways Knowledge Base were used in the analysis. For all analyses, Fisher's exact test was used to calculate a *P* value determining the probability that each biological function assigned to that data set was due to chance alone.

Patch-clamp recordings and data analysis. Spontaneous miniature excitatory postsynaptic currents (mEPSCs) were recorded in the whole-cell voltage-clamp mode using an EPC-10 patch-clamp amplifier and PULSE software (HEKA Elektronik, Lambrecht, Germany) from cultured neurons at 17 to 19DIV visualized with a charge-coupled-device (CCD) camera (VX55, TILL Photonics GmbH, Gräfelfing, Germany) mounted on an upright microscope (BX51WI, Olympus, Hamburg, Germany). Coverslips with transfected cells were constantly superfused at room temperature with a bath solution containing 156 mM NaCl, 2 mM KCl, 2 mM $CaCl_2$, 1 mM $MgCl_2$, 16.5 mM glucose, and 10 mM HEPES (pH 7.3 with NaOH) to which gabazine (5 μM) and tetrodotoxin (0.5 μM) were added during recording. The pipette solution contained 110 mM $CsMeSO_3$, 25 mM CsCl, 30 mM HEPES, 2 mM $MgCl_2$, 0.362 mM $CaCl_2$, 1 mM EGTA, 4 mM MgATP, and 0.1 mM Na_2GTP (pH 7.2 with CsOH). Patch pipettes were pulled from borosilicate glass (Science Products, Hofheim, Germany) and had resistances of 3 to 5.5 MΩ when filled with the pipette solution. Neurons were held at a potential of −70 mV, and mEPSCs were analyzed from 100- to 300-s current recordings made after 10 min of equilibration in the whole-cell configuration. Experiments were performed blindly with respect to the transfection (miR-181a or control duplex RNA [control]). Data were acquired at a sampling rate of 20 kHz and filtered at 3 kHz. Series resistance was controlled every 5 min, and only experiments with uncompensated series resistances of <25 MΩ were accepted. Mean event amplitude and frequency were determined off-line with the Mini Analysis program (Synaptosoft Inc.) using an amplitude threshold of −5 pA. The statistical significance of results was tested by Student's two-tailed *t* test using GraphPad Prism 4 (GraphPad Software, San Diego, CA) and Microsoft Excel. *P* values of <0.05 were considered statistically significant.

Statistics. Experiments are reported as mean ± standard deviation (SD) (or standard error of the mean [SEM] for electrophysiology) and based on three or more independent replications. Significance was determined using Student's *t* test.

RESULTS

High-throughput screening for the identification of miRNAs enriched at nucleus accumbens synapses. In order to identify miRNAs with functional relevance in drug-induced synaptic plasticity, we chose to profile miRNAs from neurons of the nucleus accumbens, specifically with the emphasis on identifying miRNAs that are enriched within the synaptodendritic compartment. The nucleus accumbens is the primary site of action of most drugs of abuse, and it plays a key role in reward, motivation, and addiction, in response to the release of the neurotransmitter dopamine. To detect and identify miRNAs, the nucleus accumbens from both hemispheres of P15 rat brains were carefully microdissected and synaptoneurosomes were immediately prepared. Synaptoneurosomes are biochemical preparations that are highly enriched in synaptic membranes and also preserve most components of local protein synthesis machinery, including polyribosomes, mRNAs, and regulatory RNAs (such as miRNAs) (14, 45, 49, 50, 53). We confirmed the purity of the synaptoneurosome preparations by the enrichment and depletion of BC1 RNA and U6 snRNA, respectively. Furthermore, the nuclear and soma-resident protein EEA-1 was absent whereas the synaptic proteins PSD-95 and GluA2 were enriched (data not shown). We therefore went on to compare total RNA that was extracted from nucleus accumbens synaptoneurosomes with total RNA prepared from whole tissue by competitive hybridization to microarrays that contained probes for all *Rattus norvegicus* mature miRNAs listed in the Sanger miRBase release 13.0. In three independent microarray hybridizations, we identified 69 miRNAs that displayed differential expression in at least two hybridizations and 38 miRNAs that were differentially expressed in all three hybridizations ($P < 0.01$) (Fig. 1a). Of these 38 miRNAs, 20 miRNAs were found to be enriched in the synaptoneurosomes whereas 18 miRNAs were depleted (Fig. 1b) (see Table S2 in the supplemental material). Further stringent filtration of the data to include only those miRNAs with either ≥2-fold enrichment or ≥2-fold depletion from the synaptoneurosomes identified nine enriched miRNAs and seven depleted miRNAs (Table 1). Interestingly, there was almost no overlap between the miRNAs enriched in nucleus accumbens synaptoneurosomes and those previously identified in a screen of rat forebrain synaptoneurosomes (53), suggesting tissue-specific populations of synaptic miRNAs. Of the seven depleted miRNAs, however, four of them (miR-145, miR-126, miR-150, and miR-143) have also been previously documented to be depleted from forebrain synaptoneurosomes, implying a general absence of these miRNAs from the synaptodendritic compartment (see Table S2 in the supplemental material) (53).

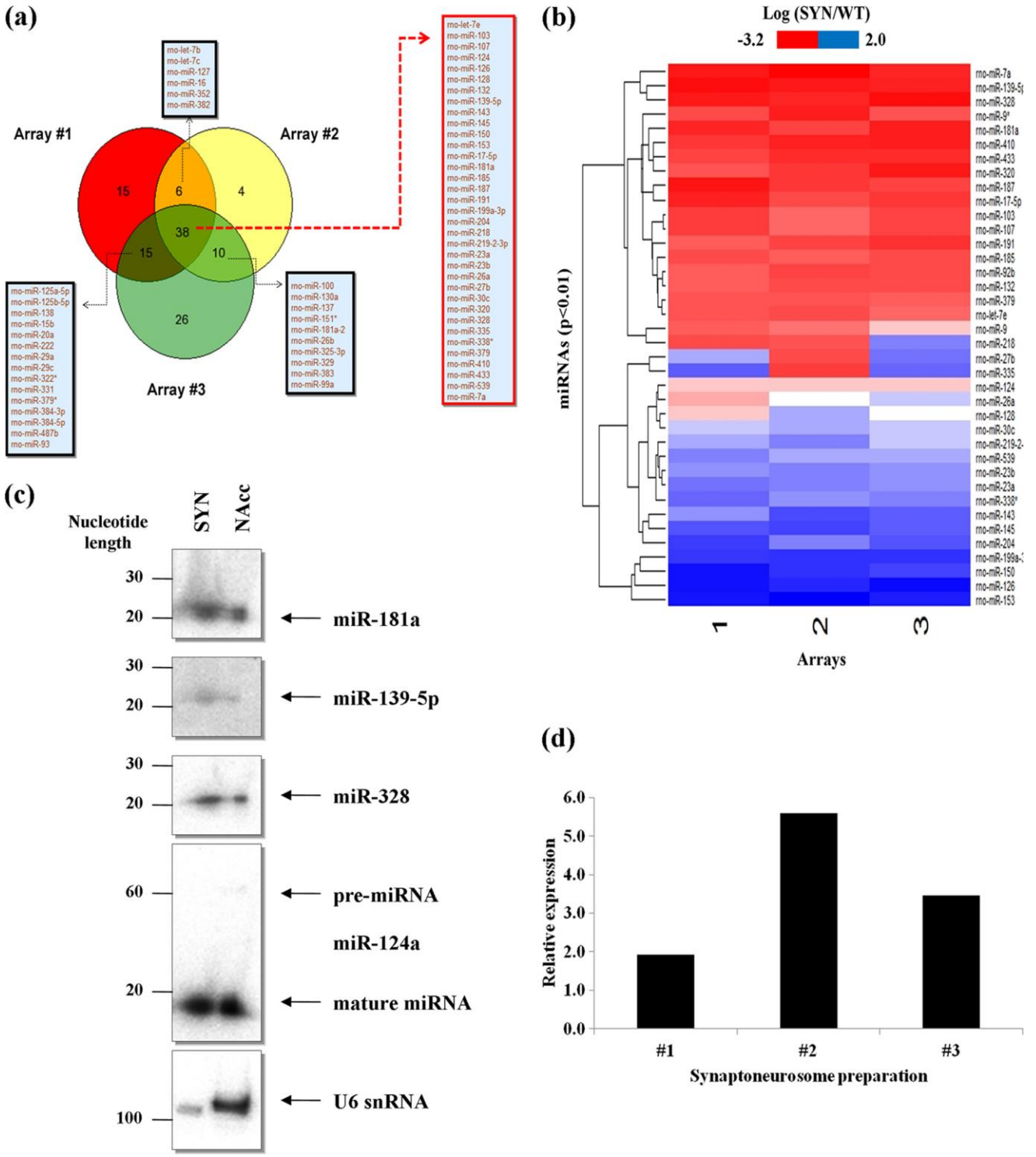

FIG 1 A subset of miRNAs are enriched at nucleus accumbens synapses. (a) miRNAs identified by microarray screening to be consistent between two or more arrays ($n = 3$; $P < 0.01$). Total RNA, including small RNA species, was extracted from synaptoneurosomes in three independent preparations and compared to total RNA prepared from whole tissue of the nucleus accumbens via competitive hybridization to microarrays ($n = 3$). miRNAs that are both enriched and depleted from synaptoneurosomes prepared from the nucleus accumbens region of P15 rats are shown. (b) Differential abundance of miRNAs in synaptoneurosomes. In three separate microarray hybridizations, we identified ~38 miRNAs that were consistently detected ($P < 0.01$). Refer to Table 1 for those miRNAs with ≥2-fold enrichment or depletion ($P < 0.01$) in the synaptoneurosomes. (c) Northern blot validation of miR-181a abundance in synaptoneurosomes (SYN) compared to that in whole tissue (NAcc). Also shown are the expression of miR-124a and U6 snRNA in the SYN and NAcc. Validation of two other miRNAs, miR-139-5p and miR-328, also found to be abundant in the synaptoneurosomes compared to whole tissue. Note the absence of pre-miR-124a from synaptoneurosomes. (d) qRT-PCR validation of miR-181a enrichment in synaptoneurosomes relative to whole tissue in three independent preparations. Data were normalized to the expression of miR-124a, which was equally distributed throughout the cell (Table 1 and Fig. 1c).

TABLE 1 miRNAs with ≥2-fold enrichment or depletion from synaptoneurosomes prepared from P15 rat nucleus accumbens region

miRNA in nucleus accumbens synaptoneurosomes[a]	Avg fold enrichment or depletion ± SD ($n = 3$)
Enriched miRNAs	
rno-miR-139-5p	3.12 ± 0.59
rno-miR-328	3.11 ± 0.76
rno-miR-410	2.41 ± 0.47
rno-miR-433	2.00 ± 0.32
rno-miR-7a	3.47 ± 1.36
rno-miR-181a	2.29 ± 0.55
rno-miR-17-5p	2.01 ± 0.51
rno-miR-187	2.24 ± 0.89
rno-miR-320	2.09 ± 0.75
Depleted miRNAs	
rno-miR-199a-3p	0.29 ± 0.02
rno-miR-145	0.40 ± 0.04
rno-miR-126	0.18 ± 0.05
rno-miR-153	0.17 ± 0.05
rno-miR-150	0.27 ± 0.10
rno-miR-204	0.44 ± 0.13
rno-miR-143	0.48 ± 0.13

[a] Enrichment or depletion of ≥2-fold; $P < 0.01$.

Validation of miR-181a enrichment in the synaptodendritic compartment of the nucleus accumbens. We next proceeded to validate the miRNAs identified in our microarray screen. In accordance with our microarray data, we found higher levels of three selected candidates (miR-139-5p, miR-328, and miR-181a) in total RNA prepared from the synaptoneurosomes compared to that in whole tissue by Northern blotting (Fig. 1c). Moreover, as expected, miR-124 was equally abundant in both the synaptoneurosome preparations and whole tissue, whereas U6 snRNA was strongly depleted from the synaptoneurosomes (Fig. 1c). Of the nine enriched miRNAs, miR-181a showed the highest relative abundance in the microarray screen (see Table S3 in the supplemental material). Additionally, miR-181a was previously found to be associated with Ago2 in the striatum (47), to be expressed in a somatodendritic gradient in hippocampal neurons (31), and to be induced by cocaine (8, 47) (see Table S2 in the supplemental material). Finally, virus-mediated overexpression of this miRNA in the rat nucleus accumbens was recently shown to enhance conditioned place preference (CPP) for cocaine (9). Due to this growing body of evidence in regard to a central role for miR-181a in the addiction process, we focused on this miRNA for further functional analysis. Quantitative RT-PCR (qRT-PCR) analysis of the three independent synaptoneurosome preparations showed a robust abundance of this miRNA, thus further confirming the microarray screen and Northern blot analysis (Fig. 1d). In summation, our results show that miR-181a is strongly enriched in the synaptodendritic compartment of the nucleus accumbens, suggesting that it might be involved in the local regulation of synaptic proteins at this site.

Computational prediction of a putative miR-181a target gene. To get insight into the biological function of miR-181a at the synapse, we went on to identify direct target genes of this miRNA. For this purpose, we used a consensus-based approach whereby we compared the target genes predicted by three of the leading target prediction algorithms (TargetScan, PicTar, MiRBase). Based on this integrative strategy, we identified 55 putative target genes of miR-181a that were common to all three algorithms (Fig. 2a) (see Table S4 in the supplemental material). Gene ontology (GO) assignment of these 55 target genes showed a strong enrichment for genes involved in neurological diseases, nervous system development and function, and cell-to-cell signaling and interaction (Fig. 2b) (see Table S5 in the supplemental material). A target gene that was common to all three programs and contained a highly conserved binding site for miR-181a, among several different mammalian species, was the gene encoding GluA2 (Fig. 2c).

The mRNA transcript encoding the GluA2 subunit of AMPA-Rs is a target gene of miR-181a. The GluA2 protein is an integral subunit of AMPA-R complexes that are highly abundant in the synaptodendritic compartment (data not shown). AMPA-Rs are postsynaptic ionotropic glutamate-gated ion channels that mediate the majority of the fast excitatory neurotransmission in the mammalian central nervous system in the process governing learning, memory and addiction-related behaviors. Interestingly, the AMPA-R subunits GluA1 and GluA2 appear to be locally translated near postsynaptic densities (23, 25, 26, 51, 57, 59, 60), suggesting that they could be subject to regulation by synaptic miRNAs (12, 35, 36, 48, 50, 53). A role for miRNAs in regulating postsynaptic glutamate receptors that show sequence similarities to mammalian AMPA-R genes (56) has recently been identified at the *Drosophila* neuromuscular junction (27), but whether such regulation occurs in vertebrates is not known. We therefore decided to study a potential functional miR-181a/GluA2 interaction in greater detail.

We used primary cortical and hippocampal cultures for our studies, since GABAergic medium spiny neurons of the nucleus accumbens lose dendritic spines upon prolonged *in vitro* culture due to the absence of excitatory input (58), thus making them an unsuitable system to study synaptic development *in vitro*. On the other hand, cortical and hippocampal neurons are widely used to study the mechanisms of plasticity in general and have also proven extremely useful in the context of drug-induced plasticity (15). Most importantly, stimulation of dopamine signaling in hippocampal neurons leads to the activation of D1 family receptors and localized protein synthesis of GluA1 (54). However, the effects of dopamine on GluA2 expression have not been studied.

To verify that the mRNA encoding the GluA2 subunit of AMPA-Rs is a genuine target gene of miR-181a, the full-length 3′ UTR of the transcript was cloned downstream of a luciferase gene in a reporter vector (Fig. 2c). The vector, along with miR-181a duplex, was then cotransfected into primary cortical neurons, and luciferase activity was monitored 48 h later. With increasing concentrations of miR-181a duplex (5→20 nM) there was a robust decrease in luciferase activity (Fig. 2d). Upon cotransfection with miR-134, an miRNA we had previously identified as being enriched in the synaptodendritic compartment of mature neurons (51) but which lacks a well-characterized binding site in the 3′ UTR of GluA2, there was no effect on luciferase activity even with increasing concentrations (5→20 nM) (Fig. 2d). Overall, these results suggest that the repression of luciferase activity in the cortical neurons was a specific effect of miR-181a overexpression.

We next tested whether the predicted miR-181a binding site located within the GluA2-3′ UTR (wild type) is responsible for miR-181a-mediated inhibition of reporter gene expression. Accordingly, point mutations were introduced into the wild-type GluA2-3′ UTR to abolish the predicted seed pairing of miR-181a

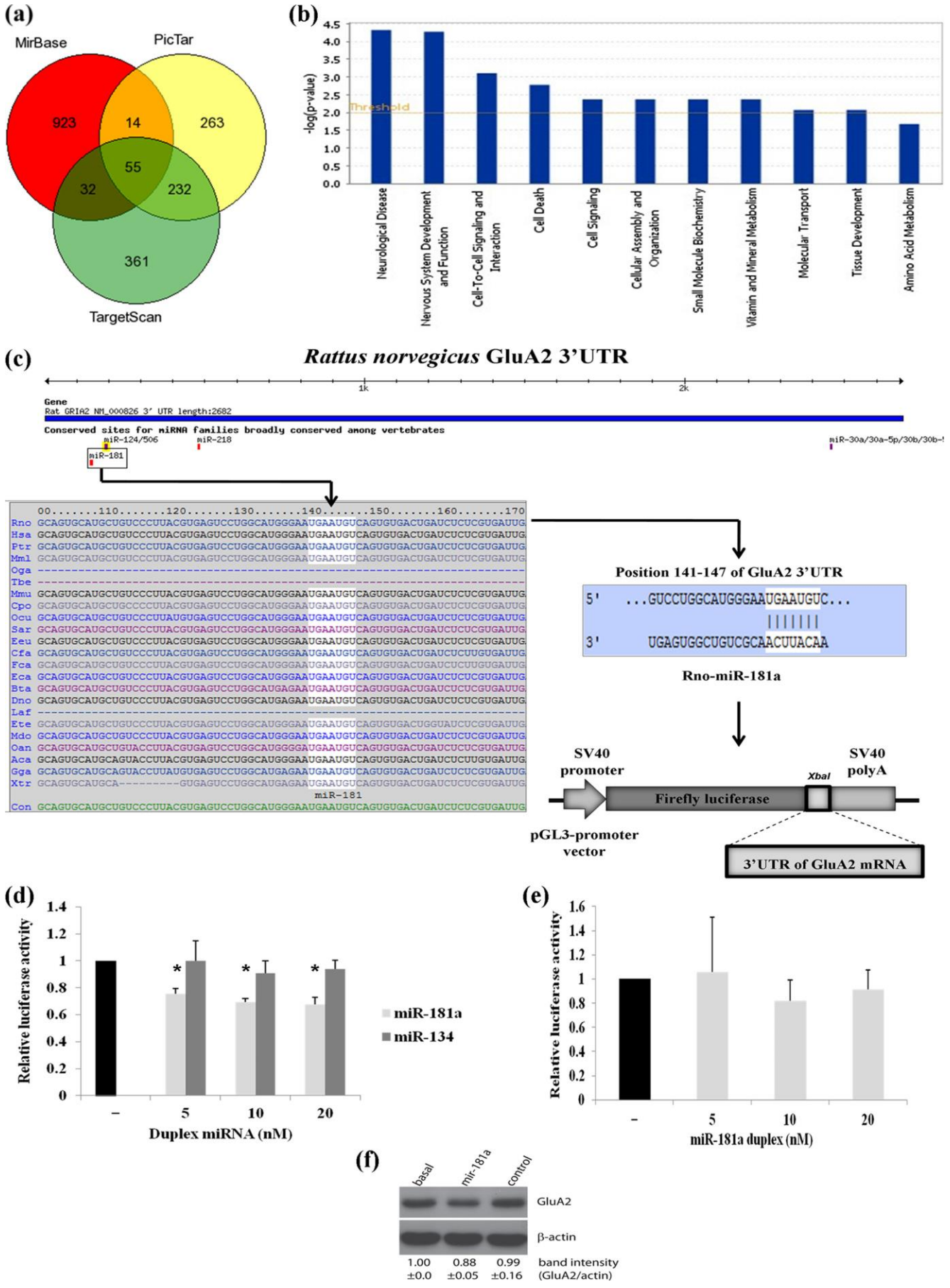
(a)
MirBase
PicTar
TargetScan
923
14
263
55
32
232
361
(b)
-log(p-value)
Threshold
Neurological Disease
Nervous System Development and Function
Cell-To-Cell Signaling and Interaction
Cell Death
Cell Signaling
Cellular Assembly and Organization
Small Molecule Biochemistry
Vitamin and Mineral Metabolism
Molecular Transport
Tissue Development
Amino Acid Metabolism
(c)
Rattus norvegicus GluA2 3'UTR
Gene
Rat GRIA2 NM_000826 3' UTR length:2682
Conserved sites for miRNA families broadly conserved among vertebrates
miR-124/506
miR-218
miR-181
miR-30a/30a-5p/30b/30b-
Rno
Hsa
Ptr
Mml
Oga
Tbe
Mmu
Cpo
Ocu
Sar
Eeu
Cfa
Fca
Eca
Bta
Dno
Laf
Ete
Mdo
Oan
Aca
Gga
Xtr
Con
miR-181
Position 141-147 of GluA2 3'UTR
5' ...GUCCUGGCAUGGGAAUGAAUGUC...
3' UGAGUGGCUGUCGCAACUUACAA
Rno-miR-181a
SV40 promoter
XbaI
SV40 polyA
Firefly luciferase
pGL3-promoter vector
3'UTR of GluA2 mRNA
(d)
Relative luciferase activity
miR-181a
miR-134
Duplex miRNA (nM)
(e)
Relative luciferase activity
miR-181a duplex (nM)
(f)
basal
mir-181a
control
GluA2
β-actin
1.00 ±0.0
0.88 ±0.05
0.99 ±0.16
band intensity (GluA2/actin)

to GluA2 mRNA (mutant GluA2-3′ UTR). Upon cotransfection of the resulting mutant, GluA2-3′ UTR, with increasing concentrations of miR-181a duplex (5→20 nM), there was no significant change in luciferase activity (Fig. 2e). These results suggest that the repressive effect of miR-181a on wild-type GluA2-3′ UTR is mediated via a single, highly conserved binding site (Fig. 2c). Western blotting using a GluA2-specific antibody confirmed that miR-181a overexpression in primary cortical neurons led to a slight but significant reduction (12% ± 5%) in the expression of total endogenous GluA2 protein levels in primary neurons (Fig. 2f).

The expression of endogenous miR-181a increases during the maturation of hippocampal neurons in cell culture (Fig. 3a). To test whether endogenous miR-181a regulates the translation of GluA2 mRNA in primary neurons, we decided to use antisense molecules that would effectively sequester endogenous miR-181a (so-called power locked nucleic acids [LNAs]; Exiqon). In an initial assessment by qRT-PCR, the anti-miR-181a molecules showed both a strong specificity and an efficacy for sequestering endogenous miR-181a (and other members of the miR-181 family that share a highly conserved seed sequence) without any effect on nonhomologous miRNAs, such as miR-124a (Fig. 3b). Upon cotransfection of the wild-type GluA2-3′ UTR luciferase reporter constructs into cortical neurons alongside anti-miR-181a molecules, there was a significant upregulation in luciferase activity. This activity increased with increasing concentrations of the anti-miR-181a LNA (5→25 nM) (Fig. 3c). Upon cotransfection with an LNA molecule of equal length but a scrambled sequence (scramble power LNA-A; 25 nM), no effect was observed on the activity of the luciferase construct (Fig. 3c). Moreover, the inhibitory function of endogenous miR-181a on the activity of the GluA2 reporter construct was dependent on the presence of an miR-181a binding site, since the mutant GluA2-3′ UTR construct was resistant to increasing amounts of anti-miR181a (5→25 nM) (Fig. 3d).

Next, we used nucleofection of anti-miR-181a (100 nM) into primary cortical neurons in order to measure changes in endogenous GluA2 mRNA and protein levels upon miR-181a inhibition. By nucleofection, it is possible to achieve ~80% transfection efficiency. In our experiments, we observed a modest but significant increase in GluA2 mRNA levels compared to those under control conditions (Fig. 3e). Additionally, equal concentrations of anti-miR-181a LNA and control LNA that were "spiked" in just prior to RNA extraction from the cortical cells had no effect on the expression level of GluA2 mRNA, eliminating the possibility that the observed increase was an artifact of altered qRT-PCR efficiency due to the presence of anti-miR-181a (data not shown). This suggests that at least part of the miR-181a-dependent repression of GluA2 expression (Fig. 3c) is due to GluA2 mRNA destabilization. We next measured the level of the GluA2 protein in response to the nucleofected anti-miR-181a (100 nM) by Western blotting. In this set of experiments, however, we could not detect significant differences in GluA2 protein levels between anti-miR-181a and control conditions (data not shown).

Taken together, these results identify GluA2 mRNA as a genuine target gene of miR-181a in primary rat neurons. Moreover, they further raise the possibility that miR-181a-mediated modulation of GluA2 expression could be involved in synaptic function.

miR-181a reduces AMPA-R surface clusters, spine volume, and mEPSC frequency in cultured hippocampal neurons. To address whether miR-181a-directed regulation of GluA2 has any consequence on AMPA-R function, we decided to monitor AMPA-R surface expression at synapses in primary hippocampal neurons. It was shown that the number of surface AMPA-R clusters correlates with the number of functional synapses, and the size of individual AMPA-R surface clusters is a good measure for postsynaptic strength (38). For this set of experiments, 13DIV hippocampal neurons were cotransfected with a vector expressing a green fluorescent protein (eGFP) together with either miR-181a duplex or a control duplex RNA of scrambled sequence. The eGFP allowed us to identify those AMPA-R clusters that were present on the dendrites of transfected neurons (Fig. 4a). Using immunocytochemistry (ICC) with an anti-GluA2-antibody on permeabilized hippocampal neurons at 18DIV, we could confirm miR-181a-mediated reduction in total GluA2 levels (Fig. 4b). The number and size of GluA2-containing surface AMPA-R clusters was subsequently measured by ICC on nonpermeabilized neurons (53). Using confocal microscopy, we found a decrease in the average size, but not in the density, of GluA2-containing AMPA-R surface clusters on dendrites of neurons transfected with miR-181a duplex compared to neurons transfected with control duplex RNA (Fig. 4a, c, and d). In accordance with the results obtained from Western blotting (data not shown), we were not able to detect a significant increase in GluA2-containing AMPA-R surface cluster size upon inhibition of miR-181a (data not shown). Additionally, we noticed that miR-181a overexpression significantly reduced dendritic spine volume and density in 18DIV hippocampal neurons in comparison to cells transfected with the control duplex (Fig. 4e and f), suggesting that this miRNA can also specifically interfere with dendritic spine morphogenesis.

Finally, we recorded mEPSCs from miR-181a overexpression neurons to detect any changes in basal synaptic transmission mediated primarily by AMPA-Rs (Fig. 5). In accordance with decreases in GluA2 surface expression and spine number and volume (Fig. 4), we observed a significant reduction in mEPSC frequency in miR-181a-overexpressing neurons compared to

FIG 2 GluA2 is a target of the synaptic miRNA miR-181a. (a) miR-181a target genes similarly predicted by three leading miRNA/target gene prediction algorithms. See Table S3 in the supplemental material for a list and detailed description of these genes. (b) Gene ontology (GO) assignment of the target genes predicted for miR-181a ($P = 0.01$). See Table S4 in the supplemental material for a list and detailed description of the GO classification. (c) The binding site for the seed sequence (nucleotides 2 to 8 from the 5′ end of the miRNA) of miR-181a in the 3′ UTR of GluA2 is highly conserved among several species. Binding site prediction information and degree of conservation in mammalian species obtained from TargetScan release 5.1. (d) Relative luciferase gene activity of a reporter vector harboring the 3′ UTR of GluA2 mRNA downstream of a luciferase gene in the presence of increasing concentrations of miR-181a or miR-134 duplex (5 to 20 nM). Cotransfection of miR-181a or miR-134 duplex, firefly luciferase reporter, and *Renilla* luciferase vector was performed on 5DIV cortical cells, and luciferase activity was measured at 7DIV. Bar plots show mean ± SD ($n = 4$). Significance was determined using Student's t test (*, $P < 0.001$). (e) Relative luciferase gene activity of a reporter vector harboring the mutant 3′ UTR of GluA2 mRNA downstream of a luciferase gene in the presence of increasing concentrations of miR-181a duplex (5 to 20 nM). Bar plots show mean ± SD ($n = 3$). (f) miR-181a expression reduces endogenous GluA2 protein levels in neurons. Primary cortical neurons (5DIV) were transfected with 50 nM the indicated duplex RNA and processed for Western blotting with anti-GluA2 and anti-ß-actin antibodies 2 days later. Results from one representative blot are shown. Quantification of the band intensities (normalized to the basal condition) from three independent blots ± SD is shown at the bottom.

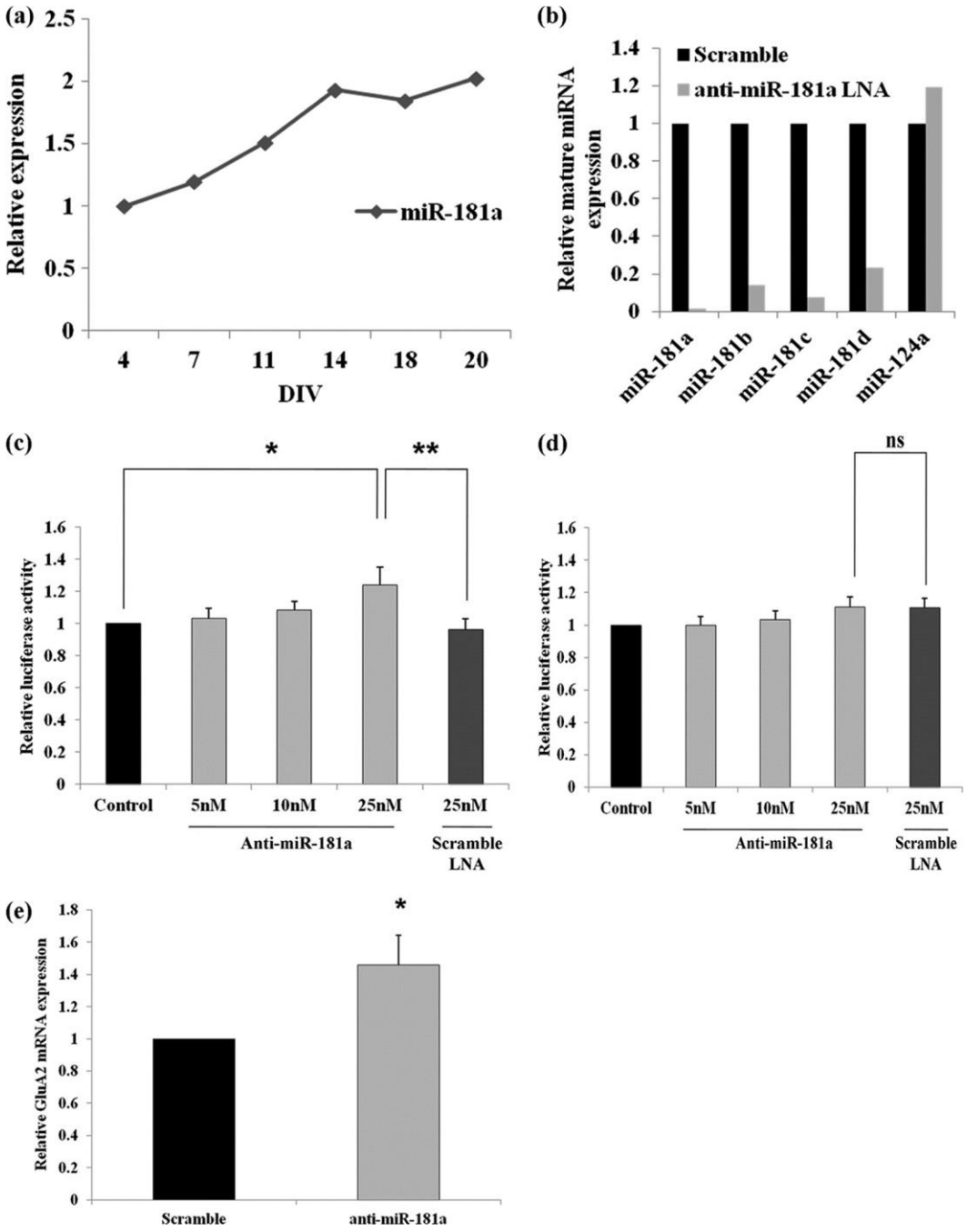

FIG 3 Endogenous miR-181a regulates a GluA2-3′ UTR reporter gene in neurons. (a) The expression of miR-181a in dissociated neuronal cell culture as measured by qRT-PCR. Data were normalized to the expression of U6 snRNA and are shown relative to expression level at 4DIV. (b) Effect of antisense-miR-181a LNA on endogenous miR-181a,-181b,-181c, and -181d levels. Data were normalized using U6 snRNA, and data are shown relative to equal amounts of scramble LNA that was nucleofected. The specificity of the miR-181a LNA on the expression of miR-124a is shown for comparison. (c) Luciferase gene activity in a reporter vector harboring the wild-type 3′ UTR of GluA2 mRNA downstream of a luciferase gene in the presence of increasing concentrations of miR-181a LNA (5 to 25 nM). Cotransfection of anti-miR-181a LNA or scramble LNA (25 nM) with firefly luciferase reporter and *Renilla* luciferase vector was performed on 5DIV cortical cells, and luciferase expression was measured at 7DIV. Data are shown relative to basal conditions for each type of plasmid transfected. Bar plots show mean ± SD ($n = 4$). Significance was determined using Student's *t* test (*, $P < 0.03$; **, $P < 0.005$). (d) Luciferase gene activity in a reporter vector harboring the mutant 3′ UTR of GluA2 mRNA downstream of a luciferase gene in the presence of increasing concentrations of miR-181a LNA (5 to 25 nM). (e) Change in endogenous GluA2 mRNA levels upon sequestration of endogenous miR-181a through the use of antisense molecules that target miR-181a. Change in mRNA levels was measured by qRT-PCR using GAPDH as the endogenous control, and data are shown relative to equal amounts of scrambled LNA that was nucleofected. Cortical cells were nucleofected with LNA at the time of plating, and mRNA levels were measured at 7DIV. Bar plots show mean ± SD ($n = 3$); *, $P < 0.03$.

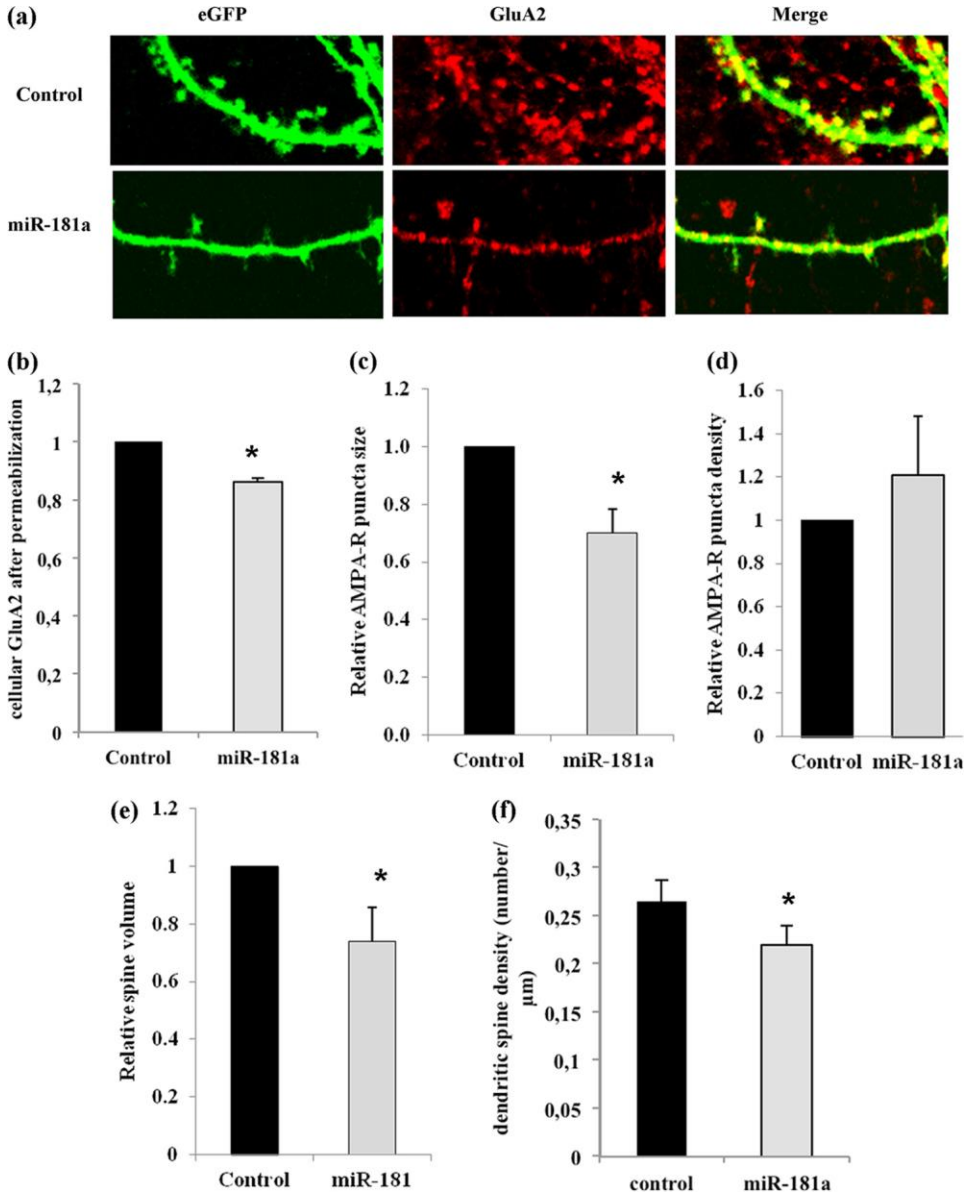

FIG 4 miR-181a reduces GluA2 surface expression and dendritic spine volume in hippocampal neurons. Primary rat hippocampal neurons were transfected with eGFP plasmid and either miR-181a duplex (25 nM) or scramble pre-miR (control, 25 nM) at 11DIV and processed for immunostaining at 18DIV. (a) Representative images of dendrites from transfected neurons stained with anti-GluA2 under nonpermeablizing conditions. (b) Quantification of anti-GluA2 immunostaining performed under permeabilizing conditions. Data are relative to control transfected cells. Bar graphs represent the mean ± SD ($n = 4$); *, $P < 0.05$ (Student's *t* test). (c) Quantification of anti-GluA2 immunostaining performed under nonpermeabilized conditions. Data are relative to control-transfected cells. Bar graphs represent the mean ± SD ($n = 4$). *, $P < 0.01$ (Student's *t* test). (d) Quantification of the average density (total number/cell area [μm^2]) of surface GluA2 clusters. Data are relative to control transfected cells. Bar graphs represent the mean ± SD ($n = 4$). (e) Quantification of the average spine volume (average mean eGFP intensity of individual spines/total intensity of whole cell) ($n = 4$; *, $P < 0.01$). (f) Quantification of the average spine density (total number of spines/dendritic length [μm]). Data are relative to control-transfected cells. Bar graphs represent the mean ± SD ($n = 4$; *, $P < 0.05$).

control transfected neurons (Fig. 5a to c). In contrast, miR-181a overexpression led to only a subtle reduction in the average mEPSC amplitude (Fig. 5d and e), which according to the cumulative probability plot appeared to be restricted mostly to events of larger amplitude (Fig. 5e). The potential mechanisms that could underlie these differential effects on frequency versus amplitude are highlighted in the discussion. Together, our results indicate that miR-181a might play a negative regulatory role in the expression of surface GluA2-containing AMPA-R, spine morphogenesis, and basal synaptic transmission, likely due to the inhibition of GluA2 mRNA translation and/or the promotion of GluA2 mRNA degradation at synapses.

Stimulation of dopamine signaling induces miR-181a expression in hippocampus neurons. The neurotransmitter dopamine has a central role in motivational control, as most drugs of abuse modulate dopamine signaling in order to elicit persistent structural and functional plasticity in neurons (28, 66). Therefore, we tested whether dopamine signaling would modulate the ex-

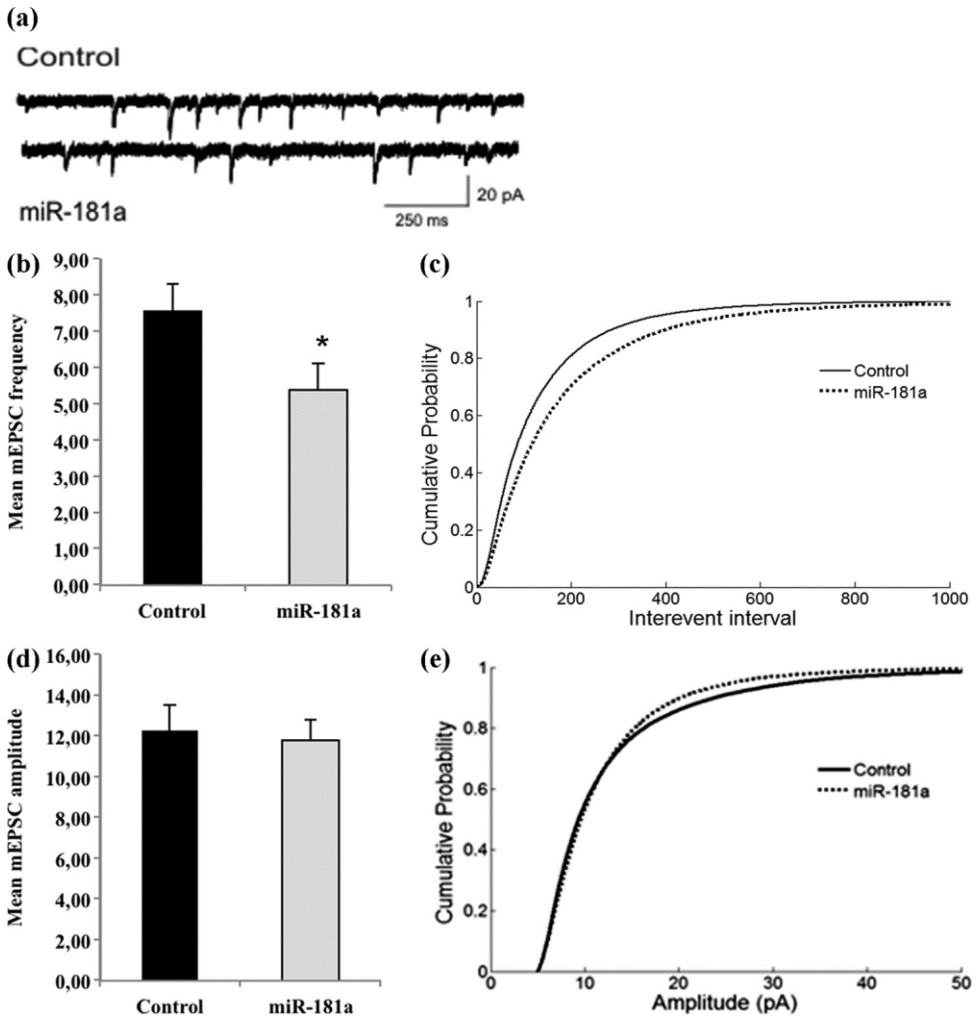

FIG 5 miR-181a reduces the frequency of mEPSCs in hippocampal neurons. Neurons were transfected as described for Fig. 4 and subjected to patch-clamp recordings between 17 and 19DIV. (a) Representative current traces from neurons transfected with either miR-181a or a control RNA. (b) Average mEPSC frequencies of neurons transfected either with miR-181a or a control RNA. $n = 13$ neurons per condition, originating from three independent transfections. $P < 0.05$. (c) Cumulative probability of interevent intervals from neurons analyzed in panel b. $n = 26224$ (control), 18285 (miR-181a). $P < 0.001$ by Kolmogorov-Smirnov (KS) test. (d) Average mEPSC amplitudes of events from neurons analyzed in panel b. $P = 0.78$. (e) Cumulative probability plot of amplitudes of events from neurons analyzed in panel b. $n = 26309$ (control), 18388 (miR-181a). $P < 0.001$ by KS test.

pression of miR-181a in dissociated hippocampal neurons that express endogenous dopamine receptors (15, 54). For this set of experiments, we simulated dopamine signaling through the bath application of D1/D5 dopamine receptor agonist SKF-38393 (52). When the expression of the mature miR-181a form was measured by qRT-PCR upon SKF-38393 treatment over a period of 4 h, maximum induction was observed after 1 h of treatment (Fig. 6a). Therefore, we used this time point for further studies. Upon stimulation with variable amounts of SKF-38393 (10 nM→100 μM), we observed maximum induction of miR-181a at 10 nM (Fig. 6b and data not shown). At this concentration, other miRNAs that were either enriched (miR-100 and miR-99a) (Fig. 1a) or equally distributed in synaptoneurosomes (miR-124a) (Fig. 1c) were not affected by agonist treatment (Fig. 6b), suggesting that dopamine signaling selectively activates miR-181a. Dopamine signaling was effectively induced as judged by the robust activation of the immediate-early genes Arc and c-Fos (Fig. 6c). Moreover, at 10 nM the agonist did not significantly activate the two potential miR-181a precursors, pre-miR-181a and -b, implying that the activation might involve a posttranscriptional regulation step (Fig. 6c). This is further supported by the presence of pre-miR-181a-2, and not the pre-miR-181a-1, in nucleus accumbens synaptoneurosomes as judged by microarray (Fig. 1a) (see Table S6 in the supplemental material). Taken together, these results suggest that the stimulation of dopamine signaling in hippocampus neurons leads to an increase in mature miR-181a, possibly due to increased pre-miR-181a processing.

We next examined whether the increased levels of miR-181a in response to dopamine agonist signaling affect GluA2 expression. For this experiment, either wild-type or mutant GluA2-3′ UTR fused to the luciferase gene was transfected into 13DIV hippocampal cells and treated with 10 nM SKF-38393 at 18DIV and luciferase activity was measured 24 h later. The agonist treatment led to a significant decrease in the activity of the wild-type, but not of the mutant, GluA2-3′ UTR construct (Fig. 6d). From this, it can be deduced that the induction of miR-181a by dopamine agonist

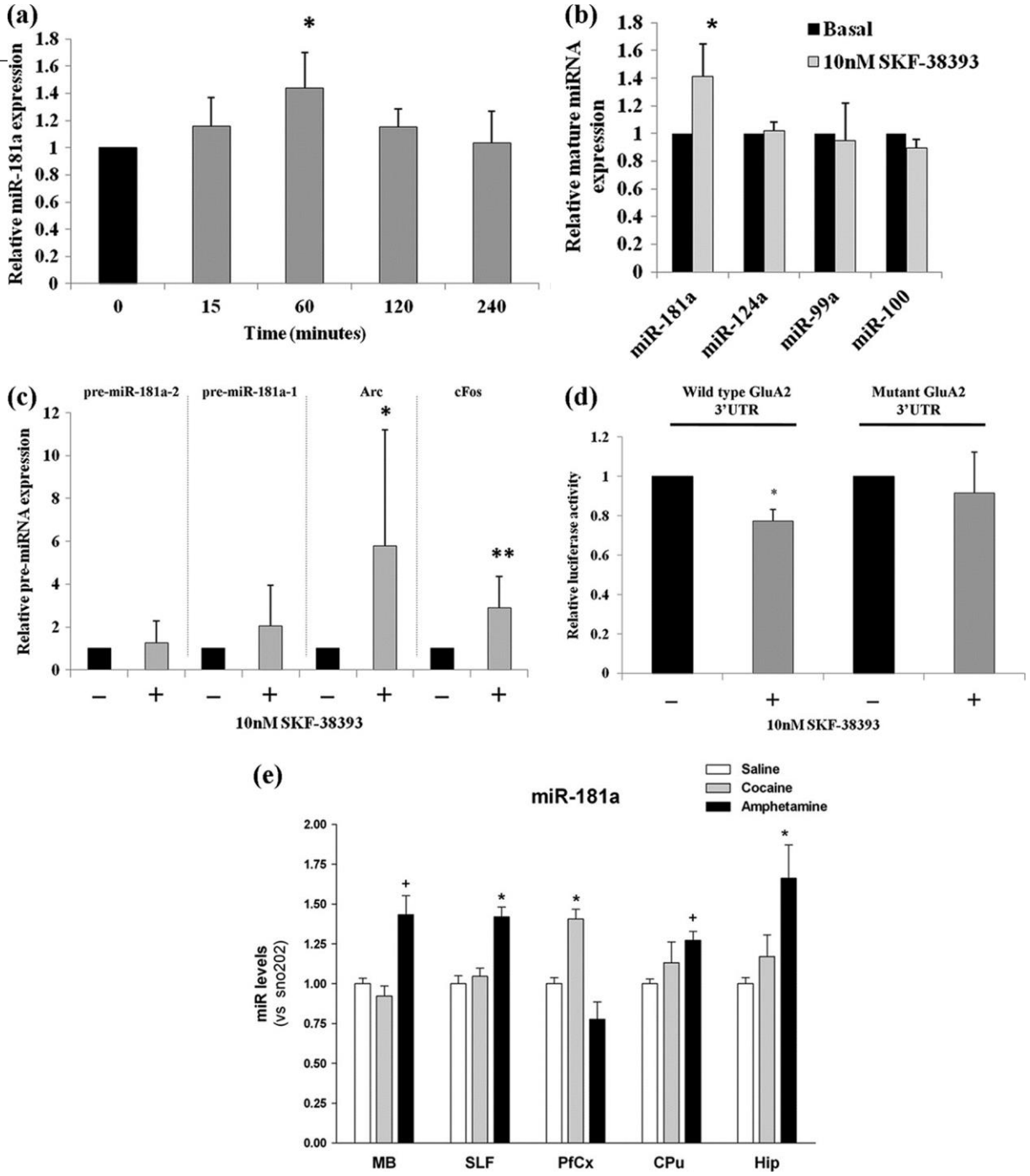

FIG 6 Dopamine agonist induces miR-181a expression in neurons. (a) Expression of mature miR-181a in hippocampal neuronal cells during dopamine treatment. 18DIV hippocampal neurons were treated with 10 nM SKF-38393 for 15 min to 4 h. At each time point, cells were washed and lysed and the expression of miR-181a was measured by qRT-PCR. Data are relative to mock-treated cells and are normalized to U6 snRNA. Bar plots show mean ± SD ($n = 3$); *, $P < 0.05$. (b) Expression of mature miR-181a in hippocampal neuronal cells in the presence of 10 nM SKF-38393. Also shown are the expressions of other miRNAs (miR-99a, miR-100, and miR-124a) at this concentration of the agonist. 18DIV hippocampal neurons were treated with 10 nM SKF-38393 for 1 h at 37°C. After 1 h of treatment, cells were washed and lysed and the expression of miR-181a was measured by qRT-PCR. Data are relative to mock-treated cells and are normalized to the expression of U6 snRNA. Bar plots show mean ± SD ($n = 3$). Significance was determined using Student's *t* test (*, $P < 0.009$). (c) Expression of pre-miR-181a-1, pre-miR-181a-2, Arc, and c-Fos transcripts in hippocampal neuronal cells in the presence of 10 nM SKF-38393. 18DIV hippocampal neurons were treated with 10 nM SKF-38393 for 1 h at 37°C. After 1 h of treatment, cells were washed and lysed and the expression of the transcripts was measured by qRT-PCR. Data are relative to mock-treated cells and are normalized to the expression of GAPDH mRNA. Bar plots show mean ± SD ($n = 5$). *, $P = 0.073$; **, $P < 0.05$. (d) Effect of dopamine agonist signaling on GluA2-3′ UTR luciferase construct activity (wild type or mutant), *in vitro*. Wild-type or mutant GluA2-3′ UTR luciferase construct was transfected into 13DIV hippocampal cells and treated with 10 nM SKF-38393 on 18DIV for 1 h at 37°C. After treatment, cells were washed and reincubated at 37°C for an additional 24 h, after which time the luciferase activity was measured. Data are shown relative to untreated cells transfected with either the wild-type or mutant construct, respectively. Bar plots show mean ± SD ($n = 5$ for wild-type construct; $n = 3$ for mutant construct); *, $P < 0.0002$. (e) Expression of miR-181a in various regions of the mouse brain in response to chronic treatment with psychotropic drugs. C57BL6 mice (four or five per group) were exposed to saline, cocaine (10 mg/kg), or amphetamine (5 mg/kg) for 5 days (1 injection/day) and sacrificed 4 h after the last injection. Total RNA (including small RNA species) was analyzed by qRT-PCR. Data were normalized to snoRNA 202, and data are shown relative to saline-treated mice. Hip, hippocampus; PFCx, prefrontal cortex; SLF, sublimbic forebrain, VMB, ventral midbrain. Bar plots show mean ± SD ($n = 4$ or 5 per group). *, $P < 0.05$; +, $0.1 > P > 0.05$.

signaling leads to the generation of functional miR-181a that is potentially capable of downregulating GluA2 expression.

Upregulation of miR-181a in chronically drug-treated mice. It is well established that chronic exposure to addictive psychotropic drugs can lead to neuroplastic changes in the brain (46, 63). Additionally, several recent studies have further demonstrated changes in miRNA abundance due to treatment with psychotropic drugs that are known to engage dopamine signaling (8, 9, 18, 22, 33). To monitor whether miR-181a expression is altered *in vivo* in response to chronic exposure to psychotropic drugs, C57BL/6 mice (four to five per group) were exposed to saline, cocaine (10 mg/kg), or amphetamine (5 mg/kg) for 5 days (1 injection/day) and sacrificed 4 h after the last injection. For each animal, the hippocampus, prefrontal cortex, sublimbic forebrain (nucleus accumbens region), and ventral midbrain were carefully microdissected and total RNA (including small RNA species) was extracted for the screening of miR-181a expression by qRT-PCR. Chronic drug exposure led to a significant induction of miR-181a expression in a drug-dependent and brain region-specific manner (Fig. 6e; data not shown for the induction of miR-181b and c). Of the two psychotropic drugs tested, amphetamine showed the most significant induction of miR-181a, which was observed in multiple regions of the brain, with the hippocampus showing the greatest degree of induction. In contrast, cocaine induced the expression of miR-181a most robustly in the prefrontal cortex. Taken together, these results demonstrate that drugs of abuse that are known to engage dopamine signaling potently induce miR-181a expression in relevant brain areas *in vivo*, notably the hippocampus and prefrontal cortex.

DISCUSSION

It is now well accepted that the intake of drugs of abuse can lead to fundamental changes in neuronal processes that regulate synaptic plasticity (46, 63). These changes can manifest in long-lasting neuroadaptations in several key regions of the mesolimbic dopamine system that may, in turn, contribute to behavioral changes characterized by altered processing of contextual information. However, the exact molecular mechanisms governing these neuroadaptations are far from clear and are the subject of intense scientific inquiry.

In this study, we explored the role of miRNAs in contributing to the neuroadaptations caused by drugs of abuse due to their extensive reach into gene-regulatory mechanisms in the brain, most notably their widespread role at synapses of the hippocampus and cortex (48, 50, 53). Moreover, several recent studies have now identified a role for miRNAs in the rewarding effects of a number of addictive drugs of abuse (8, 9, 18, 19, 20, 22, 33, 44). In our study, we identified a total of 20 miRNAs that were significantly enriched in nucleus accumbens synaptoneurosomes, with 9 of them showing ≥2-fold enrichment (Fig. 1a and 1b; Table 1). miR-181a, an miRNA that was previously implicated in immune function (10), displayed a particularly robust and reproducible enrichment in synaptoneurosomes as judged by both Northern blotting and qRT-PCR analysis (Fig. 1c and d). miR-181a was also identified to be associated with Ago2 in the striatum and induced by cocaine in Drd2-expressing neurons, suggesting a likely role in cocaine addiction (47). Additionally, a somatodendritic gradient has been shown for miR-181a with over 2-fold enrichment in dendritic regions, further corroborating the detection of this miRNA at synaptic sites (31). Interestingly, a significant number of other miRNAs from our screen were also identified to be associated with Ago2 in the striatum, were induced by cocaine in Drd2-expressing neurons, and possessed a somatodendritic gradient. miRNAs falling into each of these categories are summarized in Table S2 in the supplemental material. In addition to the validation of miR-181a, we also verified the enrichment of two other miRNAs, miR-139-5p and miR-328, in our synaptoneurosome preparations (Fig. 1c). Similarly to miR-181a, these two miRNAs were also previously found to be associated with striatal Ago2 and favor a somatodendritic gradient distribution (see Table S2). The functional characterizations of these miRNAs are under way in our lab.

Among the computationally predicted targets for miR-181a, there was an apparent bias toward genes involved in various brain functions (Fig. 2a and 2b; see Tables S4 and S5 in the supplemental material). One of the target genes that we specifically focused on was the transcript encoding the GluA2 subunit of AMPA-Rs (Fig. 2c). A potential interaction between miR-181 family member miR-181b and GluA2 was previously investigated within the context of schizophrenia, where miR-181b showed elevated levels in the gray matter of the superior temporal gyrus (4). However, this study used a glioblastoma cell culture model and did not address the functional consequences with regard to synapse morphology and physiology. In our work, we observed a specific reduction in GluA2 surface expression and mEPSC frequency upon miR-181a expression, demonstrating for the first time an important functional role for miR-181a at the synapse. The regulation of AMPA-Rs is of particular interest for understanding the molecular mechanisms contributing to neuroadaptations caused by drugs of abuse, and also for synaptic plasticity in general, since the expression and subunit composition of AMPA-Rs at synapses are critical determinants of excitatory synaptic strength (6, 61). Interestingly, reduced GluA2 surface expression upon miR-181a overexpression correlates with a significant reduction in mEPSC frequency (Fig. 5b and c). The effects on frequency are most easily explained by a reduction in functional postsynaptic specializations. Consistent with this, dendrites of miR-181a overexpressing neurons have fewer and smaller spines (Fig. 4e and f). Spine defects could be a direct consequence of decreased GluA2 surface expression, since GluA2 was shown to promote spine growth via its extracellular N-terminal domain (43). However, although we monitor synapse morphology and physiology exclusively in cells where miR-181a was expressed postsynaptically, we cannot formally rule out the possibility that changes in mEPSC frequency are due to a retrograde signal that alters presynaptic function (e.g., probability of vesicle release) of synaptically connected nontransfected neurons. Furthermore, presynaptic changes occurring in termini that synapse onto the neuron they originate from (so-called autapses) could account for frequency alterations. A detailed electrophysiological characterization will be required to distinguish between these various possibilities. Surprisingly, the reduction in mEPSC frequency was accompanied by only a very subtle reduction in amplitude (Fig. 5d and e). Perhaps miR-181a triggers a selective removal of GluA2 from a small subset of synapses that subsequently become silent, whereas the majority of synapses would preserve their GluA2 content and therefore keep their original strength (21). This could be important for synapse-specific modifications, for example during long-term depression (LTD).

Intriguingly, other GluA receptors (in particular GluA1) lack canonical miR-181a binding sites in their 3′ UTRs, suggesting that miR-181a selectively targets GluA2 for translational repression. Therefore, we speculate that miR-181a could also contribute to alterations in the subunit composition of AMPA-Rs by selectively

reducing the expression of GluA2 subunits. Specifically, miR-181a may block local synthesis of GluA2 but not of GluA1, possibly leading to an increase in calcium-permeable GluA2-lacking (Cp) AMPA-Rs at synapses. Cp-AMPA-Rs are transiently inserted into synapses during several forms of Hebbian and homeostatic plasticity (40), where they seem to play an important role in the induction phase of plasticity. A relative increase in Cp-AMPA-Rs upon miR-181a expression could also compensate for the loss of GluA2-containing AMPA-Rs, providing an additional explanation why we observed only subtle reductions of mEPSC amplitudes under these conditions (Fig. 5d and e).

In the context of addiction, drugs of abuse are known to influence AMPA-R assembly in order to provoke abnormal plasticity that contributes to reward-seeking behavior(s) (65, 66). For example, cocaine is known to alter postsynaptic AMPA-R components by promoting the exchange of GluA2-containing AMPA-Rs (i.e., GluA1/2 or GluA2/3 receptors) for GluA2-lacking AMPA-Rs (i.e., GluA1/1 or GluA1/3) (1, 3, 39). Furthermore, GluA2-lacking AMPA-Rs are required for drug-craving behavior following prolonged cocaine withdrawal (11). As such, the regulation of GluA2 expression by miR-181a could be part of a homeostatic plasticity mechanism in response to increased dopamine signaling. Indeed, we found that the expression of miR-181a (and other members of this family such as miR-181b and -c) is upregulated by dopamine signaling in cell culture (Fig. 6a to d) and by psychotropic drugs in mouse models of chronic drug addiction (Fig. 6e and data not shown for miR-181b and -c). Moreover, dopamine agonist treatment reduced the expression of the GluA2 reporter in an miR-181a binding site-dependent manner (Fig. 6d). Consistent with our results, Schuman and colleagues recently observed dopamine-dependent increases in local GluA1, but not GluA2, synthesis in dendrites of hippocampal neurons (54). Together, these results are consistent with the idea that aberrantly expressed miR-181a, in response to drugs of abuse/dopamine signaling, can lead to perturbation in AMPA-R subunit assembly by preferentially targeting the GluA2 subunit for posttranscriptional downregulation. In turn, this might contribute to some of the altered neuroadaptations associated with drug-afflicted areas of the brain. In this regard, it will be very interesting to test the potential involvement of miR-181a in drug-induced alterations in plasticity and behavior in animal models in future studies.

Since the 3′ UTR of mRNAs is usually targeted by multiple microRNAs (2), miR-181a is likely not the only posttranscriptional regulator of GluA2-expression. Interestingly, the highly conserved and exclusively neuronal miR-124 (30) also has a conserved binding site in the vicinity of the binding site for miR-181a (Fig. 2c). Moreover, miR-124 has also been shown to respond to cocaine treatment (downregulation) (8, 9), which might translate into increased expression of target gene(s), like GluA2. However, in our work, we found that miR-124 was not enriched at MSN synapses (Fig. 1c), and we did not see significant alterations in the expression pattern of this miRNA upon dopamine signaling (Fig. 6b). Clearly, more work is needed to elucidate the exact contribution of other posttranscriptional regulators, at the level of both miRNAs and RNA binding proteins (RBPs), in the regulation of GluA2 expression.

A finding from this work that needs more clarification is the mechanism by which miR-181a is induced in response to dopamine signaling in different brain areas. There are two possibilities by which this may occur: (i) increased transcriptional output of the gene encoding miR-181a or (ii) increased processing of miR-181a from its precursor molecule (pre-miRNA). In our study, we found some preliminary experimental support for the latter. Specifically, by microarray screening, we were able to detect one of the miR-181a precursors, pre-miR-181a-2 (but not pre-miR-181a-1) in the synaptoneurosomes prepared from the nucleus accumbens tissue (see Table S6 in the supplemental material). This could indicate synapto-dendritic transport and/or local processing of pre-miR-181a-2 in response to dopamine signaling. Consistent with this model, proteins of the miRNA processing machinery (e.g., Dicer, eIF2C2) have been found within the vicinity of dendrites close to synapses (35, 36).

Taken together, our work identifies mammalian AMPA-Rs as targets of neuronal miRNAs, with important implications for both physiological and pathological plasticity mechanisms. Furthermore, our results suggest that perturbations in the GluA2 subunit composition of AMPA-Rs in response to drug-induced expression of the nucleus accumbens-enriched miRNA miR-181a may lead to maladaptive changes in synaptic transmission and plasticity in brain regions critical to the drug reward pathway. miR-181a could therefore represent a novel and promising target for therapeutic intervention in situations of excessive dopamine signaling, including but not limited to drug abuse.

ACKNOWLEDGMENTS

We gratefully acknowledge the excellent technical assistance of Tatjana Wüst. We thank Roberto Fiore for cloning the GluA2-3′ UTR. We also thank Roberto Fiore and Sharof Khudayberdiev for critical reading of the manuscript.

This work was supported by the Deutsche Forschungsgemeinschaft (SFB488 to G.M.S.), the Human Frontier Science Program (Career Development Award to G.M.S.), and the National Institute on Drug Abuse (1R21DA025102-01 to G.M.S.). G.M.S. is an EMBO Young Investigator.

We declare that we have no conflict of interest.

REFERENCES

1. **Argilli E, Sibley DR, Malenka RC, England PM, Bonci A.** 2008. Mechanism and time course of cocaine-induced long-term potentiation in the ventral tegmental area. J. Neurosci. 28:9092–9100.
2. **Bartel DP.** 2004. MicroRNAs: genomics, biogenesis, mechanism, and function. Cell 116:281–297.
3. **Bellone C, Luscher C.** 2006. Cocaine triggered AMPA receptor redistribution is reversed in vivo by mGluR-dependent long-term depression. Nat. Neurosci. 9:636–641.
4. **Beveridge NJ, et al.** 2008. Dysregulation of miRNA 181b in the temporal cortex in schizophrenia. Hum. Mol. Genet. 17:1156–1168.
5. **Bolstad BM, Irizarry RA, Astrand M, Speed TP.** 2003. A comparison of normalization methods for high density oligonucleotide array data based on variance and bias. Bioinformatics 19:185–193.
6. **Burnashev N, Monyer H, Seeburg PH, Sakmann B.** 1992. Divalent ion permeability of AMPA receptor channels is dominated by the edited form of a single subunit. Neuron 8:189–198.
7. **Bussey KJ, et al.** 2003. MatchMiner: a tool for batch navigation among gene and gene product identifiers. Genome Biol. 4:R27.
8. **Chandrasekar V, Dreyer JL.** 2009. microRNAs miR-124, let-7d and miR-181a regulate cocaine-induced plasticity. Mol. Cell. Neurosci. 42:350–362.
9. **Chandrasekar V, Dreyer JL.** 2011. Regulation of MiR-124, Let-7d, and MiR-181a in the accumbens affects the expression, extinction, and reinstatement of cocaine-induced conditioned place preference. Neuropsychopharmacology 36:1149–1164.
10. **Chen CZ, Li L, Lodish HF, Bartel DP.** 2004. MicroRNAs modulate hematopoietic lineage differentiation. Science 303:83–86.
11. **Conrad KL, et al.** 2008. Formation of accumbens GluR2-lacking AMPA receptors mediates incubation of cocaine craving. Nature 454:118–121.
12. **Cougot N, et al.** 2008. Dendrites of mammalian neurons contain special-

ized P-body-like structures that respond to neuronal activation. J. Neurosci. 28:13793–13804.
13. Di Chiara G. 2002. Nucleus accumbens shell and core dopamine: differential role in behavior and addiction. Behav. Brain Res. 137:75–114.
14. Fiore R, et al. 2009. Mef2-mediated transcription of the miR379-410 cluster regulates activity-dependent dendritogenesis by fine-tuning Pumilio2 protein levels. EMBO J. 28:697–710.
15. Gao C, Sun X, Wolf ME. 2006. Activation of D1 dopamine receptors increases surface expression of AMPA receptors and facilitates their synaptic incorporation in cultured hippocampal neurons. J. Neurochem. 98: 1664–1677.
16. Grimson A, et al. 2007. MicroRNA targeting specificity in mammals: determinants beyond seed pairing. Mol. Cell 27:91–105.
17. He Y, Yang C, Kirkmire CM, Wang ZJ. 2010. Regulation of opioid tolerance by let-7 family microRNA targeting the mu opioid receptor. J. Neurosci. 30:10251–10258.
18. Hollander JA, et al. 2010. Striatal microRNA controls cocaine intake through CREB signalling. Nature 466:197–202.
19. Huang W, Li MD. 2009. Differential allelic expression of dopamine D1 receptor gene (DRD1) is modulated by microRNA miR-504. Biol. Psychiatry 65:702–705.
20. Huang W, Li MD. 2009. Nicotine modulates expression of miR-140*, which targets the 3′-untranslated region of dynamin 1 gene (Dnm1). Int. J. Neuropsychopharmacol. 12:537–546.
21. Huang YH, et al. 2009. In vivo cocaine experience generates silent synapses. Neuron 63:40–47.
22. Im HI, Hollander JA, Bali P, Kenny PJ. 2010. MeCP2 controls BDNF expression and cocaine intake through homeostatic interactions with microRNA-212. Nat. Neurosci. 13:1120–1127.
23. Job C, Eberwine J. 2001. Localization and translation of mRNA in dendrites and axons. Nat. Rev. Neurosci. 2:889–898.
24. John B, et al. 2004. Human MicroRNA targets. PLoS Biol. 2:e363.
25. Ju W, et al. 2004. Activity-dependent regulation of dendritic synthesis and trafficking of AMPA receptors. Nat. Neurosci. 7:244–253.
26. Kacharmina JE, Job C, Crino P, Eberwine J. 2000. Stimulation of glutamate receptor protein synthesis and membrane insertion within isolated neuronal dendrites. Proc. Natl. Acad. Sci. U. S. A. 97:11545–11550.
27. Karr J, et al. 2009. Regulation of glutamate receptor subunit availability by microRNAs. J. Cell Biol. 185:685–697.
28. Kauer JA, Malenka RC. 2007. Synaptic plasticity and addiction. Nat. Rev. Neurosci. 8:844–858.
29. Krek A, et al. 2005. Combinatorial microRNA target predictions. Nat. Genet. 37:495–500.
30. Krichevsky AM, King KS, Donahue CP, Khrapko K, Kosik KS. 2003. A microRNA array reveals extensive regulation of microRNAs during brain development. RNA 9:1274–1281.
31. Kye MJ, et al. 2007. Somatodendritic microRNAs identified by laser capture and multiplex RT-PCR. RNA 13:1224–1234.
32. Le Moal M, Simon H. 1991. Mesocorticolimbic dopaminergic network: functional and regulatory roles. Physiol. Rev. 71:155–234.
33. Lippi G, et al. 2011. Targeting of the Arpc3 actin nucleation factor by microRNA-29a/b regulates dendritic spine morphology. J. Cell Biol. 194: 889–904.
34. Livak KJ, Schmittgen TD. 2001. Analysis of relative gene expression data using real-time quantitative PCR and the 2(-Delta Delta C(T)) method. Methods 25:402–408.
35. Lugli G, Larson J, Martone ME, Jones Y, Smalheiser NR. 2005. Dicer and eIF2c are enriched at postsynaptic densities in adult mouse brain and are modified by neuronal activity in a calpain-dependent manner. J. Neurochem. 94:896–905.
36. Lugli G, Torvik VI, Larson J, Smalheiser NR. 2008. Expression of microRNAs and their precursors in synaptic fractions of adult mouse forebrain. J. Neurochem. 106:650–661.
37. Luscher C, et al. 1999. Role of AMPA receptor cycling in synaptic transmission and plasticity. Neuron 24:649–658.
38. Malenka RC, Nicoll RA. 1999. Long-term potentiation—a decade of progress? Science 285:1870–1874.
39. Mameli M, Bellone C, Brown MT, Luscher C. 2011. Cocaine inverts rules for synaptic plasticity of glutamate transmission in the ventral tegmental area. Nat. Neurosci. 14:414–416.
40. Man HY. 2011. GluA2-lacking, calcium-permeable AMPA receptors—inducers of plasticity? Curr. Opin. Neurobiol. 21:291–298.
41. Miranda RC, et al. 2010. MicroRNAs: master regulators of ethanol abuse and toxicity? Alcohol. Clin. Exp. Res. 34:575–587.
42. Nestler EJ. 2001. Molecular neurobiology of addiction. Am. J. Addict. 10:201–217.
43. Passafaro M, Nakagawa T, Sala C, Sheng M. 2003. Induction of dendritic spines by an extracellular domain of AMPA receptor subunit GluR2. Nature 424:677–681.
44. Pietrzykowski AZ, et al. 2008. Posttranscriptional regulation of BK channel splice variant stability by miR-9 underlies neuroadaptation to alcohol. Neuron 59:274–287.
45. Rao A, Steward O. 1991. Evidence that protein constituents of postsynaptic membrane specializations are locally synthesized: analysis of proteins synthesized within synaptosomes. J. Neurosci. 11:2881–2895.
46. Robinson TE, Kolb B. 2004. Structural plasticity associated with exposure to drugs of abuse. Neuropharmacology 47(Suppl. 1):33–46.
47. Schaefer A, et al. 2010. Argonaute 2 in dopamine 2 receptor-expressing neurons regulates cocaine addiction. J. Exp. Med. 207:1843–1851.
48. Schratt G. 2009. microRNAs at the synapse. Nat. Rev. Neurosci. 10:842–849.
49. Schratt GM, Nigh EA, Chen WG, Hu L, Greenberg ME. 2004. BDNF regulates the translation of a select group of mRNAs by a mammalian target of rapamycin-phosphatidylinositol 3-kinase-dependent pathway during neuronal development. J. Neurosci. 24:7366–7377.
50. Schratt GM, et al. 2006. A brain-specific microRNA regulates dendritic spine development. Nature 439:283–289.
51. Schuman EM, Dynes JL, Steward O. 2006. Synaptic regulation of translation of dendritic mRNAs. J. Neurosci. 26:7143–7146.
52. Sibley DR, Leff SE, Creese I. 1982. Interactions of novel dopaminergic ligands with D-1 and D-2 dopamine receptors. Life Sci. 31:637–645.
53. Siegel G, et al. 2009. A functional screen implicates microRNA-138-dependent regulation of the depalmitoylation enzyme APT1 in dendritic spine morphogenesis. Nat. Cell Biol. 11:705–716.
54. Smith WB, Starck SR, Roberts RW, Schuman EM. 2005. Dopaminergic stimulation of local protein synthesis enhances surface expression of GluR1 and synaptic transmission in hippocampal neurons. Neuron 45: 765–779.
55. Reference deleted.
56. Sprengel R, et al. 2001. Glutamate receptor channel signatures. Trends Pharmacol. Sci. 22:7–10.
57. Steward O, Schuman EM. 2001. Protein synthesis at synaptic sites on dendrites. Annu. Rev. Neurosci. 24:299–325.
58. Sun X, Wolf ME. 2009. Nucleus accumbens neurons exhibit synaptic scaling that is occluded by repeated dopamine pre-exposure. Eur. J. Neurosci. 30:539–550.
59. Sutton MA, Schuman EM. 2005. Local translational control in dendrites and its role in long-term synaptic plasticity. J. Neurobiol. 64:116–131.
60. Sutton MA, Wall NR, Aakalu GN, Schuman EM. 2004. Regulation of dendritic protein synthesis by miniature synaptic events. Science 304: 1979–1983.
61. Swanson GT, Kamboj SK, Cull-Candy SG. 1997. Single-channel properties of recombinant AMPA receptors depend on RNA editing, splice variation, and subunit composition. J. Neurosci. 17:58–69.
62. Tada T, Sheng M. 2006. Molecular mechanisms of dendritic spine morphogenesis. Curr. Opin. Neurobiol. 16:95–101.
63. Tang J, Dani JA. 2009. Dopamine enables in vivo synaptic plasticity associated with the addictive drug nicotine. Neuron. 63:673–682.
64. Tusher VG, Tibshirani R, Chu G. 2001. Significance analysis of microarrays applied to the ionizing radiation response. Proc. Natl. Acad. Sci. U. S. A. 98:5116–5121.
65. Wolf ME. 2010. The Bermuda Triangle of cocaine-induced neuroadaptations. Trends Neurosci. 33:391–398.
66. Wolf ME, Mangiavacchi S, Sun X. 2003. Mechanisms by which dopamine receptors may influence synaptic plasticity. Ann. N. Y. Acad. Sci. 1003:241–249.
67. Zhou R, et al. 2009. Evidence for selective microRNAs and their effectors as common long-term targets for the actions of mood stabilizers. Neuropsychopharmacology 34:1395–1405.
68. Ziviani E, et al. 2011. Ryanodine receptor-2 upregulation and nicotine-mediated plasticity. EMBO J. 30:194–204.

Supplemental Table 1. **List of primers and probes used in the study.**

Experimental procedure	Targets in *Rattus novergicus*	Applied Biosystems (AB) Assay ID	Custom primers or probe sequences (5'-3')
qRT-PCR (miRNA)			
	Hsa-miR-181a	000480	-
	Hsa-miR-181b	001098	-
	Hsa-miR-181c	000482	-
	Hsa-miR-181d	001099	-
	Mmu-miR-124a	001182	-
	Hsa-miR-99a	000435	-
	Hsa-miR-100	000437	-
	U6 snRNA	001973	-
	SnoRNA 202	001232	-
qRT-PCR (pre-miRNAs, mRNA)			
	Pre-miR-181a-1	-	F: AACATTCAACGCTGTCGGTGAGT; R: GGTACAATCAACGGTCGATGGT
	Pre-miR-181a-2	-	F: AACATTCAACGCTGTCGGTGAG; R: TACAGTCAACGGTTGGTGGT
	cFos	-	F: CATCATCTAGGCCCAGTGGC; R: AGGAACCAGACAGGTCCACATCT
	Arc	-	F: ACCGTCCCCTCCTCTCTTGA; R:TCTTTGTAATCCTATTTTCTCTGCCTT
	Beta-3-tubulin	-	F: CCCCAGGGCTCAAGATGTC; R: CGCTTGAACAGCTCCTGGAT
	Gapdh	-	F: GCCTTCTCTTGTGACAAAGTGGA; R: CCGTGGGTAGAGTCATACTGGAA
Northern Blot			
	Rno-miR-181a	-	ACTCACCGACAGCGTTGAATGTT
	Rno-miR-139-5p	-	CTGGAGACACGTGCACTGTAGA
	Rno-miR-328	-	ACGGAAGGGCAGAGAGGGCCAG
	Rno-miR-124a	-	TGGCATTCACCGCGTGCCAATT
	U6 snRNA	-	GCAGGGGCCATGCTAATCTTCTCTGTATCG
Transfection (miRNA over-expression)[a]			
	miR-181a sense	-	5'Phospho-AACAUUCAACGCUGUCGGUGAGU

	miR-181a anti-sense	-	5'Phospho-UCACCGGCAGCGUUGGGUGUUCC
	miR-134 sense	-	5'Phospho-UGUGACUGGUUGACCAGAGGGA
	miR-134 anti-sense	-	5'Phospho-CCUCUGGUCAACCAGUUAUACU
	Scramble Pre-miR	-	Proprietary sequence of Ambion
Transfection (miRNA knock down)[b]			
	Hsa-miR-181a	-	ACTCACCGACAGCGTTGAATG
	Negative control A	-	Proprietary sequence of Exiqon
Cloning primers			
	GluA2-3'UTR	-	F: CTAGTACAGGAAGTACTGGAGAAAA; R: TCTGAAGGTTTCACAACACTCTGAA
Mutagenesis primers			
	miR-181a seed sequence binding site in GluA2	-	F:GAGTCCTGGCATGGGAATCAGTGTGACTGATC; R:GATCAGTCACACTGATTCCCATGCCAGGACTC

a. Oligonucleotides were annealed to form duplex RNA with 2 nucleotide long, 3' overhangs.
b. LNA modified oligonucleotides (power LNAs from Exiqon – PN 426850-00).

Supplemental Table 2. The 38 miRNAs consistently identified in the microarray experiments ($p<0.01$; n=3).

miRNAs enriched or depleted in nucleus accumbens synaptoneurosomes (p<0.01)	Average Fold enrichment ± SD (n=3)	SAM score rank[a]	Ago2-dependent in striatum[b]	Cocaine-induced in Drd2 expressing neurons[b]	Abundance in neurites relative to cell body[c]	Reported to be depleted from syn[d]
Enriched miRNAs						
rno-miR-139-5p	3.12 ± 0.59	8.08	+		+	
rno-miR-328	3.11 ± 0.76	6.38	+		+	
rno-miR-410	2.41 ± 0.47	5.70	+			
rno-miR-433	2.00 ± 0.32	5.22	+		+	
rno-miR-379	1.40 ± 0.08	5.03				
rno-miR-132	1.47 ± 0.12	4.83			+	
rno-miR-185	1.46 ± 0.11	4.82	+		+	
rno-miR-7a	3.47 ± 1.36	4.73	+	+		
rno-miR-181a	2.29 ± 0.55	4.53	+	+	+	
rno-miR-92b	1.53 ± 0.16	4.38				
rno-miR-17-5p	2.01 ± 0.51	3.84				
rno-let-7e	1.38 ± 0.15	3.28			+	
rno-miR-191	1.64 ± 0.34	3.16			+	
rno-miR-187	2.24 ± 0.89	3.06	+			
rno-miR-320	2.09 ± 0.75	2.96	+			
rno-miR-103	1.56 ± 0.31	2.87	+		+	
rno-miR-107	1.52 ± 0.31	2.58	+			
rno-miR-9*	1.19 ± 0.10	2.40				
rno-miR-9	1.92 ± 0.78	0.41			+	
rno-miR-218	1.06 ± 0.36	0.15	+			
Depleted miRNAs						
rno-miR-199a-3p	0.29 ± 0.02	19.56				
rno-miR-145	0.40 ± 0.04	9.54				+
rno-miR-126	0.18 ± 0.05	9.47				+
rno-miR-153	0.17 ± 0.05	7.98				
rno-miR-23b	0.59 ± 0.04	7.71	+		+	
rno-miR-23a	0.57 ± 0.05	7.08			+	
rno-miR-338*	0.55 ± 0.07	5.74	+			
rno-miR-539	0.61 ± 0.06	5.65	+			
rno-miR-30c	0.69 ± 0.04	5.50			+	
rno-miR-150	0.27 ± 0.10	4.87				+
rno-miR-124	0.84 ± 0.01	4.56				
rno-miR-219-2-3p	0.64 ± 0.07	4.55	+			

rno-miR-204	0.44 ± 0.13	4.27	+			
rno-miR-143	0.48 ± 0.13	4.09				+
rno-miR-128	0.74 ± 0.07	3.39	+		+	
rno-miR-26a	0.79 ± 0.10	2.38			+	
rno-miR-335	0.88 ± 0.73	0.72				
rno-miR-27b	0.89 ± 0.53	0.62			+	

MiRNAs with ≥2-fold enrichment are highlighted in the table
a. MiRNAs were ranked based on Significance Analysis of Microarrays (SAM) score. SAM is a high-throughput t-test specific for microarrays; higher the score, higher the significance (64).
b. Reference 47
c. Reference 31
d. Reference 53

Supplemental Table 3. The relative abundance of enriched (≥2-fold) miRNAs in synaptoneurosomes ($p<0.01$; n=3).

miRNAs enriched (≥2-fold) in NAcc synaptoneurosomes (p<0.01)	**Average relative abundance of enriched miRNAs ± SD**
Enriched miRNAs	
rno-miR-139-5p	4783 ± 1184
rno-miR-328	548 ± 133
rno-miR-410	752 ± 39
rno-miR-433	4122 ± 798
rno-miR-7a	4743 ± 373
rno-miR-181a	9191 ± 1527
rno-miR-17-5p	1699 ± 260
rno-miR-187	973 ± 413
rno-miR-320	2879 ± 206

Supplemental Table 4. A detailed description of miR-181a target genes similarly predicted by all three of the miRNA/target gene algorithms employed.

Symbol	Entrez Gene Name	Location	Type(s)
ACSL1	acyl-CoA synthetase long-chain family member 1	Cytoplasm	enzyme
ACVR2A	activin A receptor, type IIA	Plasma Membrane	kinase
ARSJ	arylsulfatase family, member J	Extracellular Space	enzyme
B4GALT1	UDP-Gal:betaGlcNAc beta 1,4-galactosyltransferase, polypeptide 1	Cytoplasm	enzyme
BACH2	BTB and CNC homology 1, basic leucine zipper transcription factor 2	Nucleus	transcription regulator
CARD11	caspase recruitment domain family, member 11	Cytoplasm	kinase
CBX7	chromobox homolog 7	Nucleus	other
CD4	CD4 molecule	Plasma Membrane	transmembrane receptor
CNTN4	contactin 4	Plasma Membrane	enzyme
CPD	carboxypeptidase D	Extracellular Space	peptidase
CTDSPL	CTD (carboxy-terminal domain, RNA polymerase II, polypeptide A) small phosphatase-like	Nucleus	other
E2F7	E2F transcription factor 7	Nucleus	transcription regulator
EED	embryonic ectoderm development	Nucleus	transcription regulator
EIF4A2	eukaryotic translation initiation factor 4A2	Cytoplasm	translation regulator
EPC2	enhancer of polycomb homolog 2 (Drosophila)	unknown	other
FNDC3A	fibronectin type III domain containing 3A	Cytoplasm	other
FOS	FBJ murine osteosarcoma viral oncogene homolog	Nucleus	transcription regulator
GOLGA1	golgin A1	Cytoplasm	other
GLUA2	glutamate receptor, ionotropic, AMPA 2	Plasma Membrane	ion channel
GRM5	glutamate receptor, metabotropic 5	Plasma Membrane	G-protein coupled receptor
IL1A	interleukin 1, alpha	Extracellular Space	cytokine
KLF6	Kruppel-like factor 6	Nucleus	transcription regulator
KLHL5	kelch-like 5 (Drosophila)	unknown	other
KPNB1	karyopherin (importin) beta 1	Nucleus	transporter
LBR	lamin B receptor	Nucleus	enzyme
LRRC8D	leucine rich repeat containing 8 family, member D	Plasma Membrane	G-protein coupled receptor
MAMDC2	MAM domain containing 2	Extracellular Space	other
MAP3K10	mitogen-activated protein kinase kinase kinase 10	Cytoplasm	kinase
MMP14	matrix metallopeptidase 14 (membrane-inserted)	Extracellular Space	peptidase
NPTXR	neuronal pentraxin receptor	Plasma Membrane	transmembrane receptor
NR6A1	nuclear receptor subfamily 6, group A, member 1	Nucleus	ligand-dependent nuclear receptor
OSBPL3	oxysterol binding protein-like 3	Cytoplasm	other
PAK4	p21 protein (Cdc42/Rac)-activated kinase 4	Cytoplasm	kinase
PBX3	pre-B-cell leukemia homeobox 3	Nucleus	transcription regulator
PI4K2B	phosphatidylinositol 4-kinase type 2 beta	Cytoplasm	kinase

PIAS3	protein inhibitor of activated STAT, 3	Nucleus	transcription regulator
PLCL2	phospholipase C-like 2	Cytoplasm	enzyme
PLEKHJ1	pleckstrin homology domain containing, family J member 1	unknown	other
PPP1R12B	protein phosphatase 1, regulatory (inhibitor) subunit 12B	Cytoplasm	phosphatase
PRKCD	protein kinase C, delta	Cytoplasm	kinase
RAB11FIP2	RAB11 family interacting protein 2 (class I)	Cytoplasm	other
RAN	RAN, member RAS oncogene family	Nucleus	enzyme
RGMA	RGM domain family, member A	Plasma Membrane	other
SCHIP1	schwannomin interacting protein 1	Cytoplasm	other
SEMA4C	sema domain, immunoglobulin domain (Ig), transmembrane domain (TM) and short cytoplasmic domain, (semaphorin) 4C	Plasma Membrane	other
SLITRK1	SLIT and NTRK-like family, member 1	unknown	other
SOX6	SRY (sex determining region Y)-box 6	Nucleus	transcription regulator
TARDBP	TAR DNA binding protein	Nucleus	transcription regulator
TIMP3	TIMP metallopeptidase inhibitor 3	Extracellular Space	other
TOM1L1	target of myb1 (chicken)-like 1	Cytoplasm	other
UBP1	upstream binding protein 1 (LBP-1a)	Cytoplasm	transcription regulator
YWHAG	tyrosine 3-monooxygenase/tryptophan 5-monooxygenase activation protein, gamma polypeptide	Cytoplasm	other
ZC3H6	zinc finger CCCH-type containing 6	unknown	other
ZDHHC7	zinc finger, DHHC-type containing 7	Cytoplasm	enzyme
ZIC2	Zic family member 2 (odd-paired homolog, Drosophila)	Nucleus	transcription regulator

Supplemental Table 5. A detailed description of the gene ontology assignments of the target genes predicted for miR-181a.

Category	p-value	Molecules
Neurological Disease	4.78E-05-2.75E-02	GRM5, FOS, TIMP3, RAN, **GLUA2**, EIF4A2
Nervous System Development and Function	5.36E-05-4.61E-02	GRM5, FOS, ZIC2, **GLUA2**
Cell-To-Cell Signaling and Interaction	7.88E-04-4.61E-02	GRM5, FOS, **GLUA2**
Cell Death	1.68E-03-4.2E-02	GRM5, FOS, CD4, TARDBP, **GLUA2**
Cell Signaling	4.28E-03-2.54E-02	GRM5, **GLUA2**
Cellular Assembly and Organization	4.28E-03-4.28E-03	FOS, TARDBP
Small Molecule Biochemistry	4.28E-03-2.12E-02	GRM5, FOS
Vitamin and Mineral Metabolism	4.28E-03-2.54E-02	GRM5, **GLUA2**
Molecular Transport	8.53E-03-2.12E-02	FOS, **GLUA2**
Tissue Development	8.53E-03-8.53E-03	ZIC2
Amino Acid Metabolism	2.12E-02-2.12E-02	FOS

Supplemental Table 6. Detection of pre-miR-181a-2 in synaptoneurosome preparations by microarray screening.

Array	Pre-miRNA form[a,b]	Average relative abundance (n=8 spot replicates)		Fold enrichment in SYN (p<0.01)	SYN/NAcc whole tissue (Cy3/Cy5)[c]
		SYN(Cy3-labelled)	NAcc Whole tissue (Cy5-labeleld)		
#1	pre-miR-181a-1	nd	nd	-	-
	pre-miR-181a-2	265.76	262.91	ns	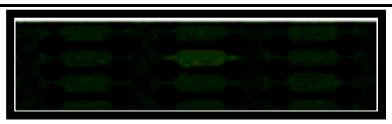
#2	pre-miR-181a-1	nd	nd	-	-
	pre-miR-181a-2	3998.22	2522.13	1.59	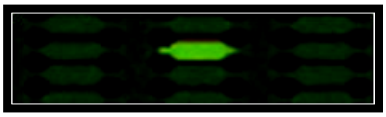
#3	pre-miR-181a-1	nd	nd	-	-
	pre-miR-181a-2	5700.88	2222.43	2.55	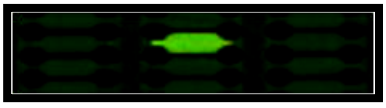

a. and **b.** Custom microarray detection probes were designed for pre-miR-181a-1 and pre-miR-181a-2 loop regions based on pre-miRNA stem-loop structures found in Sanger miRBase Release 13.0 based on accession numbers MI0000953 and MI0000925, respectively.
c. Representative regions of microarray images are shown.

Report

Cell Reports

MicroRNA-137 Controls AMPA-Receptor-Mediated Transmission and mGluR-Dependent LTD

Graphical Abstract

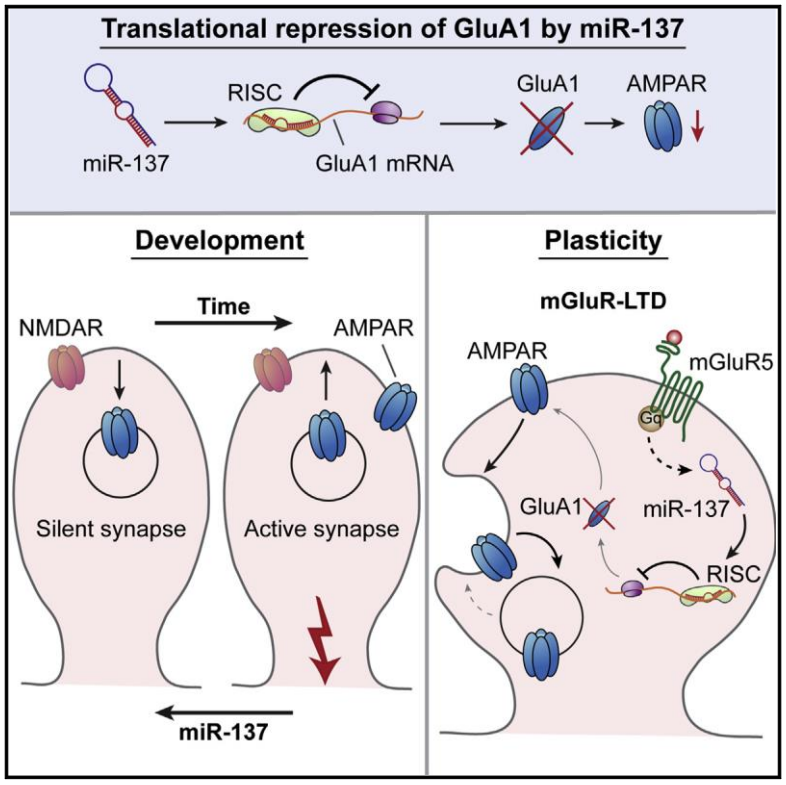

Authors

Nikkie F.M. Olde Loohuis, Wei Ba, Peter H. Stoerchel, ..., Hans van Bokhoven, Nael Nadif Kasri, Armaz Aschrafi

Correspondence

n.nadif@donders.ru.nl (N.N.K.), a.aschrafi@donders.ru.nl (A.A.)

In Brief

Olde Loohuis et al. reveal that microRNA miR-137, which is associated with intellectual disability and schizophrenia, controls AMPA-receptor-mediated transmission by targeting AMPA receptor subunit GluA1. miR-137 levels are regulated by mGluR5 activation, and, consequently, acute interference with miR-137 function impedes mGluR5-dependent synaptic plasticity.

Highlights

- AMPA receptor subunit GluA1 is a direct target of miR-137
- miR-137 represses AMPA-receptor-mediated synaptic transmission
- miR-137 is required for mGluR5-mediated long-term depression

OPEN ACCESS
CellPress

Cell Reports
Report

MicroRNA-137 Controls AMPA-Receptor-Mediated Transmission and mGluR-Dependent LTD

Nikkie F.M. Olde Loohuis,[1,5] Wei Ba,[4,5] Peter H. Stoerchel,[6] Aron Kos,[1,5] Amanda Jager,[1,5] Gerhard Schratt,[6] Gerard J.M. Martens,[3,5] Hans van Bokhoven,[1,4,5] Nael Nadif Kasri,[1,4,5,7,*] and Armaz Aschrafi[2,5,7,*]
[1]Department of Cognitive Neuroscience, Radboudumc, 6500 HB Nijmegen, the Netherlands
[2]Department of Neuroinformatics, Radboud University Nijmegen, 6525 HP Nijmegen, the Netherlands
[3]Department of Molecular Animal Physiology, Radboud University Nijmegen, 6525 HP Nijmegen, the Netherlands
[4]Department of Human Genetics, Radboudumc, 6500 HB Nijmegen, the Netherlands
[5]Donders Institute for Brain, Cognition, and Behaviour, Centre for Neuroscience, 6525 AJ Nijmegen, the Netherlands
[6]Institute of Physiological Chemistry, Biochemical-Pharmacological Center Marburg, Philipps University Marburg, 35032 Marburg, Germany
[7]Co-senior author
*Correspondence: n.nadif@donders.ru.nl (N.N.K.), a.aschrafi@donders.ru.nl (A.A.)
http://dx.doi.org/10.1016/j.celrep.2015.05.040

SUMMARY

Mutations affecting the levels of microRNA miR-137 are associated with intellectual disability and schizophrenia. However, the pathophysiological role of miR-137 remains poorly understood. Here, we describe a highly conserved miR-137-binding site within the mRNA encoding the GluA1 subunit of AMPA-type glutamate receptors (AMPARs) and confirm that GluA1 is a direct target of miR-137. Postsynaptic downregulation of miR-137 at the CA3-CA1 hippocampal synapse selectively enhances AMPAR-mediated synaptic transmission and converts silent synapses to active synapses. Conversely, miR-137 overexpression selectively reduces AMPAR-mediated synaptic transmission and silences active synapses. In addition, we find that miR-137 is transiently upregulated in response to metabotropic glutamate receptor 5 (mGluR5), but not mGluR1 activation. Consequently, acute interference with miR-137 function impedes mGluR-LTD expression. Our findings suggest that miR-137 is a key factor in the control of synaptic efficacy and mGluR-dependent synaptic plasticity, supporting the notion that glutamatergic dysfunction contributes to the pathogenesis of miR-137-linked cognitive impairments.

INTRODUCTION

Learning and memory processes rely on activity-dependent changes in synaptic strength. A fundamental mechanism for the modification of synaptic strength is the insertion or removal of alpha-amino-3-hydroxy-5-methyl-4-isoxazole propionic acid receptors (AMPARs) at the postsynaptic membrane (Bassani et al., 2013; Citri and Malenka, 2008; Huganir and Nicoll, 2013). Long-term potentiation (LTP) and long-term depression (LTD) are two central mechanisms of synaptic plasticity depending on changes in AMPAR that mediate the majority of fast synaptic transmission (Malinow and Malenka, 2002). In the hippocampus, two independent forms of LTD coexist, the N-methyl-D-aspartate receptor (NMDAR)-LTD and the group I metabotropic glutamate receptor (mGluR)-LTD, each induced through distinct signaling cascades (Collingridge et al., 2010; Oliet et al., 1997). Translation from dendritically localized mRNAs is a primary process for the induction of mGluR-LTD (Huber et al., 2000; Klann and Dever, 2004; Snyder et al., 2001). The prevailing model is that group I mGluRs rapidly trigger the local synthesis of new dendritic proteins that are required for LTD by increasing the rate of AMPAR endocytosis at active synapses (Lüscher and Huber, 2010; Waung and Huber, 2009). Among the locally translated proteins are Arc/Arg3.1 (Jakkamsetti et al., 2013; Park et al., 2008; Waung et al., 2008), Map1b (Davidkova and Carroll, 2007), STEP1 (Zhang et al., 2008), and oligophrenin-1 (Nadif Kasri et al., 2011). Interestingly, different forms of intellectual disability (ID) have been linked to defective mGluR-LTD, confirming the tight regulation of AMPAR function at mature synapses through local protein synthesis as an essential form of plasticity and cognition (Aschrafi et al., 2005; Auerbach et al., 2011; Bateup et al., 2011; Lüscher and Huber, 2010).

Local translation-dependent synaptic LTD is tightly controlled by a number of different post-transcriptional mechanisms, such as the ubiquitin-proteasome system (Hou et al., 2006; Yashiro et al., 2009), translation initiation and elongation (Costa-Mattioli et al., 2005), and by microRNAs (miRNAs) (Manakov et al., 2009). MiRNAs are small, evolutionarily conserved signaling molecules that act as silencing regulators of mRNA targets. Disruption of miRNA expression or signaling impairs synaptic plasticity and has been associated with severe cognitive impairment in mice (Hansen et al., 2013; Konopka et al., 2010) and humans (Ripke et al., 2013; Willemsen et al., 2011). Consistent with these notions, inducing LTP or LTD rapidly alters the levels of many different miRNAs in hippocampal neurons (Park and Tang, 2009; Wibrand et al., 2010). MiRNAs affect synaptic plasticity by directly targeting synaptic receptors or their downstream targets (Dutta et al., 2013; Fiore et al., 2014; Kocerha et al., 2009;

Letellier et al., 2014; Saba et al., 2012; Schratt et al., 2006), including LTD proteins such as Arc and Map1b (Chen and Shen, 2013; Wibrand et al., 2012). These findings suggest that variation in miRNA expression affects synaptic protein levels and, consequently, synaptic plasticity by controlling the stability and translation of dendritically localized transcripts.

Using SNP microarray analysis, we have identified microdeletions encompassing *MIR137* in a number of unrelated families with genetic forms of ID (Willemsen et al., 2011). These deletions cause reduced miR-137 expression and increased transcript levels for miR-137 target genes such as *KLF4*, *MITF*, and *EZH2* in ID patient-derived cell lines. Moreover, a SNP linked to *MIR137* has shown genome-wide significant association with schizophrenia (SZ) and has been associated with a number of SZ endophenotypes (Duan et al., 2014; Guella et al., 2013; Kwon et al., 2013; Ripke et al., 2013). Initial studies suggest that miR-137 modulates the proliferation and differentiation of adult neuronal stem cells in vitro and in vivo (Szulwach et al., 2010), and it negatively regulates dendrite morphogenesis and spine development in newborn neurons in the dentate gyrus (DG) by targeting the E3 ubiquitin ligase Mindbomb-1 (Smrt et al., 2010). This is in line with our recent findings showing that miR-137 is synaptically enriched (Willemsen et al., 2011), and supports the notion that cognitive deficits observed in human patients can be attributed to altered dendritic spine morphology and disrupted synaptic function (Nadif Kasri and Van Aelst, 2008; Pavlowsky et al., 2012). However, the molecular mechanisms by which miR-137 controls synaptic transmission and plasticity remain elusive.

Here, we investigated the postsynaptic function of miR-137 specifically at the CA3-CA1 synapse of the hippocampus. We identified AMPAR subunit GluA1 as a target of miR-137, and we found that this miRNA stimulates the silencing of synapses by selectively decreasing AMPAR subunit GluA1 surface expression, thereby affecting synaptic maturation. Moreover, miR-137 maturation was rapidly enhanced upon mGluR activation, which is required for the expression of mGluR-dependent LTD. Thus, our data unveil a critical role for miR-137 in controlling synaptic strength at the CA3-CA1 synapse and link genetic deficits in *MIR137* to glutamatergic dysfunction, which may ultimately contribute to the pathogenesis of cognitive impairments.

RESULTS

AMPAR Subunit GluA1 Is a Direct Target of miR-137

Bioinformatics studies revealed the presence of a highly conserved miR-137 binding site in the 3′-UTR of AMPAR subunit GluA1, but not for other AMPAR subunits (Figure 1A), suggesting that this miRNA targets GluA1. We transfected hippocampal neurons at 14 days in vitro (DIV) with either a luciferase reporter plasmid containing the GluA1 3′UTR (wild-type [WT]) or an miR-137 binding-site-mutated GluA1 3′UTR (mutant) (Figure 1B). Luciferase activity was assessed using an miR-137-sequestering sponge vector (Figure S1). Neurons infected with the sponge-miR-137 virus exhibited an increased luciferase signal when expressing the GluA1-3′UTR (Figure 1B), whereas no effect was seen with the mutated form of GluA1. Similarly, luciferase activity was increased when the GluA1-3′UTR WT neurons were exposed to a previously validated locked nucleic acid LNA-miR-137 (Willemsen et al., 2011), whereas this increase was absent in the mutant condition, suggesting a targeting of this binding site by miR-137 (Figure 1B).

Western blot analysis revealed that GluA1 protein expression was significantly increased in the sponge-miR-137-expressing neurons, whereas GluA1 expression was significantly reduced in the miR-137-expressing neurons (Figures 1C and 1D). Of note, GluA1 mRNA expression was unaffected by miR-137, suggesting that the changes in GluA1 protein levels by miR-137 is regulated at the level of translation rather than transcription (Figure 1E).

We observed a significant increase in surface GluA1 (sGluA1) expression at synapses of sponge-miR-137-expressing hippocampal neurons, whereas sGluA1 levels were reduced during miR-137 overexpression (Figures 1F and 1G), supporting the notion that AMPAR subtype GluA1 is directly targeted by miR-137.

miR-137 Regulates Excitatory Synaptic Transmission at the Hippocampal CA3-CA1 Synapse

Next, we examined the role of endogenous miR-137 on synaptic function by assessing the effects of reduced miR-137 expression on synaptic transmission at the hippocampal CA3-CA1 synapse. Simultaneous whole-cell recordings of evoked excitatory postsynaptic currents (eEPSCs) from an 8–10-DIV CA1 pyramidal neuron expressing sponge-miR-137 and an adjacent non-infected neuron were performed. miR-137 downregulation resulted in a potentiation of AMPAR-mediated transmission, but not NMDAR-mediated transmission (Figure 2A). Conversely, miR-137 overexpression significantly depressed AMPAR-mediated transmission, but not NMDAR-mediated transmission (Figure 2B), indicating that modulation of miR-137 levels is associated with opposing effects toward AMPAR-mediated synaptic transmission.

The observed changes are likely due to a postsynaptic effect, since only CA1 neurons were genetically manipulated at the CA3-CA1 synapse and we did not observe any change in presynaptic release probability, as measured by a paired-pulse stimulation paradigm (Figure 2C). Collectively, these results suggest that miR-137 controls excitatory synaptic strength in a cell-autonomous manner.

The changes in AMPAR-mediated transmission could be based on a change in synaptic AMPARs levels at individual synapses, a change in the number of functional synapses, or both. We therefore measured miniature excitatory postsynaptic currents (mEPSCs) in the sponge-miR-137- and the miR-137-infected neurons as compared to non-infected cells. While sponge-miR-137-infected neurons exhibited no change in amplitude, they showed an increase in the frequency of mEPSCs. In contrast, neurons overexpressing miR-137 showed a decreased mEPSC frequency without exhibiting any changes in amplitude (Figures 2D and 2E). A change in frequency usually reflects a change in the number of active synapses or presynaptic release probability. However, since alterations in miR-137 levels did not elicit any changes in presynaptic release probability, these results suggest that modulation of miR-137 levels in hippocampal slices resulted in a change in the number of functional synapses.

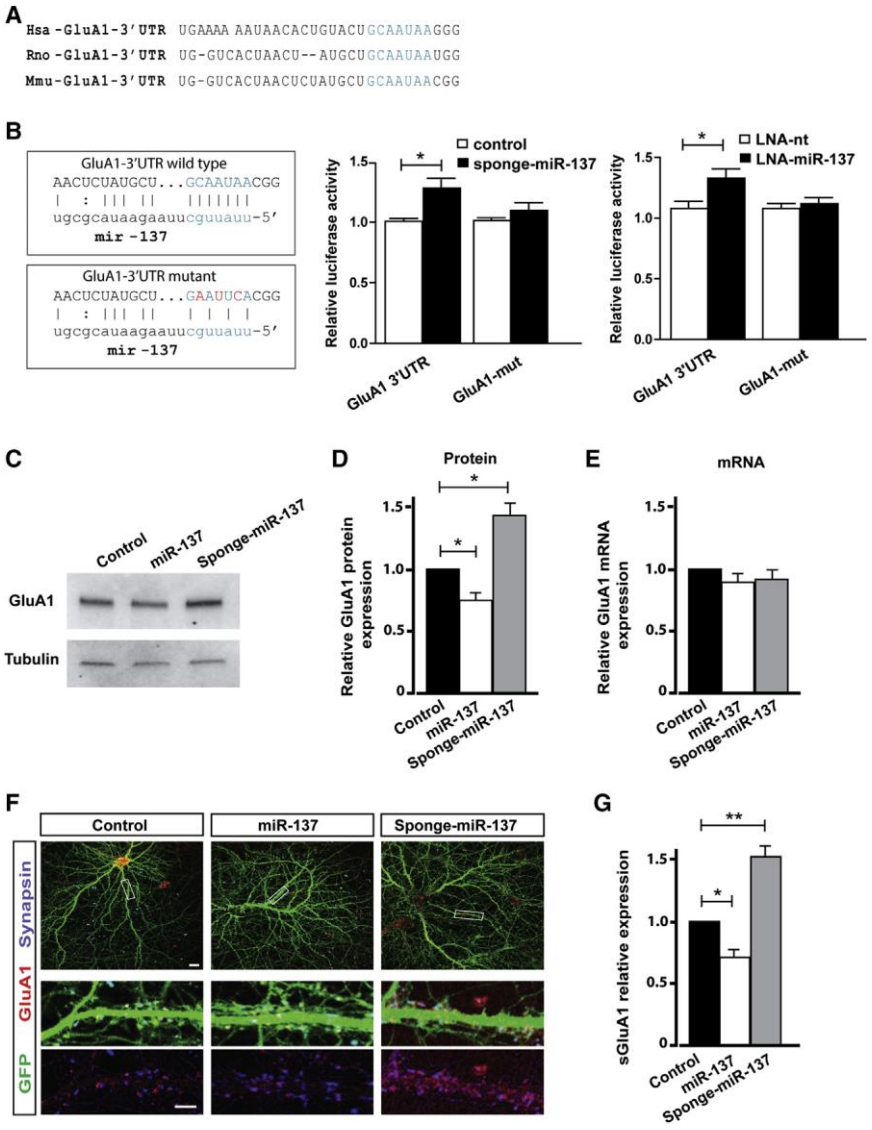

Figure 1. GluA1 Is a Direct Target of miR-137

(A) The binding site for the seed sequence for miR-37 in the 3′UTR of GluA1 is highly conserved among human (hsa), rat (rno), and mouse (mmu) sequences (shown in blue, from TargetScan release 6.2).

(B) Overview of miR-137 target site within the rat GluA1 3′UTR. miR-137 seed sequence and the nucleotide mutations inserted into the seed are indicated in blue. The graph represents the relative luciferase gene activity of a reporter vector harboring either the WT GluA1 3′UTR or mutated GluA1 3′UTR, when co-transfected with either control or sponge-miR-137 (LNA-miRNA-NT or LNA-miR-137, respectively). Luciferase activity was normalized to Renilla luciferase activity. Error bars represent the SEM for n = 8 independent experiments; *p < 0.05, Student's t test.

(C) Western blot shows GluA1 in cultured hippocampal neurons at 14 DIV, infected with lentiviruses encoding either control (GFP alone), sponge-miR-137, or miR-137 at 8 DIV; g-tubulin was used as the loading control.

(D) Mean GluA1 protein levels in the different conditions as indicated, normalized to g-tubulin levels in the same sample, are shown (n = 6; *p < 0.05, one-way ANOVA).

(E) Mean GluA1 mRNA levels in the different conditions as indicated are shown (n = 6; one-way ANOVA).

(F) Representative confocal microscopy images show sGluA1 expression, co-localizing with synapsin-1, in cultured hippocampal neurons infected with control (GFP alone), sponge-miR-137, or miR-137 lentiviruses at 8 DIV and imaged at 14 DIV. Scale bars, 10 μm (top) and 2 μm (bottom). See also Figure S1.

(G) Quantification shows the number of synaptic sGluA1 puncta at synapses (n = 20–25 neurons from three cultures/condition). Error bar represents SEM. *p < 0.05, **p < 0.01, one-way ANOVA.

miR-137 Promotes Silencing of Active Synapses

miR-137 was shown to play a critical role in neuronal morphogenesis during the development of newborn neurons in the DG in vivo (Smrt et al., 2010).

We therefore examined the role of miR-137 in dendritic spine formation or maintenance in 21-DIV hippocampal neuronal cultures. Image analysis revealed that, while no changes were observed in spine type and size by altering miR-137 levels, spine density of sponge-miR-137-infected cells was increased, whereas no effects on spine density were seen upon miR-137 overexpression (Figures 3A and 3B). Together with the finding that AMPAR mEPSC frequency is significantly altered by miR-137, we conclude that miR-137 specifically affects the number of active synapses rather than changes spine morphology at the CA3-CA1 synapse.

Next, we examined the mechanism through which miR-137 mediates synaptic depression. A plausible mechanism could involve silencing of active synapses; i.e., synapses with NMDARs but no functional AMPARs (Hanse et al., 2013). The proportion of these silent synapses rapidly decreases during the first 2 weeks of post-natal development in the hippocampus, coinciding with the maturation process of the synapses (Liao et al., 1999). We therefore measured the amount of surface NMDAR subunit NR1 co-localizing with surface AMPAR subunit GluA1 in hippocampal neurons infected at 8 DIV and immunolabeled at 14 DIV. miR-137-overexpressing neurons exhibited a significant increase in silent synapses, as fewer NR1 puncta were co-localized with GluA1 puncta, while no significant decrease in silent synapses in sponge-miR-137-infected neurons was observed (Figures 3C and 3D).

To directly probe for a role of miR-137 in synapse silencing, we measured the failure rate using a minimum stimulation protocol (Isaac et al., 1995; Liao et al., 1995). Whole-cell patch-clamp recordings were obtained from CA1 pyramidal neurons, clamped

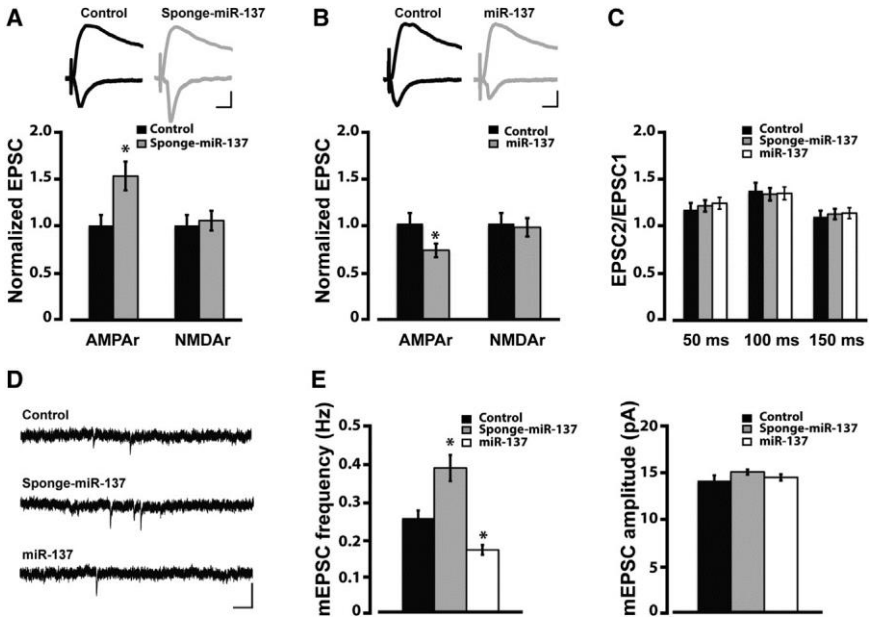

Figure 2. Postsynaptic miR-137 Regulates Synaptic Transmission

(A and B) (Top) Representative traces show EPSCs recorded simultaneously from a pair of uninfected neurons (control) and neurons infected with indicated lentiviruses. EPSCs from both −60 and +40 mV holding potentials are shown. Scale bars, 20 ms and 20 pA. (Bottom) Quantification shows the EPSCs mediated by both AMPAR and NMDAR for each experimental condition as indicated. The EPSC amplitude was normalized to the mean value of EPSCs from control neurons. (A, sponge-miR-137, n = 14; B, miR-137, n = 12). Data are shown as mean ± SEM. *p < 0.05, paired Student's t test.

(C) Paired-pulse ratio shows AMPAR-mediated EPSCs at different time intervals for control, sponge-miR-137-, and miR-137-expressing neurons (n = 5 cells for all groups). Data are shown as mean ± SEM.

(D) Representative traces show excitatory miniature events recorded at −60 mV from uninfected neurons (control) and neurons expressing sponge-miR-137 or miR-137. Scale bars, 250 ms and 20 pA.

(E) Quantification shows mEPSC frequency and amplitude for control, sponge-miR-137-, and miR-137-expressing neurons (n = 12 cells for all groups). Data are shown as mean ± SEM. *p < 0.05, one-way ANOVA.

at their resting membrane potential (−60 mV), and excitatory synaptic transmission was elicited with a weak stimulus that produced failures in ±50% of the trials (Figure 3E). Fifty trials per session were recorded at −60 and +40 mV for each cell, and the failure rate at these two holding potentials was computed. In non-infected 8-DIV CA1 neurons, the failure rate was larger at −60 than at +40 mV (Figure 3F), indicating a substantial fraction of the synapses are still silent at this stage of development (Figure 3I). Neurons infected with the sponge-miR-137 showed a similar failure rate measured at −60 mV compared with that at +40 mV (Figure 3G), indicative of fewer silent synapses due to a reduction in miR-137 levels (Figure 3I). Conversely, in CA1 hippocampal neurons overexpressing miR-137, we observed a much higher rate of failures at −60 mV compared with that at +40 mV (Figure 3H), indicative of a high fraction of silent synapses in this condition. Together these data show that the amount of silent synapses during development is significantly altered upon miR-137 expression manipulation, and they suggest that miR-137 acts as a synaptic break during development by preventing the unsilencing of silent synapses.

miR-137 Is Required for mGluR-LTD Expression

Recent findings have shown that both LTP or LTD induction rapidly alters the level of more than 50 different miRNAs in hippocampal neurons (Park and Tang, 2009). Given our results showing that miR-137 regulates AMPAR-mediated synaptic strength, we hypothesized that miR-137 might also be required for synaptic plasticity. We examined the role of miR-137 in mGluR-LTD, a form of synaptic plasticity depending on local protein translation at hippocampal neurons. We first examined the temporal expression pattern of miR-137 after mGluR-LTD induction. Using qPCR we found that LTD induced by the mGluR group I agonist (*S*)-3,5-dihydroxyphenylglycine (DHPG) rapidly increased mature miR-137 levels within 15 min after DHPG application. Interestingly, the levels of miR-137 were at baseline after 45 min (Figure 4A), suggesting a temporal regulation. The finding that precursor (pre)-miR-137 levels are concomitantly decreased 15 min after DHPG application (Figure 4B) suggested that this rapid regulation is possibly due to an increased processing of pre-miR-137 into mature miR-137 rather than enhanced miRNA transcription. Furthermore, using specific mGluR1 or mGluR5 antagonists (LY367385 and MPEP), we found that a DHPG-induced increase in mature miR-137 levels was dependent on mGluR5, but not on mGluR1, activation (Figure 4C).

Next, we examined whether mGluR5-induced miR-137 increase is required for mGluR-LTD. We reasoned that acute delivery of LNA-anti-miR-137 would only interfere with the DHPG-induced miR-137 expression, without affecting basal levels of miR-137. Indeed, introducing LNA-anti-miR-137 or control LNA-anti-miRNA-NT, into CA1 neurons of organotypic hippocampal slices via whole-cell recording pipettes, did not affect basal synaptic transmission when neurons were treated with the respective LNA-anti-miRNAs for 60 min (Figure 4D). MGluR-LTD can be induced chemically, using DHPG or by synaptic activation of mGluRs, using paired pulses of low-frequency (1 Hz) synaptic stimulation (PP-LFS). Consistent with previous studies, DHPG application (100 μM, 5 min) or PP-LFS caused an acute depression in evoked EPSCs onto both neurons treated with LNA-anti-miRNAs (Figures 4E and 4F). However, only a persistent LTD was observed in LNA-anti-miRNA-NT-treated neurons, but not in LNA-anti-miR-137 neurons (Figures 4E–4G).

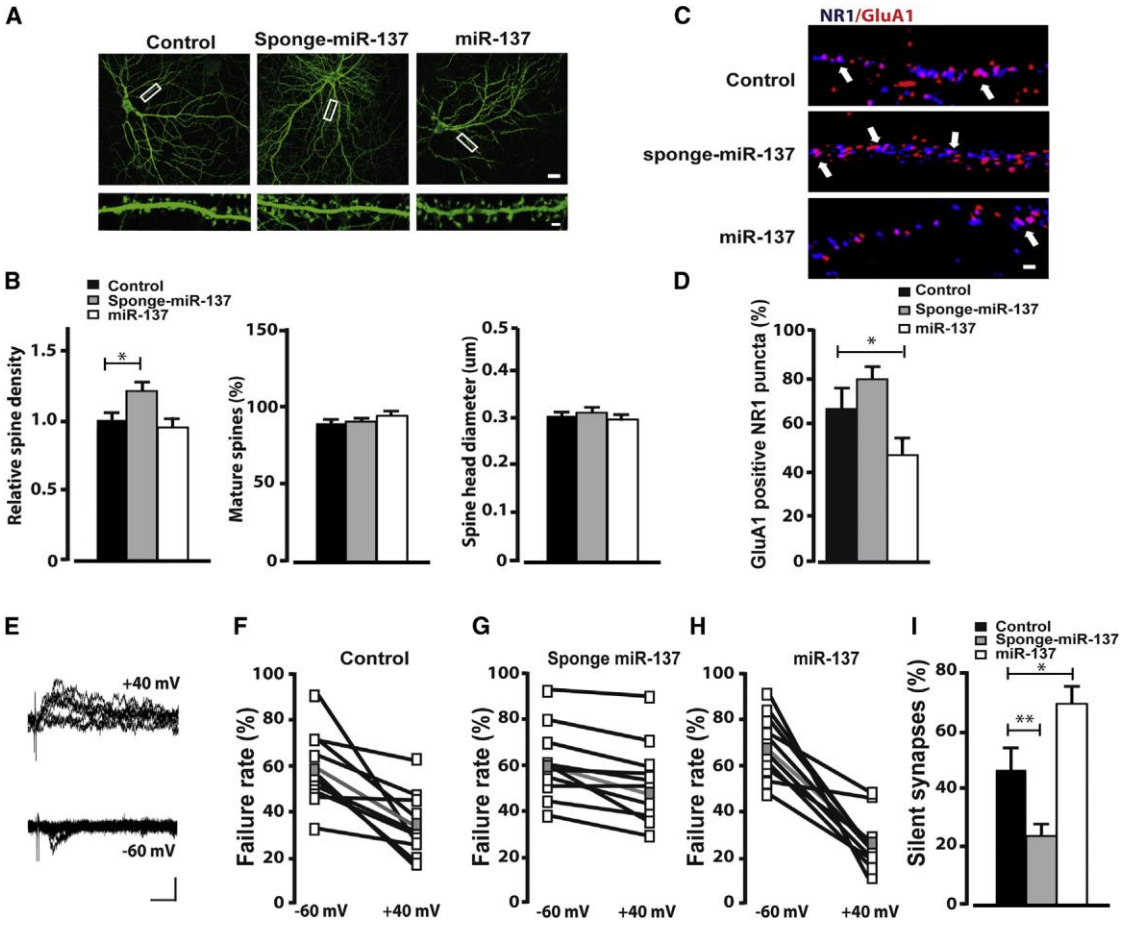

Figure 3. miR-137 Promotes Silencing of Active Synapses

(A) Representative confocal microscopy images show 21-DIV primary hippocampal neurons infected with control, sponge-miR-137, and miR-137 viruses at 8 DIV. Scale bars, 10 μm (top) and 1 μm (bottom).

(B) Quantification of spine density and size. Spine density is significantly increased in neurons expressing sponge-miR-137 compared to control neurons, whereas miR-137 overexpression shows no significant effect on spine density. miR-137 manipulation does not show an effect on the percentage of mature spines or spine size (n = 35, control; n = 26, sponge-miR-137; and n = 24, miR-137). Bars represent mean ± SEM. *p < 0.05, one-way ANOVA.

(C) Representative confocal microscopy images show surface NR1 and sGluA1 expression in cultured hippocampal neurons infected with control (GFP alone), sponge-miR-137, or miR-137 lentivirus at 8 DIV and imaged at 14 DIV. White arrows indicate GluA1/NR1 colocalization. Scale bars, 10 μm (top) and 2 μm (bottom).

(D) Quantification shows the number of NR1 puncta containing GluA1 (n = 11–14 neurons from three cultures/condition). Data are shown as mean ± SEM. *p < 0.05, one-way ANOVA followed by post hoc Bonferroni correction for multiple testing.

(E) Representative traces were recorded from CA1 hippocampal neurons under minimal stimulation conditions at −60 and +40 mV holding potentials in control neurons. Scale bars, 25 pA and 100 ms.

(F–H) Failure rates were obtained at −60 and +40 mV holding potentials in control (F), sponge-miR-137- (G), or miR-137-expressing neurons (H). Individual data points (white squares) and average (gray square) are shown.

(I) Percentages show silent synapses in conditions as indicated. Data are shown as mean ± SEM (n = 10–11; *p < 0.05, **p < 0.01, one-way ANOVA).

Finally, miR-137 was selectively required for mGluR-LTD, as no effect of manipulating miR-137 levels on NMDAR-induced LTD was observed (Figure S2). Together these data show that miR-137 is selectively required for mGluR5-mediated LTD.

DISCUSSION

miR-137 Regulates AMPAR Subunits and Synaptic Transmission in Hippocampal Neurons

Small non-coding miRNAs recently have emerged as key regulators of neuronal development and synaptic plasticity (Olde Loohuis et al., 2012). In this study, we identified AMPAR subunit GluA1 as a target of miR-137. By temporally and spatially manipulating miR-137 levels at the hippocampal CA3-CA1 pathway, we demonstrate that postsynaptic miR-137 controls maturation and plasticity of excitatory synaptic function by regulating AMPAR expression. miR-137 repressed the incorporation of AMPARs into the synaptic membrane, thereby preventing synaptic maturation and plasticity. In particular, overexpressed miR-137 in organotypic brain slices silenced active synapses, likely by the removal of sGluA1. Conversely, decreased miR-137 levels led to the accelerated maturation of excitatory

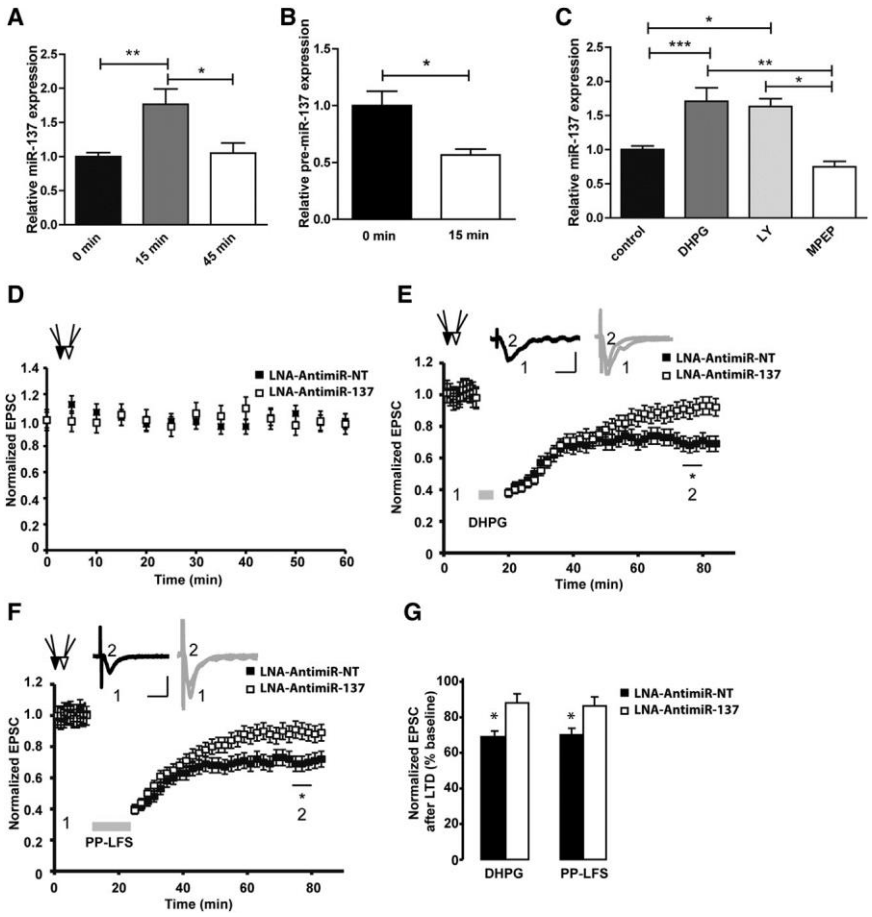

Figure 4. miR-137 Is Required for mGluR-LTD Expression

(A) mGluR-LTD induced by mGluR group 1 agonist DHPG (100 μM) enhances miR-137 levels after 15 min and miR-137 expression is decreased to baseline levels after 45 min (n = 6 for control and 15 min; n = 3 for 45 min). Data are shown as mean ± SEM. *p < 0.05, one-way ANOVA.

(B) mGluR-LTD induced by DHPG (100 μM) decreases miR-137 levels after 15 min (n = 3). Data are shown as mean ± SEM. *p < 0.05, unpaired t test.

(C) DHPG-induced increase in miR-137 levels is blocked by mGluR5 antagonist MPEP (10 μM), but not by the mGluR1 antagonist LY-367385 (100 μM) (n = 6 for control and DHPG; n = 3 for LY-367385 and MPEP). Data are shown as mean ± SEM. *p < 0.05, **p < 0.01, ***p < 0.001, one-way ANOVA.

(D) Average normalized EPSC amplitudes show CA1 neurons from hippocampal slices infused with LNA-miR-NT or with LNA-miR-137 (10 μM) for 60 min (n = 4 pairs; paired t test).

(E and F) Normalized EPSC amplitudes plotted against time from pairs of LNA-miRNA-NT and infected LNA-miR-137-injected CA1 pyramidal neurons during baseline (1) and after LTD induction (2) with DHPG (E, 100 μM, 5 min) or PP-LFS stimulation (F, 1 Hz, 15 min, 50-ms interval). (Top) Representative traces show AMPAR EPSCs before and after LTD induction for control LNA-miRNA-NT (black) and infused LNA-miR-137 (white) neurons. Scale bars represent 25 ms and 30 pA. (Bottom) EPSC amplitudes were normalized to the baseline of control LNA-miRNA-NT and LNA-miR-137-filled neurons (n = 8 pairs; data are shown as mean ± SEM; *p < 0.05, measured between 50 and 55 min after DHPG or PP-LFS treatment).

(G) AMPAR currents 50–55 min after DHPG or PP-LFS application were normalized to baseline AMPAR currents for each indicated condition. Data are shown as mean ± SEM. *p < 0.05, paired t test. See also Figure S2.

synapses, as they were prematurely converted from silent to active synapses.

Our observations could have direct implications for how experience-driven activity drives early neuronal development, particularly in the context of neurodevelopmental disorders such as ID and autism spectrum disorder (ASD) (Hanse et al., 2013). Decreased levels of miR-137 during development may lead to disturbed activity-dependent selection of AMPAR-silent synapses by excessive and premature AMPAR unsilencing and subsequent synapse stabilization. Recently, in animal models of ASD, such indiscriminative unsilencing of synapses has been shown to lead to distorted neuronal network formation. For example, haplo-insufficiency of *Syngap1* in mice leads to premature maturation of hippocampal and cortical synapses, resulting in a shortening of the critical period for plasticity (Clement et al., 2012, 2013).

The changes in synaptic AMPAR-mediated currents observed in our study are likely a result of altered total GluA1 expression by miR-137. However, we cannot exclude that molecular changes induced by altering miR-137 also could impact directly AMPAR trafficking or actin cytoskeleton dynamics. Of note, previous gene ontology (GO) analysis of the transcriptome data (Collins et al., 2014) suggests that the actin-remodeling pathway, including the Rho GTPase pathway (Govek et al., 2005), is a prominent signaling pathway that is targeted by miR-137. This is of interest since neuronal plasticity requires both actin cytoskeleton remodeling and local protein translation in response to extracellular signals (Zukin et al., 2009). Indeed, insertion and removal of AMPARs in the context of LTP and LTD has been shown to be dependent on actin polymerization (Bosch and Hayashi, 2012; Cingolani and Goda, 2008). miR-137 may thus trigger a selective removal of GluA1 from a subset of synapses that subsequently become silent by targeting directly the actin cytoskeleton pathway as well as impact directly the formation of dendritic spines. In this context, it is of note that the density of dendritic spines also were increased in sponge-miR-137-infected neurons. However, we did not observe any effects on spine density upon miR-137 overexpression, which is in accordance with a previous in vivo study in which miR-137 levels were altered in hippocampal neurons (Smrt et al., 2010). Alternatively, the effects on dendritic spines could be secondary to the effects on GluA1 expression.

miR-137 and mGluR-LTD

In this paper, we provide evidence that miR-137 is necessary for mGluR-LTD, a form of protein-synthesis-dependent synaptic plasticity (Huber et al., 2000; Klann and Dever, 2004; Snyder et al., 2001). Our experiments in organotypic hippocampal slices revealed that miR-137 levels were upregulated 15 min following LTD induction with DHPG, whereas pre-miR-137 expression decreased within the same time span, suggesting possibly increased miR-137 maturation upon DHPG-LTD. These data are in line with a previous study in which more than 50 miRNAs were found to be induced immediately after mGluR-LTD stimuli in vitro (Park and Tang, 2009). This activity-dependent regulation of miRNAs therefore suggests that they play a general role in regulating protein synthesis during LTD expression. However, to the best of our knowledge, only for miR-146a-5p and miR-125a the requirement for mGluR-LTD has been demonstrated directly (Chen and Shen, 2013; Muddashetty et al., 2011).

For miR-137, we addressed this question by using an LNA-anti-miR-137 oligonucleotide that efficiently sequestered endogenous miR-137. Using simultaneous recordings in organotypic brain slices, we found that acute inhibition of miR-137 during LTD induction blocked LTD expression, suggesting that this synaptically enriched miRNA indeed is necessary for mGluR-LTD. Of interest is the time dependency of miR-137 upregulation. This has been observed for multiple miRNAs induced after mGluR-LTD (Park and Tang, 2009), and it might represent a general mechanism by which miRNAs may play a role in restoring the repression state of mRNA translation after the transient activation (Ashraf and Kunes, 2006). Because mGluR-induced miR-137 upregulation is transient, it may be required for only a particular phase of LTD, for example, during the consolidation phase. In line with this idea, we found that only the later phase of LTD was affected and not the initial phase when miR-137 function was blocked. Rapid upregulation of miR-137 following LTD induction is thus possibly part of a precisely controlled mechanism to maintain a defined pool of synaptic proteins involved in synaptic AMPAR expression.

In the present study, we found several lines of evidence for a key role for miR-137 in controlling synaptic efficacy and plasticity. Our study suggests that endogenous miR-137 functions as a synaptic break during development and regulates excitatory synaptic strength through direct modulation of GluA1 levels. In conclusion, we link genetic deficits in *MIR137* to glutamatergic dysfunction, which may contribute to our understanding of the pathogenesis of miR-137-linked cognitive impairments.

EXPERIMENTAL PROCEDURES

Virus production, luciferase assay, western blot, immunofluorescence, and image analysis are described in the Supplemental Experimental Procedures.

miRNA Constructs

The sponge-miR-137 sequence was designed based on the rat miR-137-3p sequence according to the original publication describing the application of miRNA-sponge (Ebert et al., 2007; Kluiver et al., 2012). Briefly, the sponge-miR-137-3p sequence contains four consecutive miR-137-3p binding sites, each separated by four nucleotides. The miR-137 binding site contains bulged sites that are non-complementary to the miR-137 positions 11–14, in order to enhance sponge efficacy (Ebert et al., 2007; Gentner et al., 2009). Sponge-miR-137 oligonucleotides contained recognition sequences for the restriction enzymes BsrgI and EcoRI. Oligonucleotides (Sigma) were annealed in annealing buffer (containing 10 mM Tris [pH 7.5], 50 mM NaCl, and 1 mM EDTA) through a 5-min incubation at 90°C, followed by a slow cooldown to room temperature. Annealed sponge-miR-137 oligonucleotides were ligated into the FUGW vector (Plasmid 14883, Addgene) directly following the stop codon of the eGFP cDNA. To create a lentiviral vector construct carrying the rat pre-miR-137 cDNA, we PCR-amplified the precursor miR-137 containing flanking 70 nucleotides for both the 3′ and 5′ regions of the rat miR-137 from total rat brain RNA, and we ligated the PCR product into the FUGW vector using the BsrgI and EcoRI restriction sites.

Assessment of Sponge-miR-137 Function

The direct coupling of the concatemeric sponge-miR-137 sequence to the 3′ site of the GFP cDNA allows efficient binding of miR-137 to the GFP-sponge-miR-137-encoding transcript, ultimately resulting in an attenuation of GFP translation. Reduced GFP fluorescent signal intensity therefore can be used as a measure of sponge-miR-137 functional efficacy (Figure S1). For GFP quantification, the sponge-miR-137-containing vector was transfected into B35 rat neuroblastoma cells together with either a non-targeting (nt) mimic or a mimic-miR-137 oligonucleotide using Lipofectamine 2000 (Life Technologies), according to the manufacturer's instructions. Then, 48 hr post-transfection, cells were fixed in 4% paraformaldehyde (PFA)/sucrose in PBS and visualized with a Leica DFC 420C fluorescence microscope using a 20× magnification. GFP quantification was performed using the ImageJ software. We also detected significantly reduced endogenous miR-137 levels in sponge-miR-137-infected neurons compared to GFP-infected neurons, as measured by qPCR, suggesting that sponge-137 not only sequesters miR-137 but also results in an enhanced turnover rate of this miRNA.

Electrophysiology

Whole-cell recordings in cultured slices were obtained with Multiclamp 700B amplifiers (Axon Instruments). To study the effects of miR-137 on synaptic transmission, cultured slices from P6–8 rats (Wistar, Harlan Laboratories) were infected with control, sponge-miR-137, or miR-137 lentiviruses directly upon plating. Then, 8 to 10 days later, whole-cell recordings were obtained simultaneously from an infected and an adjacent uninfected neuron in the CA1 region under visual guidance using epifluorescence and transmitted light illumination. See the Supplemental Experimental Procedures for details.

Statistical Analysis

Statistical analyses were performed using Prism software (GraphPad). Statistical tests were used with alpha level at 0.05. Two group comparisons were evaluated using non-paired two-tailed t test. Three or more groups were evaluated using one-way ANOVA followed by post hoc Bonferroni correction for multiple testing. Data are plotted as mean ± SEM. Quantification was performed in a blinded fashion.

Animals

All experiments involving animals were evaluated and approved by the Committee for Animal Experiments of the Radboud University Nijmegen Medical Centre, Nijmegen, the Netherlands.

SUPPLEMENTAL INFORMATION

Supplemental Information includes Supplemental Experimental Procedures and two figures and can be found with this article online at http://dx.doi.org/10.1016/j.celrep.2015.05.040.

AUTHOR CONTRIBUTIONS

N.F.M.O.L., N.N.K., G.J.M.M., H.v.B., and A.A. conceived the experiments and wrote the manuscript. N.F.M.O.L., A.K., A.A., and A.J. performed all experiments except electrophysiology. N.N.K. and W.B. performed and analyzed all electrophysiology experiments. P.H.S. and G.S. contributed biochemical and molecular biology data.

ACKNOWLEDGMENTS

We thank D. Versteegden, M.L. Wieczorek, P. Roost, and M. Gazorpak for technical assistance. The research of the authors is supported by grants from the Donders Center for Neuroscience fellowship award of the Radboudumc (to A.A. and N.N.K.); the FP7-Marie Curie International Reintegration Grant (grant 276868 to A.A. and grant 277091 to N.N.K.); the Jerome Lejeune Foundation (to N.N.K.); and GENCODYS, an EU FP7 large-scale integrating project grant (grant 241995 to H.v.B.).

Received: December 15, 2013
Revised: April 13, 2015
Accepted: May 26, 2015
Published: June 18, 2015

REFERENCES

Aschrafi, A., Cunningham, B.A., Edelman, G.M., and Vanderklish, P.W. (2005). The fragile X mental retardation protein and group I metabotropic glutamate receptors regulate levels of mRNA granules in brain. Proc. Natl. Acad. Sci. USA *102*, 2180–2185.

Ashraf, S.I., and Kunes, S. (2006). A trace of silence: memory and microRNA at the synapse. Curr. Opin. Neurobiol. *16*, 535–539.

Auerbach, B.D., Osterweil, E.K., and Bear, M.F. (2011). Mutations causing syndromic autism define an axis of synaptic pathophysiology. Nature *480*, 63–68.

Bassani, S., Folci, A., Zapata, J., and Passafaro, M. (2013). AMPAR trafficking in synapse maturation and plasticity. Cell. Mol. Life Sci. *70*, 4411–4430.

Bateup, H.S., Takasaki, K.T., Saulnier, J.L., Denefrio, C.L., and Sabatini, B.L. (2011). Loss of Tsc1 in vivo impairs hippocampal mGluR-LTD and increases excitatory synaptic function. J. Neurosci. *31*, 8862–8869.

Bosch, M., and Hayashi, Y. (2012). Structural plasticity of dendritic spines. Curr. Opin. Neurobiol. *22*, 383–388.

Chen, Y.L., and Shen, C.K.J. (2013). Modulation of mGluR-dependent MAP1B translation and AMPA receptor endocytosis by microRNA miR-146a-5p. J. Neurosci. *33*, 9013–9020.

Cingolani, L.A., and Goda, Y. (2008). Actin in action: the interplay between the actin cytoskeleton and synaptic efficacy. Nat. Rev. Neurosci. *9*, 344–356.

Citri, A., and Malenka, R.C. (2008). Synaptic plasticity: multiple forms, functions, and mechanisms. Neuropsychopharmacology *33*, 18–41.

Clement, J.P., Aceti, M., Creson, T.K., Ozkan, E.D., Shi, Y., Reish, N.J., Almonte, A.G., Miller, B.H., Wiltgen, B.J., Miller, C.A., et al. (2012). Pathogenic SYNGAP1 mutations impair cognitive development by disrupting maturation of dendritic spine synapses. Cell *151*, 709–723.

Clement, J.P., Ozkan, E.D., Aceti, M., Miller, C.A., and Rumbaugh, G. (2013). SYNGAP1 links the maturation rate of excitatory synapses to the duration of critical-period synaptic plasticity. J. Neurosci. *33*, 10447–10452.

Collingridge, G.L., Peineau, S., Howland, J.G., and Wang, Y.T. (2010). Long-term depression in the CNS. Nat. Rev. Neurosci. *11*, 459–473.

Collins, A.L., Kim, Y., Bloom, R.J., Kelada, S.N., Sethupathy, P., and Sullivan, P.F. (2014). Transcriptional targets of the schizophrenia risk gene MIR137. Transl. Psychiatr. *4*, e404.

Costa-Mattioli, M., Gobert, D., Harding, H., Herdy, B., Azzi, M., Bruno, M., Bidinosti, M., Ben Mamou, C., Marcinkiewicz, E., Yoshida, M., et al. (2005). Translational control of hippocampal synaptic plasticity and memory by the eIF2alpha kinase GCN2. Nature *436*, 1166–1173.

Davidkova, G., and Carroll, R.C. (2007). Characterization of the role of microtubule-associated protein 1B in metabotropic glutamate receptor-mediated endocytosis of AMPA receptors in hippocampus. J. Neurosci. *27*, 13273–13278.

Duan, J., Shi, J., Fiorentino, A., Leites, C., Chen, X., Moy, W., Chen, J., Alexandrov, B.S., Usheva, A., He, D., et al.; Molecular Genetics of Schizophrenia collaboration; Genomic Psychiatric Cohort consortium (2014). A rare functional noncoding variant at the GWAS-implicated MIR137/MIR2682 locus might confer risk to schizophrenia and bipolar disorder. Am. J. Hum. Genet. *95*, 744–753.

Dutta, R., Chomyk, A.M., Chang, A., Ribaudo, M.V., Deckard, S.A., Doud, M.K., Edberg, D.D., Bai, B., Li, M., Baranzini, S.E., et al. (2013). Hippocampal demyelination and memory dysfunction are associated with increased levels of the neuronal microRNA miR-124 and reduced AMPA receptors. Ann. Neurol. *73*, 637–645.

Ebert, M.S., Neilson, J.R., and Sharp, P.A. (2007). MicroRNA sponges: competitive inhibitors of small RNAs in mammalian cells. Nat. Methods *4*, 721–726.

Fiore, R., Rajman, M., Schwale, C., Bicker, S., Antoniou, A., Bruehl, C., Draguhn, A., and Schratt, G. (2014). MiR-134-dependent regulation of Pumilio-2 is necessary for homeostatic synaptic depression. EMBO J. *33*, 2231–2246.

Gentner, B., Schira, G., Giustacchini, A., Amendola, M., Brown, B.D., Ponzoni, M., and Naldini, L. (2009). Stable knockdown of microRNA in vivo by lentiviral vectors. Nat. Methods *6*, 63–66.

Govek, E.-E., Newey, S.E., and Van Aelst, L. (2005). The role of the Rho GTPases in neuronal development. Genes Dev. *19*, 1–49.

Guella, I., Sequeira, A., Rollins, B., Morgan, L., Torri, F., van Erp, T.G.M., Myers, R.M., Barchas, J.D., Schatzberg, A.F., Watson, S.J., et al. (2013). Analysis of miR-137 expression and rs1625579 in dorsolateral prefrontal cortex. J. Psychiatr. Res. *47*, 1215–1221.

Hanse, E., Seth, H., and Riebe, I. (2013). AMPA-silent synapses in brain development and pathology. Nat. Rev. Neurosci. *14*, 839–850.

Hansen, K.F., Karelina, K., Sakamoto, K., Wayman, G.A., Impey, S., and Obrietan, K. (2013). miRNA-132: a dynamic regulator of cognitive capacity. Brain Struct. Funct. *218*, 817–831.

Hou, L., Antion, M.D., Hu, D., Spencer, C.M., Paylor, R., and Klann, E. (2006). Dynamic translational and proteasomal regulation of fragile X mental retardation protein controls mGluR-dependent long-term depression. Neuron *51*, 441–454.

Huber, K.M., Kayser, M.S., and Bear, M.F. (2000). Role for rapid dendritic protein synthesis in hippocampal mGluR-dependent long-term depression. Science *288*, 1254–1257.

Huganir, R.L., and Nicoll, R.A. (2013). AMPARs and synaptic plasticity: the last 25 years. Neuron *80*, 704–717.

Isaac, J.T., Nicoll, R.A., and Malenka, R.C. (1995). Evidence for silent synapses: implications for the expression of LTP. Neuron *15*, 427–434.

Jakkamsetti, V., Tsai, N.-P., Gross, C., Molinaro, G., Collins, K.A., Nicoletti, F., Wang, K.H., Osten, P., Bassell, G.J., Gibson, J.R., and Huber, K.M. (2013). Experience-induced Arc/Arg3.1 primes CA1 pyramidal neurons for metabotropic glutamate receptor-dependent long-term synaptic depression. Neuron *80*, 72–79.

Klann, E., and Dever, T.E. (2004). Biochemical mechanisms for translational regulation in synaptic plasticity. Nat. Rev. Neurosci. *5*, 931–942.

Kluiver, J., Slezak-Prochazka, I., Smigielska-Czepiel, K., Halsema, N., Kroesen, B.-J., and van den Berg, A. (2012). Generation of miRNA sponge constructs. Methods *58*, 113–117.

Kocerha, J., Faghihi, M.A., Lopez-Toledano, M.A., Huang, J., Ramsey, A.J., Caron, M.G., Sales, N., Willoughby, D., Elmen, J., Hansen, H.F., et al. (2009). MicroRNA-219 modulates NMDA receptor-mediated neurobehavioral dysfunction. Proc. Natl. Acad. Sci. USA *106*, 3507–3512.

Konopka, W., Kiryk, A., Novak, M., Herwerth, M., Parkitna, J.R., Wawrzyniak, M., Kowarsch, A., Michaluk, P., Dzwonek, J., Arnsperger, T., et al. (2010). MicroRNA loss enhances learning and memory in mice. J. Neurosci. *30*, 14835–14842.

Kwon, E., Wang, W., and Tsai, L.H. (2013). Validation of schizophrenia-associated genes CSMD1, C10orf26, CACNA1C and TCF4 as miR-137 targets. Mol. Psychiatry *18*, 11–12.

Letellier, M., Elramah, S., Mondin, M., Soula, A., Penn, A., Choquet, D., Landry, M., Thoumine, O., and Favereaux, A. (2014). miR-92a regulates expression of synaptic GluA1-containing AMPA receptors during homeostatic scaling. Nat. Neurosci. *17*, 1040–1042.

Liao, D., Hessler, N.A., and Malinow, R. (1995). Activation of postsynaptically silent synapses during pairing-induced LTP in CA1 region of hippocampal slice. Nature *375*, 400–404.

Liao, D., Zhang, X., O'Brien, R., Ehlers, M.D., and Huganir, R.L. (1999). Regulation of morphological postsynaptic silent synapses in developing hippocampal neurons. Nat. Neurosci. *2*, 37–43.

Lüscher, C., and Huber, K.M. (2010). Group 1 mGluR-dependent synaptic long-term depression: mechanisms and implications for circuitry and disease. Neuron *65*, 445–459.

Malinow, R., and Malenka, R.C. (2002). AMPA receptor trafficking and synaptic plasticity. Annu. Rev. Neurosci. *25*, 103–126.

Manakov, S.A., Grant, S.G.N., and Enright, A.J. (2009). Reciprocal regulation of microRNA and mRNA profiles in neuronal development and synapse formation. BMC Genomics *10*, 419.

Muddashetty, R.S., Nalavadi, V.C., Gross, C., Yao, X., Xing, L., Laur, O., Warren, S.T., and Bassell, G.J. (2011). Reversible inhibition of PSD-95 mRNA translation by miR-125a, FMRP phosphorylation, and mGluR signaling. Mol. Cell *42*, 673–688.

Nadif Kasri, N., and Van Aelst, L. (2008). Rho-linked genes and neurological disorders. Pflugers Arch. *455*, 787–797.

Nadif Kasri, N., Nakano-Kobayashi, A., and Van Aelst, L. (2011). Rapid synthesis of the X-linked mental retardation protein OPHN1 mediates mGluR-dependent LTD through interaction with the endocytic machinery. Neuron *72*, 300–315.

Olde Loohuis, N.F.M., Kos, A., Martens, G.J.M., Van Bokhoven, H., Nadif Kasri, N., and Aschrafi, A. (2012). MicroRNA networks direct neuronal development and plasticity. Cell. Mol. Life Sci. *69*, 89–102.

Oliet, S.H., Malenka, R.C., and Nicoll, R.A. (1997). Two distinct forms of long-term depression coexist in CA1 hippocampal pyramidal cells. Neuron *18*, 969–982.

Park, C.S., and Tang, S.-J. (2009). Regulation of microRNA expression by induction of bidirectional synaptic plasticity. J. Mol. Neurosci. *38*, 50–56.

Park, S., Park, J.M., Kim, S., Kim, J.-A., Shepherd, J.D., Smith-Hicks, C.L., Chowdhury, S., Kaufmann, W., Kuhl, D., Ryazanov, A.G., et al. (2008). Elongation factor 2 and fragile X mental retardation protein control the dynamic translation of Arc/Arg3.1 essential for mGluR-LTD. Neuron *59*, 70–83.

Pavlowsky, A., Chelly, J., and Billuart, P. (2012). Emerging major synaptic signaling pathways involved in intellectual disability. Mol. Psychiatry *17*, 682–693.

Ripke, S., O'Dushlaine, C., Chambert, K., Moran, J.L., Kähler, A.K., Akterin, S., Bergen, S.E., Collins, A.L., Crowley, J.J., Fromer, M., et al.; Multicenter Genetic Studies of Schizophrenia Consortium; Psychosis Endophenotypes International Consortium; Wellcome Trust Case Control Consortium 2 (2013). Genome-wide association analysis identifies 13 new risk loci for schizophrenia. Nat. Genet. *45*, 1150–1159.

Saba, R., Störchel, P.H., Aksoy-Aksel, A., Kepura, F., Lippi, G., Plant, T.D., and Schratt, G.M. (2012). Dopamine-regulated microRNA MiR-181a controls GluA2 surface expression in hippocampal neurons. Mol. Cell. Biol. *32*, 619–632.

Schratt, G.M., Tuebing, F., Nigh, E.A., Kane, C.G., Sabatini, M.E., Kiebler, M., and Greenberg, M.E. (2006). A brain-specific microRNA regulates dendritic spine development. Nature *439*, 283–289.

Smrt, R.D., Szulwach, K.E., Pfeiffer, R.L., Li, X., Guo, W., Pathania, M., Teng, Z.-Q., Luo, Y., Peng, J., Bordey, A., et al. (2010). MicroRNA miR-137 regulates neuronal maturation by targeting ubiquitin ligase mind bomb-1. Stem Cells *28*, 1060–1070.

Snyder, E.M., Philpot, B.D., Huber, K.M., Dong, X., Fallon, J.R., and Bear, M.F. (2001). Internalization of ionotropic glutamate receptors in response to mGluR activation. Nat. Neurosci. *4*, 1079–1085.

Szulwach, K.E., Li, X., Smrt, R.D., Li, Y., Luo, Y., Lin, L., Santistevan, N.J., Li, W., Zhao, X., and Jin, P. (2010). Cross talk between microRNA and epigenetic regulation in adult neurogenesis. J. Cell Biol. *189*, 127–141.

Waung, M.W., and Huber, K.M. (2009). Protein translation in synaptic plasticity: mGluR-LTD, Fragile X. Curr. Opin. Neurobiol. *19*, 319–326.

Waung, M.W., Pfeiffer, B.E., Nosyreva, E.D., Ronesi, J.A., and Huber, K.M. (2008). Rapid translation of Arc/Arg3.1 selectively mediates mGluR-dependent LTD through persistent increases in AMPAR endocytosis rate. Neuron *59*, 84–97.

Wibrand, K., Panja, D., Tiron, A., Ofte, M.L., Skaftnesmo, K.-O., Lee, C.S., Pena, J.T.G., Tuschl, T., and Bramham, C.R. (2010). Differential regulation of mature and precursor microRNA expression by NMDA and metabotropic glutamate receptor activation during LTP in the adult dentate gyrus in vivo. Eur. J. Neurosci. *31*, 636–645.

Wibrand, K., Pai, B., Siripornmongcolchai, T., Bittins, M., Berentsen, B., Ofte, M.L., Weigel, A., Skaftnesmo, K.O., and Bramham, C.R. (2012). MicroRNA regulation of the synaptic plasticity-related gene Arc. PLoS ONE *7*, e41688.

Willemsen, M.H., Vallès, A., Kirkels, L.A.M.H., Mastebroek, M., Olde Loohuis, N., Kos, A., Wissink-Lindhout, W.M., de Brouwer, A.P.M., Nillesen, W.M., Pfundt, R., et al. (2011). Chromosome 1p21.3 microdeletions comprising DPYD and MIR137 are associated with intellectual disability. J. Med. Genet. *48*, 810–818.

Yashiro, K., Riday, T.T., Condon, K.H., Roberts, A.C., Bernardo, D.R., Prakash, R., Weinberg, R.J., Ehlers, M.D., and Philpot, B.D. (2009). Ube3a is required for experience-dependent maturation of the neocortex. Nat. Neurosci. *12*, 777–783.

Zhang, Y., Venkitaramani, D.V., Gladding, C.M., Zhang, Y., Kurup, P., Molnar, E., Collingridge, G.L., and Lombroso, P.J. (2008). The tyrosine phosphatase STEP mediates AMPA receptor endocytosis after metabotropic glutamate receptor stimulation. J. Neurosci. *28*, 10561–10566.

Zukin, R.S., Richter, J.D., and Bagni, C. (2009). Signals, synapses, and synthesis: how new proteins control plasticity. Front Neural Circuits *3*, 14.

Supplemental Data

MicroRNA-137 controls AMPA-Receptor mediated transmission and mGluR-LTD

Nikkie FM Olde Loohuis[1,5], Wei Ba[4,5], Peter Stoerchel[6], Aron Kos[1,5], Amanda Jager[1,5], Gerhard Schratt[6], Gerard JM Martens[3,5], Hans van Bokhoven[1,4,5], Nael Nadif Kasri[1,4,5,7]*, Armaz Aschrafi[2,5,7]*

[7] Co-senior author

*Corresponding Authors

Two Supplemental Figures

Supplemental Experimental Procedures

Supplemental References

Supplemental Figures and Legends

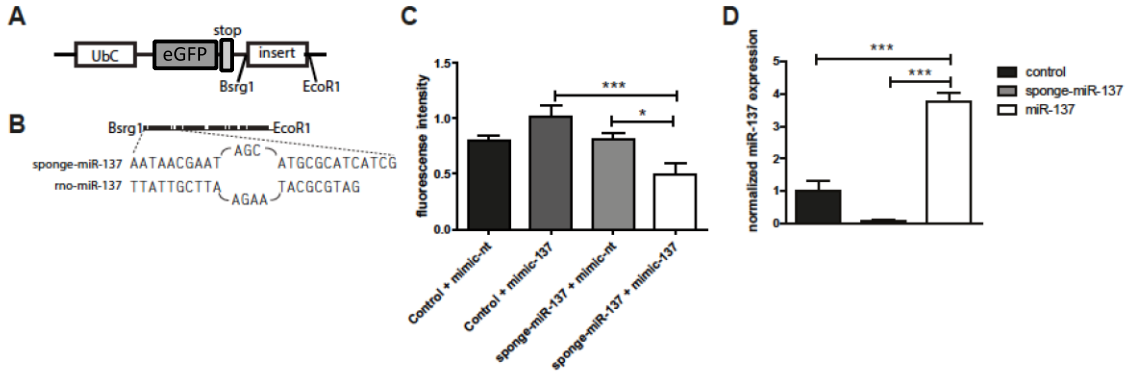

Figure S1. Validation of sponge-miR-137 and miR-137 viral constructs.
(A) To selectively reduce endogenous miR-137 levels in CA1 neurons, we used a sequestration vector called ‘‘sponge-miR-137” containing four partially complementary miR-137 binding sites (Ebert et al., 2007) followed by the coding sequence for enhanced green fluorescent protein (eGFP). The efficacy of this sponge-miR-137 in sequestering miR-137 was demonstrated by co-transfection of this sponge and a miR-137 overexpressing construct, which resulted in a reduction of eGFP fluorescence (Figure S1C). Moreover, in neurons the sponge-miR-137 construct lowered miR-137 levels, while the miR-137 overexpressing virus increased miR-137 levels in infected hippocampal neurons as compared to control neurons (Figure S1D). Map representing a lentiviral construct driven by the Ubiquitin C (UbC) promoter. The vector consists of a eGFP reporter followed by a translational stop. The insert, representing either a sponge-miR-137 or a miR-137 precursor sequence was cloned into this vector using Bsrg1 and EcoR1 restriction sites.
(B) The sponge-miR-137 sequence consists of four complementary binding sites for miR-137 in which miRNA mispairing was introduced to enhance sponge efficacy (Ebert et al., 2007; Gentner et al., 2009). Each sequestering sequence is separated by four nucleotides.
(C) Graph representing the validation of the sponge-miR-137 construct using fluorescence intensity as a measure. Co-transfection of the control construct with either mimic non-targeting (mimic-NT) as a control or mimic-137 to achieve miR-137 over expression represents the baseline signal. No change in signal intensity is observed in B35 cells co-transfected with sponge-miR-137 and mimic-miR-NT compared to the control. Fluorescence intensity is significantly decreased when sponge-miR-137 is co-transfected with mimic-137 compared to co-transfection of control with mimic-137. Data are shown as mean ±SEM, **P*< 0.05 and ****P*<0.001 by one-way ANOVA followed by post-hoc Bonferroni’s correction for multiple testing, $F_{(3, 20)} = 7.12$, $P < 0.01$
(**D)** Graph representing miR-137 expression levels in primary hippocampal neurons infected at 8 DIV with control, sponge-miR-137 and miR-137 overexpressing viruses. MiR-137 over expression results in a significant increase at 21 DIV. Data are shown as mean ±SEM, ****P*<0.001 by one-way ANOVA followed by post-hoc Bonferroni’s correction for multiple testing, $F_{(2, 8)} = 36.2$, $P < 0.001$

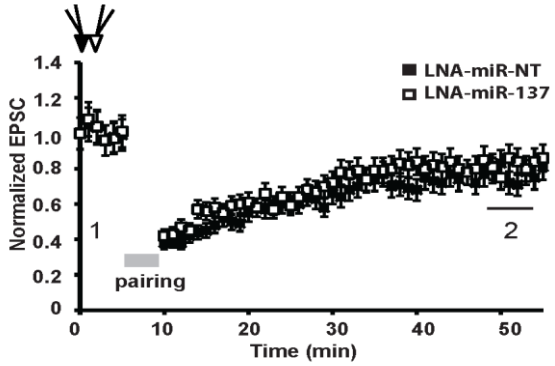

Figure S2. MiR-137 is not required for NMDAr-LTD
NMDAr dependent-LTD was induced in CA1 neurons infused with control LNA-miR-NT (black) and infused LNA-miR-137 (white) using a pairing protocol (-40 mV, 1Hz, 300 stimuli). Normalized AMPAr-mediated EPSCs before and after LTD induction. Error bars represent SEM. n = 5, significance was measured between 35 and 40 min, paired t-test.

Supplemental Experimental Procedures

Animals. Wistar rats (Harlan laboratories, USA) were housed per 2 or 3 animals on a 12-h light cycle in a temperature-controlled (21 ± 1°C) environment with ad libitum access to food and water. Rats were used at E18 or P6-8 for primary neuronal cultures or organotypic hippocampal slices, respectively. All experiments involving animals were evaluated and approved by the Committee for Animal Experiments of the Radboud University Nijmegen Medical Centre, Nijmegen, The Netherlands.

Cloning of GluA1 3'UTR. The 3'UTR of GluA1 was PCR amplified from mouse brain cDNA (C57BL/6) and the 2.6 kb-fragment was ligated to the XbaI-site of pGL4 (Promega). The miR-137 binding site was mutated by site-directed mutagenesis.
The following primers were used:
GluA1-3'UTR(XbaI)-fw: GATCTCTAGACTGGAGCAGACAGGAAACCCTTGGG;
GluA1-3'UTR(Nhe)-rv:
GATCGCTAGCTAATGGGTCCACAGTGATTTAATTCTTGTG
GluA1-3'UTR-137mut-fw: CTAACTCTATGCTGAATTCACGGGAGAGATCC
GluA1-3'UTR-137mut-rv: GGATCTCTCCCGTGAATTCAGCATAGAGTTAG

Luciferase assay. Primary rat hippocampal neurons (14 DIV) were co-transfected with pGL4-GluA1 3'UTR and pGL4-RL (pGL4 carrying a humanized Renilla ORF for normalization) plus 10 nM miR-137 pLNA or control B pLNA (Exicon). Luciferase activity was measured after 3 days using the Dual Luciferase Reporter System (Promega). For the gene activity experiments involving the miR-137 sponge, 4 DIV hippocampal neurons were infected with lentiviral particles encoding either the miR-137-sponge or the GFP, followed by transfection of luciferase vectors at 14 DIV. Luciferase activity was measured at DIV 17.

Quantitative real-time PCR (qPCR) Analysis. Total RNA was extracted from primary neurons or slice cultures using the miRNeasy Mini Kit following manufacturer

instructions (Qiagen). Total RNA was reverse-transcribed using the miScript II RT Kit (Qiagen). qPCR was performed with the miScript SYBR Green PCR Kit (Qiagen). Mature miR-137 was detected using the miScript Primer Assay (Qiagen) and precursor-miR-137 was amplified using the following primers (5'➔3'): pre-miR-137 forward: GTGACGGGTATTCTTGGGT; pre-miR-137 reverse: GACTACGCGTATTCTTAAGCAA. MiR expression was normalized to rat U6 and β-actin using GeNorm (Vandesompele et al., 2002). GluA1 forward, CGAGTTCTGCTACAAATCCCG; GluA1 reverse, TGTCCGTATGGCTTCATTGATG; β-Actin forward, CCAGATCATGTTTGAGACCTTC3; β-Actin reverse, AGGATCTTCATGAGGTAGTCTG; U6 snRNA forward, GCTTCGGCAGCACATATA; U6 snRNA reverse, CGCTTCACGAATTTGCGT. Each sample was examined at least three independent times by qPCR.

Western blot. Primary hippocampal neurons were infected at 8 DIV with control (GFP alone), sponge-miR-137, or miR-137 expressing lentivirus. Neurons were harvested at 14 DIV and homogenized in ice-cold lysis buffer (50 mM Tris [pH 7.4], 150 mM NaCl, 1 mM EDTA, 1% TritonX-100, 5 mM NaF, 2 mM Na_3VO_4, 4 mM $Na_2P_2O_7$ and protease inhibitors). Total lysates were subjected to Western blot analysis with anti-GluA1 (MAB2263, Millipore) and anti-γ-tubulin (T5326, Sigma) as a loading control.

Virus production. Viral particles were prepared by cotransfection of HEK-293T cells with a FUGW plasmid, the HIV-1 packaging vector Δ8.9, and the VSVG envelope glycoprotein vector using the calcium phosphate co-precipitation method. HEK293T cells were placed overnight in a 3% CO2 humidified 37°C incubator. The following day, medium was replaced by fresh ultraculture (Lonza) containing 4 mM valproate (Sigma) and the CO2 percentage was set to 10 %. Supernatants were collected 24h and 48h later.

Viral particles were purified over a 20 % sucrose cushion by ultracentrifugation for 3 hours at 21.000 RPM. Viral particles were resuspended in PBS without Ca^{2+} and Mg^{2+} (Life technologies), and stored at -80°C until use.

Electrophysiology. Whole-cell recordings in cultured slices were obtained with Multiclamp 700B amplifiers (Axon Instruments). To study the effects of miR-137 on synaptic transmission, cultured slices from P6-8 rats (Wistar) were infected with either control, sponge-miR-137, or miR-137 lentiviruses directly upon plating. Eight to ten days later, whole-cell recordings were obtained simultaneously from an infected and an adjacent uninfected neuron in the CA1 region under visual guidance, using epifluorescence and transmitted light illumination. The recording chamber was perfused with artificial cerebrospinal fluid (ACSF) containing 119 mM NaCl, 2.5 mM KCl, 4 mM $CaCl_2$, 4 mM $MgCl_2$, 26 mM $NaHCO_3$, 1 mM NaH_2PO_4, 11 mM glucose, 0.1 mM picrotoxin, 4 μM 2-chloroadenosine [pH 7.4], and gassed with 5% CO_2/95% O_2. Recordings were made at 30°C. Patch recording pipettes (3–5 MΩ) were filled with intracellular solution containing 115 mM cesium methanesulfonate, 20 mM CsCl, 10 mM HEPES, 2.5 mM $MgCl_2$, 4 mM Na_2ATP, 0.4 mM Na_3GTP, 10 mM sodium phosphocreatine, and 0.6 mM EGTA [pH 7.25]. Evoked responses were induced using bipolar electrodes (FHC) placed on Schaffer collateral pathway (0.1 Hz). Responses were recorded at both -60 mV (for AMPAr-mediated responses) and +40 mV (for NMDAr-mediated responses). NMDAr-mediated responses were quantified as the mean between 60 and 65 ms after stimulation. All recordings were performed by stimulating two independent synaptic inputs. Results from each pathway were averaged and counted as n = 1. All data are reported as mean ± SEM. Statistical significance was determined by the paired Student's t-test (for paired recordings). Failure rate experiments were performed using minimum stimulation. Failure rate was calculated as a percentage of failed evoked responses over 50 sweeps at a holding potential of -60 and +40 mV. We used the peak amplitudes of individual responses as the criterion for defining success or failure. The peak amplitudes of each response were measured in Clampfit (Axon). We used a threshold (10 pA for responses at -60 mV and 20 pA for responses at +40 mV) as a cutoff criterion—responses with a peak amplitude above the threshold were counted as success.

The success trials had a clear response above the baseline and all displayed kinetics in line with evoked responses. The percentage of silent synapses was calculated as 1-(LN failure rate -60mV)/(LN failure rate +40 mV) (Isaac et al., 1995; Liao et al., 1995)

Spontaneous responses were recorded at -60 mV (mEPSC) in ACSF containing 2.5 mM $CaCl_2$ and 1.2 mM $MgCl_2$ at 30°C. mEPSCs were recorded in the presence of 1 μM TTX and 0.1 mM picrotoxin. Five to ten min of recordings were analyzed from each cell. Data were acquired at 5 kHz, filtered at 2 kHz, and analyzed using the Mini Analysis Program (Synaptosoft, Decatur, USA).

For mGluR-LTD experiments, 130 mM potassium gluconate and 5 mM KCl were substituted for cesium methansulfonate and CsCl in the internal solution. mGluR-LTD was performed on 12 DIV organotypic cultures and was induced by 5 min bath application of 100 μM (R,S)-3,5-dihydroyphenylglycine (DHPG). The cell was held in current clamp during DHPG application and 5 min afterwards (Hsieh et al., 2006; Huber et al., 2001). All recordings were done by stimulating two independent synaptic inputs; results from each pathway were averaged and counted as n = 1. Only recordings with a stable series resistance before and after DHPG application were retained for analysis. PP-LFS induced LTD was induced by a 15 min, 1Hz pair-pulse stimulation (50 ms inter-stimulus interval) in the presence of APV to block NMDArs. NMDAr-LTD was induced by pairing presynaptic stimulation at 1 Hz for 5 min (300 stimuli) with depolarization of the post-synaptic neuron at -40 mV. The EPSC amplitude was normalized to the average baseline amplitude before pairing. For all LTD experiments neurons were filled with intracellular solution containing either LNA-miR-NT or LNA-miR-137 (10 μM) via the patch pipette and baseline recordings was performed for 30 minutes before LTD induction. Please note that all LTD experiments were performed within the same slice using two simultaneous patch-clamp recordings of neighboring CA1 cells; each pipette was filled with one of the LNAs, allowing for a direct comparison between conditions. All data are reported as mean ± SEM. Statistical significance was determined by the paired Student's t- test (for paired recordings) or the Mann-Whitney test (for un-paired recordings). Significance was set to $P < 0.05$.

Primary neuronal cultures and hippocampal slice cultures. All media and reagents were purchased from Life Technologies. Dissociated hippocampal cultures were prepared form gestational day 18 fetal rats (Wistar). Pregnant rats were anaesthetized with isoflurane and sacrificed by cervical dislocation. Embryonic brains were dissected in ice-cold Hank's buffer (HBSS without Ca^{2+} and Mg^{2+}, 100 U/ml penicillin, 100 µg/ml streptomycin, 1x Glutamax). The hippocampi were separated from the cortices and incubated with 0.025% trypsin for 15 min at 37°C. Neurons were mechanically dissociated in NeuroBasal medium containing 10% FCS and 1x GlutaMax (Invitrogen) using fire-polished Pasteur pipettes. The cell suspension was filtered through a 70 µm cell strainer (BD Falcon) and plated on poly-D-lysine (Invitrogen, 70.000-150.000) pre-coated glass coverslips in 24-wells plates at a density of 25.000 neurons per well. Medium was replaced after 6 hours with Neurobasal medium containing B27 supplement, and 1x GlutaMax. Neurons were maintained in a 5% CO2 humidified 37°C incubator. One-third of the medium was refreshed every three to four days.
Hippocampal slice cultures were prepared from P6-8 rats. Slices were infected on the same day of preparation (0 DIV) with lentiviral particles in the CA1 pyramidal cell layer using a pico-liter injector (Warner instruments). Slices were maintained in a 5 % CO2 humidified 35°C incubator on slice culture medium (pH 7.3, osmolarity 325) consisting of MEM, 20 % horse serum, 1 mM L-Glutamine, 1 mM $CaCl_2$, 2 mM $MgSO_4$, 0.25 mg Insulin, 1.25 mM Ascorbic acid, 12.87 mM D-Glucose, 5.25 mM $NaHCO_3$ and 30 mM Hepes. Medium was refreshed every 2 days.

Pharmacological treatment of cultured slices. Organotypic hippocampal slices were stimulated with 100 µM of the mGluR agonist (S)-3,5-dihydroxyphenylglycine (DHPG) (Tocris bioscience) for 15 minutes. The antagonists LY367385 (100 µM, Tocris Bioscience) and 2-Methyl-6-(phenylethynyl)pyridine (MPEP, 10 µM, Tocris Bioscience) were used (with a 30 min preincubation) to block mGluR1, and mGluR5, respectively. Following drug treatment slices were snap-frozen in liquid nitrogen and stored at -80 °C until RNA isolation.

*Immunocytochemistry***.** For immunocytochemistry, primary hippocampal neurons were fixed at 21 DIV in prewarmed 4% PFA/sucrose in PBS for 20 min at room temperature. For surface labeling of the AMPAr, non-permeabilized neurons were washed with PBS and blocked with 1% Bovine Serum Albumin (BSA) in PBS for 30 min. Surface AMPArs were labeled with extracellular N-terminal domain-specific antibodies anti-GluA1 (MAB2263, Millipore) or anti-NR1 (N308/48, NeuroMab) in 1% BSA in PBS at 4 °C overnight. After thorough washing, neurons were permeabilized using 0,1% triton X-100 for 5 min, washed, and blocked with 1% BSA in PBS for 30 min. Neurons were incubated overnight with anti-GFP (A10262 life technologies) diluted 1/500 in 1% BSA at 4 °C. Secondary antibody incubation was done the next day with Alexa-488, Alexa-568 and/or Alexa-647 (Molecular Probes) for 1 hour at room temperature. Coverslips were mounted in ProLong Gold (Life Technologies).

Image analysis. For AMPAr expression analysis images of infected neurons were captured using a Leica TCS SP2 AOBS Confocal Laser Scanning Microscope (CLSM) at 63x magnification. All the parameters (pinhole, gain, contrast, and brightness) were kept constant for neuronal cells from the same experiment. Quantitative analysis was performed using ImageJ software. Pictures were corrected for background fluorescence. GluA1 and NR1 immunoreactive puncta were defined as discrete points along a dendrite within 50 μm from the soma. Puncta were analyzed in 2 to 3 dendrites for each neuron. The number of puncta for each dendrite was averaged, which represent the value of that cell, and this value equals an n of 1. For calculating the % of silent synapses we counted the amount of NR1 puncta co-localizing with GluA1 puncta versus NR1 puncta without co-localizing GluA1 puncta. For dendritic spine analysis spines were imaged using CLSM above using an optical zoom of eight. Neuronstudio software was used to quantify spine density by determining the amount of spines per um of dendrite. Spines were assigned mature or immature and spine head diameter was measured.

Supplemental References

Gentner, B., Schira, G., Giustacchini, A., Amendola, M., Brown, B.D., Ponzoni, M., and Naldini, L. (2009). Stable knockdown of microRNA in vivo by lentiviral vectors. Nat Methods *6*, 63–66.

Hsieh, H., Boehm, J., Sato, C., Iwatsubo, T., Tomita, T., Sisodia, S., and Malinow, R. (2006). AMPAR removal underlies Abeta-induced synaptic depression and dendritic spine loss. Neuron *52*, 831–843.

Huber, K.M., Roder, J.C., and Bear, M.F. (2001). Chemical induction of mGluR5- and protein synthesis-dependent long-term depression in hippocampal area CA1. J Neurophysiol *86*, 321–325.

4.3 Störchel et al., 2015

Synopsis

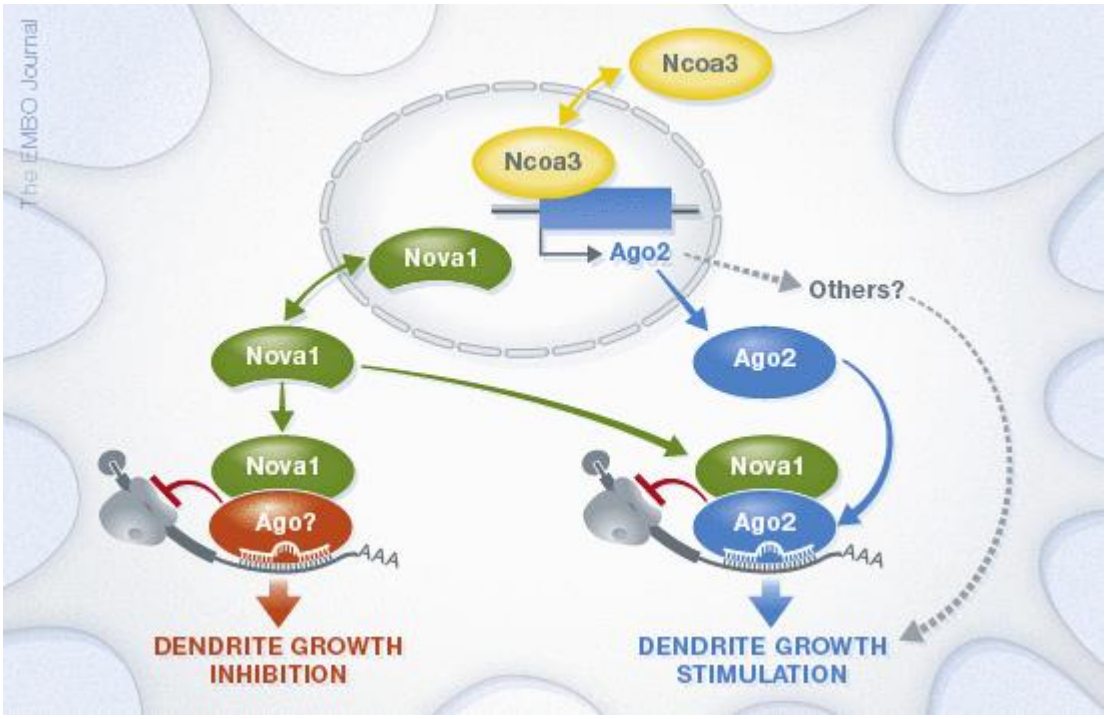

The identification of two novel modulators of miRNA function reveals an additional layer of transcriptional and post-transcriptional control of Argonaute proteins and adds further insight on the central role for miRNAs in neurogenesis.

- Large-scale RNAi screen identifies novel miRNA regulatory proteins in primary neurons.
- Ncoa3 and Nova1 are required for the repressive activity of the spine-regulating miR-134.
- Nova1 is a general, miRISC-associated miRNA regulatory RBP in neurons.
- Ncoa3 regulates a specific subset of miRNA target interactions involved in the control of dendritogenesis.
- Ncoa3-dependent transcriptional regulation of the miRISC protein Ago2 is required for the control of miRNA activity and dendritogenesis.

Keywords: Ago2, dendrite, miRNA, Ncoa3, Nova1
Received November 24, 2014.
Revision received May 8, 2015.
Accepted May 20, 2015.

Published online: June 23, 2015

Article

SOURCE DATA | TRANSPARENT PROCESS

THE EMBO JOURNAL

A large-scale functional screen identifies Nova1 and Ncoa3 as regulators of neuronal miRNA function

Peter H Störchel‡, Juliane Thümmler‡, Gabriele Siegel†, Ayla Aksoy-Aksel, Federico Zampa, Simon Sumer & Gerhard Schratt*

Abstract

MicroRNAs (miRNAs) are important regulators of neuronal development, network connectivity, and synaptic plasticity. While many neuronal miRNAs were previously shown to modulate neuronal morphogenesis, little is known regarding the regulation of miRNA function. In a large-scale functional screen, we identified two novel regulators of neuronal miRNA function, Nova1 and Ncoa3. Both proteins are expressed in the nucleus and the cytoplasm of developing hippocampal neurons. We found that Nova1 and Ncoa3 stimulate miRNA function by different mechanisms that converge on Argonaute (Ago) proteins, core components of the miRNA-induced silencing complex (miRISC). While Nova1 physically interacts with Ago proteins, Ncoa3 selectively promotes the expression of Ago2 at the transcriptional level. We further show that Ncoa3 regulates dendritic complexity and dendritic spine maturation of hippocampal neurons in a miRNA-dependent fashion. Importantly, both the loss of miRNA activity and increased dendrite complexity upon Ncoa3 knockdown were rescued by Ago2 overexpression. Together, we uncovered two novel factors that control neuronal miRISC function at the level of Ago proteins, with possible implications for the regulation of synapse development and plasticity.

Keywords Ago2; dendrite; miRNA; Ncoa3; Nova1
Subject Categories Neuroscience; RNA Biology
DOI 10.15252/embj.201490643 | Received 24 November 2014 | Revised 8 May 2015 | Accepted 20 May 2015

Introduction

MicroRNAs (miRNAs) are a large family of small non-coding RNAs that regulate gene expression post-transcriptionally. Over the last 10 years, miRNAs have been implicated in the regulation of virtually every aspect of mammalian nervous system development, including neurogenesis, neuronal differentiation, and plasticity (Fiore *et al*, 2011; Im & Kenny, 2012). A subset of neuronal miRNAs localizes within the synapto-dendritic compartment, where they constitute a regulatory layer in local mRNA translation and the control of synaptic plasticity (Siegel *et al*, 2011). Arguably, the best studied synaptic miRNA is miR-134, which (i) is required for activity-dependent dendritogenesis and synaptic scaling by inhibiting Pumilio2 (Fiore *et al*, 2009, 2014), (ii) mediates spine shrinkage by repressing Lim-domain protein kinase 1 (Schratt *et al*, 2006), and (iii) impairs synaptic plasticity and memory in the mouse hippocampus *in vivo* by downregulating CREB (Gao *et al*, 2010). Other examples of functionally important miRNAs are miR-138, which restricts the growth of dendritic spines by targeting the depalmitoylating enzyme APT1, and the highly conserved let-7, which regulates BDNF-dependent dendritogenesis and axon regeneration (Huang *et al*, 2012; Zou *et al*, 2013).

MiRNAs bind the 3′ untranslated region (UTR) of target mRNAs via partial base-pair complementarity, thereby inducing translational repression and/or decay of their targets (Eulalio *et al*, 2008; Krol *et al*, 2010). The miRNA-induced silencing complex (miRISC) is a large multi-protein complex that mediates miRNA activity (Tang, 2005). The Argonaute (Ago) family of proteins are the main catalysts of miRNA function as they serve as a platform for miRISC assembly on the target mRNA (Meister, 2013). The mammalian genome comprises four genes encoding for Ago subfamily proteins (Ago1–4), all of which are capable of miRNA-mediated gene silencing. Ago2 is the only member that possesses nuclease ("slicer") activity (Liu *et al*, 2004), and therefore is capable of endonucleolytic cleavage of targets in the case of perfect complementarity between the miRNA and the target, which is a rare event in mammals. GW182 (Tnrc6a-c in mammals) proteins represent other core components of miRISC, which help to recruit different effector complexes onto miRNA target mRNAs to induce translational repression and/or mRNA decay (Fabian & Sonenberg, 2012).

miRISC activity is regulated by signal-dependent modification of accessory factors in response to environmental cues. In neurons, activity-dependent degradation of Mov10 was shown to impair miRISC activity, thereby allowing local protein synthesis at synapses

Institute for Physiological Chemistry, Biochemical-Pharmacological Center Marburg, Philipps-University Marburg, Marburg, Germany
*Corresponding author. Tel: +49 6421 28 65020; E-mail: schratt@staff.uni-marburg.de
‡These authors contributed equally to this work
†Present address: Division of Psychiatry Research, Systems and Cell Biology of Neurodegeneration, University of Zurich, Schlieren, Switzerland

to occur (Banerjee *et al*, 2009). A similar mechanism involving the Mov10 homologue Armitage is further involved in the formation of long-term memories in *Drosophila* (Ashraf *et al*, 2006). Finally, dephosphorylation of FMRP in response to elevated activity leads to a release of miRISC from target mRNAs at synapses, thereby allowing synaptic protein synthesis to occur (Muddashetty *et al*, 2011). In addition, several RNA-binding proteins (RBPs) that do not directly associate with miRISC, but are recruited to the same targeted mRNA, have been previously shown to modulate the effect of miRNAs in non-neuronal cells, including Pumilio (Kedde *et al*, 2010), HuR (Bhattacharyya *et al*, 2006), and DND1 (Kedde *et al*, 2007). However, a comprehensive analysis of miRISC regulation by RBPs in neurons has not been performed.

Here, we interrogated the function of 286 RBPs in neuronal miRISC regulation using siRNA screening in primary mouse cortical neurons. Thereby, we identified Nova1 as a neuron-specific miRISC component and Ncoa3 as a regulator of Ago2 expression. We suggest that neuron-specific modulators of miRISC function such as Nova1 and Ncoa3 could play important roles in activity-dependent gene regulation during synapse development and plasticity.

Results

To identify RBPs that modulate the repressive activity of miRNAs in neurons, we combined siRNA-mediated RBP knockdown with a luciferase-based reporter gene readout (Fig 1A). Our siRNA library consisted of three different synthetic siRNAs for each of the 286 RBPs which had been shown to be expressed in the postnatal mouse cortex (McKee *et al*, 2005) (Supplementary Dataset S1). For the screen, each individual siRNA was co-transfected into primary mouse cortical neurons (5 days *in vitro* DIV) along with a miR-134-responsive luciferase reporter gene (UBE3A-luc) (Valluy *et al*, 2015) and synthetic miR-134 duplex RNA. miR-134 duplex RNA is directly loaded into miRISC, thereby allowing us to focus on the effects of RBPs downstream of Dicer-dependent pre-miRNA processing. We observed a highly reproducible about 40% repression of UBE3A-luc expression by miR-134 in the absence of additional siRNA. If a given RBP was required for the repressive function of miR-134, the knockdown of the RBP should completely (100%) relieve the miR-134-mediated repression of UBE3A-luc. Because individual siRNAs display different degrees of efficacy, we considered RBPs as positive hits if at least two of three RBP-targeting siRNAs resulted in an at least 50% relief of miR-134-mediated repression averaged over the three independent screen replicates. Results of the analysis using this cutoff are shown in Fig 1B (complete study results in Supplementary Dataset S2). Two known miRISC-associated proteins (Tnrc6c, Ddx6) fulfilled our hit selection criteria (Chu & Rana, 2006; Landthaler *et al*, 2008). In addition, 31 out of 36 siRNAs directed against twelve known regulators of miRNA function (Ago family proteins, Fmr1, Pabpc family members, Tnrc6a) relieved repression of the miR-134 reporter, although the effect was not strong enough to qualify them as hits. This demonstrates that (i) our screen setup allows the identification of miRISC regulatory RBPs; and (ii) our criteria for the selection of hits are very stringent, thereby reducing the number of false positives. In addition to Tnrc6c and Ddx6, ten novel RBPs that had not been previously reported to be involved in miRNA function were identified as hits (Fig 1B). These include RBPs implicated in mRNA translation (Rpl5) (Meskauskas & Dinman, 2001), mRNA decay (Lsm7) (Tharun *et al*, 2000), splicing (Nova1, U2af1, Rbm25) (Jensen *et al*, 2000; Mollet *et al*, 2006; Zhou *et al*, 2008), mRNA nuclear export (Nxf1, Nxt1) (Stutz & Izaurralde, 2003), and transcription (Ewsr1, Fubp1, Ncoa3) (Law *et al*, 2006; Xu *et al*, 2009; Zhang & Chen, 2013). Since most of the identified candidates are involved in general RNA metabolism, we considered the possibility that knockdown of these RBPs could affect reporter gene expression independent of miRNAs. Therefore, we conducted a secondary RNAi screen for all the hits where we now also included a condition without miR-134 ("−miR" condition; Fig 1C). If the RBP regulates reporter gene expression independent of the transfected miRNA, a similar upregulation of reporter gene expression would be observed in the "+miR" and the "−miR" conditions compared to the respective basal or control siRNA conditions and the ratio "+miR/−miR" would be comparable over all experimental conditions. The validation experiments were performed in rat neurons using siRNAs with conserved target sequences between mouse and rat mRNAs. In addition, an improved reporter gene system (pGL4) was used to further minimize non-specific effects. Using this experimental setup, knockdown of three (Nova1, Ncoa3, Ewsr1) out of the original ten positive hits resulted in a significant increase in the ratio +miR/−miR, suggesting that only these three RBPs specifically affect miR-134-dependent repression of UBE3A-luc. Specific derepression of miRNA target expression by RBP knockdown was further confirmed by our results using a plasmid without miR-134-binding site (Supplementary Fig S1A). The efficacy of the siRNAs targeting Nova1, Ncoa3, and Ewsr1 was validated by Western blot. Each of the three siRNAs led to a specific knockdown of the respective GFP-tagged proteins in HEK293 (Supplementary Fig S1B). Together, we could identify three novel proteins (Nova1, Ncoa3, and Ewsr1) that are specifically required for the repressive function of miR-134. To assess whether these RBPs modulate miRNA activity in a more general fashion, we extended our analysis to another neuronal miRNA, miR-138, and its validated target APT1 (Siegel *et al*, 2009). Knockdown of Nova1 and Ncoa3 led to a significant derepression of APT1-luc reporter expression (Fig 1D) which was comparable to the effects observed with UBE3A-luc. In contrast, the Ewsr1-targeting siRNA had no effect on APT1-luc expression. We conclude that Nova1 and Ncoa3 are required for the repressive function of multiple neuronal miRNAs and therefore decided to focus on these RBPs for further characterization.

We next studied the expression of Nova1 and Ncoa3 proteins in post-mitotic neurons by Western blot analysis. Nova1 was expressed throughout the *in vitro* development of primary rat hippocampal (Fig 2A) and cortical neurons (Supplementary Fig S2A). The anti-Nova1 antibody was specific, since the Nova1 band was absent when Western blots were performed with total brain lysates from Nova knockout mice (Supplementary Fig S2B). Ncoa3 expression in hippocampal neurons peaked at seven DIV, declined until 14 DIV, and became undetectable at 18 DIV (Fig 2B; Supplementary Fig S2C). Using immunocytochemistry (ICC), we observed that both proteins localized to the nuclear and cytoplasmic compartment of hippocampal neurons (14 DIV: Fig 2C–F; 7 DIV: Supplementary Fig S2D). The majority of cytoplasmic Nova1 protein was detected as granular structures in the neuronal soma, but some Nova1-positive granules extended into proximal dendrites that could be identified by co-staining for the dendritic marker MAP2 (arrows in Fig 2D).

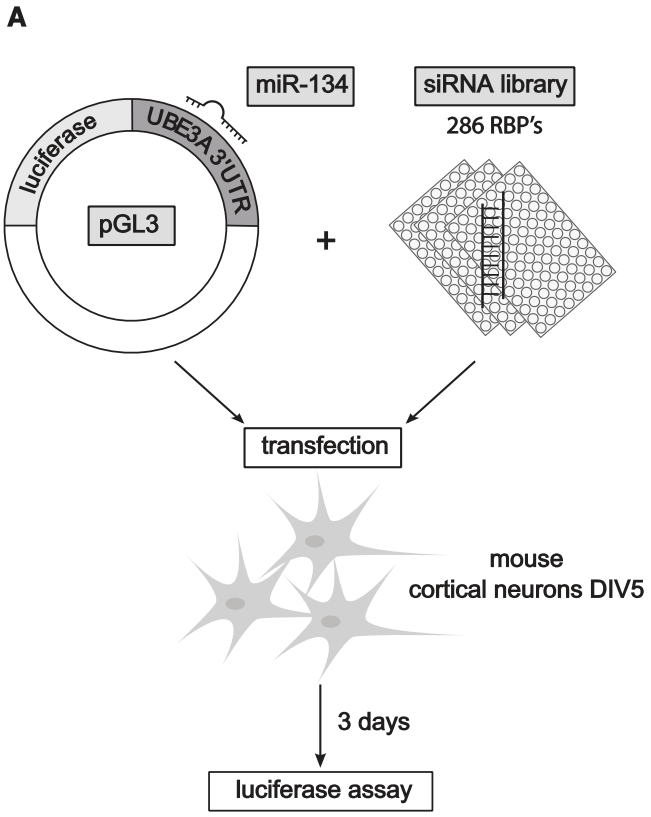

B

	gene	siRNA1	siRNA2	siRNA3
known genes	Ago1	-45.3	7.7	98.5
	Ago2	10.4	19.8	8.9
	Ago3	-4.5	11.1	17.0
	Ago4	21.1	19.8	21.0
	Fmr1	34.7	23.3	37.6
	Pabpc1	-44.1	-1.2	46.0
	Pabpc2	49.1	23.2	52.0
	Pabpc4	81.5	25.7	35.5
	Pabpc5	-2.9	23.0	11.6
	Tnrc6a	121.9	16.6	42.6
	Tnrc6c	77.9	51.9	54.5
	Ddx6	94.7	105.2	127.1
hits	Ewsr1	104.1	43.8	170.9
	Fubp1	108.9	83.9	14.5
	Lsm7	-2.8	157.6	154.6
	Ncoa3	27.4	79.5	107.9
	Nova1	47.9	215.0	84.1
	Nxf1	183.4	137.8	154.4
	Nxt1	16.0	96.8	86.3
	Rbm25	74.8	150.0	89.2
	Rpl5	276.3	173.1	-6.4
	U2af1	98.3	15.6	94.0

% relief of miRNA-mediated repression

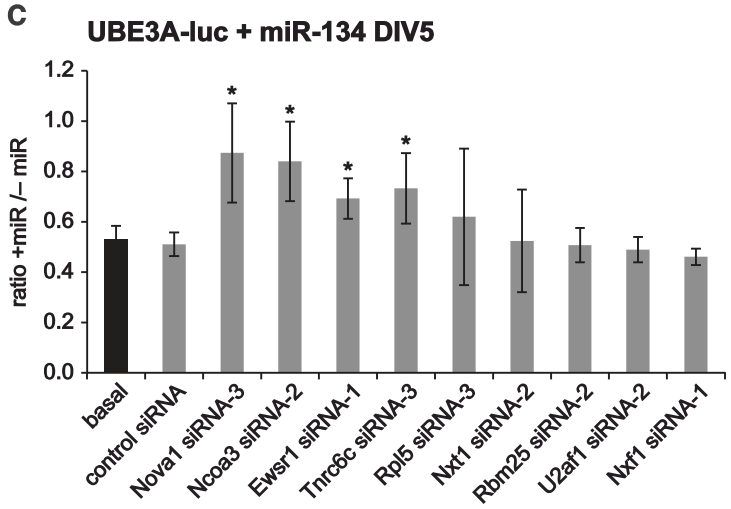

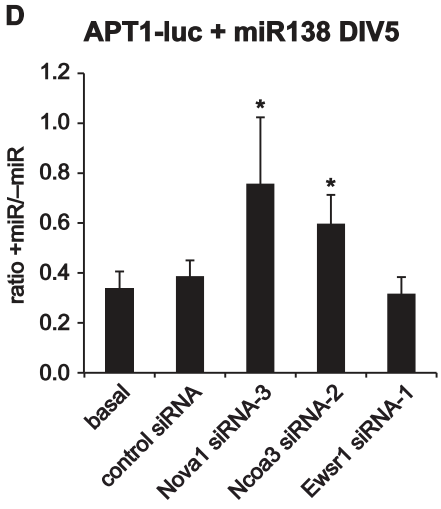

Figure 1. Identification of 12 RNA-binding proteins required for miR-134 repressive function in primary neurons using siRNA-based screening.

A Setup of the RNAi screen in mouse primary cortical neurons. Neurons (5 days *in vitro* (DIV)) were co-transfected with the miR-134-responsive pGL3-UBE3A-3′UTR luciferase reporter (pGL3-UBE3A-luc) together with miR-134 duplex RNA and siRNA (one per condition) directed against 286 RBPs expressed in the mouse cortex (3 siRNAs per RBP). Luciferase activity was determined 3 days after transfection.

B Table of genes which are either known to be involved in the regulation of miRNA activity ("known genes") or whose knockdown led to an at least 50% relief of miRNA-mediated repression for at least two out of the three siRNAs tested ("hits"). Values are the average of three replicate experiments and represent the percent relief of miRNA-mediated repression for the indicated siRNA compared to a condition without siRNA. Note that two known genes (Tnrc6c, Ddx6) were also present within the 12 hits.

C Luciferase reporter assay in primary rat cortical neurons transfected with pGL4-UBE3A-luc and the indicated siRNAs in the presence or absence of miR-134 duplex RNA. The ratio of normalized luciferase activity from neurons with ("+miR") to neurons without co-transfected miR-134 ("−miR") is plotted. Values are the average from three independent experiments ± standard deviation. *$P < 0.05$ (unpaired *t*-test compared to control siRNA).

D Luciferase reporter assay as in (C) with pGL4-APT1 3′UTR (APT1-luc) in the presence ("+miR") or absence ("−miR") of miR-138. $n = 3$. *$P < 0.05$ (unpaired t-test compared to control siRNA).

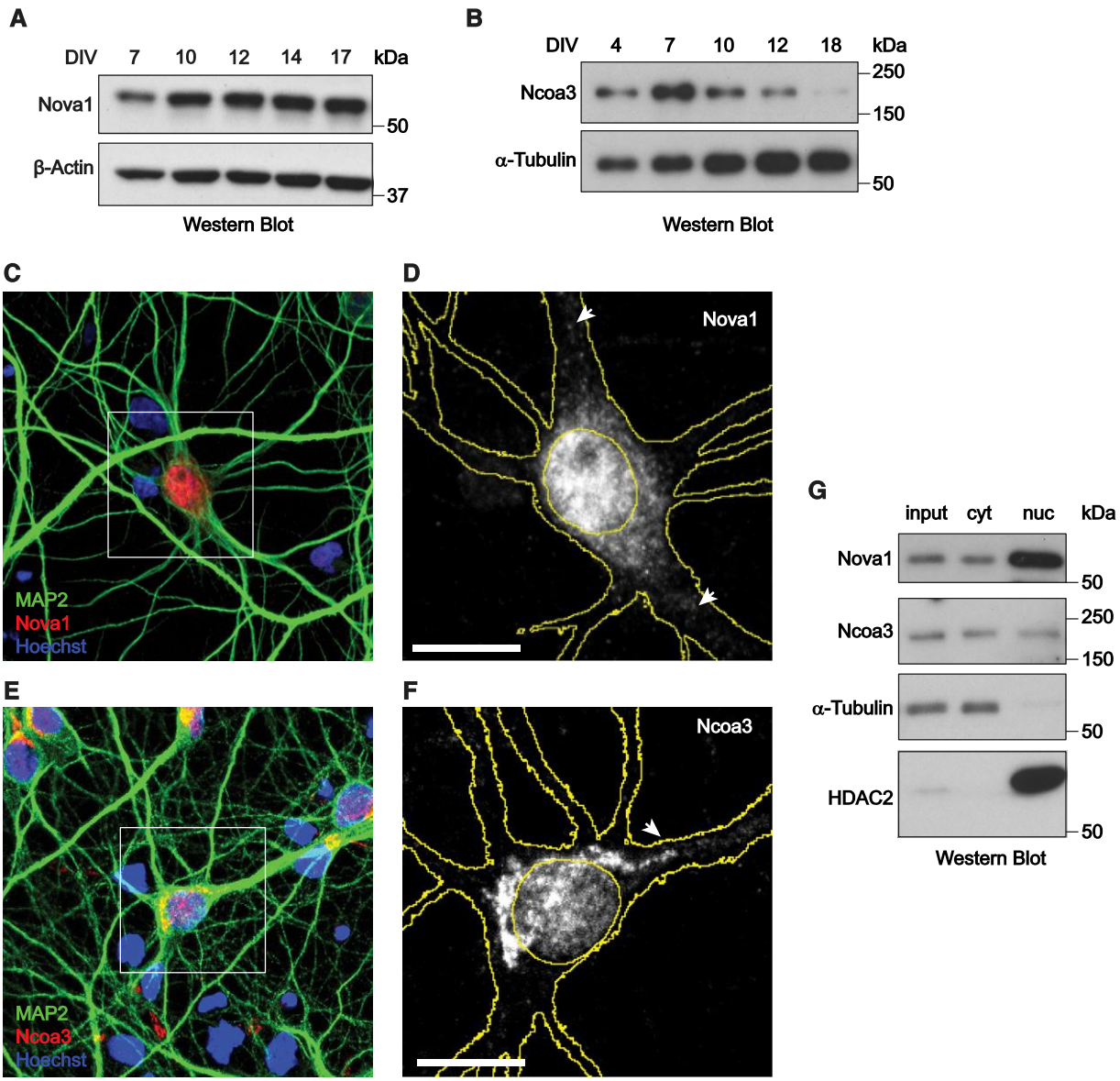

Figure 2. Nova1 and Ncoa3 are expressed in developing rat hippocampal neurons in culture.

A, B Western blot analysis of Nova1 (A) and Ncoa3 (B) proteins using whole-cell extracts harvested from FUDR-treated (B) or non-treated (A) rat hippocampal neurons at the indicated days of *in vitro* (DIV) culture. α-tubulin or β-actin was used as a loading control.

C–F Immunocytochemistry analysis of Nova1 (C, D) and Ncoa3 (E, F) expression (red) in hippocampal neuron cultures at 14 DIV. MAP2 staining (green) was used to visualize neurons and Hoechst staining (blue) to visualize nuclei. (D, F) Magnification of insert depicted in (C) or (E), respectively. For simplicity, only the Nova1 (D) or Ncoa3 (F) signal is shown in grayscale. Cell and nuclear outlines derived from MAP2 and Hoechst staining, respectively, are shown in yellow. Scale bar = 10 μm.

G Western blot analysis of Nova1 and Ncoa3 using whole-cell lysates (input), cytoplasmic (cyt) or nuclear (nuc) fractions from FUDR-treated rat hippocampal neurons at seven DIV. α-tubulin was used as a cytoplasmic and HDAC2 as a nuclear marker protein.

Source data are available online for this figure.

Similarly, some of the Ncoa3-positive cytoplasmic granules extended into the proximal part of apical dendrites (arrow in Fig 2F), whereas Ncoa3 expression at distal dendrites was generally low. Importantly, the Ncoa3 ICC signal was significantly reduced in cells expressing Ncoa3 shRNA which demonstrates the specificity of the antibody (Supplementary Fig S2E and F). The results obtained by ICC could be confirmed by Western blot analysis of cytoplasmic and nuclear extracts (Fig 2G). Taken together, our results demonstrate that Nova1 and Ncoa3 are expressed in both the nuclear and cytosolic compartments of post-mitotic hippocampal neurons at times of synapse development (7–14 DIV).

We next investigated whether Nova1 and Ncoa3 are required for the repressive function of endogenously expressed miRNAs in rat hippocampal neurons. To this end, we constructed a series of luciferase reporter plasmids consisting of the 3′UTRs of mRNAs targeted by let-7 (LIN41 3′UTR), miR-138 (APT1 3′UTR), or miR-134 (LIMK1 3′UTR). Importantly, these miRNAs are endogenously expressed in post-mitotic neurons and were previously shown to regulate

neuronal morphogenesis via their respective mRNA targets (Schratt *et al*, 2006; Siegel *et al*, 2009; Huang *et al*, 2012). In addition, we cloned luciferase reporters with mutated miRNA-binding sites in order to account for potential miRNA-independent effects. Efficient knockdown of Nova1 and Ncoa3 in rat neurons was achieved by shRNA vectors containing conserved siRNA sequences used in the screen (Supplementary Fig S3A and B). Both Nova1 and Ncoa3 knockdown significantly increased the expression of reporter constructs containing a wild-type APT1 (Fig 3A and B), LIN41 (Fig 3C and D), and LIMK1 3′UTR (Fig 3E). The stimulatory effect of Nova1 and Ncoa3 shRNAs was specific, since reintroduction of shRNA-resistant GFP-fusion proteins at least partially restored basal APT1-luc expression (Fig 3A and B). Mutation of the two let-7-binding sites in the context of the LIN41 3′UTR (Fig 3C and D) or of the miR-134-binding site in the context of the LIMK1 3′UTR (Fig 3E) largely abolished Nova1 and Ncoa3 shRNA-mediated upregulation of the reporters, suggesting that the effects are to a large extent miRNA-dependent. The miR-134 target UBE3A-luc was selectively upregulated by the Nova1, but not by the Ncoa3 shRNA (Supplementary Fig S3C). Similar observations were made for the miR-124 target IQGAP1 (Lim *et al*, 2005) and another let-7 target, HMGA2 (Nishino *et al*, 2008) (Supplementary Fig S3D and E). Finally, repression of a reporter construct containing multiple sequential miR-138-binding sites, but lacking a specific 3′UTR context ("miR-138 sponge-luc"), was specifically relieved by Nova1 knockdown (Fig 3F). In addition, Nova1 overexpression significantly reduced the expression of APT1 and UBE3A-luc reporters in neurons (Supplementary Fig S3F and G). Collectively, these results suggest that Nova1 is a general stimulator of neuronal miRNA activity, whereas Ncoa3 regulates a specific subset of neuronal miRNA targets depending on the 3′UTR sequence context.

We next examined whether the observed regulation of miRNA reporter genes by Nova1 and Ncoa3 translated into alterations in endogenous miRNA target protein levels in neurons. Therefore, we focused on the regulation of Limk1 by miR-134, which is important during dendritic spine morphogenesis (Schratt *et al*, 2006). We observed increased levels of Limk1 in hippocampal neurons infected with recombinant adeno-associated virus (rAAV) expressing Nova1 shRNA compared to control shRNA-infected cells (Fig 4A; Supplementary Fig S4A and B). Similarly, rAAV-mediated Ncoa3 knockdown was accompanied by significantly elevated Limk1 protein levels (Fig 4B; Supplementary Fig S4C–E). Taken together, both Nova1 and Ncoa3 are required for efficient repression of the miR-134 target Limk1, consistent with a positive regulation of miR-134 activity by these RBPs. To directly examine the functional significance of Nova1- and Ncoa3-dependent Limk1 regulation, we investigated whether these proteins are involved in spine shrinkage following miR-134 overexpression (Schratt *et al*, 2006). As expected, miR-134 overexpression led to a significant reduction in average spine volume in control cells, an effect that was almost completely abolished in the presence of both the Nova1 and Ncoa3 shRNA (Fig 4C and D). These results indicate that the positive regulation of miR-134 activity by Nova1 and Ncoa3 is functionally relevant during spine morphogenesis.

We next investigated the mechanisms underlying the miRNA regulatory function of Nova1 and Ncoa3. Our results from reporter assays suggest that Nova1 regulates the expression of miRNA targets independent of the 3′UTR context (Fig 3). This raises the question whether Nova1 is directly associated with the neuronal miRISC. To address this, we studied a potential interaction between Nova1 and Ago using co-immunoprecipitation (co-IP) assays in rat hippocampal lysates. Western blot analysis demonstrated efficient pull-down of Ago proteins using a mouse monoclonal anti-pan-Ago antibody (Fig 5A, upper panel). Importantly, we were able to specifically detect Nova1 in pan-Ago IPs, but not in control IgG IPs (Fig 5A; Supplementary Fig S5A, middle panels). The interaction of Nova1 with Ago was weak, since only 2% of Nova1 present in the input could be recovered by Ago IP (Supplementary Fig S5B). The amount of co-precipitated Nova1 was unaltered in the presence of RNase (Supplementary Fig S5C and D), suggesting that Nova1 and Ago reside in a protein complex. To further confirm an interaction of Nova1 with endogenous miRNA targets, we performed RNA immunoprecipitation (RIP) experiments (Fig 5B). A protocol was chosen that preserves protein–protein interactions, so that indirect Nova1 target mRNA interactions that are mediated by associated RBPs (e.g., Ago) could also be detected. Limk1 mRNA, in contrast to GAPDH mRNA, was significantly enriched in Nova1-RIP samples compared to IgG-RIP controls, suggesting a specific interaction between Nova1 and endogenous Limk1 mRNA (Fig 5B). The previously reported Nova1 target Rgs4 served as a positive control (Licatalosi *et al*, 2008). We have previously shown that the miR-134-dependent repression of Limk1 is reversed by BDNF stimulation (Schratt *et al*, 2006). Having shown that Nova1 interacts with Ago and Limk1 mRNA, we asked whether Nova1 was involved in BDNF-regulated Limk1 synthesis. We observed that the stimulatory effect of BDNF on a destabilized Limk1-luc reporter (Limk1-lucPEST) was occluded by Nova1 knockdown (Fig 5C), consistent with a role of Nova1 in the dynamic regulation of the Limk1-associated miRISC in response to BDNF. To get further mechanistic insight into the gene regulatory function of Nova1 within miRISC, we performed tethering assays (Pillai *et al*, 2005). Hereby, a protein of interest is artificially recruited to target RNAs by virtue of an N-terminal fusion of the lambda-phage N-peptide that allows binding to stem-loop sequences (boxB) present in the 3′UTR of a reporter RNA. This allowed us to study potential gene regulatory functions of Nova1 on target RNAs independent of the RNA sequence context and the interaction with Ago proteins. When NHA-Nova1 is tethered in this way downstream of a luciferase reporter gene, we observed a significant reduction in luciferase activity compared to a NHA-GFP control construct (Fig 5D). The magnitude of repression was comparable to tethering NHA-Tnrc6c, a known miRISC component. Thus, Nova1 is able to repress mRNA translation when recruited to target RNAs, consistent with a function downstream of Ago. The use of deletion constructs further revealed that both the Nova1 N-terminus (containing the NLS, KH1 and KH2 domains) and C-terminus (containing the NES and KH3 domain) are required for the repressive activity of Nova1 (Fig 5E). Importantly, all NHA-fusion proteins were expressed to comparable levels and localized in hippocampal neurons as expected (Supplementary Fig S5F and G). Nova1 tethering was further sufficient to reduce reporter gene expression in HEK293 cells (Supplementary Fig S5H). Together, our results suggest that Nova1 is part of neuronal miRISC and possesses the ability to repress mRNA translation independent of its sequence-specific RNA-binding activity.

In contrast to Nova1, Ncoa3 is involved in the regulation of a specific subset of miRNA target interactions (Fig 3). Moreover, Ncoa3 did not interact with Ago based on our co-IP experiments

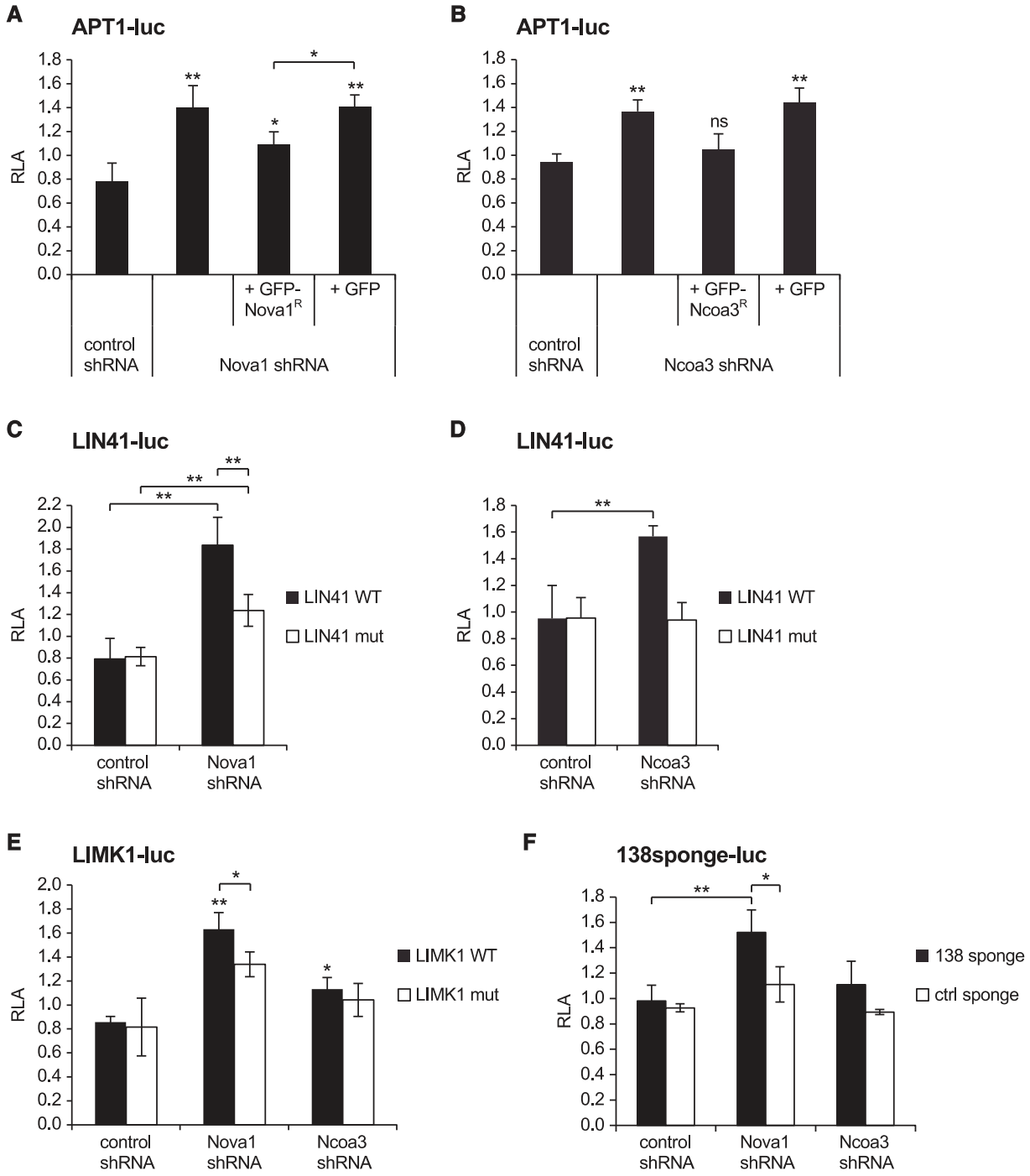

Figure 3. Nova1 and Ncoa3 are required for the repressive activity of a subset of neuronal miRNAs.

A–F Luciferase reporter gene assays performed in rat cortical neurons (14 DIV) (rat hippocampal neurons in (D)) that had been transfected at 11 or 12 DIV with the indicated 3′UTRs fused to the luc gene of pGL4 together with the given shRNA expression construct. In (A, B), additional shRNA-resistant (^{R}) expression constructs for Nova1 and Ncoa3, respectively, or the empty expression vector (GFP) were co-transfected. Relative luciferase activity (RLA) represents the ratio of firefly reporter activity to *Renilla* control reporter activity normalized to a basal condition without shRNA expression vector. Values are the mean ± standard deviation from at least three independent experiments. One-way ANOVA: $P < 0.0001$ (A, C, E), $P < 0.005$ (B, D, F). Tukey's HSD (A–D) and unpaired *t*-test (E, F): $^*P < 0.05$, $^{**}P < 0.01$.

(Fig 5A; Supplementary Fig S5A, lower panels), and tethering of Ncoa3 to a target RNA was not sufficient to cause translational repression (Fig 5F; Supplementary Fig S5F). Together, these results argue against a direct function of Ncoa3 within neuronal miRISC.

Given that Nova1 and Ncoa3 are required for the function of neuronal miRNAs that play important roles in neuronal morphogenesis (Fig 3), we decided to assess their role in dendrite and spine development. Nova1 knockdown in hippocampal neurons

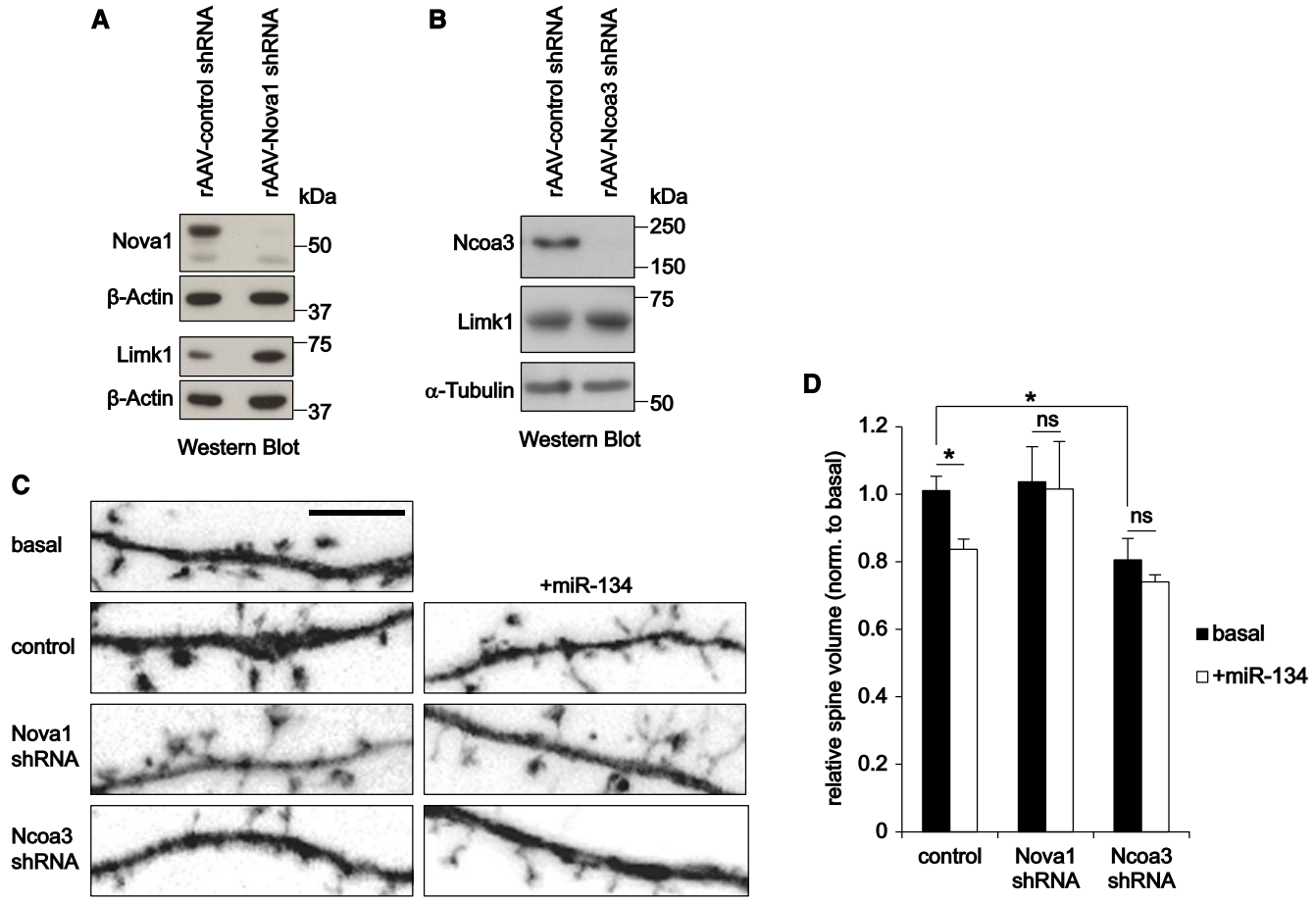

Figure 4. Nova1 and Ncoa3 are required for miR-134-mediated repression of Limk1 and spine morphogenesis.

A, B Western blot analysis of Nova1, Ncoa3, and Limk1 protein in whole-cell extracts from hippocampal neurons (14 DIV) that had been infected with rAAV expressing the indicated shRNAs at four DIV. β-actin or α-tubulin was used as a loading control.

C Representative dendritic segments with dendritic spines from hippocampal neurons (19 DIV) transfected with the indicated shRNA expression construct (empty plasmid served as a control) in the presence or absence of miR-134 duplex RNA (+miR-134, 20 nM) on 13 DIV. Scale bar = 5 μm.

D Quantification of the average relative spine volume of hippocampal neurons from (C). Values were normalized to a basal condition without shRNA expression vector and represent averages ± standard deviation from three independent experiments (each including six cells per condition). *$P < 0.05$ (unpaired *t*-test).

Source data are available online for this figure.

(12 DIV) under basal conditions had no significant effect on dendritic complexity or spine morphogenesis (Fig 4D; Supplementary Fig S6A and B). In contrast, Ncoa3 knockdown resulted in a highly significant increase in dendritic complexity, which was quantified by Sholl analysis (Fig 6A–C). Increased dendritic complexity was rescued by molecular replacement with Ncoa3-GFP^R, but not with a control vector (unmodified pEGFP_N1), demonstrating that the phenotype is caused by a specific reduction of Ncoa3 expression (Fig 6A–C). Expression and shRNA resistance of Ncoa3^R-GFP were confirmed by Western blotting (Supplementary Fig S6C). Therefore, we uncovered a novel function of Ncoa3 in neuronal morphogenesis and decided to investigate the underlying mechanisms in more detail.

If the observed regulation of miRNA activity by Ncoa3 (Fig 3) was functionally important, one would expect that Ncoa3 knockdown should not cause phenotypic alterations in the absence of miRNAs. To test this hypothesis, we combined the Ncoa3 shRNA with knockdown of Drosha, a component of the microprocessor that is crucial for the biogenesis of the vast majority of miRNAs (Gregory *et al*, 2004). Efficient knockdown of Drosha in neurons was verified by Western blotting (Supplementary Fig S6D) and qPCR (Supplementary Fig S6E). We could also confirm a reduction in the levels of several mature miRNAs upon Drosha knockdown (Supplementary Fig S6F). Using dendritic complexity as readout, we found that Ncoa3 shRNA was no longer able to increase dendritic complexity in the absence of Drosha (Fig 6D–F). We therefore conclude that the dendritic phenotype caused by Ncoa3 knockdown is due to aberrant miRNA function in these neurons.

In addition, knockdown of Ncoa3 significantly reduced the average dendritic spine volume (Figs 4D and 7A and B), which was rescued by co-expression of Ncoa3^R-GFP (Fig 7A and B). We were interested in whether the morphological phenotypes observed upon Ncoa3 knockdown translated into altered excitatory synapse function. Thus, we measured miniature excitatory postsynaptic currents (mEPSCs) using patch-clamp electrophysiological recordings (Fig 7C). Consistent with our previous observation that Ncoa3 knockdown results in reduced spine volume, we detected reduced

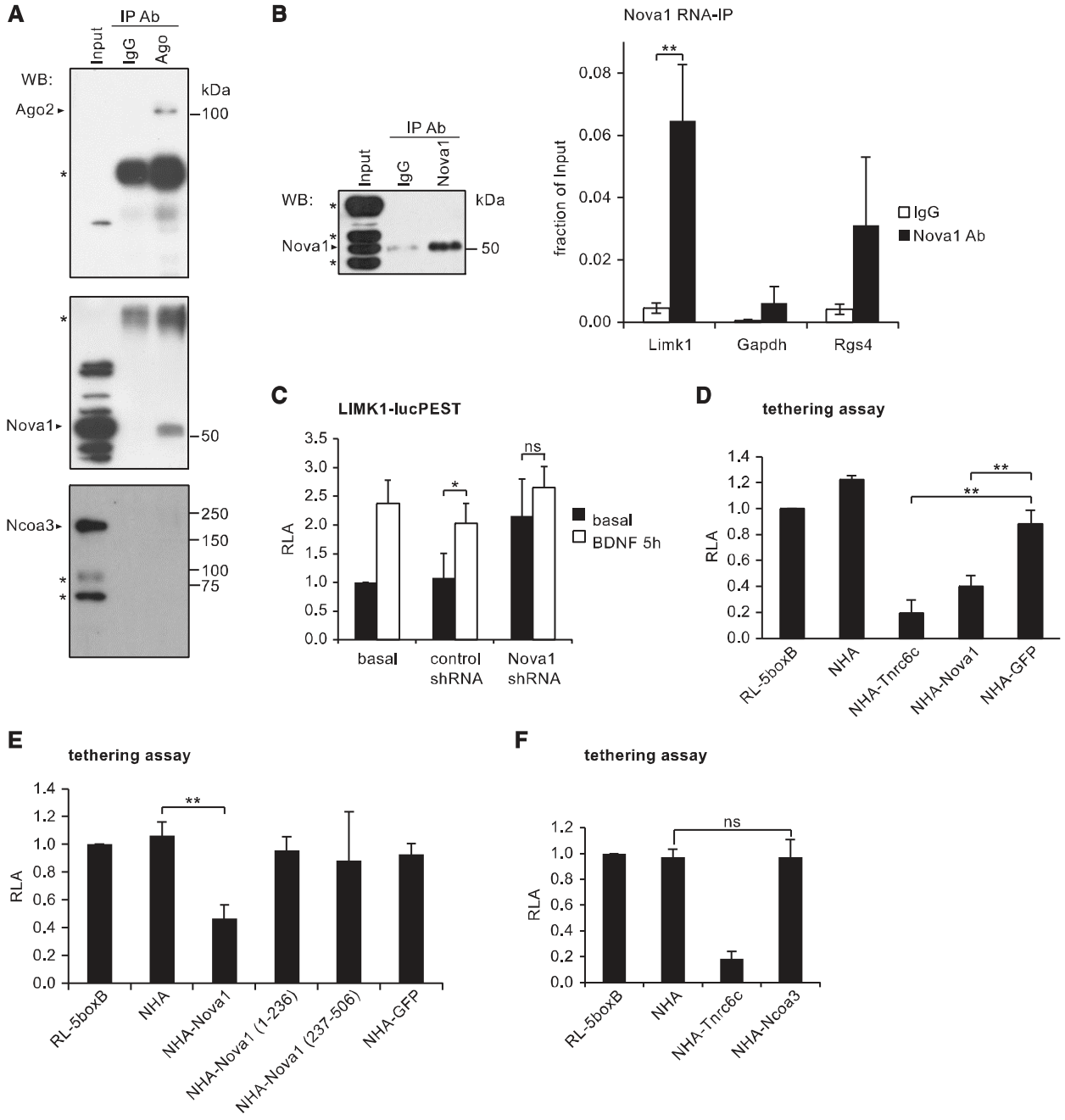

Figure 5. Nova1 and Ncoa3 stimulate neuronal miRNA function by different mechanisms.

A Representative co-immunoprecipitation experiment in hippocampal lysates from adult rat using a pan-Ago antibody. Upper panel: anti-Ago2 Western blot demonstrates specific pull-down of Ago2 in pan-Ago IP. Lower panel: anti-Nova1 Western blot demonstrates specific co-precipitation of Nova1 (52 kDa) and Ago proteins. *Non-identified cross-reactive proteins.

B RNA immunoprecipitation (RIP) in adult rat hippocampus using an anti-Nova1 antibody. Left: specific IP of Nova1 with the applied antibody was confirmed by Western blot analysis. *Non-identified cross-reactive proteins. Right: qPCR for the indicated transcripts is presented as the ratio of mRNA present in Nova1 or control IgG IPs compared to the input material. Data is the average ± standard deviation from three independent experiments. $^{**}P < 0.005$ (unpaired Student's *t*-test).

C Luciferase assay in cortical neurons (five DIV) transfected with a reporter gene which harbors the Limk1 3′UTR fused to a destabilized firefly ORF (Limk1-lucPEST) and with the indicated shRNAs. Neurons were stimulated with BDNF (100 ng/ml) or mock-treated for 5 h before processing for luminometry. Values were normalized to a co-transfected *Renilla* reporter and the basal condition without shRNA was set as 1. Data is the average ± standard deviation of four independent experiments. $^{*}P < 0.05$ (unpaired *t*-test). ns: not significant.

D–F Luciferase assay in cortical neurons (five DIV) transfected with RL-5boxB (tethering plasmid) together with plasmids expressing the indicated NHA-fusion proteins. Values were normalized to a co-transfected firefly reporter, and a basal condition without additional NHA protein was set as 1. Data is the average ± standard deviation of four independent experiments. One-way ANOVA: $P < 0.0001$ (D, F), $P < 0.005$ (E); Tukey's HSD test: $^{**}P < 0.01$; ns: not significant.

Source data are available online for this figure.

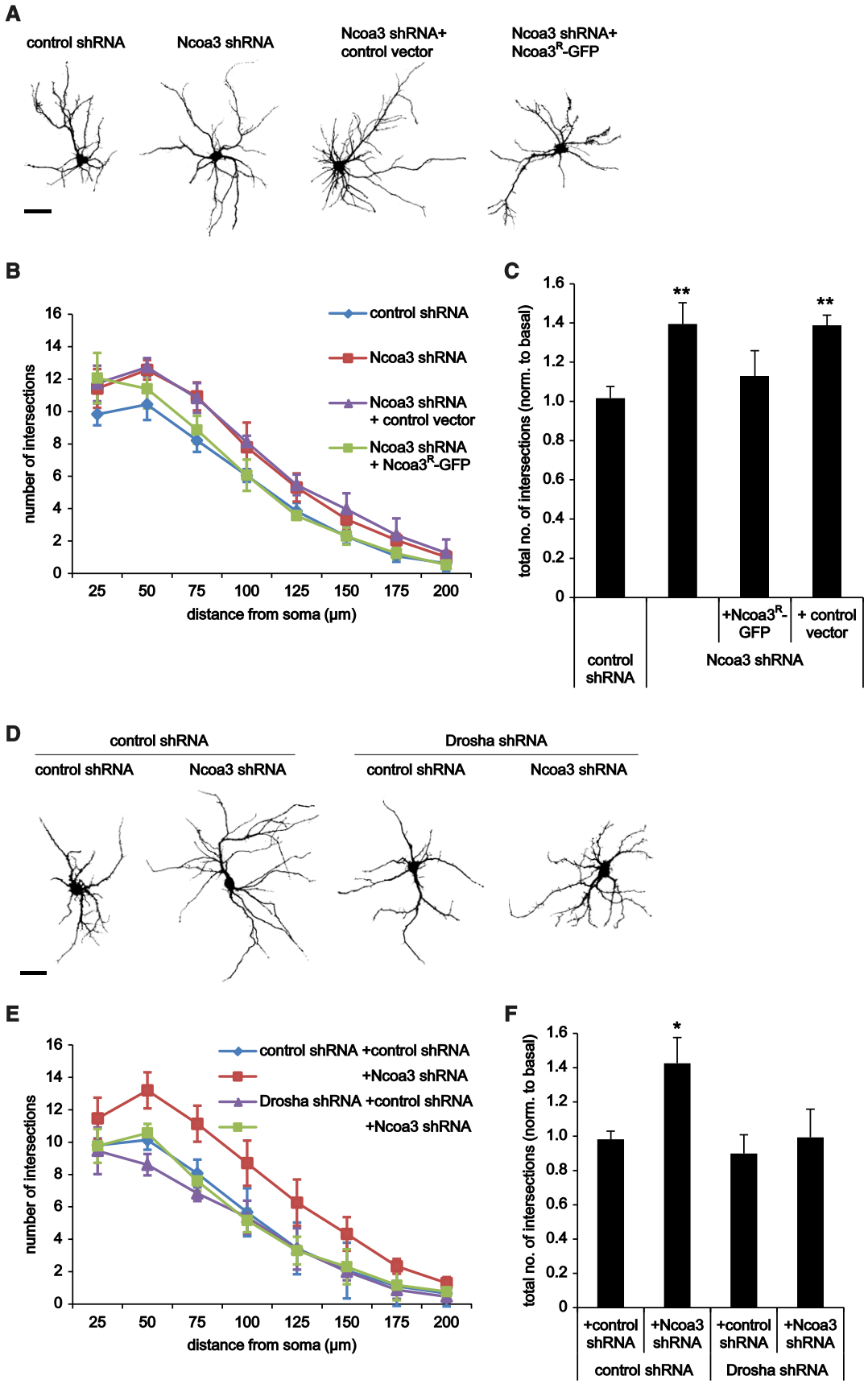

Figure 6.

Figure 6. Ncoa3 regulates dendritic complexity in rat hippocampal neurons.

A Representative traces of rat hippocampal pyramidal neurons (12 DIV) that had been transfected with GFP and the indicated shRNA or expression vectors at six DIV. Ncoa3^{R}: Noca3-shRNA resistant. Scale bar = 50 μm.

B Sholl analysis of hippocampal neurons from (A). The average number of intersections with concentric circles drawn around the cell soma at distances from 25 to 200 μm is shown. Values are the average ± standard deviation from three independent experiments (in each 10–12 cells per condition).

C Sholl analysis as in (B), except that the total number of intersections was calculated for each condition. Values were normalized to a basal condition without shRNA. Data is the average ± standard deviation of three independent experiments. One-way ANOVA: $P = 0.0029$, Tukey's HSD test: $^{**}P < 0.01$ (to control shRNA condition).

D Representative traces of rat hippocampal pyramidal neurons (12 DIV) that had been transfected with GFP and the indicated shRNA vectors. Scale bar = 50 μm.

E, F Results from Sholl analysis performed as in (B, C). Data is the average ± standard deviation of four independent experiments. One-way ANOVA: $P = 0.0037$; Tukey's HSD test: $^{*}P < 0.05$ (to control shRNA condition).

average mEPSC amplitudes (Fig 7D and E), but not frequencies (Fig 7F), in Ncoa3 shRNA-transfected neurons compared to control conditions. Therefore, Ncoa3 knockdown affects both morphological and electrophysiological properties of excitatory synapses of hippocampal neurons.

Given the well-documented function of Ncoa3 as transcriptional co-activator, we hypothesized that Ncoa3 promotes the expression of gene(s) that play important roles in miRNA biogenesis and/or activity. To address this hypothesis, we isolated RNA from hippocampal neurons that had been infected with either rAAV expressing Ncoa3 shRNA or a control shRNA (Supplementary Fig S7A). We validated a reduction in Ncoa3 mRNA levels in Ncoa3 shRNA compared to control shRNA-infected neurons (Fig 8A). We subsequently subjected isolated RNA to comparative microarray hybridizations using the Affymetrix platform Rat Gene 2.0 ST, which covers a total of 36,685 different transcripts. Hybridization signals from the individual arrays were strongly correlated, demonstrating high reproducibility of the experiments (Supplementary Fig S7B). In total, we identified 100 annotated transcripts that were differentially expressed between Ncoa3 shRNA and control shRNA conditions (cutoff 1.3-fold, $P < 0.05$, $n = 3$), among which 68 were downregulated and 32 were upregulated upon Ncoa3 knockdown (Fig 8B, complete expression analysis is provided in Supplementary Dataset S3). Intriguingly, among the 15 most downregulated transcripts, we identified the miRISC core component Ago2 and, as expected, Ncoa3 itself (Fig 8B, bold). Ncoa3-dependent regulation of Ago2 and three other candidates identified by microarray (Cyb5r3, Map9, and Spast) was independently confirmed by qPCR (Fig 8C). In contrast, several other components of miRNA regulatory complexes were not affected by Ncoa3 knockdown (Supplementary Fig S7C). Since downregulation of Ago2 could in principle explain elevated expression of a subset of miRNA targets in Ncoa3 knockdown cells (Fig 3; Supplementary Fig S3), we decided to study the regulation of Ago2 in more detail. Using Western blot analysis, we further observed a robust downregulation of Ago2 protein upon infection of neurons with rAAV-expressed Ncoa3 shRNA (Fig 8D; Supplementary Fig S7D). To interrogate whether Ncoa3 promotes Ago2 transcription by directly binding to the Ago2 promoter, we performed chromatin immunoprecipitation (ChIP) assays. Ncoa3-ChIP specifically enriched DNA fragments corresponding to the promoter regions of Ago2 and two other Ncoa3-regulated genes (Map9 and Spast) but not Cyb5r3 or the β-globin control (Fig 8E; Supplementary Fig S7E and F). The specificity of the Ncoa3-ChIP was further confirmed by the reduced recovery of Ago2, Map9, and Spast promoter fragments from Ncoa3 knockdown neurons. Next, we tested whether Ncoa3 was involved in the regulation of Ago2 transcription using luciferase reporter assays. Therefore, we inserted a fragment of the mouse Ago2 promoter upstream of a minimal promoter driving the luciferase reporter gene. This fragment contains a conserved motif that could serve as a retinoic acid receptor alpha (RXRA)-binding site (JASPAR database; Supplementary Fig S7G). Ncoa3 was required for the induction of this reporter by retinoic acid (RA), suggesting that Ncoa3 functions as a co-activator of RXRA in the context of the Ago2 promoter (Fig 8F). Taken together, our experiments establish Ago2 as a direct transcriptional target gene of Ncoa3 in neurons.

We were then prompted to test whether the functional role of Ncoa3 in miRNA regulation and neuronal morphogenesis is mediated via transcriptional control of Ago2. Therefore, we used a Flag/HA-Ago2 construct which was efficiently expressed in neurons and HEK293 cells as judged by ICC and Western blotting, respectively (Supplementary Fig S8A and B). The quantification of Ago2 levels after Flag/HA-Ago2 overexpression showed that total Ago2 was elevated in control neurons by 1.5-fold and that Ago2 was restored to normal levels in Ncoa3 knockdown neurons (Fig 9A; Supplementary Fig S8C). We investigated further the involvement of Ago2 in Ncoa3-mediated miRNA function using the LIN41 3′UTR reporter assay. Importantly, co-expression of Flag/HA-Ago2 in the context of the Ncoa3 shRNA nearly restored reporter expression to basal levels, demonstrating that Ago2 downregulation is required for the loss in let-7 activity in response to Ncoa3 knockdown (Fig 9B). Importantly, expression of Flag/HA-Ago2 alone had no repressive activity (Fig 9B), suggesting that Ago2 is indeed downstream of Ncoa3 in the regulation of miRNA activity. Finally, we determined the role of Ago2 in Ncoa3-dependent neuronal morphogenesis (Fig 9C–E). Neurons expressing Ncoa3 shRNA showed a robust increase in dendritic complexity, which was almost completely rescued upon co-expression of Flag/HA-Ago2, but not the control vector. Similar to the observations from miRNA reporter gene assays, the expression of Flag/HA-Ago2 alone did not significantly affect dendritic complexity. Taken together, our results from miRNA reporter assays and neuromorphological analysis strongly suggest that the transcriptional regulation of Ago2 is responsible for Ncoa3-mediated regulation of miRNA activity and dendritogenesis.

Discussion

In this study, we present the first large-scale RNAi-based functional screen designed to identify RBPs that modulate miRISC activity in primary neurons. In addition to previously reported miRISC factors (Trnc6c, Ddx6/RCK/p54), we uncovered three novel regulators of miRNA activity: Nova1, Ncoa3, and Ewsr1. The fact that these regulators were missed in previous screens (Chu & Rana, 2006; Eulalio *et al*, 2007) suggests that neurons employ specific regulatory mechanisms

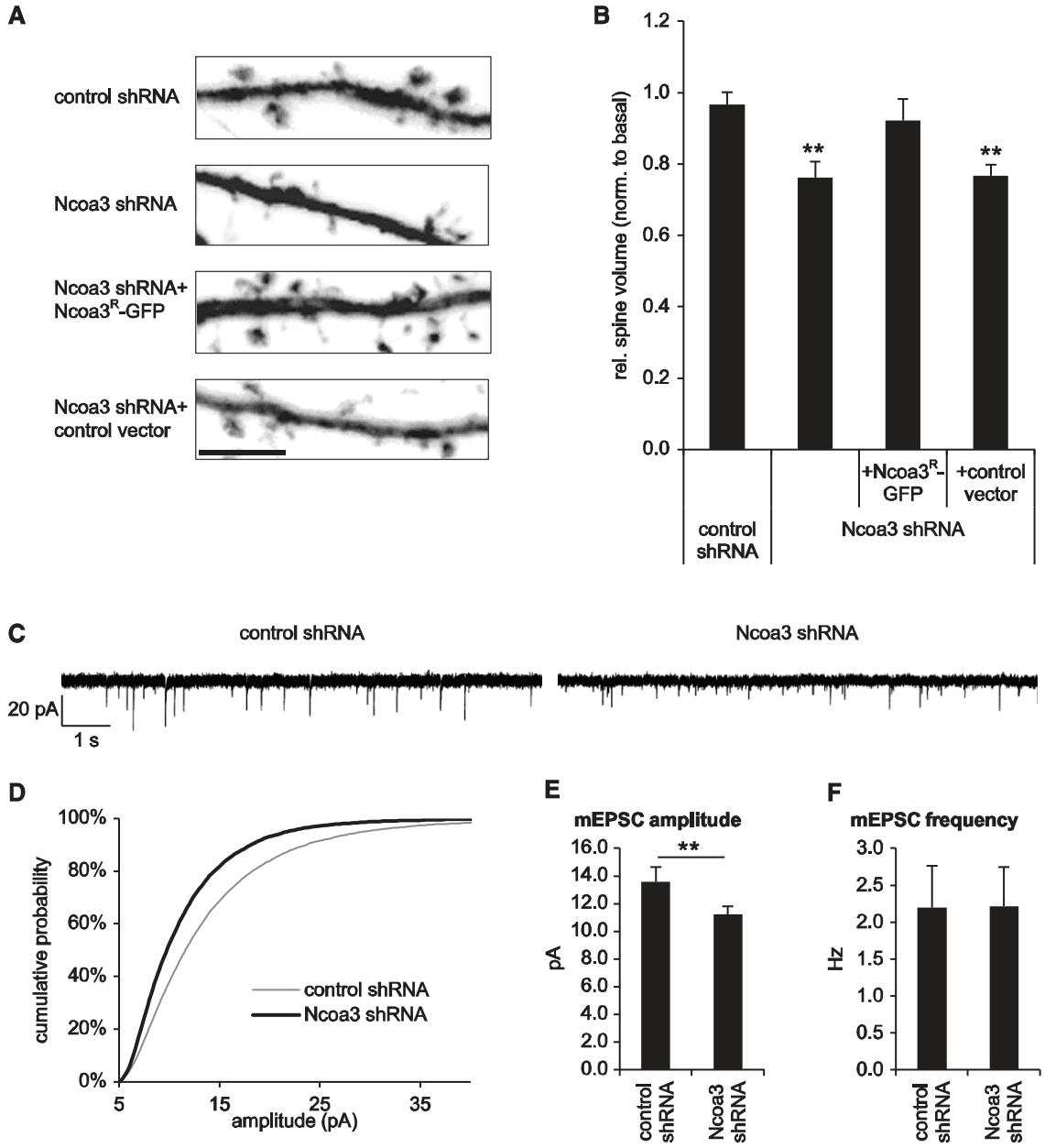

Figure 7. Ncoa3 regulates dendritic spine size and mEPSC amplitudes in rat hippocampal neurons.

A Representative dendritic segments with dendritic spines from hippocampal neurons (19 DIV) transfected with GFP and the indicated shRNA or expression vectors at 13 DIV. Scale bar = 5 μm.

B Quantification of the average relative spine volume of hippocampal neurons from (A). Values were normalized to a basal condition without shRNA and represent the average ± standard deviation from three independent experiments (in each six cells per condition). One-way ANOVA: $P = 0.0009$; Tukey's HSD test: $^{**}P < 0.01$ (to control shRNA condition).

C–F Dissociated hippocampal neurons were transfected with indicated shRNA expression vectors on 12–13 DIV, and mEPSCs were measured on 18–21 DIV. (C) Exemplary traces from representative recordings. (D) Cumulative probability plot distribution of mEPSC amplitudes; $P < 10^{-6}$ (Kolmogorov–Smirnov test). (E) Average mEPSC amplitudes ± standard error, $^{**}P < 0.01$ (unpaired *t*-test). (F) Average mEPSC frequency ± standard error. Cells were collected from five independent experiments (control shRNA: $n = 18$; Ncoa3 shRNA: $n = 19$; one Ncoa3 shRNA cell was qualified as outlier).

which involve both neuron-specific (such as Nova1) and ubiquitously expressed RBPs (such as Ncoa3 and Ewsr1) to control miRNA activity. In general, our discovery of cell-type specific regulators of miRNA function underscores the need for experiments that address the function and regulation of miRNAs in their natural cellular context.

Nova1 as a novel component of neuronal miRISC

Nova1 was originally identified as an autoantigen in paraneoplastic opsoclonus myoclonus ataxia (POMA), a disorder associated with breast cancer and motor dysfunction (Buckanovich *et al*, 1993).

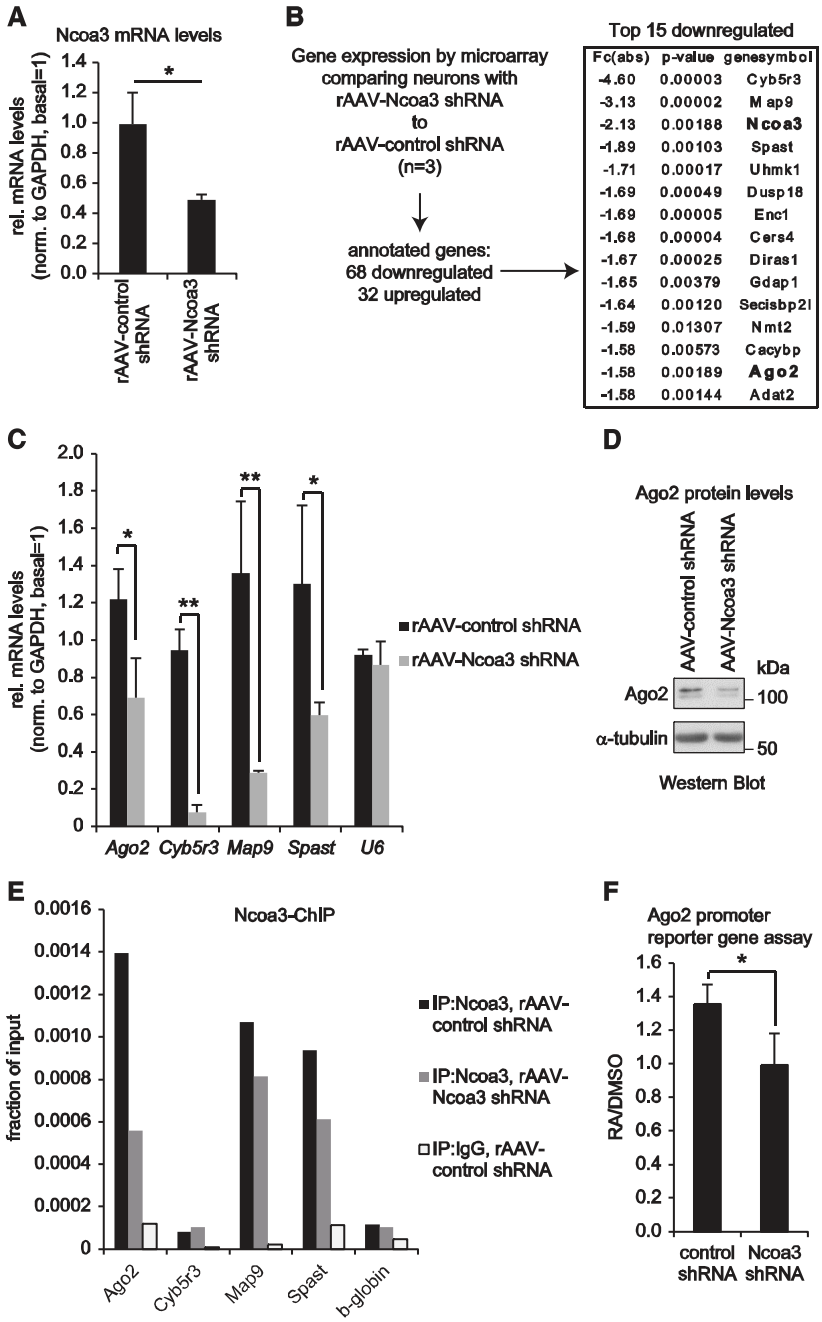

Figure 8. Microarray analysis identifies Ago2 as an Ncoa3-regulated transcript.

A qPCR analysis of Ncoa3 mRNA levels in hippocampal neurons (14 DIV) that had been infected with the indicated rAAV-expressed shRNAs at four DIV. The ratio of average Ncoa3 levels compared to the internal GAPDH control is shown after normalization to a non-infected basal condition. Data is the average ± standard deviation of three independent experiments. *$P < 0.05$ (unpaired *t*-test).

B Flow chart for the identification of Ncoa3-regulated genes by microarray in hippocampal neurons treated as in (A). Absolute fold changes (Fc(abs)), *P*-values (*t*-test), and corresponding gene symbols are given on the right for the top 15 downregulated transcripts. Ncoa3 and Ago2 are highlighted in bold.

C qPCR analysis of indicated Ncoa3-regulated transcripts in hippocampal neurons treated as in (A). The ratio of average candidate mRNA levels compared to the internal GAPDH mRNA control is shown after normalization to a non-infected basal condition. U6 was used as a negative control. Data is the average ± standard deviation of three independent experiments. *$P < 0.05$, **$P < 0.01$ (unpaired *t*-test).

D Western blot analysis of Ago2 protein in whole-cell extracts from hippocampal neurons treated as in (A). α-tubulin was used as a loading control.

E qPCR analysis of indicated Ncoa3-regulated genes from a representative Ncoa3-ChIP experiment performed in either control shRNA (black) or Ncoa3 shRNA (gray) infected neurons. As a specificity control, ChIP with an unrelated IgG was performed in control shRNA-transfected neurons (white). Values are presented as fraction of the respective input DNA used for ChIP.

F Average luciferase activity in retinoic acid (RA)- or mock (DMSO)-treated neurons transfected with an Ago2 promoter reporter gene together with the indicated shRNA constructs. Values are presented as the ratio from RA- to DMSO-treated neurons and represent the average ± standard deviation from three independent experiments. *$P < 0.05$ (unpaired *t*-test).

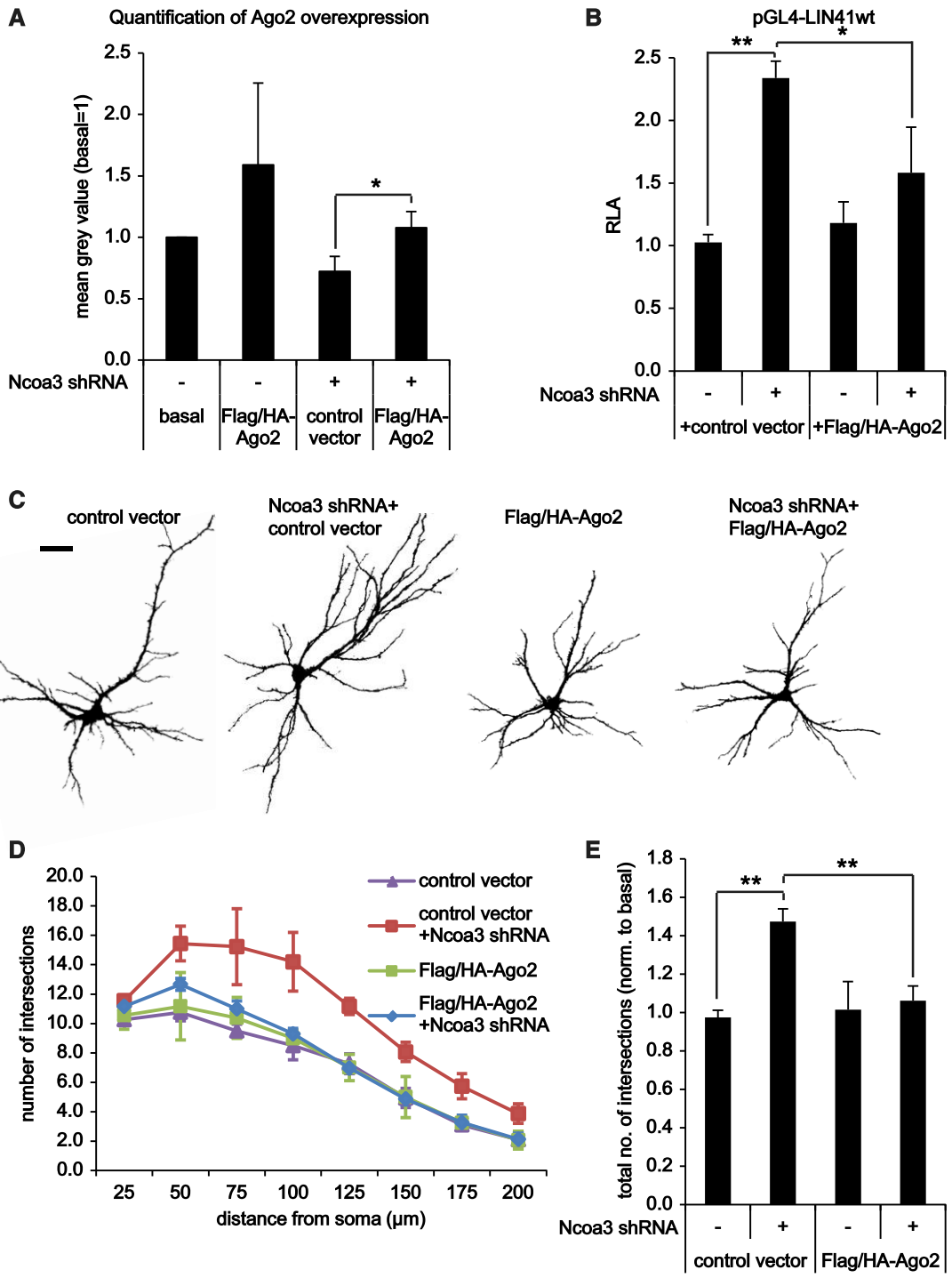

Figure 9. The regulation of Ago2 is required for Ncoa3-dependent miRNA activity and dendritogenesis.

A Quantification of Ago2 overexpression in hippocampal neurons (12 DIV) that have been transfected with GFP, the indicated shRNA expression vectors, and either empty Flag/HA (control vector) or Flag/HA-Ago2 after six DIV by anti-Ago2 immunocytochemistry. Measured was the average signal intensity in the neuronal soma (exemplary images in Supplementary Fig S8C), and values presented are the mean ± standard deviation from three independent experiments (in each 12 cells per condition). *$P < 0.05$ (pairwise *t*-test).

B Reporter gene assay performed in rat hippocampal neurons (14 DIV) that had been transfected with pGL4-LIN41 WT 3′UTR together with the indicated shRNA vectors and either empty Flag/HA (control vector) or Flag/HA-Ago2 three days before. Relative luciferase activity (RLA) represents the ratio of firefly reporter to the internal *Renilla* control reporter activity normalized to basal condition without additional expression vector. Values are the mean ± standard deviation from three independent experiments. One-way ANOVA: $P < 0.0003$; Tukey's HSD test: **$P < 0.01$.

C Representative traces of neurons (12 DIV) that have been transfected as described in (A). Scale bar = 50 µm.

D, E Results from Sholl analysis performed as in Fig 6 with neurons treated as in (A). One-way ANOVA: $P = 0.0005$; Tukey's HSD test: **$P < 0.01$.

Later, it was shown that Nova1 is a sequence-specific RNA-binding protein that functions in pre-mRNA splicing (Jensen *et al*, 2000). Two recent studies indicated that Nova proteins (Nova1 and Nova2) might also have regulatory functions in the cytoplasm. First, CLIP analysis of mouse brain indicated that a fraction of cellular Nova binds to consensus sequence elements within 3′UTR and regulates alternative polyadenylation of target mRNAs (Licatalosi *et al*, 2008). Second, Nova was shown to co-localize with target RNAs, including GlyRa2 and GIRK2, in dendrites of spinal cord motor neurons (Racca *et al*, 2010). These reports are consistent with our results from cellular fractionation and immunocytochemistry experiments in hippocampal neurons (Fig 2) and with a potential function of Nova1 in the regulation of miRISC activity in the cytoplasm. Surprisingly, although Nova1 associates with the miR-134 target Limk1 mRNA (Fig 5B), we found that the modulatory activity toward miRISC does apparently not require sequence-specific interaction of Nova1 with miRNA target RNAs. This conclusion is based on our observations that Nova1 regulates miRNA reporters independent of the 3′UTR context (Fig 3) and that artificial tethering of Nova1 to an mRNA is sufficient to induce translational repression (Fig 5D). Moreover, Nova1 interacts with Ago in an RNA-independent manner (Supplementary Fig S5C and D), arguing that Nova1 contacts Ago via protein–protein interaction(s), either directly or via additional bridging proteins. Since Nova1 knockdown leads to a residual activation of reporters containing mutated miRNA-binding sites (Fig 3), Nova1 might in addition regulate mRNA translation in a miRNA-independent manner. Importantly, Nova1 is also required for miRNA-dependent regulation of neuronal function, in particular miR-134-dependent spine morphogenesis. Since Nova1 deficiency by itself does not cause dendrite or spine abnormalities (Fig 4D; Supplementary Fig S6), we speculate that Nova1 function is specifically required for dynamic activity-dependent changes in neuronal morphology, such as those occurring during synaptic plasticity. Our finding that Nova1 is involved in BDNF-dependent Limk1 expression (Fig 5C) is consistent with this hypothesis. In this regard, it will be interesting to investigate the potential activity-dependent modifications of the Ago-Nova1 complex.

Ncoa3 as a positive regulator of Ago2 expression

Ncoa3 (SRC-3, AIB-1) is a member of the nuclear receptor co-activator (Ncoa) family of transcriptional co-activators consisting of Ncoa1–3 (also known as SRC1-3) (Leo & Chen, 2000; Dasgupta *et al*, 2014). In addition to its extensively characterized function in transcription, two reports suggest a post-transcriptional cytosolic function of Ncoa3 in non-neuronal cells (Yu *et al*, 2007; Long *et al*, 2010). Using microarray analysis, qPCR, ChIP, and reporter gene assays (Fig 8), we could identify the miRISC core factor Ago2 as novel direct transcriptional target gene of Ncoa3. Together with our results from rescue experiments (Fig 9), this provides strong evidence that Ncoa3 regulates miRNA function by activating Ago2 transcription in the nucleus. Although Ncoa3 does not interact with Ago (Fig 5A) or miRNA target RNAs (data not shown), it is possible that Ncoa3 in addition modulates miRNA function by different mechanisms. Surprisingly, we observed that a relatively subtle reduction of Ago2 levels (30–40%) in Ncoa3 knockdown cells is sufficient to cause profound impairments in miRNA regulation and neuronal morphogenesis, which are rescued by expression of Flag/HA-Ago2. These findings are consistent with previous observations that Ago2 is a rate-limiting factor in RNAi and that titrating endogenous Ago2 levels by excessive supply of small interfering RNAs can affect cellular physiology (Grimm *et al*, 2006; Borner *et al*, 2013). In contrast to Nova1, Ncoa3 is only required for the repression of a specific subset of neuronal miRNA targets (Fig 3; Supplementary Fig S3). This implies that miRNA targets display a differential susceptibility toward alterations in Ago2 levels. One possible explanation is that some specific miRNAs are preferentially loaded into Ago2. However, there are conflicting data concerning sequence-specific sorting of miRNAs into Ago proteins in mammalian cells (Burroughs *et al*, 2011; Dueck *et al*, 2012; Wang *et al*, 2012). Our observation that mRNAs targeted by the same miRNAs respond differently to Ncoa3 knockdown (e.g., the let-7 targets LIN41 and HMGA2, Fig 3D; Supplementary Fig S3D) further argues against this possibility. Alternatively, the miRNA target site context could influence recruitment of specific Ago proteins to mRNAs. In this regard, genome-wide mapping of binding sites for different Ago proteins in conjunction with the interacting miRNAs would be highly informative.

Our results further suggest that the specific pool of miRNA targets affected by the Ncoa3-Ago2 pathway plays an important role in the inhibition of dendrite growth and/or branching. Therefore, interesting candidate Ncoa3-regulated miRNAs might be those with a reported inhibitory role in dendritogenesis, such as miR-137, miR-181a, miR-34a, and miR-375 (Abdelmohsen *et al*, 2010; Smrt *et al*, 2010; Agostini *et al*, 2011; Liu *et al*, 2013). However, a more systematic analysis of Ncoa3-regulated, Ago2-associated miRNAs and their targets is needed to fully characterize the physiologically important miRNA target interactions that affect neuronal morphogenesis downstream of Ncoa3. The lack of a dendritic phenotype in neurons in which miRNA function is generally perturbed, for example, due to Drosha or Nova1 knockdown, is surprising at first, but could be explained by a perturbed function of both dendrite growth-promoting (e.g., miR-132 (Magill *et al*, 2010)) and growth-inhibiting (see above) miRNAs. If inhibitory and stimulatory activities balance each other, no net effect on dendritogenesis would be expected upon a global loss of miRNAs.

In summary, we have identified Nova1 and Ncoa3 as novel miRISC regulators that stimulate miRNA activity by different mechanisms converging on Ago proteins. We speculate that signal-dependent regulation of these pathways could be involved in neuronal plasticity and possibly other cellular contexts.

Materials and Methods

Cell culture, transfection, and recombinant AAV production

Dissociated primary hippocampal and cortical neurons from embryonic day (E)18 Sprague–Dawley rats (Charles River Laboratories) were prepared and cultured as described (Schratt *et al*, 2004). Transfection of neurons was generally performed with Lipofectamine 2000 (Invitrogen) as described (Siegel *et al*, 2009).

Where indicated, the given amount of plasmid was electroporated to cortical neurons using the Nucleofector™ X-unit (Lonza) as described earlier (Siegel *et al*, 2009). For the time course

experiment of Ncoa3, preparation of cytosolic and nuclear fractions as well as rAAV infections, the culture medium was supplemented with 10 μM of 5-fluorodeoxyuridine (FUDR) to inhibit glial proliferation.

HEK293 cells were cultivated at subconfluent density in MEM containing 10% FCS, 2 mM L-glutamine, and Pen/Strep (all from Gibco). Co-transfection of GFP-fusion constructs and siRNAs was carried out in this medium with Lipofectamine 2000 as described for neurons. For NHA-fusion constructs and rAAV production, HEK293 cells were transfected using the calcium phosphate method as described (Christensen *et al*, 2010). A titer of 1.8×10^6 IFU/ml was used to infect hippocampal neurons (four DIV).

RNAi screen experiment

Mouse cortical neurons were co-transfected in a 48-well format at five DIV with 62.5 ng of pGL3-UBE3A, 62.5 ng of pGL3-*Renilla*, 5 pmol of miR-134 duplex RNA, and 7.5 pmol of one synthetic siRNA derived from a custom siRNA library (Ambion) in a total volume of 250 μl using Lipofectamine 2000. Three individual siRNAs for 286 candidate genes were tested. Luciferase assay was performed 3 days after the transfection. Each condition was transfected in duplicates, and the entire screen was repeated three times.

Subcellular fractionation and protein extraction

After one wash with ice-cold PBS, hippocampal cultures were detached in HLB (10 mM KCl, 1 mM EDTA, 1 mM DTT, 10 mM Tris–HCl (pH 7.5), protease inhibitors (Roche)) containing 0.2% NP-40 for 10 min on a shaker at 4°C followed by lysis through 20 strokes with a Teflon potter. After an aliquot was taken as input, nuclei were pelleted at 800 *g* for 5 min at 4°C and the supernatant was recovered as cytosolic fraction. The nuclei were washed once with HLB containing 0.25 M sucrose. After 10× RIPA (0.5 M Tris pH 8.0, 1.5 M NaCl, 10% Triton X-100, 5% sodiumdeoxycholate, 0.5% SDS, 20 mM EDTA) was diluted to 1× in the input and the nuclear pellet was dissolved in 1× RIPA (containing protease inhibitors), lysis of these two fractions was enforced by sonication. All fractions were subsequently spun down by 16,000 *g* for 10 min at 4°C, and the respective supernatant was recovered as protein extract. Whole-cell extracts were prepared by lysis in 1× RIPA followed by sonication, centrifugation, and recovery of supernatants as above, or in lysis buffer (150 mM NaCl, 50 mM Tris pH 7,5, 1% Triton) containing protease inhibitors.

Co-immunoprecipitation

Dissected hippocampi from adult brain (E18) were transferred to a 15-ml potter and homogenized on ice by 14 strokes in lysis buffer (20 mM Tris pH 7,5, 150 mM NaCl, 1% NP-40, 2 mM EDTA) containing protease inhibitors (Roche) followed by 10-min centrifugation at 16,000 *g* at 4°C. For RNase treatment, RNase A (1:20; Ambion) was added to one half of the cell lysate. Lysates were incubated with either mouse anti-pan-Ago (1:200; 2A8, Millipore) or mouse IgG (SCBT) rotating overnight at 4°C. Protein G beads (25 μl per condition; Sigma) were equilibrated in lysis buffer, blocked for 2 h in BSA (1 mg/ml; NEB), washed, resuspended in lysis buffer, and incubated with lysate and antibody for 1 h at 4°C followed by four washes in lysis buffer (last two containing 350 mM NaCl).

RNA immunoprecipitation (RIP)

The hippocampi of an adult female rat were dissected and homogenized in a Dounce potter (20 strokes) in lysis buffer (10 mM Hepes (pH 7.5), 200 mM NaCl, 30 mM EDTA, 0.5% Triton X-100, 0.5 U/μl SUPERase inhibitor (Ambion), complete protease inhibitors (Roche)). Homogenate was then passed five times through a 26-G needle. After centrifugation at 70,000 *g* (4°C) for 20 min, the supernatant was supplemented with 100 μg/ml yeast tRNA (Sigma-Aldrich) and precleared with Protein G Dynabeads for 30 min at 4°C. After input collection, immunoprecipitation was performed by the addition of 10 μg antibody (rabbit anti-Nova1 (Abcam) or normal rabbit IgG (SCBT)) and 30 μl Protein G Dynabeads for 2 h at 4°C. The beads were washed five times with lysis buffer (0.1 U/ml SUPERase inhibitors and 10 μg/ml yeast tRNA) and once with lysis buffer without additives. Total RNA was extracted using the mirVana Isolation Kit (Ambion) and treated with TURBO DNase (Ambion).

Chromatin immunoprecipitation (ChIP)

Hippocampal neurons were infected with rAAV-expressed Ncoa3 shRNA or rAAV-expressed control shRNA (9×10^5 IFU/well) at four DIV. On 12 DIV, cells were treated with 1% formaldehyde for 10 min followed by the addition of 0.125 M glycine for 5 min. After one wash with cold PBS, cells were lysed (50 mM Hepes–KOH (pH 7.5), 140 mM NaCl, 1 mM EDTA, 1% Triton X-100, 0.2% Na-deoxycholate, 0.1% SDS, and protease inhibitors (Roche)) by gently shaking at 4°C for 10 min, detached with a cell scraper, and sonicated with a Branson sonifier 250 for 24 cycles with 20 pulses (output 2, 90% duty cycle) and 1-min incubation on ice. After centrifugation at 8,000 *g* (4°C) for 5 min, the supernatant was precleared for 30 min at 4°C with Protein G Dynabeads (Life Technologies) and used for immunoprecipitation with anti-Ncoa3 (5E11, cell signaling) or normal rabbit IgG (Santa Cruz) antibodies (2 h at 4°C) which were previously coupled to Protein G Dynabeads for 30 min. Beads were washed twice with lysis buffer, four times with high salt buffer (20 mM Tris (pH 8), 1 M NaCl, 2 mM EDTA, 1% Triton X-100, 0.1% SDS), twice with Li wash buffer (10 mM Tris (pH 8), 250 mM LiCl, 1 mM EDTA, 1% NP-40, 1% Na-deoxycholate), and once with TE (20 mM Tris (pH 8), 1 mM EDTA) at 4°C for 5 min. The complexes were eluted in elution buffer (100 mM $NaHCO_3$, 1% SDS) for 15 min at 30°C, and cross-links in the supernatant were reversed by the addition of NaCl (final concentration 370 mM) and incubation at 65°C for 4 h. The input was taken after preclearing, supplemented with proteinase K (10 μg/100 μl lysate from NEB), and incubated at 65°C for 4 h. The DNA was subsequently recovered by phenol/chloroform/isoamyl alcohol extraction (Carl Roth).

Western blot analysis

Western blotting was performed in principle as described (Siegel *et al*, 2009). Please see Supplementary Materials and Methods for further details.

Immunocytochemistry, microscopy, and image processing

Immunocytochemistry and confocal microscopy were in principle performed as described (Siegel *et al*, 2009). Please see Supplementary Materials and Methods for further details.

Analysis of neuronal morphology

For analysis of dendritic complexity, random pyramidal neurons (12 DIV) were imaged in epifluorescence mode and analyzed by counting intersections of dendrites with circles of 25 μm incremental radii (range: 25–200 μm) around the soma. The total number of intersections was obtained by summing up intersections between dendrites and circles at each distance. Exemplary traces of analyzed cells are shown. Background signals were removed for clearer presentation. For dendritic spine analysis, confocal images (7 *z*-stacks at 0.4-μm interval) of pyramidal neurons (19 DIV) were projected to a single-plane image and the individual spine size was quantified by its mean gray value in a 2.2-μm^2 circle. More than 100 spines per cell were measured and normalized to the cell's mean gray values. Analysis was carried out blinded to the experimental conditions.

Luciferase assay

Luciferase assays in primary rat hippocampal or cortical neurons were performed with the Dual-Luciferase Reporter Assay System (Promega). Please see Supplementary Materials and Methods for further details.

DNA constructs and molecular cloning

A detailed description of cloning procedures and primer sequences is provided in the Supplementary Materials and Methods.

RNA extraction and reverse transcription–quantitative PCR (RT–qPCR)

RNA extraction and qPCR were performed according to the manufacturer's instructions. See Supplementary Materials and Methods for further details.

Microarray

For microarray analysis, total RNA was extracted as described above. RNA quality was confirmed with the Experion System (Bio-Rad). Three independent RNA preparations, each consisting of rAAV-expressed control shRNA and rAAV-expressed Ncoa3 shRNA conditions, were submitted to the GeneCore Facility of EMBL, Heidelberg, Germany, for microarray analysis. Briefly, libraries prepared with the WT Expression Kit (Ambion) were analyzed on the Rat Gene 2.0 ST arrays (Affymetrix). The analysis was performed with Expression Console (Affymetrix) and GeneSpring (Agilent) softwares. In the latter, $\log_2$ values below the background control were removed leaving 11,206 transcript IDs for filtering by volcano plot with thresholds of 1.3-fold change and $P < 0.05$ (moderate *t*-test). Microarray data are deposited in the GEO database with accession number GSE69131.

Antibodies

A complete list of antibodies used in this study is provided in the Supplementary Materials and Methods.

Statistical analysis

For pairwise comparison, a two-tailed, unpaired Student's *t*-test was carried out. For multiple conditions, one-way ANOVA was first applied (http://vassarstats.net/) followed by Tukey's HSD test for comparing single conditions pairwise.

Supplementary information for this article is available online: http://emboj.embopress.org

Acknowledgements
We thank D. Bartel, R. Darnell, W. Filipowicz, G. Meister, R. Pillai, and T. Tuschl for sharing reagents; G. Jarosch, E. Becker, R. Gondrum, U. Beck, and H. Kaiser for outstanding technical support; and A. Antoniou and R. Fiore for critical reading of the manuscript. J. Pistolic assisted with the microarray analysis. B. Honrath, L. Greifenberg, and S. Khudayberdiev generated reagents. This work was funded by grants from the DFG (SFB488, SFB593, SPP1738) and an ERC Starting Grant "Neuromir."

Author contributions
PHS and JT designed, performed, and analyzed most of the experiments. GaS performed the initial RNAi screen (Fig 1) and the Nova1 dendritogenesis assays (Supplementary Fig S5). AAA carried out and analyzed electrophysiological recordings (Fig 7). FZ and SS contributed to Supplementary Figs S6 and S8, respectively. GeS supervised the study and wrote the manuscript.

Conflict of interest
The authors declare that they have no conflict of interest.

References

Abdelmohsen K, Hutchison ER, Lee EK, Kuwano Y, Kim MM, Masuda K, Srikantan S, Subaran SS, Marasa BS, Mattson MP, Gorospe M (2010) miR-375 inhibits differentiation of neurites by lowering HuD levels. *Mol Cell Biol* 30: 4197 – 4210

Agostini M, Tucci P, Steinert JR, Shalom-Feuerstein R, Rouleau M, Aberdam D, Forsythe ID, Young KW, Ventura A, Concepcion CP, Han YC, Candi E, Knight RA, Mak TW, Melino G (2011) microRNA-34a regulates neurite outgrowth, spinal morphology, and function. *Proc Natl Acad Sci USA* 108: 21099 – 21104

Ashraf SI, McLoon AL, Sclarsic SM, Kunes S (2006) Synaptic protein synthesis associated with memory is regulated by the RISC pathway in Drosophila. *Cell* 124: 191 – 205

Banerjee S, Neveu P, Kosik KS (2009) A coordinated local translational control point at the synapse involving relief from silencing and MOV10 degradation. *Neuron* 64: 871 – 884

Bhattacharyya SN, Habermacher R, Martine U, Closs EI, Filipowicz W (2006) Relief of microRNA-mediated translational repression in human cells subjected to stress. *Cell* 125: 1111 – 1124

Borner K, Niopek D, Cotugno G, Kaldenbach M, Pankert T, Willemsen J, Zhang X, Schurmann N, Mockenhaupt S, Serva A, Hiet MS, Wiedtke E, Castoldi M, Starkuviene V, Erfle H, Gilbert DF, Bartenschlager R, Boutros M, Binder M, Streetz K *et al* (2013) Robust RNAi enhancement via human Argonaute-2

overexpression from plasmids, viral vectors and cell lines. *Nucleic Acids Res* 41: e199

Buckanovich RJ, Posner JB, Darnell RB (1993) Nova, the paraneoplastic Ri antigen, is homologous to an RNA-binding protein and is specifically expressed in the developing motor system. *Neuron* 11: 657–672

Burroughs AM, Ando Y, de Hoon MJ, Tomaru Y, Suzuki H, Hayashizaki Y, Daub CO (2011) Deep-sequencing of human Argonaute-associated small RNAs provides insight into miRNA sorting and reveals Argonaute association with RNA fragments of diverse origin. *RNA Biol* 8: 158–177

Christensen M, Larsen LA, Kauppinen S, Schratt G (2010) Recombinant adeno-associated virus-mediated microRNA delivery into the postnatal mouse brain reveals a role for miR-134 in dendritogenesis in vivo. *Front Neural Circuits* 3: 16

Chu CY, Rana TM (2006) Translation repression in human cells by microRNA-induced gene silencing requires RCK/p54. *PLoS Biol* 4: e210

Dasgupta S, Lonard DM, O'Malley BW (2014) Nuclear receptor coactivators: master regulators of human health and disease. *Annu Rev Med* 65: 279–292

Dueck A, Ziegler C, Eichner A, Berezikov E, Meister G (2012) microRNAs associated with the different human Argonaute proteins. *Nucleic Acids Res* 40: 9850–9862

Eulalio A, Rehwinkel J, Stricker M, Huntzinger E, Yang SF, Doerks T, Dorner S, Bork P, Boutros M, Izaurralde E (2007) Target-specific requirements for enhancers of decapping in miRNA-mediated gene silencing. *Genes Dev* 21: 2558–2570

Eulalio A, Huntzinger E, Izaurralde E (2008) Getting to the root of miRNA-mediated gene silencing. *Cell* 132: 9–14

Fabian MR, Sonenberg N (2012) The mechanics of miRNA-mediated gene silencing: a look under the hood of miRISC. *Nat Struct Mol Biol* 19: 586–593

Fiore R, Khudayberdiev S, Christensen M, Siegel G, Flavell SW, Kim TK, Greenberg ME, Schratt G (2009) Mef2-mediated transcription of the miR379-410 cluster regulates activity-dependent dendritogenesis by fine-tuning Pumilio2 protein levels. *EMBO J* 28: 697–710

Fiore R, Khudayberdiev S, Saba R, Schratt G (2011) MicroRNA function in the nervous system. *Prog Mol Biol Transl Sci* 102: 47–100

Fiore R, Rajman M, Schwale C, Bicker S, Antoniou A, Bruehl C, Draguhn A, Schratt G (2014) MiR-134-dependent regulation of Pumilio-2 is necessary for homeostatic synaptic depression. *EMBO J* 33: 2231–2246

Gao J, Wang WY, Mao YW, Graff J, Guan JS, Pan L, Mak G, Kim D, Su SC, Tsai LH (2010) A novel pathway regulates memory and plasticity via SIRT1 and miR-134. *Nature* 466: 1105–1109

Gregory RI, Yan KP, Amuthan G, Chendrimada T, Doratotaj B, Cooch N, Shiekhattar R (2004) The Microprocessor complex mediates the genesis of microRNAs. *Nature* 432: 235–240

Grimm D, Streetz KL, Jopling CL, Storm TA, Pandey K, Davis CR, Marion P, Salazar F, Kay MA (2006) Fatality in mice due to oversaturation of cellular microRNA/short hairpin RNA pathways. *Nature* 441: 537–541

Huang YW, Ruiz CR, Eyler EC, Lin K, Meffert MK (2012) Dual regulation of miRNA biogenesis generates target specificity in neurotrophin-induced protein synthesis. *Cell* 148: 933–946

Im HI, Kenny PJ (2012) MicroRNAs in neuronal function and dysfunction. *Trends Neurosci* 35: 325–334

Jensen KB, Dredge BK, Stefani G, Zhong R, Buckanovich RJ, Okano HJ, Yang YY, Darnell RB (2000) Nova-1 regulates neuron-specific alternative splicing and is essential for neuronal viability. *Neuron* 25: 359–371

Kedde M, Strasser MJ, Boldajipour B, Oude Vrielink JA, Slanchev K, le Sage C, Nagel R, Voorhoeve PM, van Duijse J, Orom UA, Lund AH, Perrakis A, Raz E, Agami R (2007) RNA-binding protein Dnd1 inhibits microRNA access to target mRNA. *Cell* 131: 1273–1286

Kedde M, van Kouwenhove M, Zwart W, Oude Vrielink JA, Elkon R, Agami R (2010) A Pumilio-induced RNA structure switch in p27-3′UTR controls miR-221 and miR-222 accessibility. *Nat Cell Biol* 12: 1014–1020

Krol J, Loedige I, Filipowicz W (2010) The widespread regulation of microRNA biogenesis, function and decay. *Nat Rev Genet* 11: 597–610

Landthaler M, Gaidatzis D, Rothballer A, Chen PY, Soll SJ, Dinic L, Ojo T, Hafner M, Zavolan M, Tuschl T (2008) Molecular characterization of human Argonaute-containing ribonucleoprotein complexes and their bound target mRNAs. *RNA* 14: 2580–2596

Law WJ, Cann KL, Hicks GG (2006) TLS, EWS and TAF15: a model for transcriptional integration of gene expression. *Brief Funct Genomic Proteomic* 5: 8–14

Leo C, Chen JD (2000) The SRC family of nuclear receptor coactivators. *Gene* 245: 1–11

Licatalosi DD, Mele A, Fak JJ, Ule J, Kayikci M, Chi SW, Clark TA, Schweitzer AC, Blume JE, Wang X, Darnell JC, Darnell RB (2008) HITS-CLIP yields genome-wide insights into brain alternative RNA processing. *Nature* 456: 464–469

Lim LP, Lau NC, Garrett-Engele P, Grimson A, Schelter JM, Castle J, Bartel DP, Linsley PS, Johnson JM (2005) Microarray analysis shows that some microRNAs downregulate large numbers of target mRNAs. *Nature* 433: 769–773

Liu J, Carmell MA, Rivas FV, Marsden CG, Thomson JM, Song JJ, Hammond SM, Joshua-Tor L, Hannon GJ (2004) Argonaute2 is the catalytic engine of mammalian RNAi. *Science* 305: 1437–1441

Liu Y, Zhao Z, Yang F, Gao Y, Song J, Wan Y (2013) microRNA-181a is involved in insulin-like growth factor-1-mediated regulation of the transcription factor CREB1. *J Neurochem* 126: 771–780

Long W, Yi P, Amazit L, LaMarca HL, Ashcroft F, Kumar R, Mancini MA, Tsai SY, Tsai MJ, O'Malley BW (2010) SRC-3Delta4 mediates the interaction of EGFR with FAK to promote cell migration. *Mol Cell* 37: 321–332

Magill ST, Cambronne XA, Luikart BW, Lioy DT, Leighton BH, Westbrook GL, Mandel G, Goodman RH (2010) microRNA-132 regulates dendritic growth and arborization of newborn neurons in the adult hippocampus. *Proc Natl Acad Sci USA* 107: 20382–20387

McKee AE, Minet E, Stern C, Riahi S, Stiles CD, Silver PA (2005) A genome-wide in situ hybridization map of RNA-binding proteins reveals anatomically restricted expression in the developing mouse brain. *BMC Dev Biol* 5: 14

Meister G (2013) Argonaute proteins: functional insights and emerging roles. *Nat Rev Genet* 14: 447–459

Meskauskas A, Dinman JD (2001) Ribosomal protein L5 helps anchor peptidyl-tRNA to the P-site in Saccharomyces cerevisiae. *RNA* 7: 1084–1096

Mollet I, Barbosa-Morais NL, Andrade J, Carmo-Fonseca M (2006) Diversity of human U2AF splicing factors. *FEBS J* 273: 4807–4816

Muddashetty RS, Nalavadi VC, Gross C, Yao X, Xing L, Laur O, Warren ST, Bassell GJ (2011) Reversible inhibition of PSD-95 mRNA translation by miR-125a, FMRP phosphorylation, and mGluR signaling. *Mol Cell* 42: 673–688

Nishino J, Kim I, Chada K, Morrison SJ (2008) Hmga2 promotes neural stem cell self-renewal in young but not old mice by reducing p16Ink4a and p19Arf Expression. *Cell* 135: 227–239

Pillai RS, Bhattacharyya SN, Artus CG, Zoller T, Cougot N, Basyuk E, Bertrand E, Filipowicz W (2005) Inhibition of translational initiation by Let-7 MicroRNA in human cells. *Science* 309: 1573–1576

Racca C, Gardiol A, Eom T, Ule J, Triller A, Darnell RB (2010) The Neuronal Splicing Factor Nova Co-Localizes with Target RNAs in the Dendrite. *Front Neural Circuits* 4: 5

Schratt GM, Nigh EA, Chen WG, Hu L, Greenberg ME (2004) BDNF regulates the translation of a select group of mRNAs by a mammalian target of rapamycin-phosphatidylinositol 3-kinase-dependent pathway during neuronal development. *J Neurosci* 24: 9366–9377

Schratt GM, Tuebing F, Nigh EA, Kane CG, Sabatini ME, Kiebler M, Greenberg ME (2006) A brain-specific microRNA regulates dendritic spine development. *Nature* 439: 283–289

Siegel G, Obernosterer G, Fiore R, Oehmen M, Bicker S, Christensen M, Khudayberdiev S, Leuschner PF, Busch CJ, Kane C, Hubel K, Dekker F, Hedberg C, Rengarajan B, Drepper C, Waldmann H, Kauppinen S, Greenberg ME, Draguhn A, Rehmsmeier M *et al* (2009) A functional screen implicates microRNA-138-dependent regulation of the depalmitoylation enzyme APT1 in dendritic spine morphogenesis. *Nat Cell Biol* 11: 705–716

Siegel G, Saba R, Schratt G (2011) microRNAs in neurons: manifold regulatory roles at the synapse. *Curr Opin Genet Dev* 21: 491–497

Smrt RD, Szulwach KE, Pfeiffer RL, Li X, Guo W, Pathania M, Teng ZQ, Luo Y, Peng J, Bordey A, Jin P, Zhao X (2010) MicroRNA miR-137 regulates neuronal maturation by targeting ubiquitin ligase mind bomb-1. *Stem Cells* 28: 1060–1070

Stutz F, Izaurralde E (2003) The interplay of nuclear mRNP assembly, mRNA surveillance and export. *Trends Cell Biol* 13: 319–327

Tang G (2005) siRNA and miRNA: an insight into RISCs. *Trends Biochem Sci* 30: 106–114

Tharun S, He W, Mayes AE, Lennertz P, Beggs JD, Parker R (2000) Yeast Sm-like proteins function in mRNA decapping and decay. *Nature* 404: 515–518

Valluy J, Bicker S, Aksoy-Aksel A, Lackinger M, Sumer S, Fiore R, Wust T, Seffer D, Metge F, Dieterich C, Wohr M, Schwarting R, Schratt G (2015) A coding-independent function of an alternative Ube3a transcript during neuronal development. *Nat Neurosci* 18: 666–673

Wang D, Zhang Z, O'Loughlin E, Lee T, Houel S, O'Carroll D, Tarakhovsky A, Ahn NG, Yi R (2012) Quantitative functions of Argonaute proteins in mammalian development. *Genes Dev* 26: 693–704

Xu J, Wu RC, O'Malley BW (2009) Normal and cancer-related functions of the p160 steroid receptor co-activator (SRC) family. *Nat Rev Cancer* 9: 615–630

Yu C, York B, Wang S, Feng Q, Xu J, O'Malley BW (2007) An essential function of the SRC-3 coactivator in suppression of cytokine mRNA translation and inflammatory response. *Mol Cell* 25: 765–778

Zhang J, Chen QM (2013) Far upstream element binding protein 1: a commander of transcription, translation and beyond. *Oncogene* 32: 2907–2916

Zhou A, Ou AC, Cho A, Benz EJ Jr, Huang SC (2008) Novel splicing factor RBM25 modulates Bcl-x pre-mRNA 5′ splice site selection. *Mol Cell Biol* 28: 5924–5936

Zou Y, Chiu H, Zinovyeva A, Ambros V, Chuang CF, Chang C (2013) Developmental decline in neuronal regeneration by the progressive change of two intrinsic timers. *Science* 340: 372–376

Expanded view

Material and Methods

DNA constructs

The firefly reporter constructs UBE3A-luc, APT1-luc, LIN41-luc WT, LIN41-luc mutant and LIMK1-luc were generated by inserting the corresponding 3'UTRs downstream of the firefly gene into the XbaI restriction site of pGL3-promoter or pGL4.13 (Promega). UBE3A-luc contains a 606 bp fragment of the rat UBE3A 3'UTR (Valluy J. et al., 2015). APT1-luc is derived from pGL3-Apt1 (Siegel et al., 2009). The wildtype and mutant 3'UTRs of *C.elegans* LIN41 were kindly provided by D. Bartel. LIN41 WT 3'UTR was excised by NotI and MssI and LIN41 mutant 3'UTR was PCR amplified. The LIMK1 3'UTR was PCR amplified from pGL3-Limk1 (Schratt et al., 2006). The 138-sponge-luc reporter was generated by inserting six binding sites for miR-138 carrying a bulge at position 9-12 (Ebert et al., 2007) into the XbaI site of pGL4.13. The ctrl sponge was created by inserting the reverse sequence of 138 sponge in pGL4.13. The renilla gene from phRL-TK was first cloned into pGL3-promoter using unique NcoI and XbaI sites and subsequently excised with HindIII and XbaI to generate pGL4-RL. For GFP-fusion proteins, open reading frames from a mouse brain cDNA library (C57BL/6) were PCR amplified and inserted into pEGFP_C1 (Clonetech) using the indicated restriction sites. The open reading frame (ORF) of Ncoa3 was amplified by PCR from a mouse cDNA clone (Clone ID: 30104508, Openbiosystems) and inserted to KpnI and AgeI restriction sites of pEGFP_N1 (Clontech). Silent mutations were introduced by site directed mutagenesis to generate shRNA-resistant Nova1 ($Nova1^R$) and Ncoa3 ($Ncoa3^R$). A predicted nuclear receptor binding site in the mouse Ago2 promotor (GRCm38/mm10, chr. 15 pos. 73185409-73185468) was cloned into the BglII and HindIII sites of pGL4.

For improved expression, a minimal promoter was further inserted to the HindIII site by oligo annealing and ligation. The Flag/HA-Ago2 expression vector was kindly provided by Thomas Tuschl. For both types of shRNA expression vectors, pSuper basic (oligoengine) and AAV (Christensen et al., 2009), the same DNA oligos were annealed and ligated into the BglII and HindIII restriction sites.

Plasmids containing wild-type and mutant 3'UTRs of mouse IQGAP1 and HMGA2 were kindly provided by D. Bartel. The 3'UTRs were excised using the SacI/XbaI and XbaI/NotI restriction sites respectively and ligated to the XbaI site of pGL4 after blunt end generation.

Antibodies

Immunohistochemistry (ICC) or Western Blot analysis (WB) at the given dilution: rabbit anti-Ncoa3 (SRC-3 clone 5E11 from Cell Signaling, WB 1:1000, ChIP), mouse anti-Ncoa3 (AIB-1 clone34 from BD Biosciences, ICC: 1:200), rabbit anti-MAP2 (Cell Signaling cat.# 4542 , ICC: 1:200), mouse anti-MAP2 (clone HM-2 from Sigma-Aldrich, ICC: 1:2000), rabbit anti-α-Tubulin (Cell Signaling cat.# 2144, WB: 1:5000), mouse anti-β-Actin (clone AC-15 from Sigma-Aldrich, WB: 1:10,000), rabbit anti-HDAC2 (ab32117 from Abcam, WB: 1:5000), mouse anti-Limk1 (clone 42 from BD Biosciences, WB: 1:750), mouse anti-Ago2 (clone 2D4 from Wako, WB: 1:1000), rabbit anti-Ago2 (ab32381 from Abcam, ICC: 1:200), chicken anti-GFP (ab13970 from Abcam, WB: 1:10,000), rabbit anti-Nova1 (Merck Millipore cat.# 07-637, WB: 1:1500; ICC: 1:250), rabbit anti Nova-pan (obtained from R. Darnell; WB: 1:5000), rabbit anti-HA (ab9110 from Abcam, ICC: 1:500), mouse anti-Flag (clone M2 from Sigma-Aldrich, WB: 1:1000), rabbit anti-Drosha (sc-33778 from SCBT, WB: 1:500).

Species specific secondary antibodies for WB were HRP-conjugated (Calbiochem) and applied at 1:20,000 dilutions.

Secondary antibodies for ICC were anti-rabbit conjugated to Alexa 488, anti-mouse conjugated to Alexa 647 and anti-rabbit conjugated to Alexa 647 (Life technologies) at a dilution of 1:1000.

RNA extraction and Reverse Transcription-quantitative PCR (RT-qPCR)

For RNA extraction, hippocampal neurons were cultured in the presence of FUDR and infected on 4DIV. Total RNA was extracted on 14DIV using mirVana miRNA isolation Kit (Ambion). RNA was further treated with Turbo DNase (Ambion) according to the manufacturer's protocol. After denaturation of the DNase for 10 min. at 75°C in the presence of 15 mM EDTA we reverse transcribed 1 μg total RNA to cDNA using the iScript cDNA synthesis Kit (BioRad) supplemented with Mg^{2+} (final concentration 6 mM $MgCl_2$ and 12 mM EDTA). Quantitative PCR was processed in triplicates with 10μl total volume (0.67 μl cDNA and 0.25 μM primer concentration) using the iTaq SYBR Green Supermix with ROX (BioRad) on a Step One Plus instrument (Applied Biosystems).

Luciferase assay

Hippocampal neurons (11DIV) or cortical neurons (5DIV, 12DIV) were transfected as above in duplicates with 50-100 ng of the indicated pGL4 construct, equal amount of pGL4-RL and either 10 ng of the given pSuper vector or 7,5 pmol of siRNA duplex, or co-transfected with 5 pmol of miRNA duplex RNA (miR-134 or miR-138) (amount for one well of 24 well plate). Lysis was carried out 2-3 days later and the activity of both firefly and renilla was measured using the Dual Luciferase Reporter System (Promega) on the GloMax R96 Microplate Luminometer (Promega). Firefly activity was normalized to renilla activity and a basal condition which did not contain a shRNA expression vector

or siRNA was set as 1. Tethering experiments were performed by co-transfecting cortical neurons at 5DIV with 150 ng pCI-Neo-NHA or 250-400 ng NHA-fusion constructs, 50 ng of pRL-5boxB (obtained from R. Pillai) and 50 ng of pGL4.13 (Promega). Luciferase assay was performed 2 days after transfection and renilla activity was normalized to firefly activity.

Western blot analysis

The concentration of extracts was determined by BCA assay (Pierce) and equal protein amounts were separated on a SDS-PAGE. After wet transfer (BioRad) to a PVDF membrane (Millipore) unspecific binding was blocked by incubation with 5% milk powder in Tris-buffered saline containing 0.1% Tween 20 (TBS-T). The same milk solution was used to dilute primary and secondary antibodies which were incubated at 4°C overnight or for 1 h at RT respectively, each followed by 3 wash steps with (TBS-T) for 10 min. Secondary HRP-conjugated antibodies were detected using the ECL Prime Western Blotting Detection Reagent (GE Healthcare). Band intensities of scanned films were measured with Image J.

Immunocytochemistry and confocal microscopy

For microscopic analysis hippocampal neurons were fixed by 4% paraformaldehyde/sucrose in PBS for 15 min. followed by three PBS washes. For analysis of neuronal morphology (see below), the GFP expressing cells were mounted directly in Aquapoly (Polysciences). For immunocytochemistry the cells were pre-incubated with GDB (20 mM $NaPO_4$ pH 7.4, 450 mM NaCl, 0.3% Triton X-100, 0.1% Gelatine) for 10 min. followed by incubation with the primary antibody for 1 h at RT diluted in GDB. After the cells were washed four times with PBS, the secondary antibody was applied for 1 h at RT diluted in GDB. After three further PBS washes,

Hoechst was incubated at 1:5000 in PBS for 5 min. and the cells were mounted as above.

All images were acquired with a LSM 5 Pascal (Zeiss) microscope. Presented immunocytochemistry images are the maximum projections of 2-4 confocal stacks with a *z*-distance of 0.5-1 μm. Measurements of average signal intensity and *x*-*y*-distance as well as further image cropping/magnification steps were carried out with Image J software.

Primers

All primer sequences are given 5' to 3'. The following primers were used for qPCR:

Ncoa3 FW: GCTTCGTCTCGACCCACTTC

Ncoa3 REV: GGTCGGATGCCTTGTCCTAC

Ago1 FW: TCATTATCGTCATCCTGCCCG

Ago1 REV: GGCAGAGGTTGGACAGAGTC

Ago2 FW: TCACATTCATCGTGGTGCAGA

Ago2 REV: TCTTTGTGTCGACGGTTGTG

Ago3 FW: GCTGTAGGCGACGCAAGTTC

Ago3 REV: TGAAAGCTCCAGGCAGAAGAG

Ago4 FW: GTTCAGTCAGGAGGTCGTGC

Ago4 REV: TGGCCAAGCTACCTGTTTCA

Tnrc6a FW: GCTCAAGTGCCTCCTCCATT

Tnrc6a REV: GGTTCAGCATGGCTACCTGT

Tnrc6b FW: CCCATAGGACACAACCCCAC

Tnrc6b REV: CTCCAAGGAGATGCCGGTTT

Tnrc6c FW: CACTTTTGCCAGAACTTACTAAGAC

Tnrc6c REV: ACAGGCAGATGCACGTTTG

Dicer FW: CAGTTGTCCATCATGCCCTC

Dicer REV: CTCAGCGCCACTCTTGAGAA

Trbp FW: CAGTCTGAGTGCAACCCTGT

Trbp REV: TGGTGAACTCTTTGCGGTGA

Arhgdib FW: TACAGAGACACACAGGGCGG

Arhgdib REV: CGGCTTGTAGTTGAGCTTGC

Htra4 FW: GGCTCCGGAACTCCGATATG

Htra4 REV: ATCCCAATCACCTCGCCATC

Gpr3 FW: AACCCGGTCATTTACGCCTT

Gpr3 REV: CTGGCGGACCTAACCTTCTG

Spast FW: GCGCATCGACGAGGAAGAG

Spast REV: TGTTCACCTTGGCCCGTAAC

Cyb5r3 FW: TTCAAGGACACGCATCCCAA

Cyb5r3 REV: GGACTTCTTGTCTGCACGGA

Map9 FW: GGCAGCGGTTTATCAGGAGT

Map9 REV: CCAGGCCTCAAATGACGCTA

U6 snRNA FW: CTCGCTTCGGCAGCACA

U6 snRNA REV: AACGCTTCACGAATTTGCGT

GAPDH FW: GCCTTCTCTTGTGACAAAGTGGA

GAPDH REV: CCGTGGGTAGAGTCATACTGGAA

Limk1 FW: CCTCCGAGTGGTTTGTCGA

Limk1 REV: CAACACCTCCCCATGGATG

Rgs4 FW: ACAAGCCGGAACATGTTAGAG

Rgs4 REV: AGACTTGAGGAAACGACGGT

The following oligos were used to create shRNA expression constructs:

Control shRNA FW1: GATCCCCAAACCTTGTGGTCCTTAGGTTCAAGAGA

FW2: CCTAAGGACCACAAGGTTTTTTTTA

REV1: AGCTTAAAAAAAACCTTGTGGTCCTTAGGTCTCTTGAA

REV2: CCTAAGGACCACAAGGTTTGGG

Ncoa3 shRNA#1 FW1: GATCCCCGCAGCAGTAATGATGGATCTTCAAGAGA

FW2: GATCCATCATTACTGCTGCTTTTTA

REV1:

AGCTTAAAAAGCAGCAGTAATGATGGATCTCTCTTGAA

REV2: GATCCATCATTACTGCTGCGGG

Ncoa3 shRNA#2 FW1: GATCCCCGGAGACAGTGAGACAGATATTCAAGAGA

(used in all major FW2: TATCTGTCTCACTGTCTCCTTTTTA

experiments) REV1:

AGCTTAAAAAGGAGACAGTGAGACAGATATCTCTTGAA

REV2: TATCTGTCTCACTGTCTCCGGG

Nova1 shRNA FW1: GATCCCCGGTACTACTGAGAGGGTTTTCAAGAGA

FW2: AAACCCTCTCAGTAGTACCTTTTTA

REV1: AGCTTAAAAAGGTACTACTGAGAGGGTTTTCTCTTGAA

REV2: AAACCCTCTCAGTAGTACCGGG

Drosha shRNA FW1: GATCCCCCAACATAGACTACACGATTTTCAAGAGA

FW2: AATCGTGTAGTCTATGTTGTTTTTGGAAA

REV1: AGCTTTTCCAAAAACAACATAGACTACACGATTTCTCTTGAA

REV2: AATCGTGTAGTCTATGTTGGGG

DGCR8 shRNA FW1: GATCCCCAACAATTTGGAGACTAGATGAATTCAAGAGA

FW2: TTCATCTAGCTCCAAATTGTTTTTTTGGAAA

REV1:

AGCTTTTCCAAAAAAACAATTTGGAGCTAGATGAATCTCTTGAA

REV2: TTCATCTAGCTCCAAATTGTTGGG

The following primers were used to clone the mouse Ncoa3 ORF to pEGFP_N1:

Ncoa3-KpnI-FW: GACTGGTACCATGAGTGGACTAGGCGAAAG

Ncoa3-AgeI-REV: GACTACCGGTGTGCAGTATTTCTGATCGG

The following primers were used to clone the mouse Nova1 ORF to pEGFP_C1:

Nova1-XhoI-FW: GACTCTCGAGGCATGGCGGCAGCTCCCATTC

Nova1-SmaI-REV: GACTCCCGGGTCAACCCACTTTCTGAGGATTGGC

The following primers were used to clone the mouse Ewsr1 ORF to pEGFP_C1:

Ewsr1-XhoI-fw: GACTCTCGAGGCGCGTCCACGGATTACAGT

Ewsr1-SmaI-rev: GACTCCCGGGCTAGTAGGGCCGGTCTCTG

The following primers were used for site directed mutagenesis:

Ncoa3^{R}-FW: GTGCCATCCTAAAGGAGACCGTTCGCCAGATACGGCAAATAAAAG

Ncoa3^{R}-REV: CTTTTATTTGCCGTATCTGGCGAACGGTCTCCTTTAGGATGGCAC

Nova1^{R}-FW: GATTTTTATCCAGGTACCACCGAGCGGGTTTGCTTGATCCAGG

Nova1^{R}-REV: CCTGGATCAAGCAAACCCGCTCGGTGGTACCTGGATAAAAATC

The following primers were used to clone 3’UTRs to pGL4:

LIN41-FW: GATCTCTAGACACTTTCTTCTTGCTCTTTAC

LIN41-REV: GATCGCTAGCTTTATTCCAATTATGTTATCAG

LIMK1-FW: CTTCTAGAGATACTTGGAGGATAGACCCTCACC

LIMK1-REV: GCCCCGACTCTAGCTAGCGGGAGCACAGAATTGAT

The following primers were used for cloning of NHA-fusion constructs:

NHA-Nova1-Xba1-FW: TCTCTAGAATGGCGGCAGCTCCCATTCAGCAGAACG

NHA-Nova1-Not1-REV:

CCGGTGGCGGCCGCGTCAACCCACTTTCTGAGGATTGGCAG

NHA-Nova1-del1-Not1-REV:

CTGTGGATCCTCTGCGGCCGCCTGCTAGATAAGTTCAACAG

NHA-Nova1-del2-Xba1-FW:

TGAATCTAGAATCCAGAAGATACAAGAGGATCCACAGAGTG

NHA-EGFP-FW: CCACCGGTCGACACCATGGTGAGCAAGGGCG

NHA-EGFP-REV: ATCTAGAGTCGCGGCCGCTTTACTTGTAC

NHA-Ncoa3-MluI-FW: GACTACGCGTATGAGTGGACTAGGCGAAAG

NHA-Ncoa3-XbaI-REV: GATCTCTAGATCAGCAGTATTTCTGATCGGGG

The following primers were used for cloning of the mouse Ago2 nuclear receptor element and the minimal promotor to pGL4.13:

Ago2-RE-FW1: GATCTGCCGGGAGGTGGCGGTGTGGTCACG

Ago2-RE-FW2: CGCACGGGTCTGGCCGCGTCCAAGTTCAAGCTCTGA

Ago2-RE-REV1: ACCCGTGCGCGTGACCACACCGCCACCTCCCGGCA

Ago2-RE-REV2: AGCTTCAGAGCTTGAACTTGGACGCGGCCAG

Min-prom-FW1: AGCTTAGACACTAGAGGG

Min-prom-FW2: TATATAATGGAAGCTCGACTTCC

Min-prom-FW1: AGCTGGAAGTCGAGCTTCC

Min-prom-REV2: ATTATATACCCTCTAGTGTCTA

The following primers were used to amplify rat genomic regions proximal to the transcriptional start site in ChIP experiments:

Ago2-genomic-FW: ATGGTGCACCCTAAGCTTCC

Ago2-genomic-REV: TGTGATGAAGTGGATCTGCACG

Cyb5r3-genomic-FW: AGAATGGCAGTGAAGCACCA

Cyb5r3-genomic-REV: ATCTGCCCTGGAAGATTGCC

Map9-genomic-FW: ATAAGCTGATAGGGCACTGCG

Map9-genomic-REV: AACCGACTGGTCTCTTGGGT

Spast-genomic-FW: CCAGTCAGACTCCTGCGAAC

Spast-genomic-REV: AGATCTGGGGTTTCGATGGC

beta-globin-genomic-FW: TCTAGAAGGTACCCTCATGGCTGAA

beta-globin-genomic-REV: GGATATGCCCTGTGGAGTGTTGAC

Figure legends

Figure E1: Validation of siRNA specificity in luciferase reporter assays.

A) Primary rat cortical neurons were transfected with the unmodified pGL4 (empty-luc) and luciferase activity was quantified as in Fig. 1 C and D. B) Western blot analysis with lysates obtained from HEK293 cells that had been co-transfected with the indicated GFP-tagged protein expression constructs and different siRNAs. Upper panels: anti-GFP Western. Lower panel: anti-ß-Actin Western (loading control). For GFP-Ewsr1, a non-specific band (*) serves as internal loading control.

Figure E2: Nova1 expression in cortical neurons and validation of the anti-Ncoa3 antibody for ICC.

A) Western blot analysis of Nova1 protein using whole cell extracts harvested from rat cortical neurons at the indicated days of *in vitro* (DIV) culture. ß-actin was used as a loading control. B) Western blot analysis of Nova1 protein using brain extracts from Nova1 knockout mice. C) Western blot analysis of Ncoa3 protein using whole cell extracts harvested from FUDR-treated rat hippocampal neurons at the indicated days of *in vitro* (DIV) culture. α-Tubulin was used as a loading control. D) Immunocytochemistry analysis of Ncoa3 expression (red) in hippocampal neuron cultures at 7DIV. MAP2 staining (green) was used to visualize neurons, Hoechst (blue) to visualize nuclei. Right: Magnification of insert depicted on the left. For simplicity, only the Ncoa3 signal is shown in greyscale. Cell and nuclear outlines derived from MAP2 and Hoechst staining, respectively, are shown in yellow. Scale bar = 10 μm. E) Immunocytochemistry for Ncoa3 (white in left panel, red in right panel) in hippocampal neurons (14DIV) that were transfected with the indicated shRNA expression vectors and GFP. F) Quantification of the average Ncoa3 signal intensity in the soma of

transfected neurons (right panel). Presented values are mean ± standard deviation from three independent experiments (10 cells per condition) with normalization to a basal condition without shRNA. **p<0.01 (student's t-test). Scale bar = 50 μm.

Figure E3: Validation of Ncoa3/Nova1 knockdown and target regulation.

A, B) Western blot analysis of Nova1 (A) and Ncoa3 (B) protein using whole cell extracts from cortical neurons (4-6DIV) that have been nucleofected with the indicated shRNA expression vectors. Migration of the Nova1-specific band is marked by an arrowhead. ß-Actin was used as a loading control. C-E) Reporter gene assay performed in either rat hippocampal neurons (14DIV, C) or cortical neurons (14DIV, D, E) that have been transfected with pGL4 vectors carrying the indicated 3'UTR together with either control, Nova1 or Ncoa3 shRNA expression vectors 3 days before. Relative luciferase activity (RLA) represents the ratio of firefly reporter activity to renilla control reporter activity which is normalized to a basal condition without shRNA expression vector. Presented are averages ± standard deviations from three independent experiments. One-way ANOVA: p<0.0001 (E), p<0.001 (D), p<0.05 (C). Tukey HSD test (C) and unpaired student's t-test (D, E): *p<0.05, **p<0.01.(student's t-test to control shRNA). F, G) Reporter gene assays in cortical neurons (14DIV) were performed in principle as described in C-E), instead that GFP expression vectors were used. Presented are averages ± standard deviations from three independent experiments. unpaired student's t-test: *p<0.05.

Figure E4: Validation of Nova1 and Ncoa3 dependent regulation of Limk1.

A) Technical replicate of the experiment in Fig. 4A) and the corresponding quantification of n=2 in B). C, D) Technical replicates of the experiments in Fig. 4B) and the quantification of n=3 in E). *p<0.05 (student's t-test).

Figure E5: Validation of Nova1-Ago interaction by co-IP.

A) This experiment is a biological replicate of Fig. 5A. B) Nova1 band intensities from figures 5A and E5A were quantified using ImageJ software. Values are given as percent intensity compared to the input signal and represent the average of two independent experiments. C, D) Equal experimental setup as in Fig. 5A) and E5A) except that RNAse A was added to the lysate before IP. E) Validation of anti-pan-Nova antibody. Western blot analysis using brain lysate from Nova knockout mice. F) Western blot analysis in lysates from HEK293 cells transfected with the indicated NHA-fusion constructs. Upper panel: anti-HA Western Blot; lower panel: anti-ß-Actin Western Blot as loading control. * non-identified cross-reactive protein. G) Immunocytochemistry in neurons transfected with the indicated NHA-Nova1 constructs. Upper panel: anti-HA. Middle panel: Hoechst (nuclei); lower panel: MAP2 (dendrites). H) Tethering assay in HEK293 cells with the indicated expression constructs as in Fig. 5D-F. Presented are averages ± standard deviations from three independent experiments. One-way ANOVA: p<0.001. Tukey HSD test: *p<0.05, **p<0.01, ns= not significant.

Figure E6: Dendritic outgrowth after Nova1 knock-down and validation of Ncoa3 and Drosha shRNA efficacy.

A) Dendritic outgrowth of cultured hippocampal neurons was analyzed by Sholl's method after transfection with GFP and Nova1 shRNA, control shRNA expression vector, or no additional vector as in Fig. 6. B) Summation of the intersection number

over all analyzed distances from the data in A). C) Western blot analysis of GFP-Ncoa3 in cell extracts from HEK293 cells that had been transfected with indicated shRNA constructs together with GFP-Ncoa3 expression vectors. Expression of co-transfected GFP was used as a loading control. Note that GFP-Ncoa3^{R} is not resistant to Ncoa3 shRNA#1, but to shRNA#2 which is used for all experiments in the main body. D) Western blot analysis of Drosha in hippocampal neurons (19DIV) that had been infected with rAAV expressing the indicated shRNAs after 12DIV. ß-Actin was used as a loading control. E) qPCR analysis of indicated mRNAs in rAAV-Drosha or control shRNA infected neurons. Values are normalized to the rAAV control shRNA condition for each target mRNA. N=3. F) Taqman qPCR analysis of indicated mature miRNAs in rAAV-Drosha or control shRNA infected neurons. Values are normalized to the rAAV control shRNA condition for each target mRNA. N=2.

Figure E7: Figure 7 does not have an expanded view.

Figure E8: rAAV-infection efficacy, microarray validation and additional Ncoa3-ChIP experiments.

A) Immunocytochemistry in hippocampal neurons (14DIV) that had been infected with rAAV expressing the indicated shRNAs after 4DIV. MAP2 staining (red) was used to visualize neurons, Hoechst (blue) to visualize cell nuclei. Co-expression of GFP from rAAV vectors in MAP2-positive cells was used to determine transfection efficiency with approx. 80% from 3 independent infections (approx. 80%). Scale bar = 100 µm. B) Matrix of Pearson's correlation coefficients of signals obtained from 6 independent microarray hybridizations. C) qPCR analysis of indicated mRNAs in hippocampal neurons (14DIV) that had been infected with rAAV for the expression of indicated shRNAs at 4DIV. mRNA levels were normalized to GAPDH and a non-infected basal

condition was set to 1. Presented are averages ± standard deviations from three independent infections. **p<0.01 (unpaired student's t-test). D) Quantification of Ago2 protein levels in hippocampal neurons from three independent Western Blots performed as in Fig. 8D. Band densities were normalized to α-Tubulin and a non-infected condition (basal) was set as 1. Presented are averages ± standard deviations. *p<0.05 (unpaired student's t-test). E, F) qPCR analysis of indicated Ncoa3-regulated transcripts from two additional Ncoa3-ChIP experiments performed in either control shRNA (black) or Ncoa3 shRNA (grey) infected neurons. Values are presented as fraction of the respective input DNA used for ChIP. As a specificity control, ChIP with an unrelated IgG was performed in control shRNA transfected neurons (white). G) Alignment of mouse, rat and human Ago2 promoter sequences for the construction of the Ago2 luciferase promoter reporter used in Fig. 8F. The putative RXRA binding site is depicted in bold. Non-conserved nucleotides are shown in italics.

Figure E9: Validation of Flag/HA-Ago2 expression in hippocampal neurons and HEK293 cells.

A) Left panel: Immunocytochemistry using anti-HA antibody (red) in hippocampal neurons (14DIV) that had been transfected with either Flag/HA-Ago2 (top) or an empty Flag/HA plasmid (control vector, bottom) three days before. Co-transfection of GFP (green) was used to outline neuronal morphology. Hoechst counterstain (blue) was used to visualize nuclei. Scale bar = 40 μm. Right panel: Higher magnification of the neurons shown on the left, illustrating the predominant cytoplasmic localization of Flag/HA-Ago2. Scale bar = 15 μm. B) Western blot analysis of Flag/HA-Ago2 using anti-Flag antibody in cell extracts from HEK293 cells that had been transfected with Flag/HA-Ago2 or empty Flag/HA plasmid (control vector). α-Tubulin was used as a

loading control. C) Immunocytochemistry using anti-Ago2 antibody (upper panel) in hippocampal neurons (12DIV) treated as described in Fig. 9A. Co-transfection of GFP (green, lower panel) served to outline the neuronal soma and was used for quantification of the signal. Scale bar = 10 μm.

Extended dataset 1: List of all siRNAs used for in initial screen.

Extended dataset 2: Results of the initial screen.

Extended dataset 3: Complete list of genes altered by rAAV-Ncoa3 shRNA (Fc>1.3, p<0.05) including non-annotated transcripts.

Expanded View

Figure E1

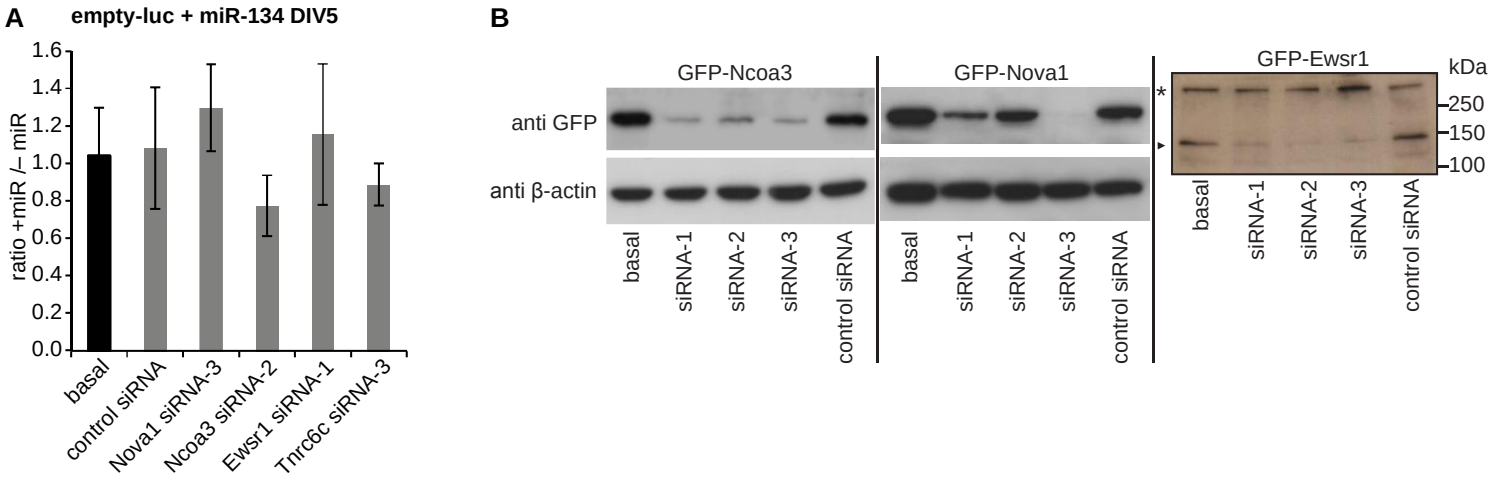

Figure E2

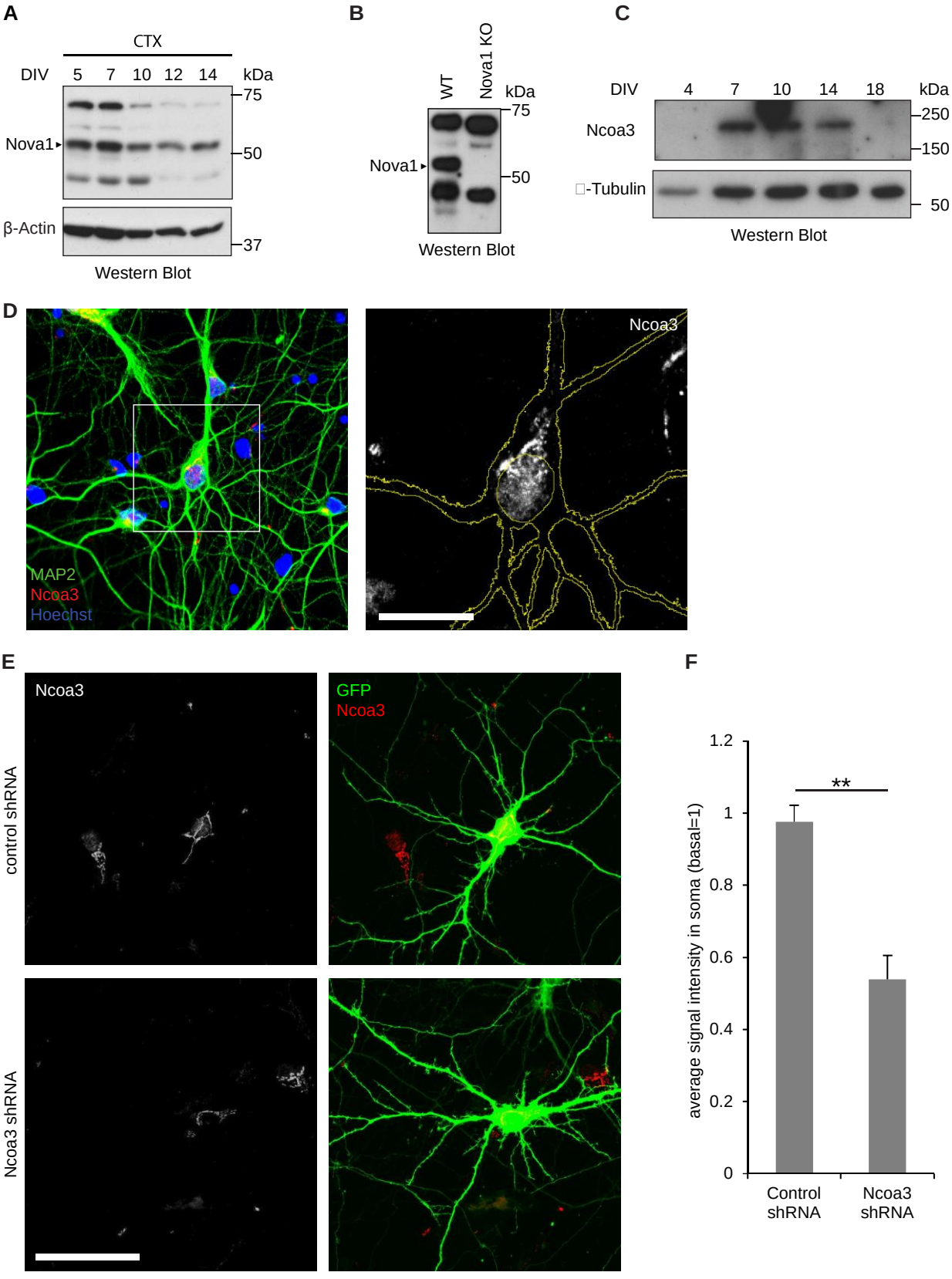
A
CTX
DIV 5 7 10 12 14 kDa
75
Nova1
50
β-Actin
37
Western Blot
B
WT
Nova1 KO
kDa
75
Nova1
50
Western Blot
C
DIV 4 7 10 14 18 kDa
250
Ncoa3
150
□-Tubulin
50
Western Blot
D
MAP2
Ncoa3
Hoechst
Ncoa3
E
Ncoa3
GFP
Ncoa3
control shRNA
Ncoa3 shRNA
F
average signal intensity in soma (basal=1)
1.2
1
0.8
0.6
0.4
0.2
0
**
Control shRNA
Ncoa3 shRNA

Figure E3

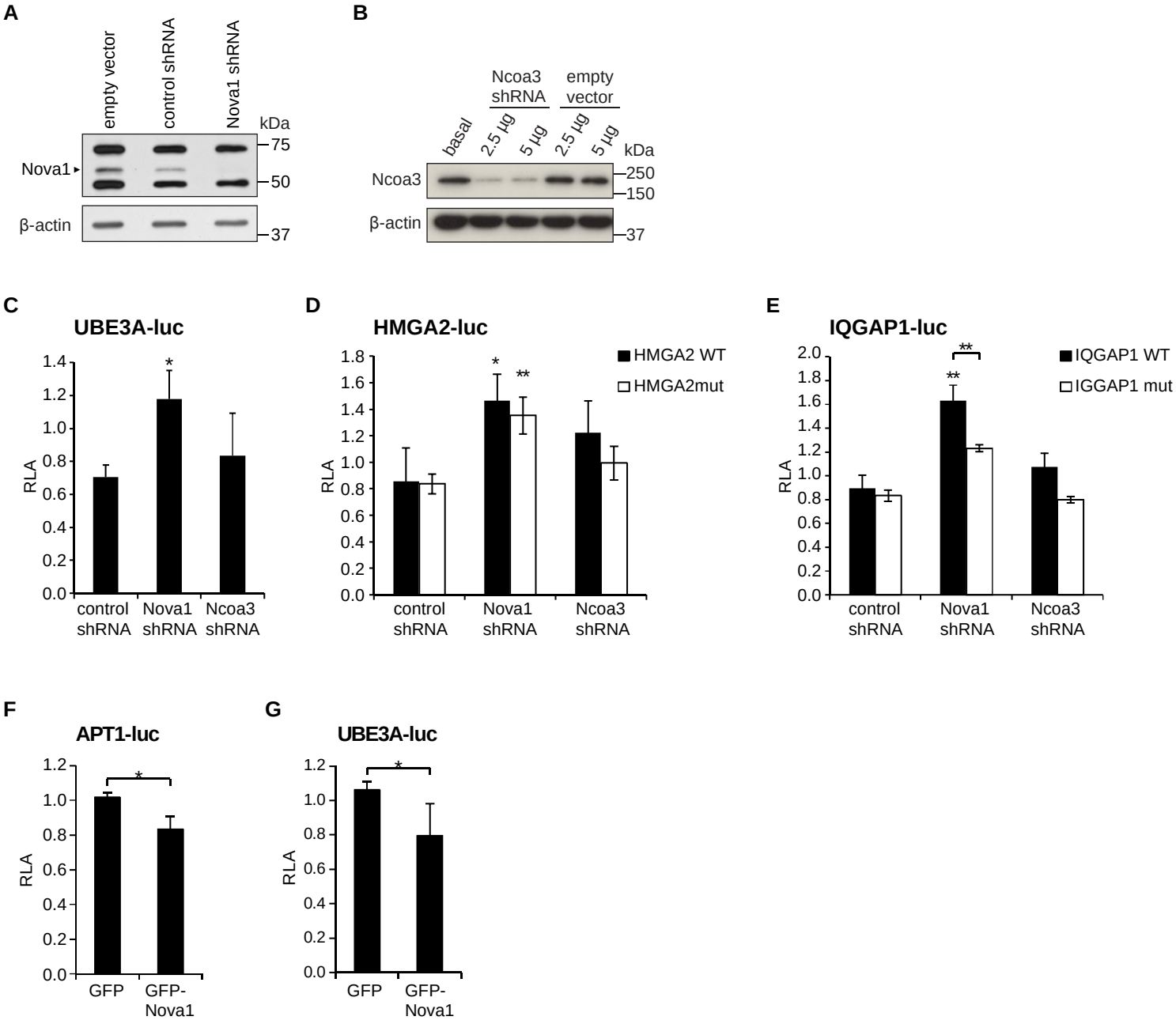
A
empty vector
control shRNA
Nova1 shRNA
kDa
Nova1
75
50
β-actin
37
B
Ncoa3 shRNA
empty vector
basal
2.5 µg
5 µg
2.5 µg
5 µg
kDa
Ncoa3
250
150
β-actin
37
C
UBE3A-luc
RLA
control shRNA
Nova1 shRNA
Ncoa3 shRNA
D
HMGA2-luc
HMGA2 WT
HMGA2mut
RLA
control shRNA
Nova1 shRNA
Ncoa3 shRNA
E
IQGAP1-luc
IQGAP1 WT
IGGAP1 mut
RLA
control shRNA
Nova1 shRNA
Ncoa3 shRNA
F
APT1-luc
RLA
GFP
GFP-Nova1
G
UBE3A-luc
RLA
GFP
GFP-Nova1

Figure E4

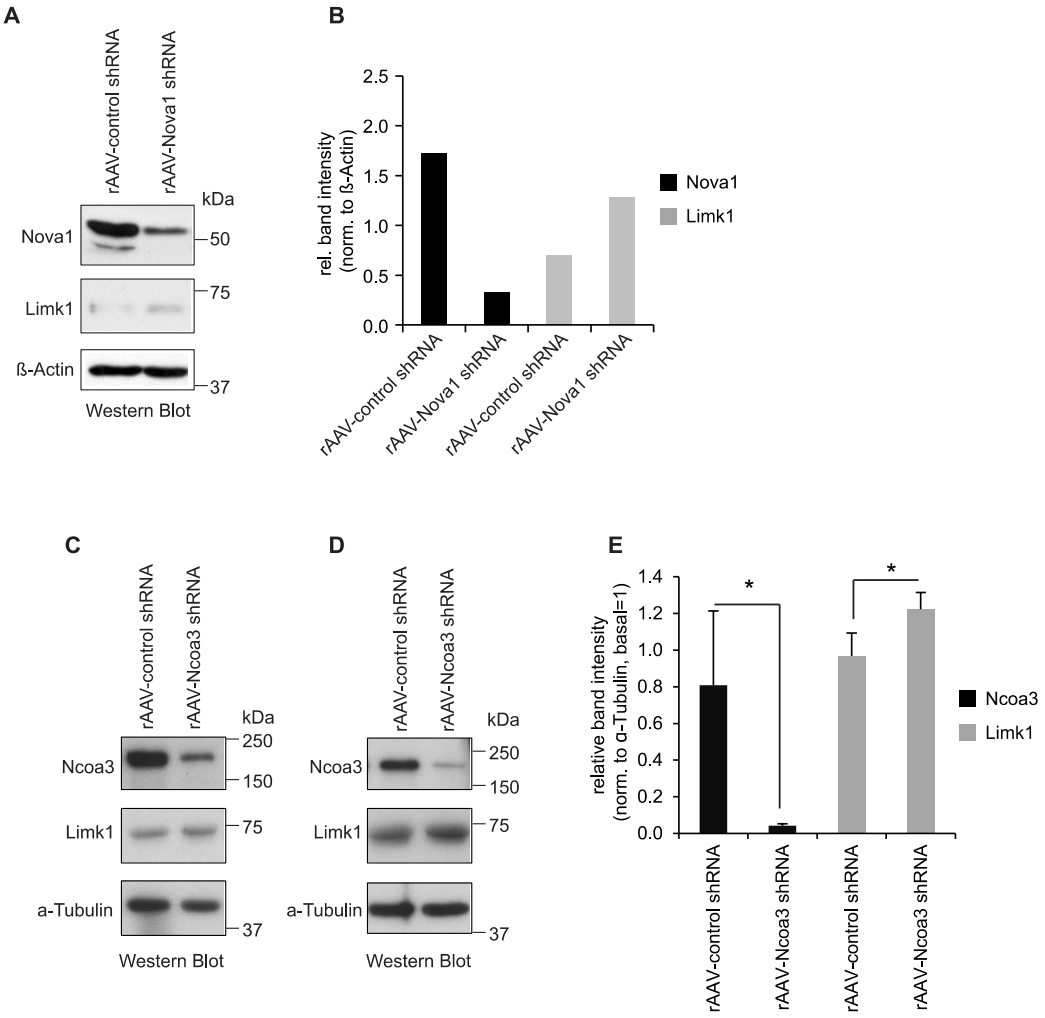
A
rAAV-control shRNA
rAAV-Nova1 shRNA
kDa
Nova1
50
Limk1
75
ß-Actin
37
Western Blot
B
rel. band intensity (norm. to ß-Actin)
2.5
2.0
1.5
1.0
0.5
0.0
Nova1
Limk1
rAAV-control shRNA
rAAV-Nova1 shRNA
rAAV-control shRNA
rAAV-Nova1 shRNA
C
rAAV-control shRNA
rAAV-Ncoa3 shRNA
kDa
Ncoa3
250
150
Limk1
75
a-Tubulin
37
Western Blot
D
rAAV-control shRNA
rAAV-Ncoa3 shRNA
kDa
Ncoa3
250
150
Limk1
75
a-Tubulin
37
Western Blot
E
relative band intensity (norm. to α-Tubulin, basal=1)
1.4
1.2
1.0
0.8
0.6
0.4
0.2
0.0
*
*
Ncoa3
Limk1
rAAV-control shRNA
rAAV-Ncoa3 shRNA
rAAV-control shRNA
rAAV-Ncoa3 shRNA

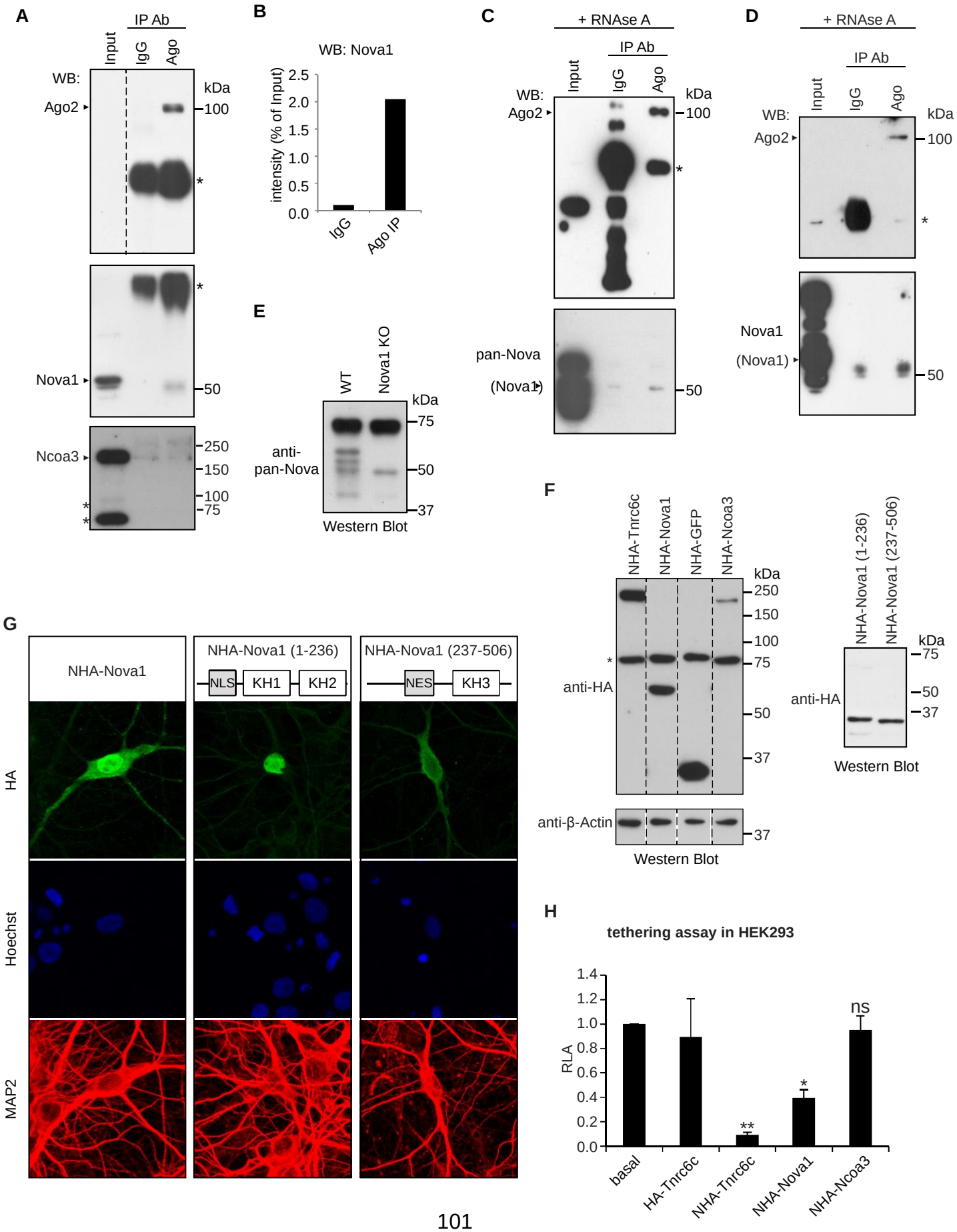
A
IP Ab
Input
IgG
Ago
WB:
kDa
Ago2
100
*
Nova1
50
Ncoa3
250
150
100
75
B
WB: Nova1
intensity (% of Input)
2.5
2.0
1.5
1.0
0.5
0.0
IgG
Ago IP
C
+ RNAse A
IP Ab
Input
IgG
Ago
WB:
Ago2
kDa
100
*
pan-Nova
(Nova1)
50
D
+ RNAse A
IP Ab
Input
IgG
Ago
WB:
Ago2
kDa
100
*
Nova1
(Nova1)
50
E
WT
Nova1 KO
kDa
anti-
pan-Nova
75
50
37
Western Blot
F
NHA-Tnrc6c
NHA-Nova1
NHA-GFP
NHA-Ncoa3
kDa
250
150
100
75
50
37
anti-HA
anti-β-Actin
Western Blot
NHA-Nova1 (1-236)
NHA-Nova1 (237-506)
kDa
75
50
37
anti-HA
Western Blot
G
NHA-Nova1
NHA-Nova1 (1-236)
NLS
KH1
KH2
NHA-Nova1 (237-506)
NES
KH3
HA
Hoechst
MAP2
H
tethering assay in HEK293
RLA
1.4
1.2
1.0
0.8
0.6
0.4
0.2
0.0
ns
*
**
basal
HA-Tnrc6c
NHA-Tnrc6c
NHA-Nova1
NHA-Ncoa3

Figure E6

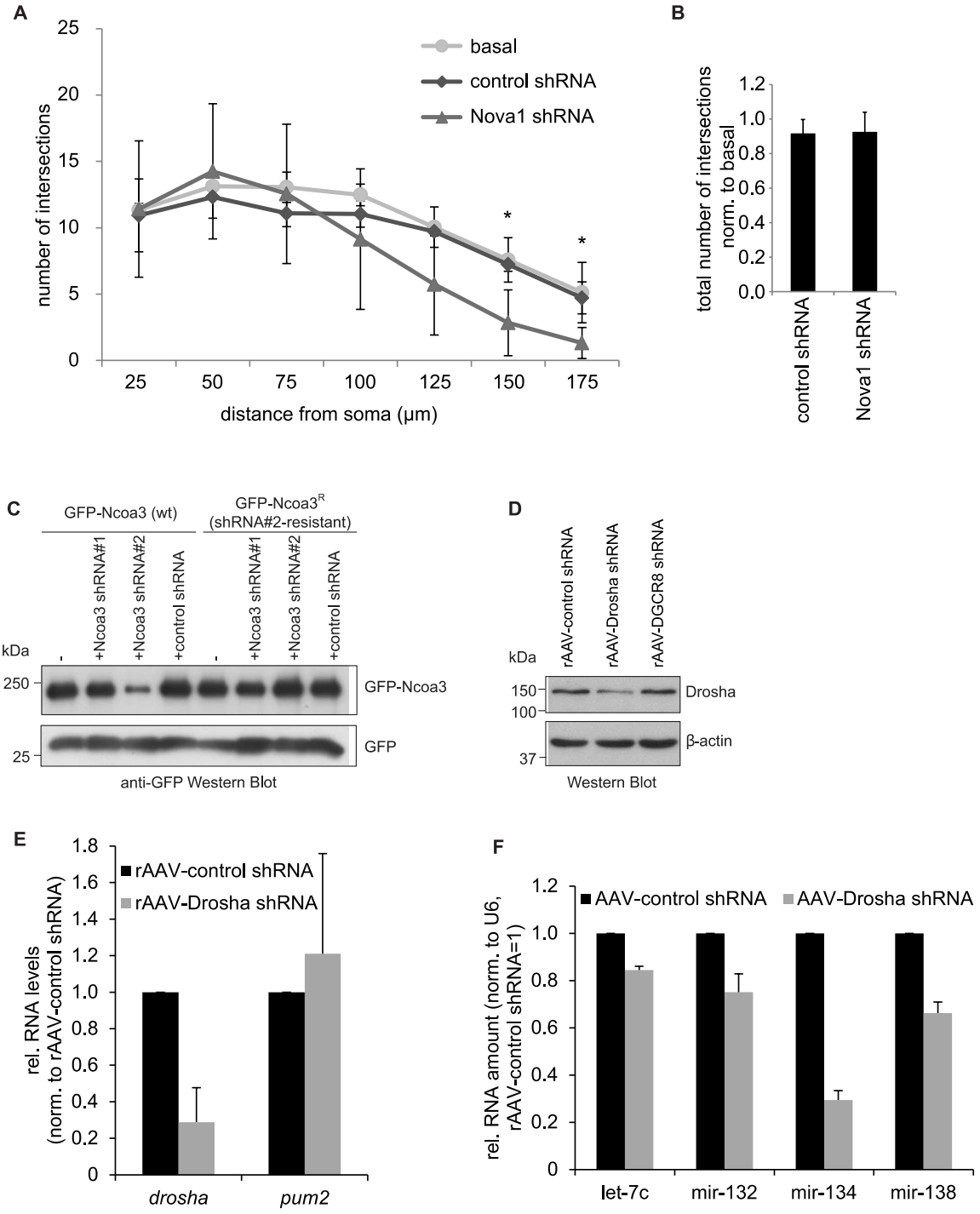
A
number of intersections
distance from soma (µm)
basal
control shRNA
Nova1 shRNA
B
total number of intersections norm. to basal
control shRNA
Nova1 shRNA
C
GFP-Ncoa3 (wt)
GFP-Ncoa3R (shRNA#2-resistant)
+Ncoa3 shRNA#1
+Ncoa3 shRNA#2
+control shRNA
kDa
250
GFP-Ncoa3
25
GFP
anti-GFP Western Blot
D
rAAV-control shRNA
rAAV-Drosha shRNA
rAAV-DGCR8 shRNA
kDa
150
100
Drosha
37
β-actin
Western Blot
E
rAAV-control shRNA
rAAV-Drosha shRNA
rel. RNA levels (norm. to rAAV-control shRNA)
drosha
pum2
F
AAV-control shRNA
AAV-Drosha shRNA
rel. RNA amount (norm. to U6, rAAV-control shRNA=1)
let-7c
mir-132
mir-134
mir-138

Figure E8

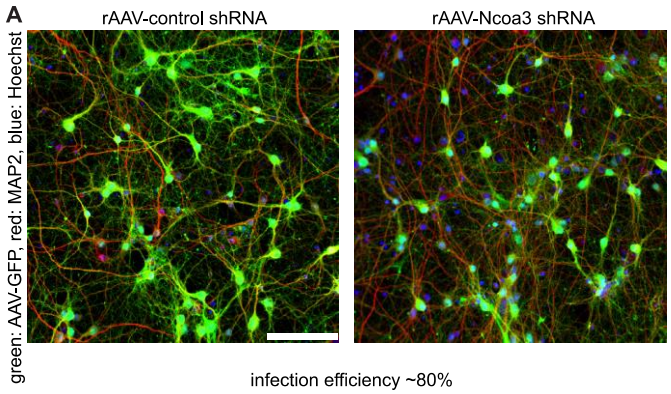

B

Pearson's correlation coefficients

		rAAV-control shRNA			rAAV-Ncoa3 shRNA		
		I	II	III	I	II	III
rAAV-control shRNA	I	1	0.994	0.976	0.995	0.992	0.975
	II	0.994	1	0.974	0.993	0.992	0.973
	III	0.976	0.974	1	0.974	0.975	0.994
rAAV-Ncoa3 shRNA	I	0.995	0.993	0.974	1	0.993	0.974
	II	0.992	0.992	0.975	0.993	1	0.975
	III	0.975	0.973	0.994	0.974	0.975	1

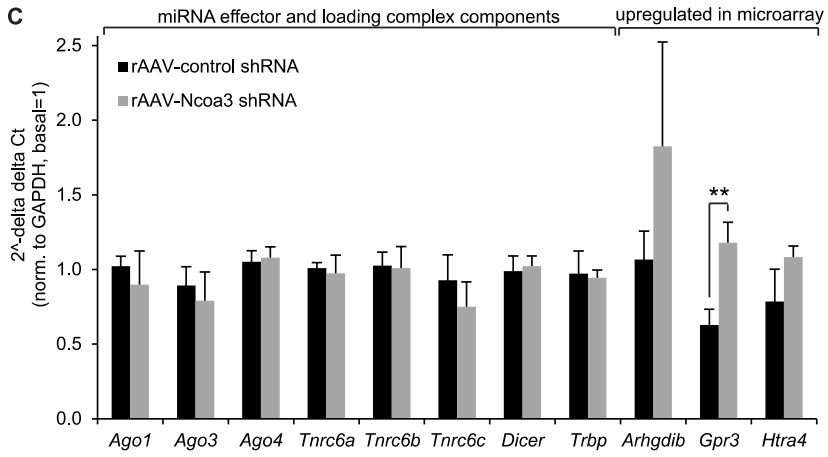

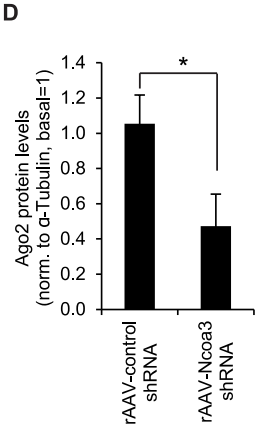

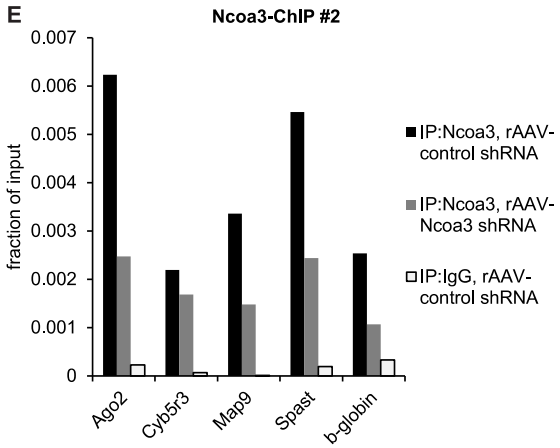

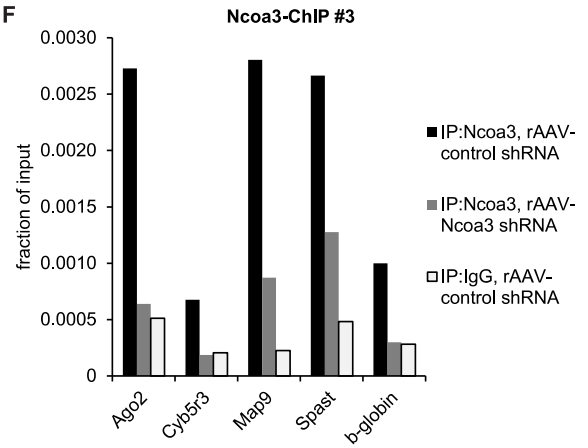

G

```
Mmu: GCCGGGAGGTGGCGGTGTGGTCACGCGCACGGGTCTGGCCGCGTCCAAGTTCAAGCTCTG
Rno: GCCGGGAGGTGGCGGTGTGGTCACGCGCACGGGTCTGGCCGCGTCCAAGTTCAAGNNNNN
Hsa: GCCGGGAGGTGGCGGTGTGGTCCTGCGCGAGCGGCCGGCCGCGTTCAAGTTCAAGCTCCG
```

Figure E9

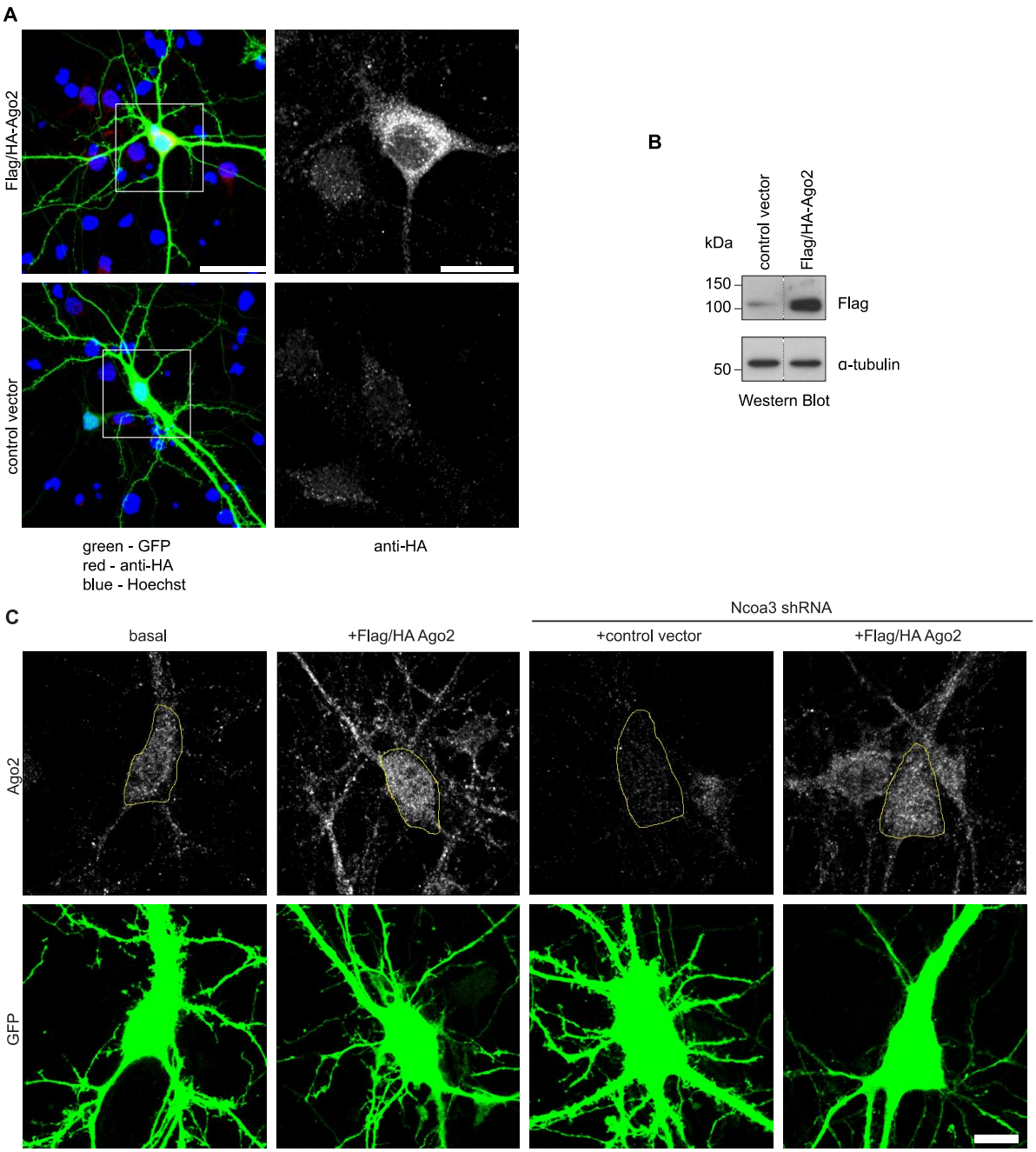
A
Flag/HA-Ago2
control vector
green - GFP
red - anti-HA
blue - Hoechst
anti-HA
B
kDa
control vector
Flag/HA-Ago2
150
100
Flag
50
α-tubulin
Western Blot
C
basal
+Flag/HA Ago2
Ncoa3 shRNA
+control vector
+Flag/HA Ago2
Ago2
GFP

5. References

Abdelmohsen, K., Hutchison, E.R., Lee, E.K., Kuwano, Y., Kim, M.M., Masuda, K., Srikantan, S., Subaran, S.S., Marasa, B.S., and Mattson, M.P., et al. (2010). miR-375 Inhibits Differentiation of Neurites by Lowering HuD Levels. Molecular and Cellular Biology *30*, 4197-4210.

Agostini, M., Tucci, P., Steinert, J.R., Shalom-Feuerstein, R., Rouleau, M., Aberdam, D., Forsythe, I.D., Young, K.W., Ventura, A., and Concepcion, C.P., et al. (2011). microRNA-34a regulates neurite outgrowth, spinal morphology, and function. Proc Natl Acad Sci U S A *108*, 21099-21104.

Amazit, L., Pasini, L., Szafran, A.T., Berno, V., Wu, R.-C., Mielke, M., Jones, E.D., Mancini, M.G., Hinojos, C.A., and O'Malley, B.W., et al. (2007). Regulation of SRC-3 Intercompartmental Dynamics by Estrogen Receptor and Phosphorylation. Molecular and Cellular Biology *27*, 6913-6932.

Aoto, J., Nam, C.I., Poon, M.M., Ting, P., and Chen, L. (2008). Synaptic Signaling by All-Trans Retinoic Acid in Homeostatic Synaptic Plasticity. Neuron *60*, 308-320.

Azuma-Mukai, A., Oguri, H., Mituyama, T., Qian, Z.R., Asai, K., Siomi, H., and Siomi, M.C. (2008). Characterization of endogenous human Argonautes and their miRNA partners in RNA silencing. Proceedings of the National Academy of Sciences of the United States of America *105*, 7964-7969.

Banerjee, S., Neveu, P., and Kosik, K.S. (2009). A Coordinated Local Translational Control Point at the Synapse Involving Relief from Silencing and MOV10 Degradation. Neuron *64*, 871-884.

Bellone, C., and Lüscher, C. (2006). Cocaine triggered AMPA receptor redistribution is reversed in vivo by mGluR-dependent long-term depression. Nature neuroscience *9*, 636-641.

Beveridge, N.J., Tooney, P.A., Carroll, A.P., Gardiner, E., Bowden, N., Scott, R.J., Tran, N., Dedova, I., and Cairns, M.J. (2008). Dysregulation of miRNA 181b in the temporal cortex in schizophrenia. Human Molecular Genetics *17*, 1156-1168.

Bhattacharyya, S.N., Habermacher, R., Martine, U., Closs, E.I., and Filipowicz, W. (2006). Relief of microRNA-Mediated Translational Repression in Human Cells Subjected to Stress. Cell *125*, 1111-1124.

Bicker, S., Khudayberdiev, S., Weiss, K., Zocher, K., Baumeister, S., and Schratt, G. (2013). The DEAH-box helicase DHX36 mediates dendritic localization of the neuronal precursor-microRNA-134. Genes & Development *27*, 991-996.

Börner, K., Niopek, D., Cotugno, G., Kaldenbach, M., Pankert, T., Willemsen, J., Zhang, X., Schürmann, N., Mockenhaupt, S., and Serva, A., et al. (2013). Robust RNAi enhancement via human Argonaute-2 overexpression from plasmids, viral vectors and cell lines. Nucleic Acids Research *41*, e199.

Cajigas, I.J., Tushev, G., Will, T.J., tom Dieck, S., Fuerst, N., and Schuman, E.M. (2012). The Local Transcriptome in the Synaptic Neuropil Revealed by Deep Sequencing and High-Resolution Imaging. Neuron *74*, 453-466.

Cambray, S., Pedraza, N., Rafel, M., Garí, E., Aldea, M., and Gallego, C. (2009). Protein kinase KIS localizes to RNA granules and enhances local translation. Molecular and Cellular Biology *29*, 726-735.

Chai, Z., Yang, L., Yu, B., He, Q., Li, W.-I., Zhou, R., Zhang, T., Zheng, X., and Xie, J. (2009). p38 mitogen-activated protein kinase-dependent regulation of SRC-3 and involvement in retinoic acid receptor alpha signaling in embryonic cortical neurons. IUBMB Life *61*, 670-678.

Chaki, S., and Hikichi, H. (2011). Targeting of metabotropic glutamate receptors for the treatment of schizophrenia. Current pharmaceutical design *17*, 94-102.

Chandrasekar, V., and Dreyer, J.-L. (2009). microRNAs miR-124, let-7d and miR-181a regulate cocaine-induced plasticity. Molecular and cellular neurosciences *42*, 350-362.

Chandrasekar, V., and Dreyer, J.-L. (2011). Regulation of MiR-124, Let-7d, and MiR-181a in the accumbens affects the expression, extinction, and reinstatement of cocaine-induced conditioned place preference. Neuropsychopharmacology : official publication of the American College of Neuropsychopharmacology *36*, 1149-1164.

Cheloufi, S., Dos Santos, C.O., Chong, M.M.W., and Hannon, G.J. (2010). A dicer-independent miRNA biogenesis pathway that requires Ago catalysis. Nature *465*, 584-589.

Cifuentes, D., Xue, H., Taylor, D.W., Patnode, H., Mishima, Y., Cheloufi, S., Ma, E., Mane, S., Hannon, G.J., and Lawson, N.D., et al. (2010). A novel miRNA processing pathway independent of Dicer requires Argonaute2 catalytic activity. Science (New York, N.Y.) *328*, 1694-1698.

Cummings, E., Donohoe, G., Hargreaves, A., Moore, S., Fahey, C., Dinan, T., McDonald, C., O'Callaghan, E., O'Neill, F., and Waddington, J., et al. (2013). Mood congruent psychotic symptoms and specific cognitive deficits in carriers of the novel schizophrenia risk variant at MIR-137. Neuroscience Letters *532*, 33-38.

Dan, C., Jinjun, B., Zi-Chun, H., Lin, M., Wei, C., Xu, Z., Ri, Z., Shun, C., Wen-Zhu, S., and Qing-Cai, J., et al. (2015). Modulation of TNF-α mRNA stability by human antigen R and miR181s in sepsis-induced immunoparalysis. EMBO molecular medicine *7*, 140-157.

Dasgupta, S., Lonard, D.M., and O'Malley, B.W. (2014). Nuclear receptor coactivators: master regulators of human health and disease. Annual review of medicine *65*, 279-292.

Diederichs, S., and Haber, D.A. (2007). Dual role for argonautes in microRNA processing and posttranscriptional regulation of microRNA expression. Cell *131*, 1097-1108.

Edbauer, D., Neilson, J.R., Foster, K.A., Wang, C.-F., Seeburg, D.P., Batterton, M.N., Tada, T., Dolan, B.M., Sharp, P.A., and Sheng, M. (2010). Regulation of Synaptic Structure and Function by FMRP-Associated MicroRNAs miR-125b and miR-132. Neuron *65*, 373-384.

Engels, B., Jannot, G., Remenyi, J., Simard, M.J., and Hutvagner, G. (2012). Polypyrimidine tract binding protein (hnRNP I) is possibly a conserved modulator of miRNA-mediated gene regulation. PLoS ONE *7*, e33144.

Fiore, R., Khudayberdiev, S., Christensen, M., Siegel, G., Flavell, S.W., Kim, T.-K., Greenberg, M.E., and Schratt, G. (2009). Mef2-mediated transcription of the miR379–410 cluster regulates activity-dependent dendritogenesis by fine-tuning Pumilio2 protein levels. EMBO J *28*, 697-710.

Fiore, R., Rajman, M., Schwale, C., Bicker, S., Antoniou, A., Bruehl, C., Draguhn, A., and Schratt, G. (2014). MiR-134-dependent regulation of Pumilio-2 is necessary for homeostatic synaptic depression. The EMBO journal *33*, 2231-2246.

Flavell, S.W., and Greenberg, M.E. (2008). Signaling mechanisms linking neuronal activity to gene expression and plasticity of the nervous system. Annual review of neuroscience *31*, 563-590.

Gao, J., Wang, W.-Y., Mao, Y.-W., Gräff, J., Guan, J.-S., Pan, L., Mak, G., Kim, D., Su, S.C., and Tsai, L.-H. (2010). A novel pathway regulates memory and plasticity via SIRT1 and miR-134. Nature *466*, 1105-1109.

Gojis, O., Rudraraju, B., Gudi, M., Hogben, K., Sousha, S., Coombes, R.C., Coombes, C.R., Cleator, S., and Palmieri, C. (2010). The role of SRC-3 in human breast cancer. Nature reviews. Clinical oncology *7*, 83-89.

Grimm, D., and Kay, M.A. (2006). Therapeutic short hairpin RNA expression in the liver: viral targets and vectors. Gene therapy *13*, 563-575.

Hafner, M., Landthaler, M., Burger, L., Khorshid, M., Hausser, J., Berninger, P., Rothballer, A., Ascano, M., Jungkamp, A.-C., and Munschauer, M., et al. (2010). Transcriptome-wide Identification of RNA-Binding Protein and MicroRNA Target Sites by PAR-CLIP. Cell *141*, 129-141.

Ho, V.M., Dallalzadeh, L.O., Karathanasis, N., Keles, M.F., Vangala, S., Grogan, T., Poirazi, P., and Martin, K.C. (2014). GluA2 mRNA distribution and regulation by miR-124 in hippocampal neurons. Molecular and cellular neurosciences *61*, 1-12.

Höck, J., Weinmann, L., Ender, C., Rüdel, S., Kremmer, E., Raabe, M., Urlaub, H., and Meister, G. (2007). Proteomic and functional analysis of Argonaute-containing mRNA–protein complexes in human cells. EMBO Rep *8*, 1052-1060.

Horman, S.R., Janas, M.M., Litterst, C., Wang, B., MacRae, I.J., Sever, M.J., Morrissey, D.V., Graves, P., Luo, B., and Umesalma, S., et al. (2013). Akt-Mediated Phosphorylation of Argonaute 2 Downregulates Cleavage and Upregulates Translational Repression of MicroRNA Targets. Molecular Cell *50*, 356-367.

Hu, Z., Zhao, J., Hu, T., Luo, Y., Zhu, J., and Li, Z. (2015). miR-501-3p mediates the activity-dependent regulation of the expression of AMPA receptor subunit GluA1. The Journal of Cell Biology *208*, 949-959.

Huang, P., Ye, B., Yang, Y., Shi, J., and Zhao, H. (2015). MicroRNA-181 functions as a tumor suppressor in non-small cell lung cancer (NSCLC) by targeting Bcl-2. Tumour biology : the journal of the International Society for Oncodevelopmental Biology and Medicine *36*, 3381-3387.

Huganir, R.L., and Nicoll, R.A. (2013). AMPARs and Synaptic Plasticity: The Last 25 Years. Neuron *80*, 704-717.

Huntzinger, E., and Izaurralde, E. (2011). Gene silencing by microRNAs: contributions of translational repression and mRNA decay. Nat Rev Genet *12*, 99-110.

Iorio, M.V., and Croce, C.M. (2012). Causes and consequences of microRNA dysregulation. Cancer journal (Sudbury, Mass.) *18*, 215-222.

Jimenez-Mateos, E.M., Engel, T., Merino-Serrais, P., McKiernan, R.C., Tanaka, K., Mouri, G., Sano, T., O'Tuathaigh, C., Waddington, J.L., and Prenter, S., et al. (2012). Silencing microRNA-134 produces neuroprotective and prolonged seizure-suppressive effects. Nat Med *18*, 1087-1094.

Jovicic, A., Roshan, R., Moisoi, N., Pradervand, S., Moser, R., Pillai, B., and Luthi-Carter, R. (2013). Comprehensive Expression Analyses of Neural Cell-Type-Specific miRNAs Identify New Determinants of the Specification and Maintenance of Neuronal Phenotypes. Journal of Neuroscience *33*, 5127-5137.

Kedde, M., Strasser, M.J., Boldajipour, B., Vrielink, J.A.O., Slanchev, K., Le Sage, C., Nagel, R., Voorhoeve, P.M., van Duijse, J., and Ørom, U.A., et al. (2007). RNA-Binding Protein Dnd1 Inhibits MicroRNA Access to Target mRNA. Cell *131*, 1273-1286.

Krol, J., Loedige, I., and Filipowicz, W. (2010). The widespread regulation of microRNA biogenesis, function and decay. Nat Rev Genet.

Kwon, E., Wang, W., and Tsai, L.-H. (2013). Validation of schizophrenia-associated genes CSMD1, C10orf26, CACNA1C and TCF4 as miR-137 targets. Molecular psychiatry *18*, 11-12.

Kye, M.-J., Liu, T., Levy, S.F., Xu, N.L., Groves, B.B., Bonneau, R., Lao, K., and Kosik, K.S. (2007). Somatodendritic microRNAs identified by laser capture and multiplex RT-PCR. RNA (New York, N.Y.) *13*, 1224-1234.

Leo, C., and Chen, J.D. (2000). The SRC family of nuclear receptor coactivators. Gene *245*, 1-11.

Letellier, M., Elramah, S., Mondin, M., Soula, A., Penn, A., Choquet, D., Landry, M., Thoumine, O., and Favereaux, A. (2014). miR-92a regulates expression of synaptic GluA1-containing AMPA receptors during homeostatic scaling. Nature neuroscience *17*, 1040-1042.

Li, S., Wang, L., Fu, B., Berman, M.A., Diallo, A., and Dorf, M.E. (2014). TRIM65 regulates microRNA activity by ubiquitination of TNRC6. Proceedings of the National Academy of Sciences *111*, 6970-6975.

Lippman, J., and Dunaevsky, A. (2005). Dendritic spine morphogenesis and plasticity. Journal of neurobiology *64*, 47-57.

Liu, Y., Zhao, Z., Yang, F., Gao, Y., Song, J., and Wan, Y. (2013). microRNA-181a is involved in insulin-like growth factor-1-mediated regulation of the transcription factor CREB1. J Neurochem.

Long, W., Yi, P., Amazit, L., LaMarca, H.L., Ashcroft, F., Kumar, R., Mancini, M.A., Tsai, S.Y., Tsai, M.-J., and O'Malley, B.W. (2010). SRC-3Delta4 mediates the interaction of EGFR with FAK to promote cell migration. Molecular Cell *37*, 321-332.

Lugli, G., Torvik, V.I., Larson, J., and Smalheiser, N.R. (2008). Expression of microRNAs and their precursors in synaptic fractions of adult mouse forebrain. Journal of Neurochemistry *106*, 650-661.

Matsuzaki, M., Honkura, N., Ellis-Davies, Graham C R, and Kasai, H. (2004). Structural basis of long-term potentiation in single dendritic spines. Nature *429*, 761-766.

McKee, A.E., Minet, E., Stern, C., Riahi, S., Stiles, C.D., and Silver, P.A. (2005). A genome-wide in situ hybridization map of RNA-binding proteins reveals anatomically restricted expression in the developing mouse brain. BMC Dev Biol *5*, 14.

Miska, E.A., Alvarez-Saavedra, E., Townsend, M., Yoshii, A., Sestan, N., Rakic, P., Constantine-Paton, M., and Horvitz, H.R. (2004). Microarray analysis of microRNA expression in the developing mammalian brain. Genome biology *5*, R68.

Muddashetty, R.S., Nalavadi, V.C., Gross, C., Yao, X., Xing, L., Laur, O., Warren, S.T., and Bassell, G.J. (2011). Reversible inhibition of PSD-95 mRNA translation by miR-125a, FMRP phosphorylation, and mGluR signaling. Molecular Cell *42*, 673-688.

Nolde, M.J., Saka, N., Reinert, K.L., and Slack, F.J. (2007). The Caenorhabditis elegans pumilio homolog, puf-9, is required for the 3'UTR-mediated repression of the let-7 microRNA target gene, hbl-1. Developmental Biology *305*, 551-563.

O'Carroll, D., Mecklenbrauker, I., Das, P.P., Santana, A., Koenig, U., Enright, A.J., Miska, E.A., and Tarakhovsky, A. (2007). A Slicer-independent role for Argonaute 2 in hematopoiesis and the microRNA pathway. Genes & Development *21*, 1999-2004.

Olde Loohuis, Nikkie F M, Ba, W., Stoerchel, P.H., Kos, A., Jager, A., Schratt, G., Martens, Gerard J M, van Bokhoven, H., Nadif Kasri, N., and Aschrafi, A. (2015). MicroRNA-137 Controls AMPA-Receptor-Mediated Transmission and mGluR-Dependent LTD. Cell reports *11*, 1876-1884.

Passafaro, M., Nakagawa, T., Sala, C., and Sheng, M. (2003). Induction of dendritic spines by an extracellular domain of AMPA receptor subunit GluR2. Nature *424*, 677-681.

Qi, H.H., Ongusaha, P.P., Myllyharju, J., Cheng, D., Pakkanen, O., Shi, Y., Lee, S.W., Peng, J., and Shi, Y. (2008). Prolyl 4-hydroxylation regulates Argonaute 2 stability. Nature *455*, 421-424.

Ran, I., Gkogkas, C.G., Vasuta, C., Tartas, M., Khoutorsky, A., Laplante, I., Parsyan, A., Nevarko, T., Sonenberg, N., and Lacaille, J.-C. (2013). Selective regulation of GluA subunit synthesis and AMPA receptor-mediated synaptic function and plasticity by the translation repressor 4E-BP2 in hippocampal pyramidal cells. The Journal of neuroscience : the official journal of the Society for Neuroscience *33*, 1872-1886.

Richter, J.D., and Klann, E. (2009). Making synaptic plasticity and memory last: mechanisms of translational regulation. Genes & Development *23*, 1-11.

Ripke, S., Neale, B.M., Corvin, A., Walters, James T. R., and et al. (2014). Biological insights from 108 schizophrenia-associated genetic loci. Nature *511*, 421-427.

Roll-Mecak, A., and McNally, F.J. (2010). Microtubule-severing enzymes. Current Opinion in Cell Biology *22*, 96-103.

Rybak, A., Fuchs, H., Hadian, K., Smirnova, L., Wulczyn, E.A., Michel, G., Nitsch, R., Krappmann, D., and Wulczyn, F.G. (2009). The let-7 target gene mouse lin-41 is a stem cell specific E3 ubiquitin ligase for the miRNA pathway protein Ago2. Nature cell biology *11*, 1411-1420.

Saba, R., Storchel, P.H., Aksoy-Aksel, A., Kepura, F., Lippi, G., Plant, T.D., and Schratt, G.M. (2012). Dopamine-Regulated MicroRNA MiR-181a Controls GluA2 Surface Expression in Hippocampal Neurons. Molecular and Cellular Biology *32*, 619-632.

Sasaki, Y., Gross, C., Xing, L., Goshima, Y., and Bassell, G.J. (2014). Identification of axon-enriched microRNAs localized to growth cones of cortical neurons. Developmental neurobiology *74*, 397-406.

Schaefer, A., Im, H.-I., Venø, M.T., Fowler, C.D., Min, A., Intrator, A., Kjems, J., Kenny, P.J., O'Carroll, D., and Greengard, P. (2010). Argonaute 2 in dopamine 2 receptor-expressing neurons regulates cocaine addiction. The Journal of experimental medicine *207*, 1843-1851.

Schratt, G.M., Tuebing, F., Nigh, E.A., Kane, C.G., Sabatini, M.E., Kiebler, M., and Greenberg, M.E. (2006). A brain-specific microRNA regulates dendritic spine development. Nature *439*, 283-289.

Shi, L., Cheng, Z., Zhang, J., Li, R., Zhao, P., Fu, Z., and You, Y. (2008). hsa-mir-181a and hsa-mir-181b function as tumor suppressors in human glioma cells. Brain Research *1236*, 185-193.

Shin, K.-H., Bae, S.D., Hong, H.S., Kim, R.H., Kang, M.K., and Park, N.-H. (2011). miR-181a shows tumor suppressive effect against oral squamous cell carcinoma cells by downregulating K-ras. Biochemical and Biophysical Research Communications *404*, 896-902.

Siegel, G., Obernosterer, G., Fiore, R., Oehmen, M., Bicker, S., Christensen, M., Khudayberdiev, S., Leuschner, P.F., Busch, C.J.L., and Kane, C., et al. (2009). A functional screen implicates microRNA-138-dependent regulation of the depalmitoylation enzyme APT1 in dendritic spine morphogenesis. Nat Cell Biol *11*, 705-716.

Siegert, S., Seo, J., Kwon, E.J., Rudenko, A., Cho, S., Wang, W., Flood, Z., Martorell, A.J., Ericsson, M., and Mungenast, A.E., et al. (2015). The schizophrenia risk gene product miR-137 alters presynaptic plasticity. Nature neuroscience *18*, 1008-1016.

Smrt, R.D., Szulwach, K.E., Pfeiffer, R.L., Li, X., Guo, W., Pathania, M., Teng, Z.-Q., Luo, Y., Peng, J., and Bordey, A., et al. (2010). MicroRNA miR-137 Regulates Neuronal Maturation by Targeting Ubiquitin Ligase Mind Bomb-1. STEM CELLS *28*, 1060-1070.

Störchel, P.H., Thümmler, J., Siegel, G., Aksoy-Aksel, A., Zampa, F., Sumer, S., and Schratt, G. (2015). A large-scale functional screen identifies Nova1 and Ncoa3 as regulators of neuronal miRNA function. The EMBO journal.

van Kouwenhove, M., Kedde, M., and Agami, R. (2011). MicroRNA regulation by RNA-binding proteins and its implications for cancer. Nature reviews. Cancer *11*, 644-656.

van Os, J., and Kapur, S. (2009). Schizophrenia. The Lancet *374*, 635-645.

Venoux, M., Delmouly, K., Milhavet, O., Vidal-Eychenié, S., Giorgi, D., and Rouquier, S. (2008). Gene organization, evolution and expression of the microtubule-associated protein ASAP (MAP9). BMC genomics *9*, 406.

Willemsen, M.H., Vallès, A., Kirkels, Laurens A M H, Mastebroek, M., Olde Loohuis, N., Kos, A., Wissink-Lindhout, W.M., de Brouwer, Arjan P M, Nillesen, W.M., and Pfundt, R., et al. (2011). Chromosome 1p21.3 microdeletions comprising DPYD and MIR137 are associated with intellectual disability. Journal of medical genetics *48*, 810-818.

Xu, J., Wu, R.-C., and O'Malley, B.W. (2009). Normal and cancer-related functions of the p160 steroid receptor co-activator (SRC) family. Nature reviews. Cancer *9*, 615-630.

Yu, C., York, B., Wang, S., Feng, Q., Xu, J., and O'Malley, B.W. (2007). An Essential Function of the SRC-3 Coactivator in Suppression of Cytokine mRNA Translation and Inflammatory Response. Molecular Cell *25*, 765-778.

Zeng, Y., Sankala, H., Zhang, X., and Graves, P.R. (2008). Phosphorylation of Argonaute 2 at serine-387 facilitates its localization to processing bodies. Biochem. J. *413*, 429.

6. Appendix

6.1 List of abbreviations

3’ UTR	3’ untranslated region
AAV	Adeno-associated virus
Ago	Argonaute protein
APT1	acyl-protein thioesterase 1
AMPA	α-amino-3-hydroxy-5-methyl-4-isoxazolepropionic acid
AMPA-R	AMPA-receptor
BDNF	brain-derived neurotrophic factor
CACNA1C	voltage-dependent L-type calcium channel subunit alpha-1C
CAT-1	cationic amino acid transporter 1
ChIP	chromatin immunoprecipitation
CLIP	cross-linking immunoprecipitation
CREB1	cyclic AMP-responsive element-binding protein 1
CSMD1	CUB and sushi domain-containing protein 1
DGCR8	DiGeorge syndrome critical region 8
DHPG	Dihydroxyphenylglycine
DIV	days *in vitro*
DNA	deoxyribonucleic acid
Drd2	dopamine-receptor 2
eIF4E-BP2	eukaryotic initiation factor 4E binding protein 2
Fig.	figure
FMRP	fragile X mental retardation protein
GFP	green fluorescent protein
GluA1	ionotropic glutamate receptor, AMPA-selective 1
GluA2	ionotropic glutamate receptor, AMPA-selective 2
GW182	glycine-tryptophan protein of 182 kDa
HMGA2	high mobility group AT-hook protein 2
Limk1	LIM-domain kinase 1
Lin-41	abnormal cell lineage 41
LTD	long-term depression
MAP 9	microtubule-associated protein 9

mEPSC	miniature excitatory postsynaptic current
mGluR	metabotropic glutamate receptor
Mib1	mind bomb homolog 1
miRISC	microRNA-induced silencing complex
miRNA	microRNA
Mov10	Moloney leukemia virus 10
mRNA	messenger RNA
Ncoa3	nuclear receptor co-activator 3
NMDA	N-methyl-D-aspartate
NMDA-R	NMDA-receptor
Nova1	neuro-oncological ventral antigen 1
pLNA	power locked nucleic acids
PND	post-natal day
pre-miRNA	precursor microRNA
pri-miRNA	primary microRNA
Pub.	publication
Pum2	Pumilio2
qPCR	quantitative PCR
RBP	RNA-binding protein
RNA	ribonucleic acid
RNAi	RNA interference
shRNA	short hairpin RNA
siRNA	small interfering RNA
TCF4	transcription factor 4
TNF-alpha	tumor necrosis factor alpha
Tnrc6	trinucleotide repeat-containing gene 6
TRBP	trans-activation-responsive RNA-binding protein
UHMK1	U2AF homology motif kinase 1

6.2 List of academic teachers

My academic teachers in Lübeck were:

Anemüller
Hartmann
Hilgenfeld
Jelkmann
Kalies
Keller
Laskay
Martinetz
Notbohm
Paulsen
Peters
Prestin
Rohwedel
Tantau
Weimar
Zechel
Ziegler
Zühlke

My academic teachers in Albuquerque were:

Brozik
Ho
Osgood
Toolson

My academic teachers in Dresden were:

Bergmann
Corbeil
Gelinsky
Groß
Hoflack
Mertig
Müller
Scharnweber
Schroeder
Schwille
Simons
Stewart

6.3 Acknowledgements

I would like to express my deepest gratitude to my supervisor Prof. Gerhard Schratt for making this research project possible. He offered a great scientific environment with the right balance of freedom and guidance. He was always supportive and inspired me with confidence. Thank you!

My hearty thanks belong to Juliane Thümmler for being a magnificent member of our screen team. Our countless discussions in the lab, in the kitchen, or in bars were a big source of motivation for me. She is a great person. Please stay the way you are!

Dr. Gabriele Siegel introduced me to the Lab through which I learned a lot from her. She taught me how to work independently which was essential for the success of this work. She is a genuine character and I wish her all the best for the future.

My sincere thanks go to Dr. Roberto Fiore, Dr. Silvia Bicker, Dr. Anna Antoniou and Kerstin Weiss for corrections of this thesis and for being great colleagues and persons.

My deep gratitude goes to all other present or past members of the Schratt Lab, specifically Federico Zampa, Martin Lackinger, Jeremy Valluy, Dr. Sharof Khudayberdiev, Dr. Ayla Aksoy-Aksel, Dr. Marek Rajman, Helena Martin, Miriam Montag, Dr. Bernd Kösters, Dr. Reuben Saba, Simon Sumer for all kinds of help though assistance, discussions or encouragements inside and outside the lab.

I would like to thank the teaching staff composed of Dr. Christian Wrocklage, Dr. Birgit Rost and Dr. Cecilia Patrascan for enabling enabled me to focus on my experimental work.

Thanks to Prof. Macro Rust and Sophie Meyer for the conversations at our Mensa breaks.

Special thanks to our present or past technicians Ute Beck, Eva Becker, Traudel Jarosch, Karlheinz Burk, Heinrich Kaiser, Renate Gondrum, Bettina Kowalski and Tatjana Wüst for their persistent work. Administrative paper work was greatly supported by Irena Müller.

I am thankful to my internship students Anna Tsankova, Birgit Honrath, Christian Goecke and Lea Greifenberg for their great technical support and discussions.

My deepest gratitude is extended to my parents Dr. Evelyn Störchel-Dreczko and Dr. Hajo Störchel who supported me during all my steps. I would not have made it here without them.

My love Mareike was the biggest support to me. Even though we had to give up our common apartment in Heidelberg for the continuation of this work in Marburg, she knew what she wanted and made her way. Her independence and sheer endless understanding for me always encouraged me to bring this work to an end.